Faculty of Resource Science and Technology

Integrative Multi-Omics and Environmental Analysis: Linking Transcriptomics, Soil Chemistry, and Microbial Communities to Trunking Performance in Sago Palm (*Metroxylon sagu* Rottb.)

Fifi Hafizzah Binti Pendi

Doctor of Philosophy
2026

Integrative Multi-Omics and Environmental Analysis: Linking Transcriptomics, Soil Chemistry, and Microbial Communities to Trunking Performance in Sago Palm (*Metroxylon sagu* Rottb.)

Fifi Hafizzah Binti Pendi

A thesis submitted

In fulfillment of the requirements for the degree of Doctor of Philosophy

(Genetics)

Faculty of Resource Science and Technology
UNIVERSITI MALAYSIA SARAWAK
2026

DECLARATION

I declare that the work in this thesis was carried out in accordance with the regulations of Universiti Malaysia Sarawak. Except where due acknowledgements have been made, the work is that of the author alone. The thesis has not been accepted for any degree and is not concurrently submitted in candidature of any other degree.

……

Signature

Name: Fifi Hafizzah Binti Pendi

Matric No.: 21010133

Faculty of Resource Science and Technology

Universiti Malaysia Sarawak

Date : 15 January 2026

ACKNOWLEDGEMENT

First and foremost, I am deeply grateful to my supervisor, Prof Dr. Mohd Hasnain bin Md Hussain, for his trust, expert guidance, encouragement, and unwavering support throughout the course of this research. His insight, patience, and critical feedback have been instrumental in shaping both the direction and the quality of this thesis.

I also wish to extend my sincere thanks to all staff of the Faculty of Resource Science and Technology whose support and resources in creating a conducive environment for learning and research. I also would like to thank my fellow lab members in Proteomics Laboratory, for their collaboration, technical assistance, and many stimulating discussions we shared.

I gratefully acknowledge Sarawak Research and Development Council (SRDC) and Yayasan Tun Taib for their funding and monetary aids, without their funding, this research would not have been possible.

On a personal note, I am profoundly thankful to my family for their endless patience and encouragement. To my parents, grandparents, my brother and all those who stood by me during moments of challenge and doubt, your belief in me kept me going. Lastly, I would like to thank my beloved cats, for their silent companionship and comforting presence during stressful times.

This thesis would not produce without the collective support of everyone mentioned above, and many others whose contributions are deeply appreciated, even if not named individually.

ABSTRACT

The substantial starch yield produced in the pith of *Metroxylon sagu* Rottb. palm has established it as a key staple crop in Malaysia and Indonesia. Thriving in marginal peatlands with minimal maintenance, sago palm holds promise as a sustainable supplement to other starch-producing crops. However, the occurrence of non-trunking (dwarf, trunkless) palms in plantations create instability in sago starch production. While research largely focused on non-trunking palms, trunking sago palms remain understudied, particularly in relation to the peat soils they inhabit. This thesis addresses these gaps by integrating transcriptomic, peat soil physicochemical and microbial perspectives to elucidate the mechanisms underpinning trunk formation of sago palm. Leaf RNA-seq generated a total of 85.61 Gb clean data, identifying 6,119 differentially expressed genes. Functional characterisation revealed coordinated molecular mechanism that supports persistent growth and trunk development. Functional enrichment of the upregulated genes were linked to stress response and genome stability pathways, including protective chaperone activity (*CSP1*), protein homeostasis (*ATL5*), DNA repair (*Zip4*), and chromatin organisation (RanBP2-type zinc finger proteins). The upregulation of *PHO1* mediated phosphate uptake and ABA-responsive stomatal regulation to ensure continuous assimilate synthesis and resilience under heat stress, while *AGO10* safeguarded transcriptional balance Sequestration of excess phosphate by vacuole complemented this buffering system thus maintaining osmotic stability. Conversely, the downregulated lignin and flavonoid biosynthesis redirected resources toward vascular initiation, meristem activity, and carbohydrate accumulation while maintaining vertical growth. Soil analysis showed acidic and low carbon content properties, with trunking sago palms benefitting from slightly lower nutrient concentrations that minimised ionic antagonism at roots for uptake. In contrast, ionic disequilibrium at non-trunking sago palm

soils impaired photosynthesis efficiency and nutrient turnover. Microbial profiling revealed higher levels of Desulfobacterota and Nitrospirota (*Thermodesulfovibrio*) in trunking sago palm soils contributes to enhanced nitrogen and sulphur cycling and reduced heavy metal stress, while fungal communities across all soil samples was dominated by taxa such as Ascomycota and Basidiomycota Together, these findings suggest trunking palms exhibit better environmental adaptation, mediated by synergistic regulation of macronutrient availability and hormone signalling that fine-tunes sago palm growth trajectories. Through this integrated molecular and soil studies, the work provides an insight underpinning plant developmental plasticity and provides understanding for sustainable sago cultivation and food security in tropical peatland ecosystems.

Keywords: Amplicon, boron, fungi, *Metroxylon sagu*, mineral, non-trunking, transcriptomics, trunking

Analisis Integratif Pelbagai Omik dan Alam Sekitar: Menghubungkan Transkriptomik, Kimia Tanah dan Komuniti Mikrob kepada Pertumbuhan Batang Pokok Sagu (Metroxylon sagu Rottb.)

ABSTRAK

Hasil kanji yang tinggi dihasilkan dalam empulur pokok Metroxylon sagu Rottb. *menjadikan rumbia tersebut sebagai tanaman penting di Malaysia dan Indonesia. Tumbuh meliar di kawasan tanah gambut dengan penjaan minimum, pokok sagu berpotensi dalam memastikan keselanjaran kanji. Namun, sebahagian pokok sagu diklasifikasikan sebagai pokok sagu tidak berbatang seringkali dilaporkan di ladang pokok sagu, boleh mewujudkan ketidakstabilan dalam pengeluaran kanji sagu. Justeru, banyak kajian terhadap pokok sagu tidak berbatang telah dijalankan, tetapi kajian terhadap pokok sagu berbatang serta kajian lapang terhadap sifat tanah di ladang sagu masih kekurangan. Bagi menangani jurang ilmu, tesis ini mengintegrasikan analisis transkrptom, sifat fiziokimia tanah dan pemprofilan jenis komuniti mikrob untuk menjelaskan mekanisme yang mendasari pembentukan batang pokok sagu. Analisis penjujukan RNA daripada daun pokok sagu menghasilkan sejumlah 85.61 Gb data bersih dengan jumlah gen pengekpresan pembezaan sebanyak 6,119 gen. Pencirian fungsi menunjukan mekanisma terkoordinasi menyokong pertumbuhan berterusan. Pengayaan fungsi gen yang meningkat dikaitkan dengan mekanisme tindak balas rangsangan dan kestabilan genom, termasuk aktiviti chaperone (CSP1), homeostasis protein (ATL5), pembaikan DNA (Zip4), dan organisasi kromatin (RanBP2-type zinc finger proteins). Peningkatan ekpreso PHO1 mengawal pengambilan fosfat dan regulasi stomata responsive ABA bagi memastikan sintesis asimilasi berterusan serta ketahana terhadap tekanan haba, manakala AGO10 melindungi keseimbagan transkrip. Penyimpanan fosfat berlebihan oleh vakuol melengkapi system penimbal, sekali gus mengekalkan kestabilan*

osmotik. Penurunan biosistesis lignin and flavonoid mengalih sumber nutrient daripada pengukuhan dinding sel sekunder kepada inisiasi vascular, aktiviti meristem, dan pengumpalan karbohidrat sambil mengekalkan pertumbuhan menegak. Analisis tanah menunjukkan sampel tanah berasid dan mempunyai kandungan karbon dan organic yang rendah. Kepekatan nutien yang sedikit rendah memberi manfaat kepada pokok sagu berbatang kerana meminimumkan antagonisme ionic pada akar untuk penyerapan ion. Sebaliknya, ketidakseimbangan ionic pada tanah pokok sagu tidak berbatang menjejaskan kecekapan fotosintesis dan kitaran nutrient pokok tidak berbatang. Analisis komuniti mikrob menunjukkan tahap Desulfobacterota dan Nitrospirota (Thermodesulfovibrio) lebih tinggi dalam sampel tanah pokok sagu berbatang menyumbangkan peningkatan kitaran nitrogen and sulfur serta pengurangan tekanan logam berat, manakala kelimpahan kulat pada kesemua sampel tanah menunjukkan taksa dominan yang sama seperti kulat Ascomycota dan Basidiomycota. Melalui hasil kajian ini, adalah dicadangkan bahawa pokok sagu berbatang mempunyai kadar penyesuaian dan persekitaran yang lebih baik berbanding pokok sagu tidak berbatang dimediasi oleh pengawalan sinergistik ketersediaan makronutrient dan isyarat hormon yang mambantu trajektori pertumbuhan pokok sagu. Kerja ini memberikan pemahaman baharu tentang keplastikan perkembangan tunbuhan serta asas untuk kelestarian penanaman sagu di ekosistem tanah gambut tropika.

Kata kunci: *Boron, kulat, Metroxylon sagu, mineral, penjujukan amplikon, pokok sagu berbatang, pokok sagu tidak berbatang*

TABLE OF CONTENTS

		Page
DECLARATION		i
ACKNOWLEDGEMENT		ii
ABSTRACT		iii
ABSTRAK		v
TABLE OF CONTENTS		vii
LIST OF TABLES		xiii
LIST OF FIGURES		xiv
LIST OF ABBREVIATIONS		xvii
CHAPTER 1: GENERAL INTRODUCTION		1
1.1	Introduction	1
1.2	Taxonomy and Botanical Description of *Metroxylon sagu*	2
1.3	The Centre of Diversity and Sago Distribution in the World	4
1.4	*Metroxylon sagu* Growth Stages	5
1.5	The Importance of Sago Palm to Mankind	6
1.6	Sago Industry in Sarawak	8
1.7	Tropical Peatlands Characteristics	11
1.8	Peat Soil Characteristics	12

1.9 Non-Trunking Occurrences Affects the Sago Palm Productivity 13

1.10 Previous Research Conducted Targeting the Sago Palm Growth Performance 16

1.11 Aim and Objectives 21

1.12 Significance and novelty of Study 21

CHAPTER 2: COMPARATIVE TRANSCRIPTOME ANALYSIS BETWEEN TRUNKING AND NON-TRUNKING *Metroxylon sagu* 23

2.1 Introduction 23

2.1.1 Omics technologies 23

2.1.2 Workflow for RNA-sequencing analysis 25

2.1.3 Leaf as studied organ 35

2.1.4 Research Objectives and Hypothesis 36

2.2 Materials and Methods 38

2.2.1 Leaf tissue collection 38

2.2.2 Total RNA extraction from sago palm leaf 39

2.2.3 RNA sequencing 41

2.2.4 Read mapping and quantification 41

2.2.5 Differentially Expressed Genes (DEGs) analysis 42

2.2.6 Identification and functional association of frequently shared DEGs 42

2.2.7 Identification of transcription factors 43

2.2.8 Synthesis of cDNA for RT-qPCR 43

2.2.9 Primer design for gene expression validation 44

2.2.10 RT-qPCR protocol 46

2.3 Results 47

2.3.1 Qualitative and Quantitative Analyses of RNA 47

2.3.2 Pre-processed RNA-seq data 51

2.3.3 Differential gene expression analysis 54

2.3.4 DEGs enrichment analysis 59

2.3.5 PPI network analysis of DEGs 66

2.3.6 Transcription factors 68

2.3.7 Validation of DEGs 68

2.4 Discussion 70

2.4.1 Gene Ontology Terms of Upregulated DEGs 70

2.4.2 Downregulated KEGG pathways involved in reduced lignin and flavonoids biosynthesis 82

2.4.3 MCODE of PPI network 86

2.4.4 Expression of transcription factors in sago palm leaves 88

2.5 Conclusion 97

CHAPTER 3: MICROBIAL AND PHYSICOCHEMICAL PROPERTIES IN SAGO PALMS GROWN IN PEAT SOILS 99

3.1 Introduction 99

3.1.1 Soil characteristics influences sago palm growth 99

3.1.2 Studies on peat soil microbial communities 100

3.1.3 Research Objectives and Hypothesis 102

3.2 Materials and Methods 103

3.2.1 Soil collection 103

3.2.2 Soil physicochemical analysis 105

3.2.2.1 Sample preparation 105

3.2.2.2 pH and electrical conductance (EC) 105

3.2.2.3 Soil bulk density 105

3.2.2.4 Available phosphorus content 106

3.2.2.5 Total nitrogen content 106

3.2.2.6 Total organic carbon content quantification 106

3.2.2.7 Cation Exchange Capacity (CEC) and exchangeable cations 107

3.2.2.8 Total boron (TB) 107

3.2.3 Soil amplicon study 107

3.2.3.1 Extraction of genomic DNA from soil samples 108

3.2.3.2 Sequencing pre-processing and statistical analysis 108

3.3 Results 110

3.3.1 Soil physicochemical properties 110

3.3.2 Amplicon dataset from trunking and non-trunking sago palm soils 114

3.3.3 Microbial composition in soil samples 115

3.3.4 Microbial diversities in sago palm soils 121

3.4 Discussion 125

3.4.1 Peat physicochemical characteristics in studied soil samples 125

3.4.2 Dominant microbial functions in sago palm plantation peat soils 129

3.4.3 Differences microbial relative abundance in soil samples 132

3.4.4 Microbial decomposition, nutrient cycling, and detoxification supporting trunk formation in sago palms 136

3.5 Conclusion 138

CHAPTER 4: GENERAL DISCUSSION AND CONCLUSION 139

4.1 Overview and Research Integration 139

4.2 Molecular Mechanisms Driving Trunk Formation in Sago Palms 140

4.2.1 RNA editing, transcript integrity, and hormonal crosstalk for stress resilience in trunking sago palms 140

4.2.2 Metabolic reprogramming and auxin-mediated regulation for trunk formation 142

4.2.3 Vacuolar Pi mobilisation and cytokinin-ABA regulation supporting palm trunk formation 144

4.3 Soil Nutrient and Microbial Contribution to Trunk Formation 145

4.3.1 Synergistic regulation of macronutrient N and P in regulating balanced growth and development 145

4.3.2 Plant-soil-microbe shaping hormone networks 147

4.4 Conclusion 150

4.5 Limitations and Future Recommendations 150

4.6 Recommendations to Sago Palms Plantation Management 152

REFERENCES 155

APPENDICES 220

LIST OF TABLES

		Page
Table 1.1	Previous omics technologies applied to study DEGs in non-trunking *Metroxylon sagu*	17
Table 2.1	Omics technologies adapted to elucidate cellular systems in plants	24
Table 2.2	The normalisation methods and its normalisation approaches	27
Table 2.3	Popular DGE tools for differentially expressed genes identification	29
Table 2.4	The advantages and disadvantages of popular pathway enrichment analysis tools	32
Table 2.5	Global positioning system (GPS) of each sample collection	39
Table 2.6	Chemical utilised in the preparation of 2% CTAB Miniprep Extraction buffer	40
Table 2.7	Buffers required in the synthesis of cDNA	44
Table 2.8	List of designed primers used in RT-qPCR targeting the upregulated and downregulated DEGs	45
Table 2.9	The quality and integrity of extracted RNA from sago leaf in average ± SD	47
Table 2.10	Integrity and yields of total RNA extracted from *M. sagu* leaf	49
Table 2.11	Summary of clean dataset and read alignment to the reference genome	52
Table 3.1	Peat physicochemical properties of collected soil samples from trunking and non-trunking sago palm plots	111
Table 3.2	Alpha diversity matrices from trunking and non-trunking soil samples	121

LIST OF FIGURES

Page

Figure 1.1 Illustration of *Metroxylon sagu* Rottb. A) Line drawing illstration flowering palm with suckers (1) stem or trunk with upper part covered with leaf bases (2) sago trunk (3) first oder of inflorescence branch (4) sago fruits. B) Detail picture of sago fruits. Source: *Metroxylon sagu* (Sago Palm, 2022) 3

Figure 1.2 Illustration of *Metroxylon sago* Rottb. growth according to local growth representation starting at *Pelawei*, *Pelawei manit*, *Bubul*, *Angau muda*, and *Angau tua* (Source: Flach, 1997) 6

Figure 1.3 The sago starch export overseas from Sarawak. A) Export distribution of sago starch to overseas. B) Sarawak sago starch export value between 2006 and 2024. Source: Sago starch 10 years performance in Sarawak Data Offical Portal. Assessed on 26 May 2025 10

Figure 1.4 Inverted saucer of peat dome. Source: Melling et al. (2007) 12

Figure 1.5 Comparison between A) trunking and B) non-trunking sago palm phenotypes. The normal plant exhibit taller with well-developed trunk. In contrast, the non-trunking sago palm appears to be at 'Sulur' growth stage, producing leaves and fronds with no stem development despite 29 years after planting 15

Figure 2.1 The standard workflow to process RNA-seq data following obtaining raw data in FASTQ files. The workflow shows three main procedures including raw gene expression quantification, differential gene expression, and pathway enrichment analysis. 34

Figure 2.2 RNA bands resolved under 1% TBE agarose gel stained using safe staining dye GelRed. M represents the 1 kb DNA ladder. Lanes 1-4, 5-8, 9-12, represents RNA extracted from Dalat, SgTalau, and PPaloh sago palm leaf, respectively 48

Figure 2.3 Principal Component Analysis (PCA) of trunking versus non-trunking sago palms across three locations A) Dalat vs NT; B) SgTalau vs NT; C) PPaloh vs NT show distinct clustering of samples demonstrating consistent transcriptional separation between two phenotypes. Note that NT refers to non-trunking of which the datasets were retrieved from NCBI Bioproject: PRJNA781491 53

Figure 2.4 Bar plot representing DEGs at log2 fold change of upregulated and downregulated genes in leaf transcriptome of each comparative sets against non-trunking sago palms 54

Figure 2.5 Volcano plot showing DEGs between trunking (T) and non-trunking (NT) for Dalat, PPaloh, and SgTalau sago palm plantations, with significantly up- and down-regulated genes highlighted in red. The red dots indicate significant differentially expressed transcripts ($p < 0.05$), while black dots represent transcripts without statistical significance ($p > 0.05$) 56

Figure 2.6 Venn diagram presenting the number of unique and overlapping genes among the three sampling locations Dalat (blue), SgTalau (yellow), and PPaloh (green) with overlapping regions indicating common DEGs expressed at two or all three sites 58

Figure 2.7 Gene ontology enrichment bubble plot of upregulated shared DEGs genes showing significantly enriched biological process, cellular component, and molecular function categories, with dot size indicating gene counts and colour representing adjusted *p*-values ($-\log_{10}$) 61

Figure 2.8 Gene ontology enrichment bubble plot of downregulated shared DEGs genes showing significantly enriched biological process, cellular component, and molecular function categories, with dot size indicating gene counts and colour representing adjusted *p*-values ($-\log_{10}$) 62

Figure 2.9 Bubble plot of downregulated shared DEGs genes showing significantly enriched KEGG pathways with dot size indicating gene counts and colour representing adjusted *p*-values ($-\log_{10}$) 63

Figure 2.10 Functional enrichment analyses of upregulated and downregulated common DEGs in trunking sagu palms from different locations. A) Heatmap of enriched terms across upregulated DEGs. B) Heatmap of top 20 enriched terms across downregulated DEGs. Bar plot are coloured based on *p*-values. The darker the shades the more significant the expression level 65

Figure 2.11 Interactome network and MCODE of A) 107 upregulated DEGs and B) 486 downregulated DEGs. Note that in the interactome network, the MCDOE complexes are coloured according to their identities 67

Figure 2.12 Validation of RNA-seq results by qPCR for four selected genes across Dalat, PPaloh, and SgTalau, showing A) $\log_2$ RT-qPCR ddct values and B) corresponding $\log_2$ RNA seq values with error bars indicating standard deviations 69

Figure 3.1 Soil collection were conducted at Block 3 and 5 indicated by yellow frame. Green field represents sago palm plantation. Source: Land Custody and Development Authority (LCDA) 104

Figure 3.2 Relative abundance of bacterial phyla in trunking (TP1-TP5) and non-trunking (NTP1-NTP5) sago palm soils, showing Acidobacteria, Proteobacteria, Actinobacteria, and Verrucomicrobiota dominate

across all samples, with minor contributions from multiple low-abundance phyla. Colour-coded bar plot shows the percentage of the major top 10 bacterial phyla. The y-axis represents the classification level of phyla, and the x-axis represents biological replicates 116

Figure 3.3 Differential relative abundance of key bacterial phyla (Nitrospirota, Desulfobacterota, WPS-2, Dependentiae, and Actinobacteria) in the soils of trunking and non-trunking sago palms with significance levels indicated as $p < 0.05$ (*), $p < 0.01$ (**), $p < 0.001$ (***) 117

Figure 3.4 Relative abundance of fungal phyla in trunking (TP1-TP5) and non-trunking (NTP1-NTP5) sago palm soils, showing Ascomycota, Mucoromycota, Basidiomycota, and Mortierellomycota dominate across all samples, with minor contributions from multiple low-abundance phyla. Colour-coded bar plot shows the percentage of the major top 10 fungal phyla. The y-axis represents the classification level of phyla, and the x-axis represents biological replicates 119

Figure 3.5 Differential relative abundance of key fungal phyla (Calcarisporiellomycota, Monoblepharomycota, Mortierellomycota, Chytridiomycota, and Glomeromycota) in the soils of trunking and non-trunking sago palms with significance levels indicated as $p < 0.05$ (*), $p < 0.01$ (**), $p < 0.001$ (***) 120

Figure 3.6 Alpha-diversity of the soil microbial community A) 16S and B) ITS of Chao1 and Shannon-relative abundance of microbial in trunking and non-trunking sago palm soils. No significant differences were detected, indicating that overall microbial richness and evenness are not the main drivers of trunking differences 122

Figure 3.7 Principal coordinates analysis (PCoA) based on Bray-Curtis distance showing differences in soil microbial community structure between trunking and non-trunking sago palms for A) bacteria and B) archaea, with clear separation of samples along the first two axes 124

LIST OF ABBREVIATIONS

2-DE	Two-dimensional electrophoresis
ABA	Abscisic acid
AMF	Arbuscular mycorrhizal fungi
AMF	Arbuscular Mycorrhizal Fungi
ANOSIM	Analysis of Similarity
AP	Available phosphorus
ASV	Amplicon Sequence Variant
ATL	ARABISOPSIS TÓXICOS EN LEVADURA
B	Boron
Bcc	*Burkholderia cepacia* complex
BD	Bulk density
BLASTp	Protein Basic Local Alignment Search Tool
BP	Biological Process
BWA	Burrows Wheeler Aligner
$CaCl_2$	calcium chloride
CC	Cellular Component
cDNA	Complementary deoxyribonucleic acid
CDs	Carbon nanodots
CEC	Cation Exchange Capacity
CTAB	hexadecyltrimethylammonium bromide
DAVID	Database for Annotation, Visualisation, and Integrated Discovery
ddPCR	Droplet digital PCR

DEGs	Differentially Expressed Genes
DGE	Differential Genes Expression
DNA	Deoxyribonucleic acid
EC	Electrical Conductance
EDTA	ethylenediaminetetraacetic acid
FDR	False Discovery Rate
Gb	Gigabyte
GC	Guanine-cytosine
GC-MS	Gas Chromatography-Mass Spectrometry
GHC	Greenhouse gases
GO	Gene Ontology
GSEA	Gene Set Enrichment Analysis
HCl	hydrochloric acid
IAA	Indole-3-acetic acid
$InsP_6$	Inositol hexaphosphate
iTAK	Plant Transcription factor and Protein Kinase Identifier and Classifier
K	Potassium
KEGG	Kyoto Encyclopedia of Genes and Genomes
L2FC	log_2 fold change
M	Millions
M. sagu	*Metroxylon sagu*

MALDI-TOF MS	Matrix-assisted laser desorption/ionisation time-of-flight mass spectrometry
MCODE	Molecular Complex Detection
MF	Molecular Function
$MgSO_4$	magnesium sulphate
miRNA	microRNA
mRNA	Messenger RNA
MSL	Mean sea level
N	nitrogen
NCBI	National Center for Biotechnology Information
NGS	Next Generation Sequencing
NMR	Nuclear Magnetic Resonance
Nr	Non-redundant
NT	Non-trunking
P	Phosphorus
padj	*p*-value adjusted
PCA	Principal Component Analysis
PCBs	Polychlorinated biphenyls
PCR	Polymerase Chain Reaction
PE	Paired-end
PGPR	Plant growth-promoting rhizobacteria
PGPR	Plant Growth-Promoting Rhizobacteria
PPaloh	Paya Paloh
PPI	Protein-protein Interaction

PVP	polyvinylpyrrolidone
RDA	Representational Differeces Analysis
RIN	RNA Integrity Number
RIN	RNA Integrity Number
RING	Really Interesting New Gene
RNA	Ribonucleic acid
RNA-seq	RNA-sequencing
rRNA	Ribosomal RNA
RT-qPCR	Reverse transcription-quantitative PCR
SD	Standard Deviation
SgTalau	Sungai Talau
SRA	Sequence Read Archives
SRB	Sulphate-reducing bacteria
STRING	Search Tool for the Retrieval of Interacting Genes/Proteins
STRS	Sungai Talau Research Station
TB	Total Boron
TFs	Transcription factors
TN	Total Nitrogen
UPS	Ubiquitin Proteasome System
UTR	Untranslated region

CHAPTER 1

GENERAL INTRODUCTION

1.1 Introduction

The sago palm (*Metroxylon sagu* Rottb.) is an indigenous palm to Southeast Asia. The starch-producing plant is experiencing increased in demand due to its versatile applications in the food and industrial sectors (Zhu, 2019). The global sago starch market revenue is projected to reached USD 5576.13 million by 2031. Sago starch which derived from the pith sought after in countries like Japan and Taiwan for its superior gelatinisation behaviour and gluten-free properties, appealing to health-conscious consumers (Thompson et al., 2023). Its increasing integration into bio-based material production aligns with the global move towards sustainable, eco-friendly materials, as industries explore sago starch as a renewable resource to reduce reliance on petroleum-based plastics (Afiq & Azura, 2013; Beg et al., 2016). Countries like Malaysia and Indonesia are positioned to dominate the sago starch market due to their abundance of sago palm stands and plantations (Ellen, 2006). Sago palms thrive in both arable and marginal lands, making them suitable for cultivation in areas like Sarawak where peatlands dominate the land area. This prompts the Sarawak government to initiate commercial sago palm plantation to boost economic growth and become a leading world sago starch exporter. Sago is a promising crop to supplement other starch-producing crops due to its high adaptability, minimal maintenance requirements, and high starch yield.

1.2 Taxonomy and Botanical Description of *Metroxylon sagu*

Sago palm (*Metroxylon sagu* Rottb.) is a soboliferous (clustering), hapaxanthic perennial plant commonly found in tropical countries. The palm belongs to the family Palmae Jussieu, subfamily Calamoideae Griffith, tribe Calameae Drude, subtribe Metroxylinae Blume and genus *Metroxylon* Rottboell (Flach, 1997). Initially, Sarkar (1970 cited in Flach, 1997) denoted chromosome number of *M. sagu* as n = 16. However, Verhaar (1976) established chromosome number as n = 13 and was verified by Rauwerdink (1984) through his examination on plants collected in Papua New Guinea. Beccari (1918) and Rauwerdink (1986) both studied genus *Metroxylon*. Beccari classification of the palm based on fruits and leaves parts distinguished nine species of *Metroxylon* and division of genus into subgroups: *Coelococcus* and *Eumetroxylon* based on the number of rows on the sago fruit. Rauwerdink (1986) on the other hand, reported that the number of scales on fruit samples were caused by variation which later proven by Boonsermsuk et al. (1997). Rauwerdink simplicity in genus classification is more straightforward where he classified five species under genus *Metroxylon* namely, *M. sagu* Rottb., *M. warburgii* Heim, *M. vitiense* Benth et Hook, *M. amicarum* Becc., *M. salomonense* Becc. (Flach, 1997; Ellen, 2006).

Sago palm is scientifically known as *Metroxylon sagu* Rottb., which derives from the word *meta* (pith or parenchyma), and *xylon* (xylem storing starch in central parenchyma) (Singhal et al., 2008). A healthy palm can grow its trunk up to 35-60 cm in diameter and reaches 6-16 metres tall. *M. sagu* is the only palm that is soboliferous (produce suckers) among of all the genus *Metroxylon* palms. Once planted, a cluster of succession suckers grow at the bottom of the mature/mother palm trunk composed of various growth stages. Towards reaching the end lifecycle, the palm grows branched terminal inflorescence with flowers

which later developed into sago fruits; a condition known as hapaxanthic. Figure 1.1 illustrates the *M*. *sagu* palm and its fruit.

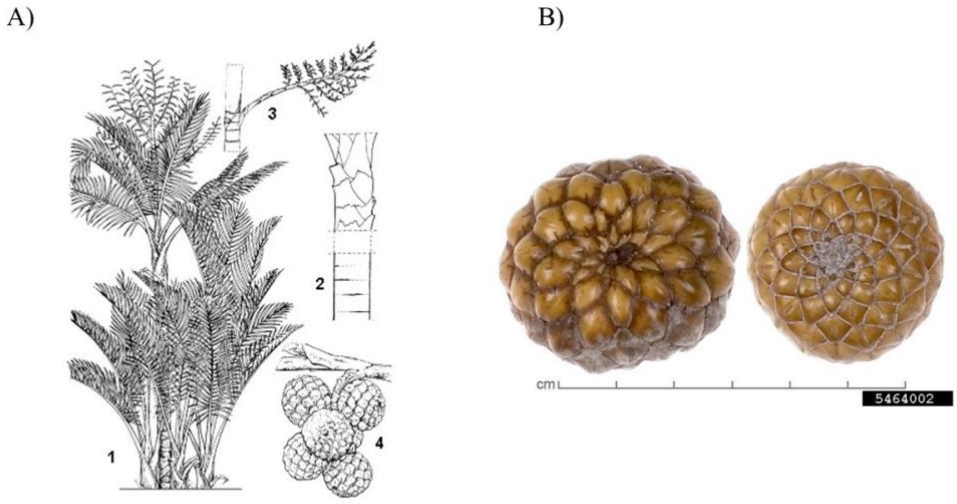

Figure 1.1: Illustration of *Metroxylon sagu* Rottb. A) Line drawing illstration flowering palm with suckers (1) stem or trunk with upper part covered with leaf bases (2) sago trunk (3) first oder of inflorescence branch (4) sago fruits. B) Detail picture of sago fruits. Source: *Metroxylon sagu* (Sago Palm, 2022)

1.3 The Centre of Diversity and Sago Distribution in the World

Sago palms are naturally found in the humid tropics of Southeast Asia, including Indonesia, Malaysia, Thailand, and Philippines, as well as northwestern Melanesia, which includes Papua New Guinea and the Solomon Islands (Ehara et al., 2021). Possesses high adaptability to hardy environments enable them to thrive well in numerous environments such as high-water table areas (Sato et al., 1979; Flach & Schuiling, 1988; Jong, 1995), marginal soils (Flach, 1997; Yamamoto et al., 2010; Ehara, 2015, Okazaki & Sasaki, 2018) and upland areas at 700 m elevation. Flach (1997) estimated an approximate 5-6 million ha of sago resource worldwide. The New Guinea island is recognised as the sago palm centre of diversity due to their vast natural sago forest and high genetic variation reported in the areas (Beccari, 1918; Flach, 1997). The sago palm is native to Indonesia and Malaysia. Given the importance of the palm to provide subsistence and emergency food to the locals especially during famine, the palms were actively distributed to nearby islands such as Samoa, Rotuma, and Tonga as early as before the pre-European times (Barrau, 1959). In Sarawak, sago palms hold deep cultural and social significance. The sago starch is traditionally prepared into *linut*, a starchy paste consumed as a staple food like rice. Beyond its dietary role, the palm itself is revered as a symbol of resilience and continuity within local communities reflecting both its ecological adaptability to marginal soils and its enduring presence in community traditions (Toyoda, 2018). The condition of sago forest varies in each country. The sago forest in Indonesia and Papua New Guinea are mostly wild stands/natural, whereas, in other countries such as Thailand, Malaysia, and Philippines, the sago forests are semi-wild/ semi-natural. Semi-wild is the condition after land clearing and sago palm planting, the sago palm area was left with minimal care (no pruning or land

clearing, no fertilizer application) with periodic sucker control leaving the sago palm stand almost resembling to a wild stand (Yamamoto et al., 2003).

1.4 *Metroxylon sagu* Growth Stages

The planting of sago palm is either through the suckers or sago fruits. The common practice by sago palm planters is propagation via suckers (Nakamura, 2018). The propagation through suckers found to have shorter growth duration and uniform sago palm variety as opposed to propagation via sago fruit (Flach, 1997; Ehara et al., 2006). The growth of sago palms is only observable after the first 4-5 years sucker transplant where the stem of the transplanted sucker elongates horizontally and produce leaves along with apparent increase in leaves and stem size. This growth stage is known as the rosette stage. After the rosette stage, the stem elongates from the horizontal direction to the vertical direction to form trunk, observed to be swelling up at the bottom part with leaves attached. Further, the stem elongates vertically, with gradual increase in stem size over time. The trunk is fallen for starch harvesting after flowering and immediately before fruiting due to starch amount rapidly decreases thereafter the development of inflorescence and fruit (Singhal et al., 2008). Normally, the maturity period of sago palm is estimated to be 9 to 12 years however, the period for sago starch harvest differs by the regions, varieties, and the palm rate of growth (Yatsugi, 1986; Flach & Schuiling, 1989). Therefore, the proper indicator to harvest the maximum amount of sago starch is vital to harvest the maximum sago starch. In Sarawak, the sago farmers come up with different approach to evaluate the sago palm growth stages. They described five growth stages of sago palm growth development starting with *Pelawei*, *Pelawei Manit*, *Bubul*, *Angau muda*, and *Angau Tua*. Each of the growth stages has its own trunk growth duration. According to the local, *Angau muda* growth stage is the best growth stage to harvest the sago starch as the starch content is at the maximum before the palm

enters *Angau tua* growth stage. Following *Angau muda*, the starch content decline rapidly to support for flower initiation and sago fruits formation and enter death phase, *Mugun* (Jong, 1995). Figure 1.2 illustrates the sago palm growth stage according to the local representation.

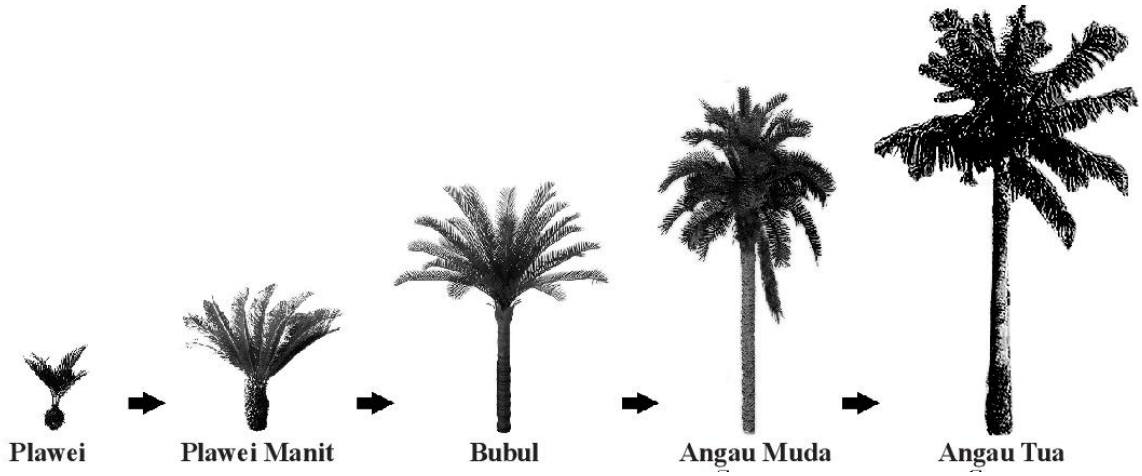

Figure 1.2: Illustration of *Metroxylon sago* Rottb. growth according to local growth representation starting at *Pelawei*, *Pelawei manit*, *Bubul*, *Angau muda*, and *Angau tua* (Source: Flach, 1997)

1.5 The Importance of Sago Palm to Mankind

Sago palm offers several products to the locals and the industry. The starch extracted from the sago palm pith has been the staple food to the locals in New Guinea, Maluku, and other areas in Melanesia (Nishimura, 2018). The sago mills converted raw sago starch into two varieties of sago starch products, namely *lemantak* (wet sago flour) and sago flour (dry crude starch). *Lemantak* is commonly produced for the local market, while sago flour is intended for export purposes (Singhal et al., 2008). In the past, sago starch was considered as poor man crop. Presently, there has been growing interest in sago starch in food industry and industrial applications thanks to their hardy characteristics against adverse environmental conditions and high starch productivity (Ehara et al., 2018). Each sago palm trunk can potentially yield up to 400 kg of dry starch. This output is six times greater than that of rice and wheat and ten times greater than potato and cassava (Bujang, 2018). The

advantage suggested sago palm as the starch crop of the century, in the event of crop failure (Karim et al., 2008).

Traditionally, sago starch is often used in the preparation of cottage delicacies such congee-based products such as *kurupun* or *papeda* and confectionary products such as sago pearls, sago cookies, and baked crackers (Hirao et al., 2018; Konuma, 2018). Physicochemical testing on gelatinisation and retrogradation properties of sago starch found superior quality of sago starch in gelatinization and retrogradation properties compared to potato, cassava, rice, and maize starches thanks to the highly branched and longer internal chain length of sago amylopectin than that of A-type starch (Vamadevan et al., 2018). This is reflected in the rheological properties of rice porridge. The porridge with sago starch as thickener gave higher viscosity and elasticity than porridge with cassava starch. It has also been suggested that sago starch has potential to aid people with dysphagia (Syahariza & Yong, 2017), and can act as prebiotics to stimulates the growth of gut microbiota particularly *Bifidobacterium* spp. and *Lactobacillus* spp. (Thompson et al., 2023).

Like other native starches, sago starch undergoes several modifications to boost their functionalities. The modifications applied enables sago starch to be use not only in food industries but also in non-food applications (Zhu, 2019). Studies by Afiq and Azura (2013) and Beg et al. (2016), found that incorporating either native or modified sago starch in the manufacturing of composite films resulted in a significant increase in the tear strength of rubber latex-based composite films and plastics-based composite films. In addition, the addition of sago starch in rubber and plastics formulations significantly increase the degradation rate of these materials. Moreover, sago starch is also actively included in the manufacturing of carbon nanodots (CDs). This fluorescent probe is commonly used in chemical and biological analytes tracing and as photocatalysts for harnessing solar energy

(Chauhan et al., 2022). These studies could have important implications for the development of more durable long-lasting products and environmentally friendly materials in the future (Mohamed et al., 2018). The sago starch is also important in pharmaceutical and medical applications. For example, pre-gelatinised sago starch is included in the formulation of drug-control release tablets (Widodo & Hassan, 2015) and hydrogels capsules to encapsulate drugs assisted in targeted therapy for colon (colonic) and eye (ocular) cancer treatments (Tan et al., 2016). In one study, sago starch and soya protein were cross-linked to make composite films for wound dressing. The study showed that the film exhibited good water vapour permeability and mechanical properties, making them suitable for wound dressing applications (Ramnath et al., 2012).

The sago starch in both native and modified forms, has the potential to be used in various applications and can perform as well as other industrially important starches such as maize, potato, and cassava starches (Zhu, 2019). It is recommended that more initiative should be taken to increase sago starch application in industries. Apart from offering cheaper and higher starch supply, sago palm tree is environmentally sustainable. Given the global concern over climate change, sago palm forests are reported to be better at carbon absorption with (28 MT CO_2 ha^{-1}) and sequestration with (8.3 MT ha^{-1}) annually (Bintoro et al., 2018). Additionally, sago palms are indigenous to Southeast Asia hence, the introduction of sago palm plantations in these areas certainly help to boost the economy of the locals without any disturbances to native plants.

1.6 Sago Industry in Sarawak

In the mid-1980s, the world first large-scale sago plantation was commenced by the Land Custody and Development Authority of Sarawak in Mukah division (Mukah Sago Plantation) and Dalat (Dalat Plantation) (Kueh et al., 1991; Chew et al., 1999) and later

further developed in Matu and Daro totalling 67,957 hectares of land including 43,426 hectares was planted by small-scales planter and the remaining 24,531 hectares was planted by commercial sago plantations (Mohamad Naim et al., 2016). New sago planting areas launched in 2016 have expanded cultivation area to 51,518 hectares aiming for 50, 000 metric tonnes of sago starch exports annually (Ehara et al., 2021). Albeit only cultivated in small land areas, Sarawak is the world major sago starch exporter despite vast sago stands in Indonesia. High export revenue of the sago starch especially to Japan made sago starch the fourth most important economic product after oil palm, pepper, and rubber (Ming et al., 2018; Trisia et al., 2020). Figure 1.3 illustrates the export value of sago starch from Sarawak.

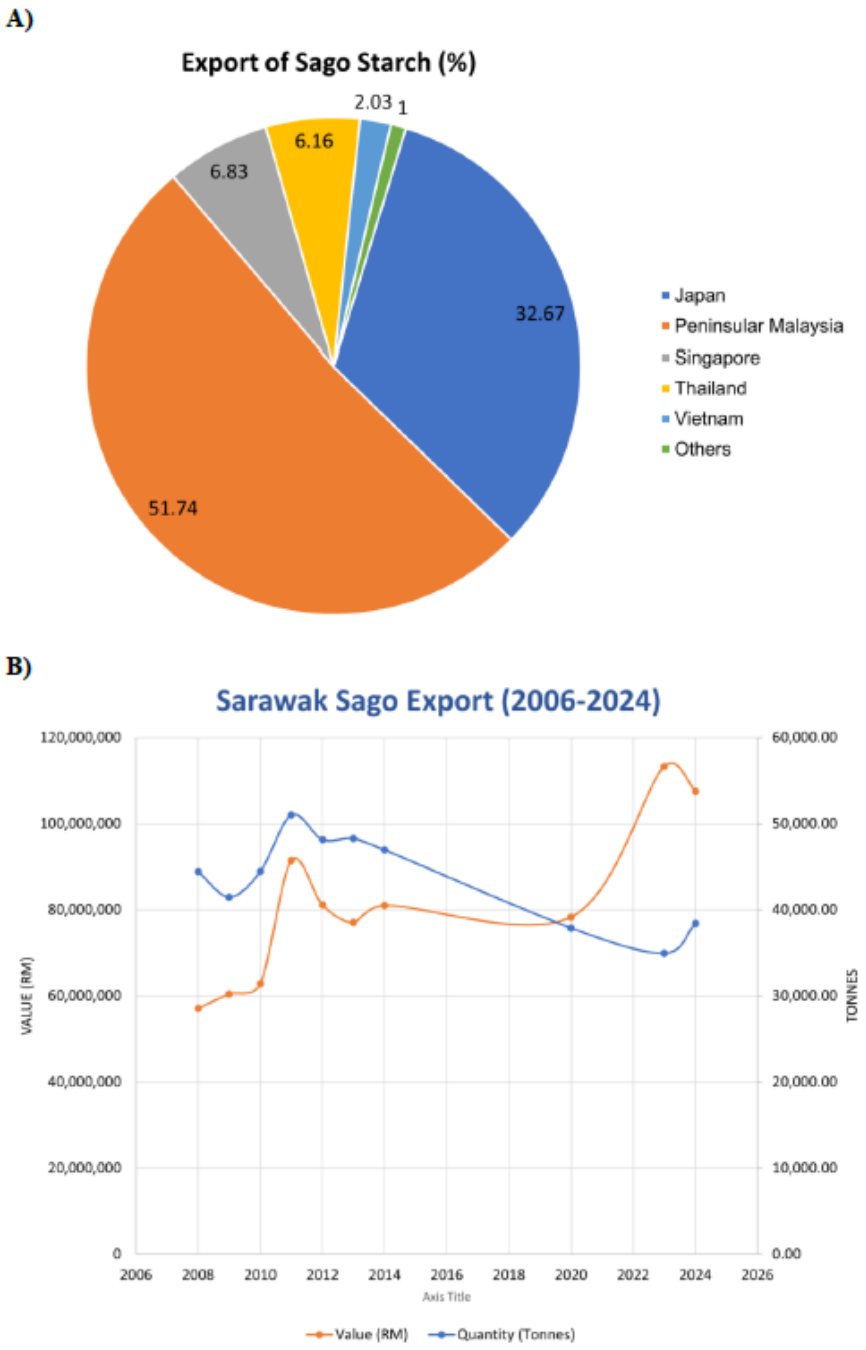

Figure 1.3: The sago starch export overseas from Sarawak. A) Export distribution of sago starch to overseas. B) Sarawak sago starch export value between 2006 and 2024. Source: Sago starch 10 years performance in Sarawak Data Offical Portal. Assessed on 26 May 2025

1.7 Tropical Peatlands Characteristics

The Sarawak land condition is distinct from that of Peninsular Malaysia. Out of the 2.6 million hectares of peatlands in Malaysia, 1.6 million hectares are in Sarawak which covering 13% of the total land area (Melling, 2016). The peatlands refer to a subset of wetlands that accumulate significant amount of soil organic matter over time (Lourenco et al., 2023). Peatlands are estimated to cover between 8% and 12% of the Earth's land surface and are found in boreal and temperate regions of the Northern Hemisphere, as well as in tropical areas (Xu et al., 2018). Unlike their boreal and temperate counterparts, tropical peatland forests are unique as they offer dual ecosystems of rainforest and peatlands (Arabia et al., 2020). The largest tropical peatlands are in Peru, South America, the Congo basin, Indonesia and Malaysia (Cole et al., 2022). These ecosystems are crucial in maintaining ecological balance by providing habitats for diverse species and acting as natural barriers that protect agricultural lands from saline water intrusion and flooding (Murdiyarso et al., 2019).

Studies of tropical peatlands in Sarawak were conducted at the Maludam National Park, Loagan Bunut National Park and several sago palm plantations in Mukah and Dalat. They described the peatlands are shaped like an inverted saucer with a prominent dome shape with shallower peat depth near the river mouths and increases inland at the peat dome centre along with irregular surface of mineral substratum (Melling, 2016). Figure 1.4 illustrates the inverted saucer shape of the peat dome.

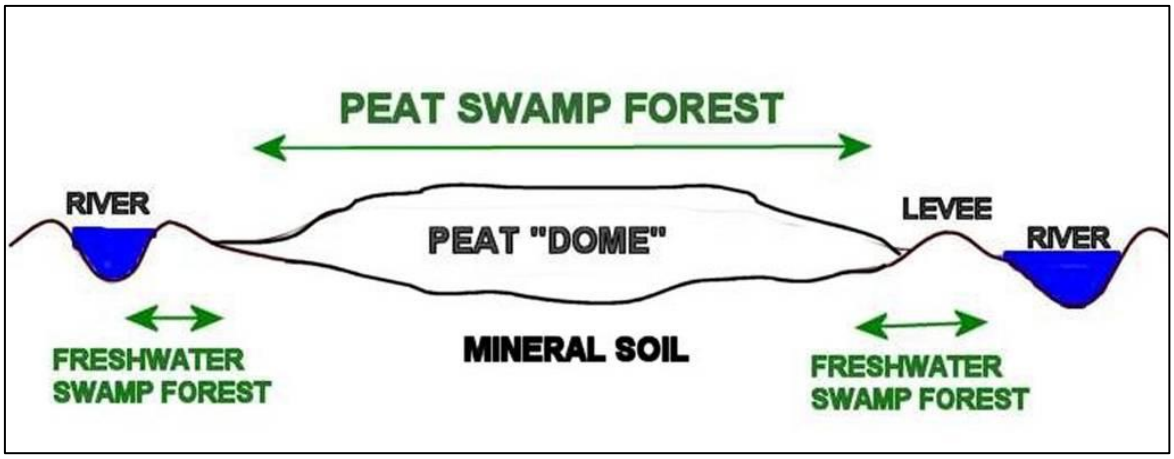

Figure 1.4: Inverted saucer of peat dome. Source: Melling et al. (2007)

1.8 Peat Soil Characteristics

Peatlands are characterised by high acidity with pH less than 4 (pH < 4), and low bulk density due to the high organic matter content. The soil in these areas is nutrient-deficient, which can limit the growth of most plants. Additionally, peatlands often have a high-water table, resulting in waterlogged conditions. These characteristics make peatlands less suitable for the cultivation of most plants. Draining is considered the most suitable method for making peatlands suitable for agriculture. However, this disturbance impacts the water table in peat domes, as this method releases broad range of greenhouse gases (GHC) and is detrimental to the environments (Jayarathne et al., 2018). Careful selection of crops planted on peatlands based on several key parameters including high yields and revenue generation, attractive for investment, less GHC emissions, and lower peat fire possibility (Applegate et al., 2022).

Sago palm is worthy of attention to be planted in peat soil. Sago palm is hardy and has a vast existence in the wetlands of Sarawak. This set off the initiation of Sarawak government to cultivate sago palms in peat soils along with grey soil, and acid sulphate soil to boost the agriculture economics of the state (Ehara et al., 2018).

1.9 Non-Trunking Occurrences Affects the Sago Palm Productivity

Depicted as the true palm, sago palm stores vast starch in the pith of the trunk. As the tree matures, it accumulates starch from the base upward until fully saturated up almost to the crown when reaching maturity (Karim et al., 2008). The productivity of sago palm per hectare land area is varied. Ruddle (2010) reported the amount of harvestable sago palm per hectare land area yearly can vary between seven to 330 sago palms. In Sarawak, a clump density of 590 sago palms/acre or 1480 sago palms/ha can produce up to 125 -140 palms/year, estimating 15 – 25 tons/ha of dry sago starch yearly (Ishizaki, 1997; Abd-Aziz, 2002).

The sago palm growth and starch production are highly dependent on the environmental conditions it grows. Previous studies have reported that starch yield in sago palm does not differ significantly among soil types, but palms cultivated on deep peat soils require a longer maturation period to achieve maximum starch accumulation (Yamamoto et al., 2003). Similar observations have been documented in earlier works, which consistently highlight the extended maturation requirement of sago palms in peat environments (Sim & Ahmed, 1978; Jong & Flach, 1995; Kaneko et al., 1996). Conversely, the delay growth rate is not applicable to sago palms grown on deep peat soil with peat thickness of more than 1.5 m. Instead, the sago palms appear stunted or described as non-trunking sago palms due to their inability to develop stem/trunk despite attaining 10-years growth cycle. This condition eliminates the economic value of the affected palms and further impacts the projected sago starch productivity. There was no study or data report conducted linking the decrease in sago starch productivity to this condition. However, it is understood that in the absence of sago stem development, starch accumulation does not occur. Hence, due to this, cultivation of

sago palm on deep peat soil is not economic and feasible (Ming et al., 2018). Figure 1.5 shows the non-trunking sago palm depicted as stunted and trunkless palm.

A)

B)

Figure 1.5: Comparison between A) trunking and B) non-trunking sago palm phenotypes. The normal plant exhibit taller with well-developed trunk. In contrast, the non-trunking sago palm appears to be at 'Sulur' growth stage, producing leaves and fronds with no stem development despite 29 years after planting

1.10 Previous Research Conducted Targeting the Sago Palm Growth Performance

The starch productivity of sago palm is highly correlated with its trunk diameter size and height (Ehara, 2009). Fertiliser application is crucial for enhanced growth to ensure sustainable production of sago palm. Research on fertiliser application effects on sago palm growth performance reported variable responses. Nitrogen-based fertiliser application studies reported small to no improvement toward sago palm growth (Watanabe, 2005). Meanwhile, Kimura et al. (2008) observed sago palm growth rate was slower when applied at high fertiliser rate (150 kg N/ha) and higher when applied at low fertiliser rate (50 kg N/ha) using slow-released fertiliser. The application of fertiliser using Phosphorus-32 (P-32) isotope dilution method on sago palms cultivated on deep peat soil (peat depth > 5 m) resulted in good vegetation during the first four years after planting. However, noticeable decline in palm growth was observed after the fifth year (Ming et al., 2018). The physicochemical studies conducted on deep peat soil (peat depth > 5 m) suggested nutrient deficit happens in the soil and confirming this soil type is not feasible for crop cultivation.

Despite numerous physiochemical studies conducted on sago palms, there is a huge gap in biological study related to the growth of sago palms. Efforts to decode responsible genes towards non-trunking sago palm phenotype is actively studied by Hussain and his colleagues using different omics approach. Several omics approaches used were metabolomics, proteomics, and genomics. Overall, the metabolites and proteins mostly expressed by the non-trunking sago palms are related to environmental stresses. Table 1.1 tabulates the past omics technologies conducted by Hussain to study the genes responsible for the non-trunking condition in sago palms.

Table 1.1: Previous omics technologies applied to study DEGs in non-trunking *Metroxylon sagu*

Omics Approach	Profiling Technology	Findings	Remarks	References
Metabolomics	NMR and GC-MS	Oils and waxes, haloalkanes, sulfite esters, phosphonates, phosphoric acid, thiophene ester, terpenes, and tocopherols were differentially expressed between trunking and non-trunking.	Highlight the presence of metabolites like acetyl-CoA, thiopenes, and tocopherol was due to environmental stress.	Hussain et al. (2020b)
Proteomics	2-DE with MALDI-ToF/ToF MS/MS	Found 865 protein spots from trunking and non-trunking. Nineteen significant proteins were found upregulated in the non-trunking. RubisCo, phosphoglycerate kinase (PGK), oxygen-evolving enhancer (OEE) proteins, carbonic anhydrase (CA), glutamine synthetase (GS), phosphoribulokinase, chloroplastic-like protein, malate dehydrogenase (MDH), and ascorbate peroxidase were among the proteins found significantly upregulated. Bioinformatics analysis described the upregulated proteins involved in photosynthesis, tricarboxylic acid cycle, glycolysis, carbon utilisation and oxidative stress metabolic pathways.	Non-trunking phenotype was caused by environmental stress and the upregulated proteins played crucial roles in the metabolism processes for palm survival.	Hussain et al. (2020a)

Table 1.1 continued

Genomics	Gene Fishing and RDA	**Gene Fishing** Nutrient-related regulations such as asparagine synthetase C (AsnC) and nonsymbiotic hemoglobin 1 (nsHb) were expressed higher in trunking and non-trunking, respectively. Transport-related proteins (ER-Golgi Soluble N-ethylmale-imide-sensitive factor-attachment Protein Receptors (SNARE) complex, TRX-m3, and peptide-2 ATP binding cassette (ABC) were expressed more in non-trunking whereas transport proteins sorting nexin (SNX), intracellular functions glucosyltransferase 2, inorganic phosphate transporter 3 (PHT3) and cobalt transport protein	Trunking sago palms has stronger defence against pathogen attacks and environmental stress as shown through higher expression of defence related and regulative proteins like beta-glucosidase and eIF-5A, respectively.	Hussain et al. (2022)

Table 1.1 continued

Genomics	Gene Fishing and RDA	**Gene Fishing** (CbiO) were found highly expressed in trunking palms. Defence mechanism proteins were also expressed in both palms. Enzymes O-antigen ligase and beta-glucosidase expressed higher in trunking whereas UDP-N-acetylmuramoyl-L-alanyl-D-glutamate lysine ligase (MurE) enzyme and mitogen-activated protein kinase (MAPK4), highly expressed in non-trunking. Eukaryotic translational initiator factor 5A (eIF-5A) complex expressed higher by 80% in trunking palms. **RDA** Eight and 16 DETs expressed differently in trunking and non-trunking, respectively DETs found in non-trunking are responsible in chemical defence, plant metabolism, signalling and salinity stress. DETs found in trunking responsible for plant growth, and stress tolerance with genes encode for neutralising imbalanced plant stress.	Non-trunking palms are nutritional challenged as denoted by expression of nsHb transcript.	Hussain et al. (2022)

Early gene expression studies that combined proteomics and metabolomics in non-trunking sago palms revealed elevated proteins and metabolites linked to stress tolerance, suggesting that these palms prioritise defence over growth. Moreover, the analytical approaches used, such as GeneFishing and representational differences analysis (RDA) by Hussain et al. (2022), were limited in scope as it covering only a narrow set of functionally expressed genes and is inefficient in pinpointing the precise responsible genes that causing differences in the phenotype of the palm. The significant gap remain in sago palm studies remain the lack in the identification of responsible genes that conveying the plant's morphology difference. Study on trunking sago palm is limited as this palm confers to the normal plant, thus scarce study was conducted targeting this plant phenotype. Therefore, the scarcity of gene expression studies in trunking sago palms leaves a significant gap in the literature especially regarding to the molecular basis of trunk formation, resource allocation, and developmental regulation.

It is hypothesised that trunking sago palms expresses a distinct set of regulatory mechanism that favours the resource allocation toward the growth of trunk, carbohydrate deposition, and vertical growth, while the non-trunking sago palms are inclined to defence-related mechanisms that suppresses their growth and trunk development. To test the hypothesis, the study combines transcriptome analysis with soil analyses, which includes physicochemical properties and microbial community composition. This study hope to uncover the gene expressed in trunking sago palms while examining soil characteristics and microbial interactions underpinning the plant growth. Such integrative approach will allow the identification of responsible genes, soil characteristics and microbial associations that defines trunk formation in trunking sago palms.

1.11 Aim and Objectives

This study aims to address the knowledge gaps related to the factors influencing *Metroxylon sagu* palm growth by integrating transcriptome from sago palm leaf tissue and soil analyses such as physicochemical properties and microbial taxonomy profiling. The general objective of this study are as follows:

i. To investigate the molecular and environmental factors associated with sago palm development through RNA sequencing of leaf tissues.
ii. To determine peat soil properties at sago palm plantation.
iii. To profile microbial taxonomy that present at the sago palm plantation.

The investigation of leaf transcriptome is presented in Chapter 2, while the investigation on environmental factors associated with sago palm growth is presented in Chapter 3 of this thesis. It is hoped that this integrative approach will provide valuable insight into the transcriptomics profile, soil characteristics, and microbial communities that may influence the sago palm growth.

1.12 Significance and novelty of Study

This study addresses the gap in understanding of the various factors influencing the growth of *M. sagu* palms by integrating molecular and environmental perspectives. Previous research has largely emphasised on agronomic practices such as fertiliser applications, with minimal incorporation of molecular biology approaches. By integrating transcriptomic analysis with soil physicochemical analysis and microbial community characterisation, this research bridges critical knowledge gaps for both the scientific and agricultural practitioners. Highlighting the fundamental purpose of comparing trunking and non-trunking sago palm traits is essential to elucidate developmental and molecular mechanisms of trunk formation,

while soil and microbial analyses will highlight environmental conditions that either support or hinder the palm development. This integrative approach offers scientific perspective to understand of the molecular regulations and environmental factors influencing sago palms performance. Identifying key soil properties and beneficial microbial taxa can inform land management strategies, including targeted fertilisation and bioaugmentation, ultimately improving yield and promoting sustainable cultivation in peatland ecosystems. In general, this research supports both scientific and agricultural communities toward sustainable and productive sago farming in marginal environments.

The novelty of this study lies in its integrative approach. This research is the first to combine transcriptomic profiling of trunking sago palms with soil physicochemical and microbial community analyses. While earlier studies have focused mainly on non-trunking palms and relied on limited gene expression methods, this research expands the scope to trunking sago palms, which represent the phenotype central to growth and productivity. By linking molecular regulation with environmental and microbiome influences, the study combine the view of genetic and environmental factors that has not been done before. This originality provides a new insight into genetic and ecological determinants of trunk formation in sago palms, offering a foundation for both scientific discovery and practical applications in sago palm cultivation.

CHAPTER 2

COMPARATIVE TRANSCRIPTOME ANALYSIS BETWEEN TRUNKING AND NON-TRUNKING *Metroxylon sagu*

2.1 Introduction

The era of sequencing holds promise in elucidating the basis of genetic traits that influence an organism's phenotypes in relation to its environment (Wang et al., 2023; Sheng et al., 2023). Plants are constantly challenged by a multitude of biotic and abiotic stresses in their environment. To survive, plants acquire sophisticated strategies by activating signal transduction pathways that triggers stress-responsive genes to produce necessary proteins. Plant resilience is crucial for achieving optimal crop productivity, as stress can significantly reduce plant yields. Elucidation of the molecular regulatory network and identification of the responsible adaptation genes are crucial for future crop enhancements (Derbyshire et al., 2022).

2.1.1 Omics technologies

Omics technologies have revolutionised the study of gene expression in plants. Aided with bioinformatics tools, these platforms enable researchers to gain insight into plant adaptation and responses, leading to more effective strategies to improve crop resilience (Mora-Poblete et al., 2023). Several omics approaches including genomics, transcriptomics, proteomics, and metabolomics, are commonly used to understand molecular biology behind plant systems. These technologies are instrumental in uncovering plant metabolic system by identifying candidate genes for crop improvement, and deepen our understanding of traits diversity of plant species. Table 2.1 tabulates several omics technologies adapted by researchers to elucidate cellular system in plants.

Table 2.1: Omics technologies adapted to elucidate cellular systems in plants

Omics	Description	Advantages	Disadvantages
Genomics	Is a systematic study of an organism nucleic acid. Provides information on an organism genetic sequence and variations (Song et al., 2023)	Enabled study of candidate genes and causal variations. Useful in revealing genetic variants, population structure, candidate genes for major economic traits, and molecular markers to accurately predict gene-to-phenotype association adding in the development of new plant traits (Bhat et al., 2020; Thudi et al., 2021)	Genomics only provide a partial view of the final products. The molecular interactions between expressed transcripts, enzyme reactions, and metabolites requires further studies (Zhang et al., 2018).
Transcriptomics	The study of transcripts that present in a cell or organisms (Guo et al., 2021).	Useful in measuring expressed genes, transcription factors associated to a certain condition/treatment. Aid in determining functions of previously unannotated genes (Tyagi et al., 2022).	RNA is sensitive to environment. Obtaining high quality RNA is crucial for RNA-sequencing (Sasi et al., 2023)
Proteomics	Study the characterisation of protein sequence that present in a cell at a particular point in time (Yan et al., 2022)	Useful in elucidating protein translated from transcriptomes, structures and protein-protein interaction (Alberton et al., 2020).	Protein is unable to be amplified like DNA thus showing relatively low sensitivity, requiring specific and expensive instruments. Proteomics cannot represent the whole genetic and chemical mechanisms (Smolikova et al., 2020)
Metabolomics	Study of global metabolite profiles in a system under certain condition (Yan et al., 2022)	Provides the final downstream product of gene transcription hence add additional layer of information to improve the accuracy of genomic prediction. The downstream product, metabolome provides more accurate result in leading to the specific phenotype of the studied organism. (Yan et al., 2022)	Plant metabolome database is relatively small (Li et al., 2022) Further investigation at upper biological level is required, as metabolic changes cannot be identified by metabolomics (Jiang et al., 2019)

2.1.2 Workflow for RNA-sequencing analysis

Transcripts identification and gene expression quantification are the distinct core activities in molecular biology. RNA-sequencing have made it possible to capture quantitative gene expression in an organism with high resolution and accuracy. The pervasive adoption of RNA-sequencing approach in life sciences has generated a large amount of data to the end user. For novice bioinformatician, the scale and complexity of these data can be undoubtedly be overwhelming. Through decades, there are many different computational algorithms and pipelines are introduced to analyse RNA-seq data and so far, there is no ultimate one approach to do it. Hence, it is important for the researcher to know the necessary workflow to analyse RNA-seq data.

Trimming of the raw data obtained following sequencing can increase the success rate to obtain meaningful differential gene expression (DGE) analysis. Trimming removes adapter sequences to remove poor quality sequences to increase sequence mapping rate to genome (Hu et al., 2021). Several trimming tools available are the Cutadapt (Martin, 2011), Trimmomatic (Bolger et al., 2014) and all-in-one fastp (Chen et al., 2018). The resultant clean reads will have to be aligned to a genome. This step maps the read sequence to selected organism genome refers as reference genome and determines the location of small sequence fragments align to the reference genome (Musich et al., 2021). Mapping tools such as Burrows Wheeler Aligner (BWA) (Li & Durbin, 2010), Bowtie2 (Langmead & Salzberg, 2012), STAR (Dobin et al., 2013), TopHat2 (Kim et al., 2013), MUMmer4 (Marçais et al., 2018), HISAT2 (Zhang et al., 2021) are the common mapping tools utilised by bioinformaticians to map read sequences to reference genome. However, in the case where available genome is absent, *de novo* approach is suggested. In this study, *de novo* is not presented as *Metroxylon sagu* genome is available. Following mapping, the counting of

reads that align to each gene known as gene quantification can be conducted using htseq-count (Anders et al., 2015). Normalisation is a vital step in data preprocessing prior to Differential Genes Expression (DGE) analysis. It adjusts the various factors that affect transcript quantification in RNA-seq data such as sequencing depth, transcript length, sample-to-sample and batch-to-batch variability to ensure reliable transcriptomic data (Abrams et al., 2019; Zhao et al., 2021). Table 2.2 tabulates common normalisation approach.

Table 2.2: The normalisation methods and its normalisation approaches

Normalisation	Description	Normalisation approach	Usage recommendation
CPM Counts per million	Counts scales by the total number of reads	Correct variations in library size only	Compare gene counts between replicates of the same sample group. Not suitable for within sample comparison
FPKM Fragments per kilobase of transcript per million fragments mapped **RPKM** Reads per kilobase of transcript per million reads mapped	Counts per length of transcript per million reads mapped	Correct variations in library size and gene length	Compare gene count between genes within a sample. Not suitable for comparisons between samples (Zhao et al., 2020)
TPM Transcripts per million	Counts per length of transcript per million reads mapped	Corrects RNA sequencing depth and gene length	Compares gene count within samples or between samples of the sample group. Comparison within samples requires normalisation within a dataset for between sample comparison (Zhao et al., 2020)
TMM Trimmed mean of M-values	Counts use a weighed trimmed mean of the log expression ratios between samples	Correct RNA sequencing depth	Compares gene count between and within samples
DESeq2 median of ratios	Counts divided by sample-specific size factors determined by median ratio of gene counts relative to geometric mean per gene	Correct RNA-sequencing depth and RNA composition	Compares gene counts between samples

Following the preprocessing steps, the resultant count matrix data is used for DGE analysis. For this purpose, many tools have been developed to facilitate the analysis to decipher lists of significant Differentially Expressed Genes (DEGs) in the experiment. Table 2.3 listed popular DGE tools by bioinformaticians to identify DEGs in a study.

Table 2.3: Popular DGE tools for differentially expressed genes identification

DGE tools	Distribution	Normalisation	Description	References
edgeR	Negative binomial	TMM	Empirical Bayes estimate and either a Fisher's exact test tailored to overdispersed data or a generalised linear model	Robinson et al. (2010)
baySeq	Negative binomial	Internal	Differential expression is empirically estimated using Bayesian statistics	Hardcastle & Kelly (2010)
EBSeq	Negative binomial	Deseq	Empirical Bayesian estimate of the posterior likelihood	Leng et al. (2013)
DESeq2	Negative binomial	Deseq	Shrinkage variance with variance-based and Cook's distance pre-filtering	Love et al. (2014)
NOIseq	Non-parametric	RPKM	Non-parametric test based on the signal-to-noise ratio	Tarazona et al. (2012)
SAMseq	Non-parametric	Internal	Mann-Whitney test with Poisson resampling	Li & Tibshirani (2013)
PoissonSeq	Poisson log-linear model	Internal	Score statistics	Li et al. (2012)
limma	Log-normal	TMM	Generalised linear model	Ritchie et al. (2015)
Sleuth	Linear model	TMM	Estimates inferential variance through kallisto quantification and bootstrap pseudo-alignment techniques	Pimentel et al. (2017)

Statistical significance cutoff selection is important for significant DEGs identification with biological significance and not simply random variation. The $\log_2$ fold change (l2FC), *p*-values and *p*-value adjusted (padj) with different correction techniques such False Discovery Rate (FDR), Bonferroni, and Benjamini-Horchberg are the common cutoff criteria in the selection of DEGs to provide reliable result and data interpretation (Liu et al., 2023). The choice of correction methods prevents false negatives whilst the l2FC can be used to rank gene differences between two experimental conditions. It is necessary to examine the distribution data and determine the appropriate threshold that reflects the biological significant variations and produce consistent and reproducible results (Rosati et al., 2024).

Once DEG analysis has been done, graphic representations such as MA plot, volcano plots, heatmaps and Venn's diagram is presented. From MA plots, it is not possible to identify significant genes as *p*-value is not evaluated meanwhile, volcano plots compare both padj and l2FC in examining differences in gene expression between two conditions. The points/genes located high on the y-axis and located far from the origin in both directions on x-axis are showing both significant and biologically relevant (McDermaid et al., 2019; Wodrich et al., 2021). The heatmaps and Venn diagrams are visualisation tools used to display the results of DGE analysis. Heatmaps use colour scales to map data values and grid with variables and observations along two axes. In contrast, Venn diagram represents the intersection and uniqueness of different data sets and the intersections between the circles show the similarities between these sets. Venn diagram is extremely useful to highlight similarities or differences between several groups or conditions concerning gene expression (Jia et al., 2021).

Upon identification of DEGs, enrichment analysis is adapted for biological interpretation of gene expression data. The enrichment analysis is a pivotal step in bioinformatics studies that highlights the relevant biological functions associated with the enriched gene lists (Chicco & Agapito, 2022). Several statistical methods can be used to associate the most enriched biological pathways in the input gene list and consider the number of genes and the likelihood of a pathway to be found enriched. There are multiple enrichment analysis tools available in the scientific literature, both as web tools and as stand-alone software programs (Rosati et al., 2024). Commonly these tools employ multiple databases such as WikiPathways (Martens et al., 2021), Kyoto Encyclopedia of Genes and Genomes (KEGG), (Kanehisa et al., 2021), Gene Ontology (GO) (Aleksander et al., 2023), Reactome (Rothfels et al., 2023), Search Tool for the Retrieval of Interacting Genes/Proteins (STRING) (Szklarczyk et al., 2021), Panther Pathways (Mi et al., 2021) and Biocarta (Adriaens et al., 2008) to facilitate and optimising pathway enrichment. Among the tools most widely used are Database for Annotation, Visualisation, and Integrated Discovery (DAVID), Metascape, Gene Set Enrichment Analysis (GSEA), Cytoscape and Enrich-r. These tools offer a variety of functionalities ranging from enrichment analysis, annotation and analysis of gene lists, visualisation and analysis of biological networks, and examination of hierarchical relationships in terms of Gene Ontology (Rosati et al., 2024). Table 2.4 enlisted bioinformatics tools for the visualisation of biological pathways and networks.

Table 2.4: The advantages and disadvantages of popular pathway enrichment analysis tools

Tools	Description	Advantages	Disadvantages	Context of Use	References
DAVID	Web-based bioinformatics tool integrating different sources of gene annotation and biological pathways. Provides clustering analysis based on gene and protein expression data.	Broad taxonomic coverage; Update annotation; gene ID conversion; user-friendly.	Requires familiarity with biological databases	In -depth analyses of gene sets emphasised on detailed annotation and molecular interactions, comparative and functional studies on different species	Sherman et al. (2022)
Metascape	Web-based tools with complete resources for gene list annotation and analysis. Integrates functional enrichment, interactome analysis, gene annotation, and membership search to interrogate more than 40 separate knowledge bases in integrated gateway. Facilitates data sets comparison from many independent orthogonal studies.	Automatic processing and recognition of gene identifier; auto clustering; supports multiple file formats, user friendly.	May generate too many enriched pathways.	Complex analyses requiring the integration of multiple omics data. Excellent for enrichment analysis and automatic gene clustering.	Zhou et al. (2019)
GSEA	Software used to determine a predefined sets of genes result in significant gene expression differences between two biological conditions.	Robust analysis method; handles large gene sets; sort genes by *p*-value and fold change leading to comprehensive biological interpretation.	Advance skills in bioinformatics are necessary. Requires processing resources and intensive system biology and statistic knowledge.	Suitable for studies determining subtle changes in gene expression between sample groups. More useful in oncology and genetics research.	Canzler & Hackermulle (2020)

Table 2.4 continued

Enrich-r	Web-based tool offering users several options for presenting results with precise statistical evidence.	Extensive collection of gene set libraries, offer visual summaries.	May overestimate results with large gene sets; no ID conversion tools.	Ideal for rapid interactive analyses of gene sets in transcriptomics and proteomics studies.	Kuleshov et al. (2016)
Cytoscape	An open-source software to visualise complex network of molecular interaction of gene expression profile.	Runs on all available operating systems that support Java; support latest and extending applications.	Require extensive memory and computational power; additional tools like R and igraph is necessary to obtain visualisation.	Ideal for complex interactions analysis as signalling pathways; gene relationship, protein-protein interactions and integration of multiomics data.	Otasek et al. (2019)

In general, a typical RNA-seq data analysis workflow involves several key steps: quality control and trimming of raw reads, alignment to a reference genome, quantification of gene expression, normalisation, and DEGs analysis. Figure 2.1 illustrates the overall workflow, and the example of tools used in each analysis step.

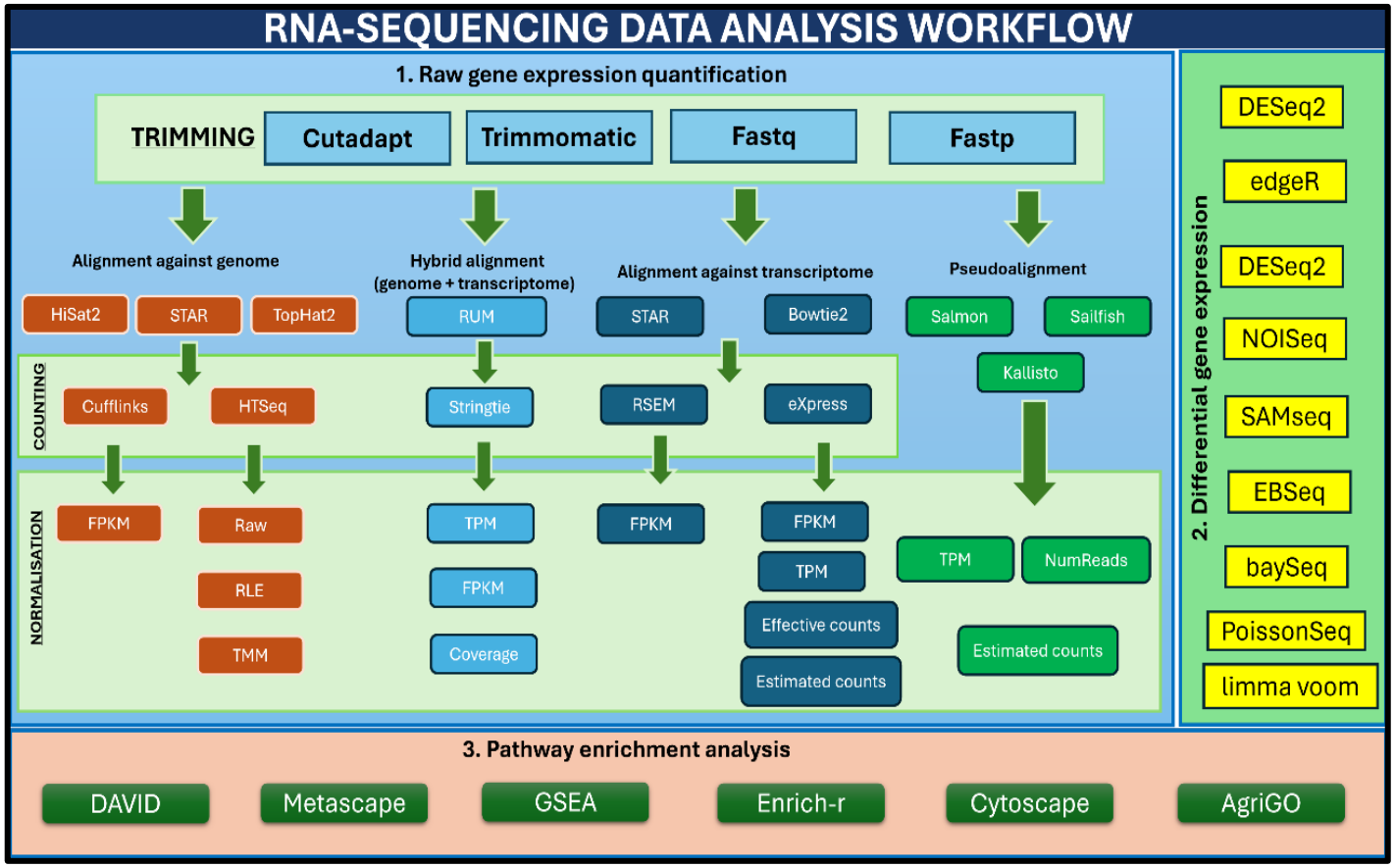

Figure 2.1: The standard workflow to process RNA-seq data following obtaining raw data in FASTQ files. The workflow shows three main procedures including raw gene expression quantification, differential gene expression, and pathway enrichment analysis.

2.1.3 Leaf as studied organ

Leaves play a crucial role in the development and overall biomass accumulation of a plant, serving as key indicators of how a plant adapts to its environment. As reservoirs of organic matter and mineral nutrients, leaves are essential for plant survival and reproduction (Shang et al., 2024). Leaf tissues are sensitive to the changes in their environments. The direct exposure of leaves to atmospheric conditions such as light, temperature and humidity is highly reflected in their morphology and physiology. Numerous transcriptomic analyses on plant leaves have revealed significant changes in plant gene expression in response to alterations in leaf metabolism. For instance, drought and cold stress have been shown to reduce leaf size and disrupt chloroplast structure in tobacco (Chen et al., 2019; Li et al., 2021; Xu et al., 2020), while similar impairments in thylakoid structure of tobacco have been observed under drought conditions (Yang et al., 2017). Moreover, analysis of rice leaves under varying nitrogen levels has uncovered nitrogen-responsive DEGs responsible for reprogramming plant hormone signal transduction, glycolysis/gluconeogenesis, ascorbate and aldarate metabolism, and photosynthesis pathways, influencing leaf senescence in rice (Zhang et al., 2024). Studies on drought-stressed rice and maize revealed downregulation of cell-cycle-related genes, affecting cell division and leaf elongation (Zhang et al., 2018; Tarun et al., 2020). Moreover, transcriptomics studies on salinity stress study in almond has shown a higher number of DEGs in leaves than in roots, suggesting a critical role of hormonal signalling in leaves tissues (Acharya et al., 2022). These findings highlight the leaf's role as the primary site of environmental and molecular adaptation.

While roots are also exposed to environmental conditions, particularly within the soil matrix, roots interact with a more localised and microbially complex environment. Root transcriptomes are often influenced by microbial associations and soil nutrient availability

which can introduce substantial variability, hence making it challenging to perform comparative analysis across plantations (Kaur et al., 2021). Moreover, root sampling is prone to contamination which can compromise RNA integrity and sequencing quality (Okamura et al., 2020). In contrast, trunk or stem tissues exhibit relatively low transcriptional activity and are less responsive to environmental stimuli (Qi et al., 2022). In addition, monocots do not have true vascular cambium like dicots. Hence, due to their primary roles in structural support and transport, trunk involvement in rapid stress signalling is limited, making it difficult to capture meaningful gene expression changes especially related to environmental adaptation (Qi et al., 2022).

In summary, while roots and trunks offer insights into specific biological processes, leaves provide the most integrative, responsive, and accessible platform for studying gene expression related to environmental adaptation and growth. The photosynthetic carbon assimilation in mature source leaves determines carbohydrate availability for growth, products of primary metabolism mediating developmental processes. Therefore, leaf transcriptome analysis offers a robust and integrative snapshot of molecular responses to environmental conditions in investigating sago palm growth and trunking development across diverse plantation environments.

2.1.4 Research Objectives and Hypothesis

This research was initiated to address the research gaps in current literature. Despite many studies conducted on non-trunking sago palms, gene expression studies specifically focused on trunking sago palms remain scarce. This lack of molecular insight has limited our understanding on the molecular mechanisms underpinning the trunking formation and growth of sago palm.

The study aim to explore the molecular mechanism underlying trunk development in sago palms by analysing leaf transcriptomes from trunking sago palms collected across different plantations. It is hypothesise that trunking sago palms expressed a set of regulatory genes and molecular pathways that promote growth and trunk development, while non-trunking sago palms exhibits genes associated with stress signalling that suppresses the palm's development. The hypothesis was conducted with the following objectives:

i) To identify commonly expressed differentially expressed genes (DEGs) in leaf tissues of trunking sago palms.

ii) To characterise the functional roles of DEGs toward sago palm growth and development through bioinformatics analyses.

2.2 Materials and Methods

This study employed an integrated workflow beginning with fastp, an all-in-one preprocessing tool used to generate clean reads efficiently. STAR aligner was then utilized for mapping due to its high precision and ability to accurately process short reads across diverse sequencing platforms. For normalization and identification of DEGs, DESeq2 was selected, as it accounts for sequencing depth and RNA composition differences between samples, enabling robust comparisons. DESeq2 also performs DGE analysis directly on the normalized count matrix. For gene enrichment analysis and visualization, web-based tools DAVID and Metascape were used. These platforms are user-friendly and require minimal bioinformatics expertise, making them ideal for researchers new to the field. The overall approach streamlines the workflow by minimizing tool-switching and maintaining high accuracy throughout the analysis pipeline.

2.2.1 Leaf tissue collection

In this study, trunking samples at *Pelawei Manit* (8-12 years) growth stage were selected. The palms were felled to obtain leaf samples. Leaf tissues were obtained at the third frond from the sago bole. Three biological replications were collected for each collection sites. The samples were collected at Dalat Sago Palm Plantation and Sungai Talau Research Station (STRS) in Mukah, and Paya Paloh Sago Palm Plantation in Kota Samarahan and denoted as Dalat, SgTalau, and PPaloh, respectively, in this study. Global positioning system (GPS) of each sample are tabulated in Table 2.5. The leaves were wiped with 70% ethanol and subsequently rolled into appropriately labelled 50 ml polypropylene tube, and snap-freeze in liquid nitrogen for transportation. Upon arrival at the laboratory, the samples were sorted and stored at -80 °C for long-term storage.

Table 2.5: Global positioning system (GPS) of each sample collection

Location	Region/Planting site	Sample ID	GPS location (DMS format)
Dalat Sago Plantation	Mukah, Dalat	Dalat_1	N02° 51' 08.3" E111° 49' 26.4"
		Dalat_2	N02° 51' 07.6" E111° 49' 34.0"
		Dalat_3	N02° 51' 06.8" E111°49' 36.7"
Sungai Talau Research Station	Mukah, Sungai Talau	SgTalau_1	N02° 48' 52.3" E 111° 54' 33.5"
		SgTalau_2	N02° 48' 52.9" E111° 54' 34.1"
		SgTalau_3	N02° 48' 52.9" E111° 54' 35.8"
Paya Paloh Sago Palm Plantation	Kota Samarahan, Paya Paloh	PPaloh_1	N02° 53' 45.6" E112° 05' 03.8"
		PPaloh_2	N01° 26' 24.6" E 110° 29' 41.5"
		PPaloh_3	N01° 26' 24.8" E 110° 29' 41.2"

2.2.2 Total RNA extraction from sago palm leaf

Total RNA from leaf tissue was extracted using conventional hexadecyltrimethylammonium bromide (CTAB) technique described by (Yan et al., 2022). The necessary buffers and solutions required in this protocol are summarised in Table 2.6. All centrifugation parameters in this technique was set at 4° C with centrifugation speed at 20,922 x g for 50 ml Nalgene tube and 16,100 x g for 1.5 ml microcentrifuge tube. All incubation steps were conducted at room temperature.

Table 2.6: Chemical utilised in the preparation of 2% CTAB Miniprep Extraction buffer

	Concentration	500 ml
CTAB	2 %	2 g
NaCl	1.4 M	40.6 g
0.5 M EDTA, pH 8.0	20 mM	20 ml
1 M Tris, pH 8.0	100 mM	50 ml
Polyvinylpyrolidone (PVP40, M.W. 40,000)	2%	10 g
Water		Add to 500 ml

An approximate 1 g of leaf tissue was ground to fine powder using a mortar and pestle under continuous liquid nitrogen environment. The powdered sample was transferred to a sterile 50 ml Nalgene Oak Ridge High-Speed PPCO centrifuge tube (Thermo Scientific, USA). A total of 15 ml CTAB lysis buffer containing 1% (v/v) β-mercaptoethanol was added to the powdered-containing centrifuge tube and vortexed for 1 min followed by incubation at room temperature for 5 min on a rotary mixer (Cole Palmer RotoFlex, Sigma-Aldrich, USA). Next, separation step was conducted twice on aqueous fraction with 15 ml of ice-cold chloroform (MACRON, USA). The mixture was gently mixed and incubated for 5 min followed by 5 min centrifugation at 20,922 x g at each wash. Then, the nucleic acid precipitation was conducted on 10 ml aqueous fraction with an equal volume of ice-cold isopropanol and the mixture was left for incubation at 5 min followed by centrifugation at 20,922 x g for 15 min. A volume of 1 ml of ice-cold 70% ethanol was added to dissolved visible pellet and the solution was transferred to a new 1.5 ml microcentrifuge tube. The solution was centrifuged at 16, 100 x g for 2 min to remove residual salts from nucleic acid pellet. This washing step was repeated twice with ice-cold 70% ethanol. Subsequently,

DNAse treatment was conducted in 100 µl of Tris-HCl buffer (40 mM Tris-HCl, 10mM $MgSO_4$, 1 mM $CaCl_2$) and treated with 2 µl of DNase (RQ1, Promega, USA). The mixture was left for incubation for 30 min. DNase treatment was terminated with 100 µl of 20 mM EDTA (pH 8.4) and centrifuged at 16, 100 x g for 15 min. A total of 540 µl of aqueous fraction was transferred to new sterile 1.5 ml microcentrifuge tube. RNA precipitation was conducted with an equal volume of ice-cold isopropanol followed by incubation for 10 min and centrifugation for 15 min. The pellet formed was washed twice with 1 ml of ice-cold 70% ethanol and centrifuged for 2 min at each wash. The resulting pellet was air-dried before resuspension in 100 µl tris-EDTA (TE) buffer and stored at -80°C.

2.2.3 RNA sequencing

High-quality RNA samples with absorbance readings A260/A280 ratios ranging between 1.80 and 2.20 and A260/A230 ratios more than 1.70 (Apryianto et al., 2024) were selected for RNA-sequencing. Samples were transported on dry ice to Apical Scientific Sdn Bhd, Seri Kembangan, Selangor for further RNA quantity and quality assessment using Agilent 2100 BioAnalyzer. RNA samples that qualified for the next generation sequencing (NGS) RNA integrity number (RIN) of 7 to 9 (Li et al., 2024) were proceed with messenger RNA (mRNA) isolation, complementary DNA (cDNA) synthesis, and cDNA library assembly. Sequencing was conducted on Illumina NovaSeq 6000 platform using paired-end (PE) strategy (150 bp) with sequencing depth of 20 million reads. The raw data from the RNA-seq libraries were submitted to the Sequence Read Archives (SRA) in the NCBI database under the project ID PRJNA922330.

2.2.4 Read mapping and quantification

The raw reads were processed and trimmed using an all-in-one FASTQ preprocessor, fastp (Chen et al., 2018). High quality reads were mapped to *Metroxylon sagu* genome

(Sago_v3: GCA_017589505.3) using STAR aligner v.2.7.10a with default parameters (Dobin et al., 2013). Alignment results were processed and sorted using SAMtools v1.19 (Li et al., 2009). Transcripts from different samples were merged using StringTie with default parameters (Pertea et al., 2015). Read counts mapped to genomic features was processed using htseq-count (Anders et al., 2015). Raw counts normalization was conducted using DESeq2 package. To avoid infinite values, a value of 1 was added to each raw count prior to $\log_2$ transformation.

2.2.5 Differentially Expressed Genes (DEGs) analysis

Differentially expressed genes (DEGs) between three comparison groups against non-trunking (NT) sago palm samples (Dalat_vs_NT; PPaloh_vs_NT; SgTalau_vs_NT) were identified using DESeq2 with default parameters (Love et al., 2014) following cut off criteria of adjusted P-value < 0.05 and $\log_2$ fold change ≥ 2. The non-trunking dataset was obtained from NCBI Bioproject: PRJNA781491 (accession: SAMN23282501, SAMN23282500; SAMN23282499), comprising leaf tissue samples collected from non-trunking sago palms at the Dalat Sago Palm Plantation. To overcome potential batch effects between the trunking samples and publicly-sourced non-trunking samples, Principal Component Analysis (PCA) was performed. Differential expression analysis was conducted separately for each of the three pairwise comparisons to minimise cross-condition variability and isolate biologically relevant transcriptional changes.

2.2.6 Identification and functional association of frequently shared DEGs

The DEGs commonly expressed in all groups were identified using Venn diagram. For functional enrichment analysis, homologous protein sequence accession ID was identified using protein Basic Local Alignment Search tool (BLASTp). The functional

enrichment analysis was performed using the Database for Annotation, Visualisation and Integrated Discovery (DAVID) tool and Metascape (Zhou et al., 2019b). The enrichment was carried out separately for upregulated and downregulated genes. Enrichment results from DAVID were visualised using SR plot software.

2.2.7 Identification of transcription factors

The identification of homologous transcription factors (TFs) was performed using iTAK (Plant Transcription factor and Protein Kinase Identifier and Classifier) (Zheng et al., 2016). Nucleotide sequences in FASTA format were uploaded to the website. This web-based portal software facilitates the recognition of plant transcriptional factors, transcriptional regulators, and protein kinases among differentially expressed genes.

2.2.8 Synthesis of cDNA for RT-qPCR

In this study, a two-step approach was performed for reverse transcription-quantitative polymerase chain reaction (RT-qPCR). Total RNA extracted from leaf tissue was reversed transcribed into complementary deoxyribonucleic acid (cDNA) (High-Capacity cDNA Reverse Transcription Kit, Applied Biosystems, USA). The details of the 2x RT master mix for a 20 µl reaction is tabulated in Table 2.7.

Table 2.7: Buffers required in the synthesis of cDNA

Component	Volume (µl) (2x reaction)	Concentration
10X RT Buffer	2.0	2X
25X dNTP Mix (100 mM)	0.8	2.5 mM
Anchored Oligo dT (VN)	2.0	1X
MultiScribe Reverse Transcriptase	1.0	5 U/µl
Nuclease-free water	3.2	-
Total per reaction	10.0	

Ten microlitre of total RNA was pipetted into the 2x RT master mix to a final volume of 20 µl. The mixture was briefly vortexed and centrifuged. The preparation for RNA conversion was done on ice. A total of 34 cycles of annealing at 25 °C for 10 min, extension at 37 °C for 120 min and inactivation at 85 °C for 5 min was programmed on the thermal cycler (T100, BioRad, USA).

2.2.9 Primer design for gene expression validation

Primer pairs were designed using Primer3 tool with default parameters (Untergasser et al., 2012). The specificity of the primer pairs was confirmed through the melt curve analysis and visualised on 1% (w/v) agarose gel. The primer pair efficiency was determined through a tenfold serial dilution. The resultant Cq values were plotted on a logarithmic scale along with the corresponding concentration. A linear regression curve (R^2) through the data points was generated and the slope of trend line was calculated according to the formula $E = (10^{-1/slope}-1) \times 100\%$. Table 2.8 tabulated the primers purchased from Integrated DNA technologies (IDT) (Singapore).

Table 2.8: List of designed primers used in RT-qPCR targeting the upregulated and downregulated DEGs

Primer name	Gene name	Primer sequence (5'-3')	Annealing temperature (°C)	PCR product size (bp)
P32	UDP-Glycosyltransferase superfamily protein	F: GTTCCATGAGGAGGAGAAGCC R: TTGAGCGTCACAGACTCCCT	57.4 58.2	150
P41	Duplicated homeodomain-like superfamily protein	F: CGGAACAGGAACGGAGGAAA R: TTGACCTCCGGCGATCTCTA	57.2 57.5	204
P51	Major facilitator superfamily protein	F: GAGGGGCATCAACAGCTTCT R: ACGCAGGAGAAGAGCATGAG	57.5 57.0	150
P58	Chalcone-flavanone isomerase family protein	F: CTGGTCCTCGGCCTCAAAAT R: GTGGTGGGCTTCTCTGGAAT	57.4 57.2	107
Act2	Actin 2	F: ACCTTGCTGGACGTGACCTTACTGAT R: GTTGTCTCGTGGATTCCAGCAGCTT	60.0 60.0	257

Note: Primers P32, P41 targeting upregulated DEGs, while P51 and P58 targeting downregulated DEGs. Actin 2 is reference gene.

2.2.10 RT-qPCR protocol

The RT-qPCR was performed on Applied Biosystem QuantStudio 5 PCR system (Thermo Scientific, USA) following the protocol condition: initial denaturation at 95 °C for 2 min, followed by 34 cycles of denaturation at 95 °C for 15 s, annealing at 60 °C for 30 s, and extension at 75 °C for 60 s with a fluorescence measurement at the last step of each cycle. A melting curve, ranging from 60 to 99 °C with fluorescence measurements at 1 °C intervals, was performed after every quantitative cycle. Each reaction was performed in 20 µl final volume containing 10 µl 2x SYBR Green PCR master mix (Fast SYBR Green; Applied Biosystem, USA), 0.8 µl of specific primer pair (0.4 µl of 0.2 µM forward and reverse primers), 1 µl of diluted cDNA sample, and 8.2 µl nuclease-free water. Each sample was tested in triplicate. The quantitative cycle (Cq), baseline correction, and threshold setting were automatically computed by the thermal cycler software. The relative messenger RNA (mRNA) expression was normalised using Actin2 as reference gene. To quantify gene expression, the relative quantification method $2^{-\Delta\Delta Ct}$ was used with primers efficiency ranges between 90% and 110% efficiency (Livak & Schmittgen, 2001).

2.3 Results

2.3.1 Qualitative and Quantitative Analyses of RNA

The quantity and quality of extracted total RNA from sago palm leaf tissue were assessed by measuring the optical density ratios (A260/280 and A260/230) using a Nanodrop (DeNovix DS-11, USA). The extracted RNA was visualised on 1% Tris Borate-EDTA (TBE) agarose gel electrophoresis to detect any sample degradation prior to sending the samples to sequencing agency (Apical Scientific Sdn. Bhd.) for downstream analysis. (Figure 2.2). Table 2.9 presents the RNA yield and the absorbance ratios in average standard deviation (SD). Figure 2.2 visualised the integrity of the extracted total RNA from sago palm leaf tissue.

Table 2.9: The quality and integrity of extracted RNA from sago leaf in average ± SD

Sample	$A_{260/280}$	$A_{260/230}$	Total RNA concentration (ng/µL)
Dalat_P1	2.12 ± 0.19	2.34 ± 0.31	257.00 ± 9.43
Dalat_P2	1.91 ± 0.04	2.54 ± 0.17	261.42 ± 51.34
Dalat_P3	1.97 ± 0.00	2.62 ± 0.07	281.11 ± 28.40
SgTalau_P1	1.97 ± 0.01	2.36 ± 0.04	281.52 ± 15.92
SgTalau_P2	1.97 ± 0.03	2.41 ± 0.12	327.24 ± 106.63
SgTalau_P3	1.96 ± 0.01	2.51 ± 0.05	310.12 ± 102.81
PPaloh_P1	1.93 ± 0.03	2.42 ± 0.27	338.10 ± 15.71
PPaloh_P2	1.99 ± 0.04	2.57 ± 0.11	273.21 ± 100.11
PPaloh_P3	1.97 ± 0.03	2.29 ± 0.06	324.87 ± 30.96

*Nanodrop reading at 1 µL of total RNA dispensed at platform.

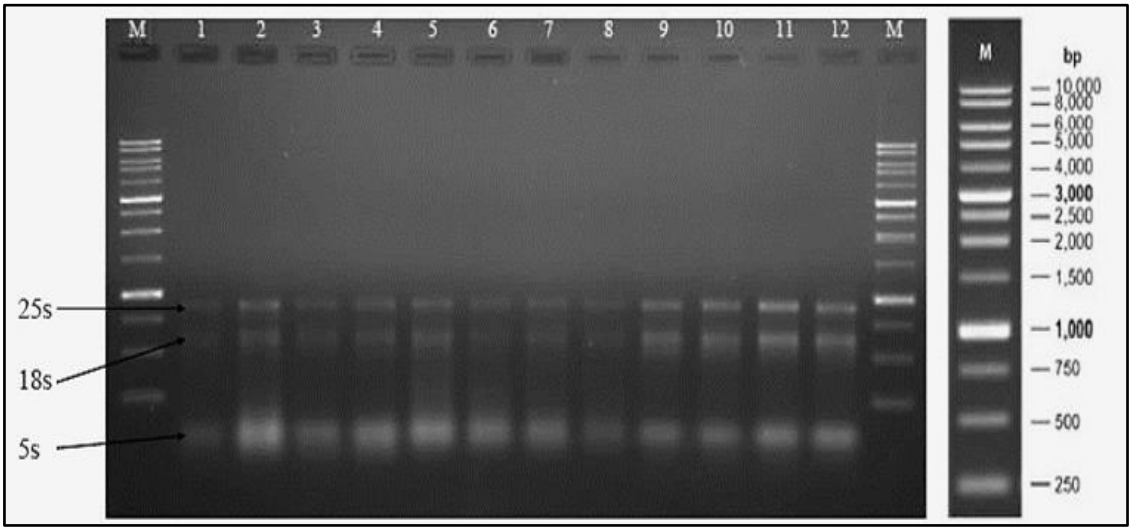

Figure 2.2: RNA bands resolved under 1% TBE agarose gel stained using safe staining dye GelRed. M represents the 1 kb DNA ladder. Lanes 1-4, 5-8, 9-12, represents RNA extracted from Dalat, SgTalau, and PPaloh sago palm leaf, respectively

The total RNA isolates undergone a secondary assessment to evaluate their purity and potential degradation during shipping. The results obtained from both the Nanodrop and Agilent 2100 Bioanalyzer systems indicated absorbance readings within the A260/280 and A260/230 ranged from 1.8 to 2.0. Additionally, the RNA Integrity Number (RIN) ranged from 3.00 to 7.00. Table 2.10 tabulates the selected total RNA samples proceed for RNA sequencing.

Table 2.10: Integrity and yields of total RNA extracted from *M. sagu* leaf

	Nanodrop				LabChip Results
Sample	**$A_{260/280}$**	**$A_{260/230}$**	**rRNA Ratio***	**RIN (Anomaly adapted)**	**RNA Total Amount (µg)**
Dalat_P1	2.03	2.03	1.70	4.70	18.80
Dalat_P2	1.88	1.84	2.00	5.10	12.36
Dalat_P3	2.00	1.94	1.50	4.80	30.94
SgTalau_P1	2.09	1.83	1.50	4.80	34.29
SgTalau_P2	1.98	1.88	1.60	4.70	18.00
SgTalau_P3	2.01	1.93	1.60	6.00	33.00
PPaloh_P1	2.06	1.97	1.00	4.00	27.81
PPaloh_P2	1.58	1.52	2.20	7.30	21.24
PPaloh_P3	1.89	1.87	1.30	3.90	21.12

*rRNA ratio for plants (25s/18s)

All samples exhibited good purity and quality, as evidence by A260/280 and A260/230 ratios falling within the range of 1.5 to 2.0 (Table 2.10). The RNA samples analysed via 1% TBE agarose gel displayed intact and sharp 25s, 18s, and 5s rRNA bands, with no noticeable bands across all loading wells (Gaafar et al., 2021). These results indicated high RNA integrity and absence of genomic DNA contamination. The Agilent 2100 Bioanalyzer system utilises automated miniaturised electrophoresis and lab-on-chip technology further evaluate RNA quality.

For RNA sample to be considered for sequencing, it must meet the following criteria such as A260/280 ≥ 1.5, A260/230 ≥ 1.9, rRNA ratio ≥ 1, and RIN ≥ 7 with total RNA concentration ≥ 3 µg (Singh et al., 2024). The RIN, scored on a numerical scale from 1 to 10 where 1 represents complete degradation and 10 signifies full integrity, serves as a critical indicator of RNA quality before subjected to sequencing. Most RNA downstream

applications emphasise the importance of high-quality RNA. As in principle, degraded RNA samples result in lower correlation of gene expression data. Consequently, many sequencing facilities recommend a minimum RIN value of 6 or higher to ensure transcript quantification accuracy (Singh et al., 2024; Steinacher et al., 2024). Interestingly, a preliminary study by (Li et al., 2024) demonstrated that both intact (RIN ~6-9) and severely degraded (RIN ~3-5) RNA samples exhibited good repeatability and reproducibility in TaqMan-qPCR and droplet digital PCR (ddPCR), with severely degraded RNA samples showing similar expression levels as intact RNA samples.

Despite the longstanding reliance on standard parameters using the Agilent Bioanalyzer system for assessing RNA quality, the RIN algorithm is fundamentally based on the distribution and relative intensity of distinct RNA fragments. The high-quality RNA typically exhibits two prominent ribosomal peaks, corresponding to 18s and 28s rRNA. The algorithm integrates these features into a standardised scale ranging from 1 to 10, where 1 represents highly degraded RNA and 10 denotes intact, high-quality RNA (Li et al., 2024). As shown in Table 2.9 the most extracted RNA displayed low RIN values ranging from 3.9 to 7.3. However, it is noteworthy that the Agilent Bioanalyzer often yields low RIN values (<8) or even no RIN values when analysing plant samples (Kim & Haj-Ahmad, 2016). Unlike mammalian RNA, plant total RNA present several challenges where it exhibits distinct peak patterns (18s and 25s) rather than the 18s and 28s of animal rRNAs peaks. These differences are frequently misinterpreted by the Bioanalyzer software as degradation artifacts. Consequently, the Agilent system inadequately evaluates intact total RNA from plant tissues as degraded RNA, resulting to lower RIN number (Shroeder et al., 2006; Gaafar et al., 2021). Thus, referring to these preliminary studies, RNA samples were subjected to RNA sequencing despite of having low RIN values.

2.3.2 Pre-processed RNA-seq data

The raw data (RNA-seq FASTQ files) obtained from the sequencing facility undergone pre-processing to remove adapter contamination, low-quality reads, and unpaired reads, resulting in clean data. Overall, a total of 85.61 Gb of clean read was generated, with an average of 6 Gb per dataset. Notably, Dalat_P2 and SgTalau_P3 datasets recorded higher reads of 100.74 M and 77.71 M, respectively, due to deeper sequencing depth of 40 million reads instead of 20 million reads. The Phred quality score of (Q30) exceeded 90%, and the guanine-cytosine (GC) content was consistently between 48-50% range. These values showed high-quality sequencing and meet the requirements for subsequent data analysis (Deng et al., 2024; Rong et al., 2024; Zou et al., 2024). The clean reads were then mapped to the *Metroxylon sagu* v3.0 (Assembly Accession: GCA_017589505.3) using the STAR aligner, resulting in more than 90% mapped reads. Table 2.11 tabulates the clean read counts and percentage of mapped reads.

Following normalisation, scree plot of principal component analysis (PCA) performed on each dataset were generated. Each comparative datasets showed a distinct gene segregation between trunking sago palm samples and the non-trunking sago palm samples (Figure 2.3). The percentage of variance by each scree plot result in high cumulative variance contribution with Dalat recorded the highest 88% followed by SgTalau (84%), and PPaloh (77%). The distinct separation, together with the elevated cumulative variance, indicates clear differentiation among sample replicates (Rong et al., 2024; Nguyen et al., 2023).

Table 2.11: Summary of clean dataset and read alignment to the reference genome

Samples	Raw Reads (M)	Clean Reads (M)	Clean Bases (Gb)	Q20 (%)	Q30 (%)	GC content (%)	Mapped reads (%)
Dalat_P1a*	41.64	41.36	6.19	97.85	93.80	48.98	94.06
Dalat_P1b*	45.49	45.19	6.76	97.55	92.97	48.97	-
Dalat_P2	56.31	55.92	8.36	97.77	93.55	49.40	94.03
Dalat_P3	101.45	100.74	15.10	97.53	93.04	48.91	94.70
PPaloh_P1	42.37	42.12	6.31	97.93	93.92	49.20	92.79
PPaloh_P2	41.74	41.48	6.21	97.96	94.01	48.39	91.88
PPaloh_P3	41.82	41.49	6.20	97.70	93.43	49.28	92.44
SgTalau_P1	43.08	42.78	6.40	97.94	94.03	49.13	93.48
SgTalau_P2a*	42.43	42.21	6.31	98.31	94.84	49.52	93.62
SgTalau_P2b*	41.26	41.01	6.13	97.91	93.91	50.10	-
SgTalau_P3	78.42	77.71	11.65	96.93	91.74	49.49	93.98
NT_1	69.96	66.66	6.67	98.00	91.78	49.57	94.33
NT_2	69.41	66.62	6.66	97.94	91.59	48.03	92.69
NT_3	69.96	67.33	6.73	97.98	91.63	47.68	94.20

Samples marked with asterisk (*) were submitted twice for sequencing. Mapped reads percentage are not shown for these samples because they were not included in the mapping analysis, as only one replicate per sample was selected for downstream, alignment. NT refers to non-trunking samples.

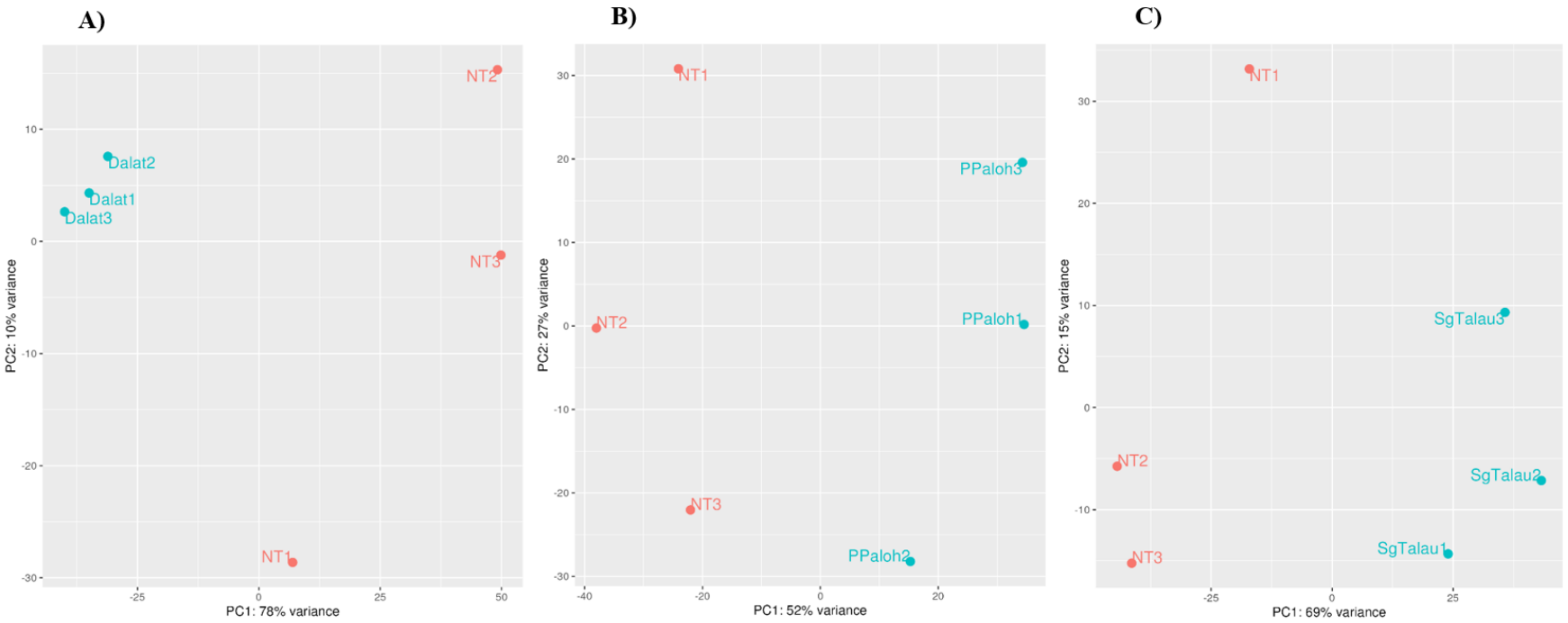

Figure 2.3: Principal Component Analysis (PCA) of trunking versus non-trunking sago palms across three locations A) Dalat vs NT; B) SgTalau vs NT; C) PPaloh vs NT show distinct clustering of samples demonstrating consistent transcriptional separation between two phenotypes. Note that NT refers to non-trunking of which the datasets were retrieved from NCBI Bioproject: PRJNA781491

2.3.3 Differential gene expression analysis

Differential gene expression analysis conducted using DESeq2 following threshold criteria of $|\log_2$ fold change (FC)$| \geq 2$ and adjusted p-value < 0.05 exhibited a total of 6, 119 differentially expressed genes (DEGs) comprised of 4,384 downregulated and 1,735 upregulated genes in the three comparative sample sets of Dalat, SgTalau, and PPaloh with non-trunking as control. Figure 2.4 illustrates the number of DEGs expressed in each comparative dataset.

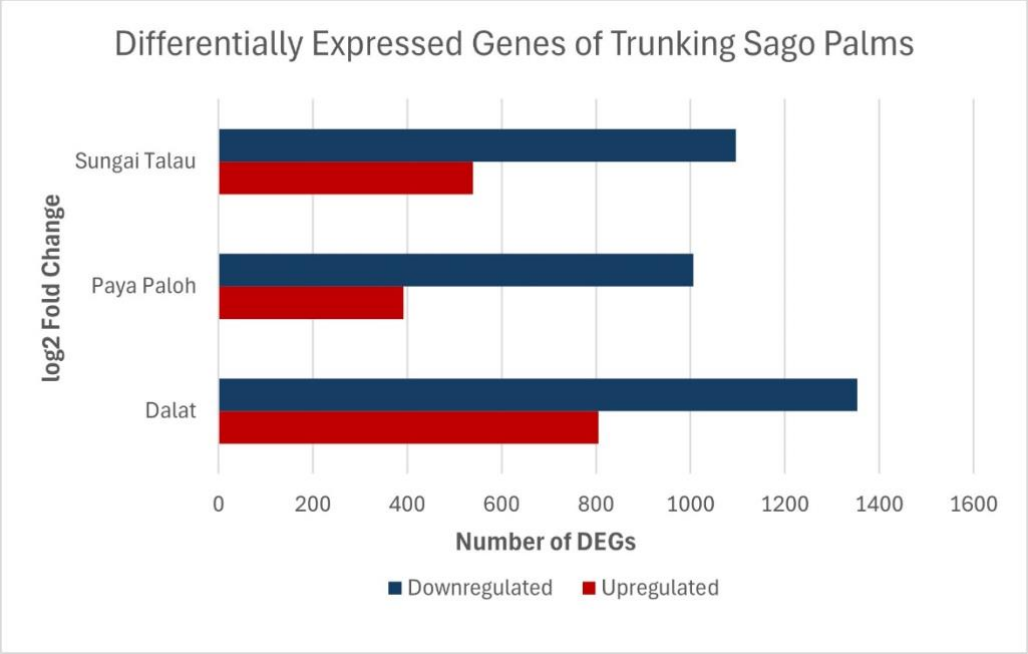

Figure 2.4: Bar plot representing DEGs at log2 fold change of upregulated and downregulated genes in leaf transcriptome of each comparative sets against non-trunking sago palms

The bar plot visualised that most of the transcriptome obtained from trunking sago palm were downregulated, regardless of their localities. It is exhibited that Dalat expressed the most downregulated genes with 1353 genes followed by SgTalau, and PPaloh with 1096 and 1006 genes, respectively. Meanwhile, upregulated genes were mostly expressed in sago palms sampled from Dalat followed by SgTalau and PPaloh with 805, 539, and 392 genes, respectively.

Volcano plot shows the distribution statistical significance versus magnitude of fold change. The most upregulated and downregulated genes are towards the right and the left, respectively, and the most statistically significant genes are towards the top (McDermaid et al., 2019). Figure 2.5 shows top 10 statistically significant transcripts. In Dalat, the most statistically significant DEGs included UDP-Glycosyltransferase superfamily, K-box region and MADs- box transcription factor (*SEP3*), SAUR-like auxin-responsive, Sec1/munc18-like (*SM*), zinc finger protein 8 (*ZFP8*), tetratricopeptide repeat (*TPR*)-like, ARF-GAP domain 6 (*AGD6*), and thioglucoside glucohydrolase 1 (*TGG1*). Meanwhile, in PPaloh the top significant DEGs were Sec1/munc18-like (*SM*), myb domain protein 48 (*MYB48)*, SAUR-like auxin-responsive, outer envelope protein of 80 kDa (*OEP80*), K-box region and MADS-box transcription factor (*SEP3*), ARF-GAP domain 6 (*AGD6*), alpha/beta-Hydrolases (*KAI2*), major facilitator superfamily protein (*GTR2*), and cationic amino acid transporter 5 (*CAT5*). Lastly Sungai Talau samples exhibited significant DEGs such as K-box region and MADS-box transcription factor (*SEP3*), histone superfamily protein, HSP20-like chaperones, GCR2-like 1 (*GCL1*), ARF-GAP domain 6(*AGD6*), Leucine-rich repeat transmembrane protein kinase (*GSO2*), thioglucoside glucohydrolase 1(*TGG1*), and zinc finger protein 8 (*ZFP8*).

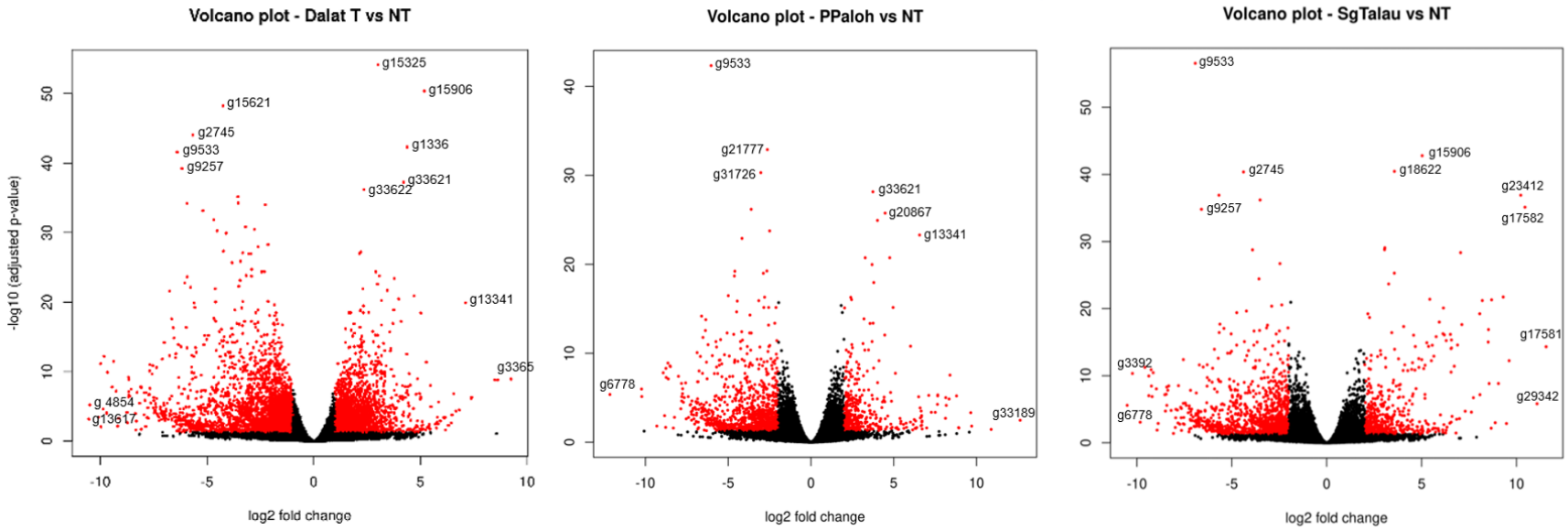

Figure 2.5: Volcano plot showing DEGs between trunking (T) and non-trunking (NT) for Dalat, PPaloh, and SgTalau sago palm plantations, with significantly up- and down-regulated genes highlighted in red. The red dots indicate significant differentially expressed transcripts ($p < 0.05$), while black dots represent transcripts without statistical significance ($p > 0.05$)

The determination of overlapping genes across all samples sets were visualised using Venn diagram (Venny 2.0.2). The diagram revealed a total of 595 commonly expressed DEGs across all datasets comprising 107 up- and 486 down-regulated DEGs, whereas 1000, 565, and 457 genes were unique to Dalat, SgTalau, and PPaloh datasets, respectively (Figure 2.6). Among the shared genes in all trunking samples were UDP-Glycosyltransferase superfamily protein (*AT4G27560*), K-box region and MADS-box transcription factor (*SEP3*), SAUR-like auxin-responsive protein family (*AT1G56150*), Sec1/munc18-like (*SM*) proteins superfamily (*ATVPS33*), duplicated homeodomain-like superfamily protein (*AT5G08520*), EXS domain (*ERD1/XPR1/SYG1*) family protein (*PHO1;H1*), and Ca^{2+} activated outward rectifying K^+ channel 6 (*KCO6*). Details of Top 25 DEGs, annotations, $\log_2$ fold-change, and adjusted p-values in each dataset are presented in Appendix A-C.

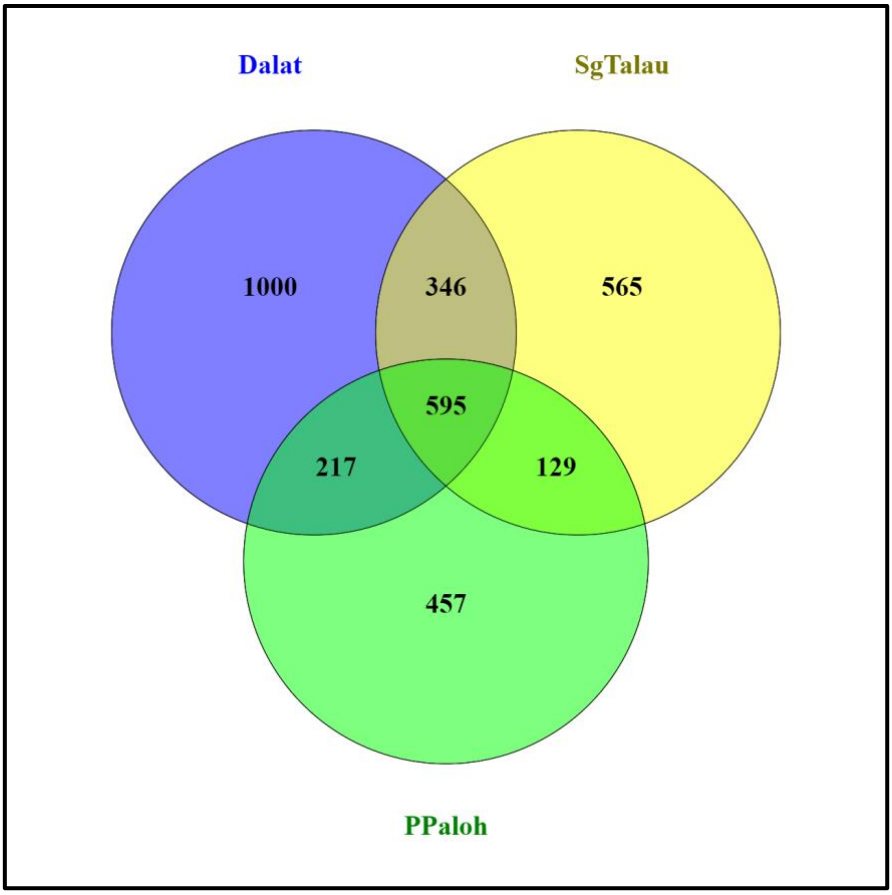

Figure 2.6: Venn diagram presenting the number of unique and overlapping genes among the three sampling locations Dalat (blue), SgTalau (yellow), and PPaloh (green) with overlapping regions indicating common DEGs expressed at two or all three sites

2.3.4 DEGs enrichment analysis

GO enrichment and KEGG pathway analyses were performed on commonly expressed DEGs using DAVID and Metascape. GO enrichment analysis classifies genes into three categories: biological process (BP), cellular component (CC), and molecular function (MF). The GO enrichment analyses of the differentially expressed genes visualised that most genes were involved in biological processes category, followed by the molecular function and cellular component categories. DAVID enriched 107 up- and 486 downregulated DEGs into 44 and 142 GO terms, respectively.

In the biological process category, resolution of DNA recombination intermediates (GO: 0071139), polyphosphate biosynthetic process (GO: 0006799), and DNA replication, synthesis of RNA primer (GO:0006269), were significantly enriched at 188.63-fold for the upregulated DEGs. Meanwhile, lignin biosynthetic process (GO: 0009809), response to oxidative stress (GO: 0006979), and cell wall organisation (GO: 0071555), were significantly enriched at 8.41-, 3.41-, 3.21-fold, respectively for downregulated DEGs. In the cellular component category, alpha DNA polymerase complex (GO: 0005658) were significantly enriched at 245.38-fold for upregulated DEGs followed by basal plasma membrane (GO:0009925) and apical part of the cell (GO: 0045177) at 81.79- and 70.10-fold, respectively. Membrane (GO: 0016020), plasma membrane (GO: 0005886), and vacuole (GO: 0005773) were significantly enriched at 1.57-, 1.57-, and 3.23-fold for downregulated DEGs in cellular component category. In molecular function category, the upregulated DEGs found 5s rRNA binding (GO: 0008097) was significantly enriched at 80.76-fold followed by inositol hexakiphosphate binding (GO: 0000822), and miRNA binding (GO: 0035198) at 50.48-, and 33.65-fold enrichment, respectively. Meanwhile, the downregulated DEGs visualised iron ion binding (GO: 0005506), heme binding (GO:

0020037), and oxidoreductase activity (GO: 0016491) were significantly enriched at 3.10-, 2.88-, and 2.70-fold enrichment, respectively. Shikimate O-hydroxycinnamoyltransferase activity (GO: 0047172), homogentisate solanesyltransferase activity (GO: 0010357), and homogentisate farnesyltransferase activity (GO: 0010355) were similarly enriched at 47.30-fold. Only top 10 significant (p-value < 0.05) GO enrichment terms were selected to generate bubble plots for GO-BP, GO-CC, and GO-MF for up- and downregulated DEGs (Figure 2.7-2.8). The detailed GO enrichment analysis results are shown in Appendix D-E.

The assigning of KEGG pathways enrichment of commonly expressed DEGs by DAVID found 15 KEGG pathways were enriched in downregulated DEGs. Among them were biosynthesis of secondary metabolites (ath01110) and metabolic pathways (ath01100) were highly represented categories followed by phenylpropanoid biosynthesis (ath00940), and flavonoid biosynthesis (ath00941) pathways (Figure 2.9). However, no KEGG pathways enrichment were identified among the upregulated DEGs. The KEGG enrichment analysis pathways are shown in Appendix F. Enrichment or over-representation analysis (ORA) is widely used in bioinformatics to infers biological pathways or processes from a set of significantly expressed genes. In this study, application of stringent criteria for DEG selection (adjusted P-value < 0.05 and $\log_2$ fold change ≥ 2) resulted in a relatively short list of upregulated genes. This limited gene set reduced the statistical power analysis, which leading enrichment tools (DAVID and Metascape) failed to identify any significantly enriched pathways (Karp et al., 2021). Furthermore, many of the upregulated DEGs may have weak or no annotations within the KEGG database, which rely on collections of predefined biological pathways collections for its enrichment calculations. This issue is particularly relevant in plants, as KEGG is known to have limited coverage of plant-specific pathways (Altman et al., 2013).

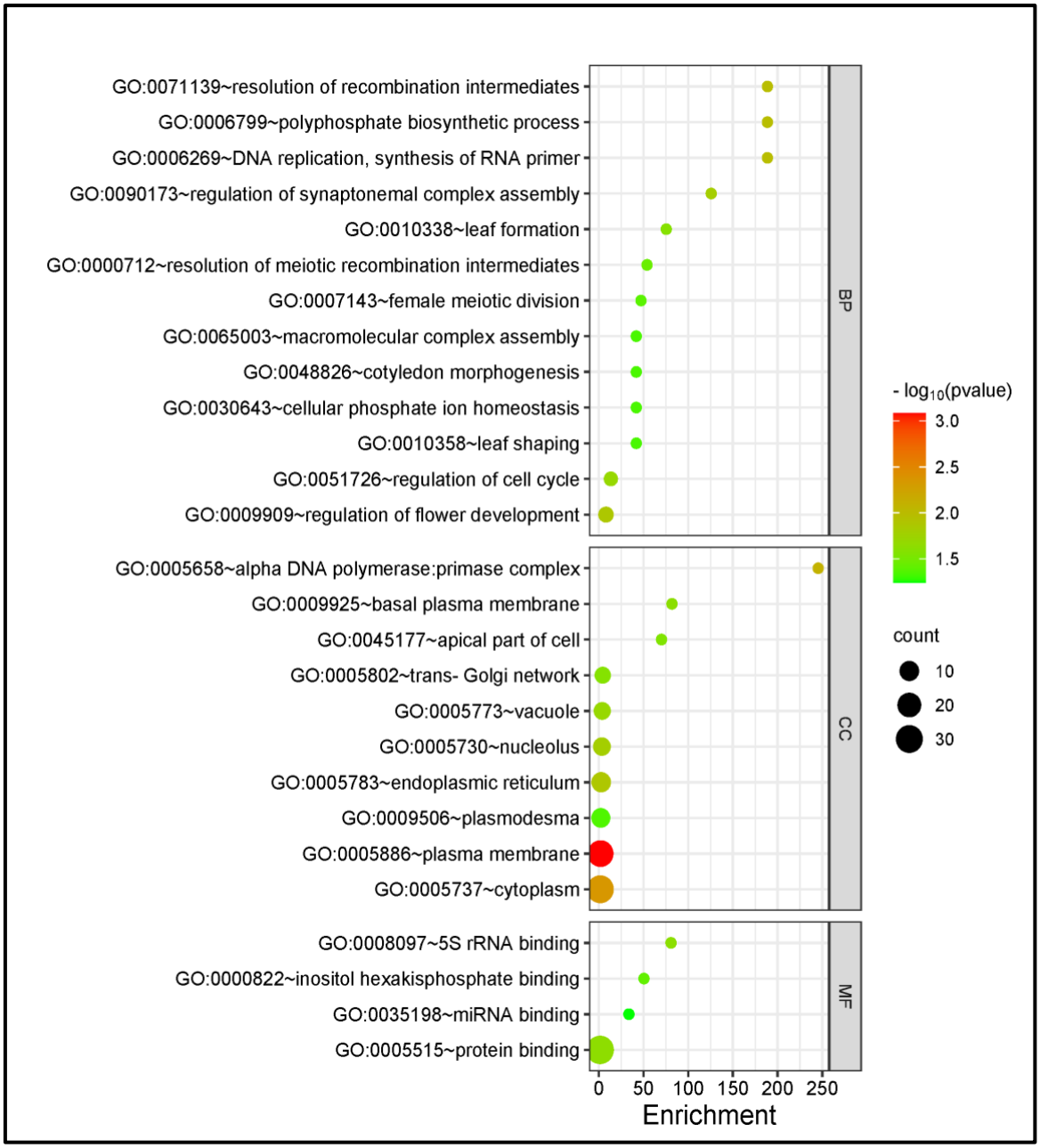

Figure 2.7: Gene ontology enrichment bubble plot of upregulated shared DEGs genes showing significantly enriched biological process, cellular component, and molecular function categories, with dot size indicating gene counts and colour representing adjusted *p*-values ($-\log_{10}$)

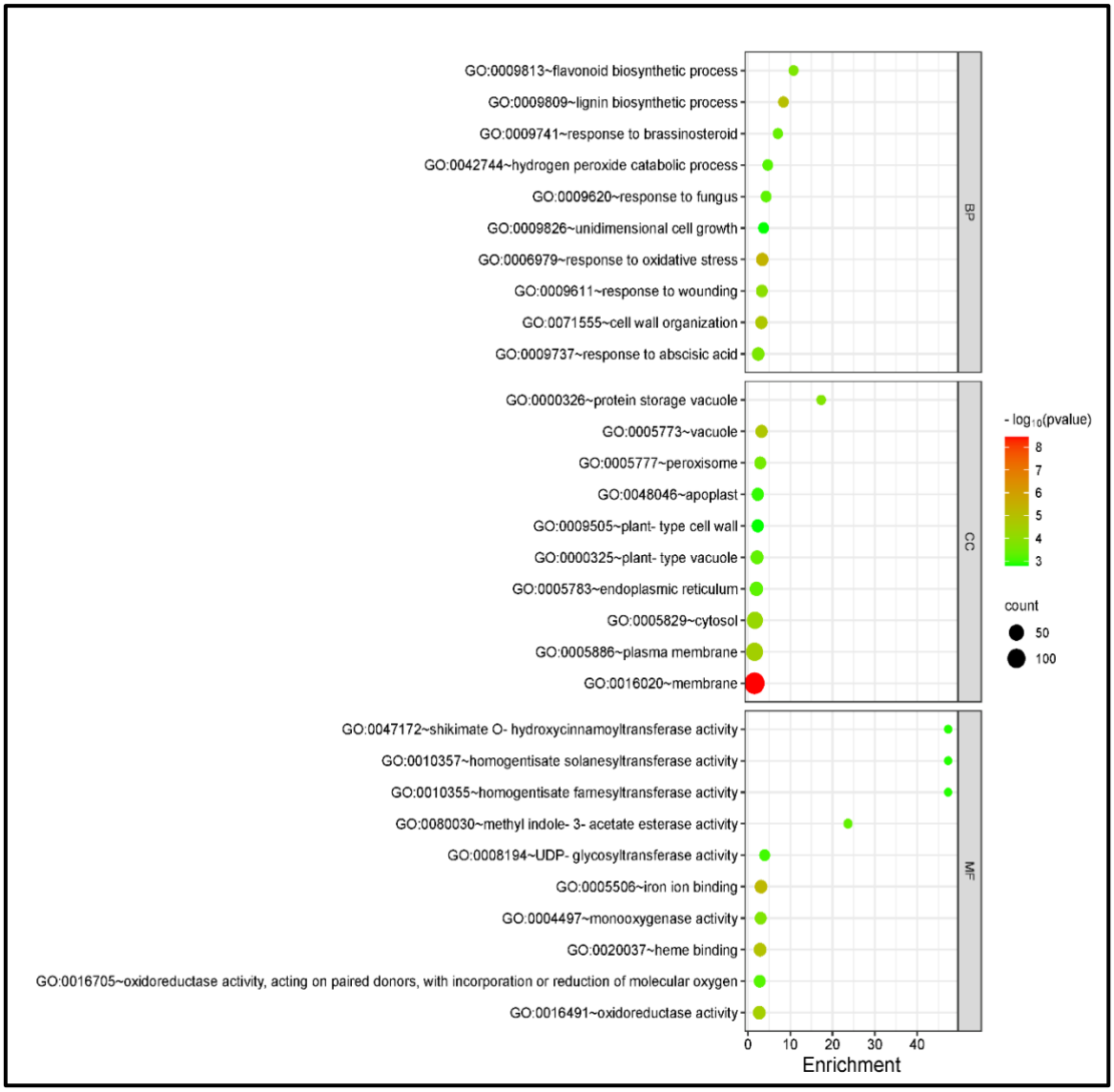

Figure 2.8: Gene ontology enrichment bubble plot of downregulated shared DEGs genes showing significantly enriched biological process, cellular component, and molecular function categories, with dot size indicating gene counts and colour representing adjusted *p*-values ($-\log_{10}$)

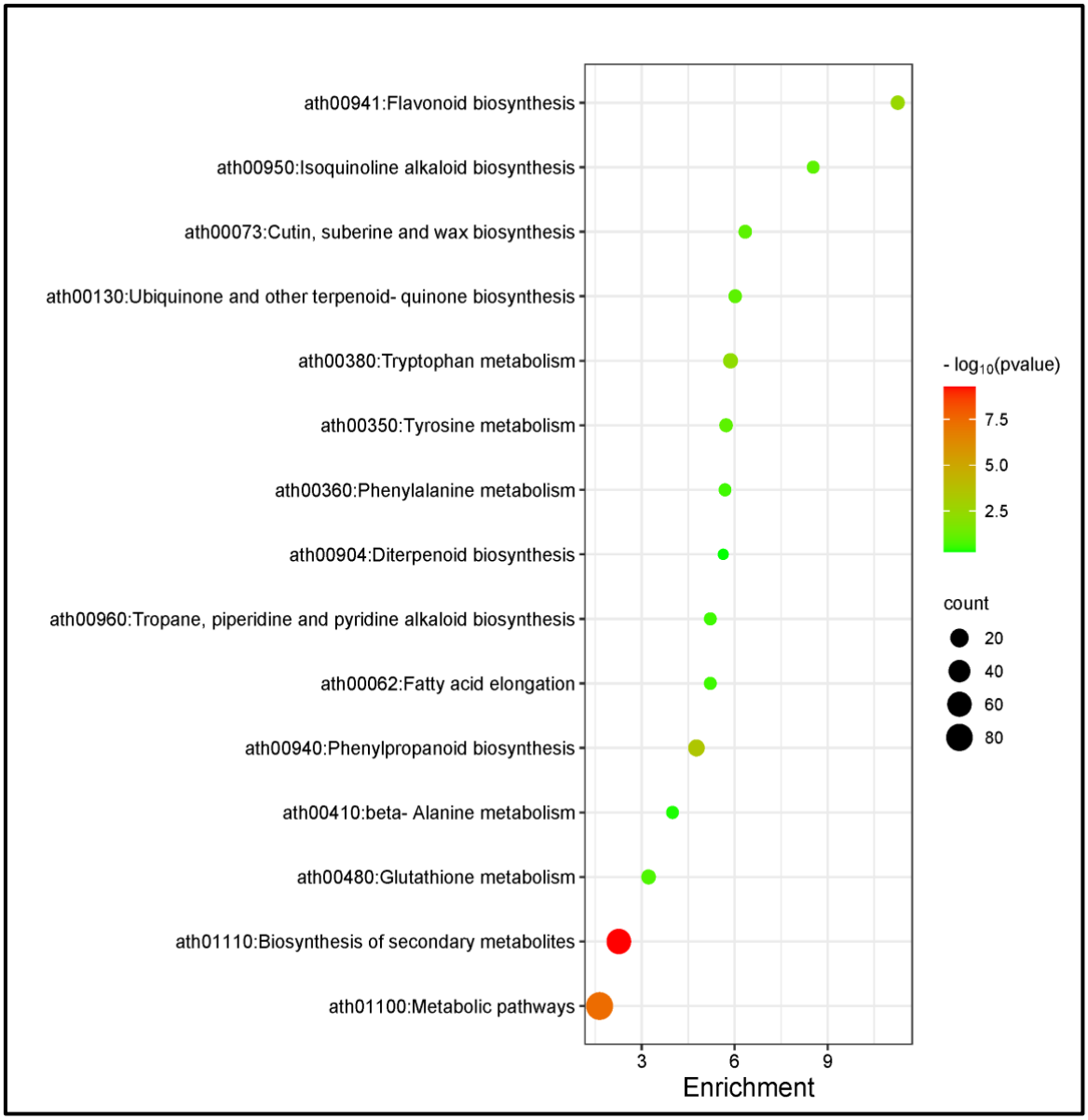

Figure 2.9: Bubble plot of downregulated shared DEGs genes showing significantly enriched KEGG pathways with dot size indicating gene counts and colour representing adjusted *p*-values ($-\log_{10}$)

Enrichment analysis using Metascape showed the heatmap mainly enriched vacuole organisation (GO:0007033), DNA-templated transcription (GO:0006351), regulation of flower development (GO: 0009909), response to heat (GO: 0009408), inorganic anion transport (GO: 0015698), and carboxylic acid transport (GO: 0046942) for upregulated DEGs. The heatmap for downregulated DEGs mainly enriched in secondary metabolic process (GO: 0019748), response to oxidative stress (GO: 0006979), lipid biosynthetic process (GO: 0008610), response to fatty acid (GO: 0070542), and cutin-based cuticle development. Several KEGG pathways were found enriched in downregulated DEGs including tryptophan metabolism (ath00380), cutin, suberine and wax biosynthesis (ath00073), isoquinoline alkaloid biosynthesis (ath00950), ubiquinone and other terpenoid-quinone biosynthesis (ath00130), and glucosinolate biosynthesis from aromatic amino acid (WP4598). Likewise, no KEGG pathway were detected for upregulated DEGs by Metascape. Figure 2.10 illustrates the function enrichment analyses for shared DEGs using Metascape software.

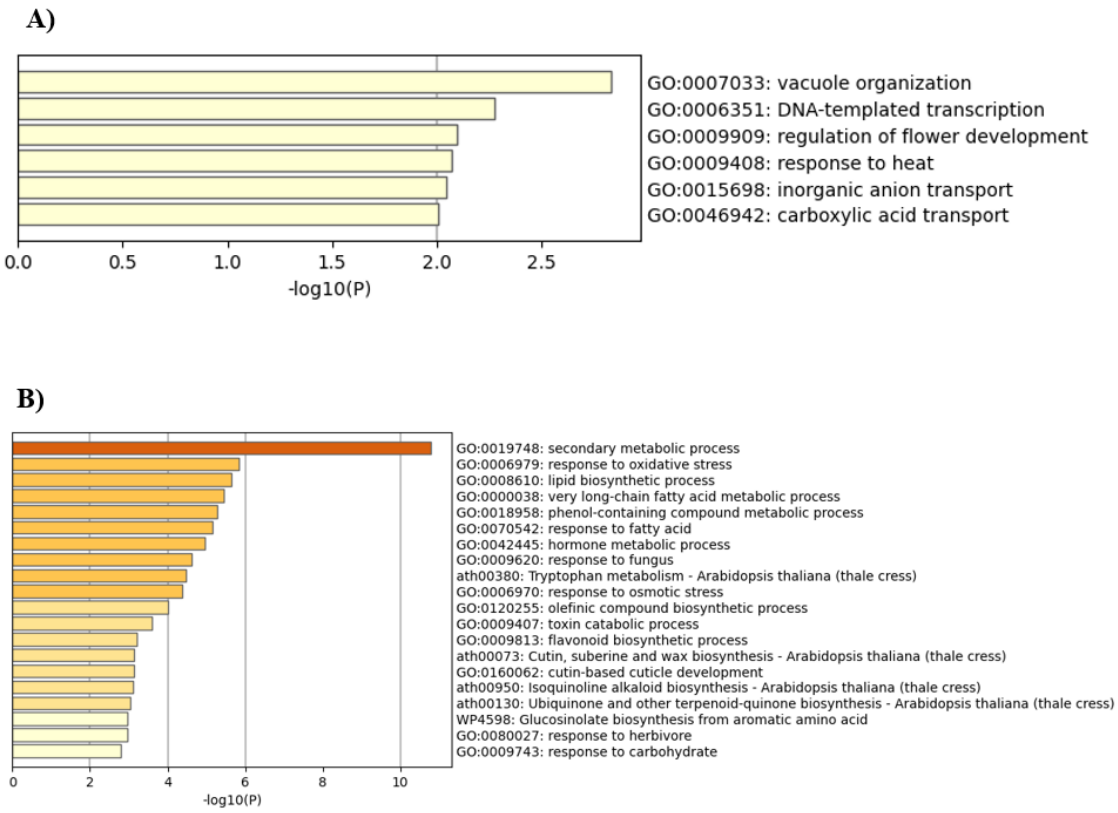

Figure 2.10: Functional enrichment analyses of upregulated and downregulated common DEGs in trunking sagu palms from different locations. A) Heatmap of enriched terms across upregulated DEGs. B) Heatmap of top 20 enriched terms across downregulated DEGs. Bar plot are coloured based on *p*-values. The darker the shades the more significant the expression level

2.3.5 PPI network analysis of DEGs

Considering the critical role of protein interactions in protein functions, the Protein-protein interaction (PPI) network analysis was conducted using Metascape software. The PPI analysis on upregulated shared DEGs contained 29 nodes and 39 edges. The Molecular Complex Detection (MCODE) screened out one cluster with four DEGs; AT1G67325, CSDP1, NRPD1B, and NRPB5. PPI on downregulated shared DEGs contained 185 nodes and 300 edges. The MCODE screened out five clusters. Cluster I contained 15 DEGs namely AT1G31690, GH9C2, BGLU12, BGLU29, AAT, AT2G22360, AT4G31140, AT3G52260, AT1G31710, AAS, RPL27, AT4G15630, ATOBGM, J11, and BGLU11. Cluster II contained six DEGs including KCS17, NRPB5, LDL2, KCS10, KCS6, and KCS1. The remaining clusters contained three DEGs each with STT3A, AT2G16210, and TRB1 (Cluster III), RWP1, FACT, and CYP704B1 (Cluster IV), EXO70B2, EXO70H1, and PUP3 for Cluster V. Figure 2.11 illustrates PPI network of both upregulated and downregulated shared DEGs.

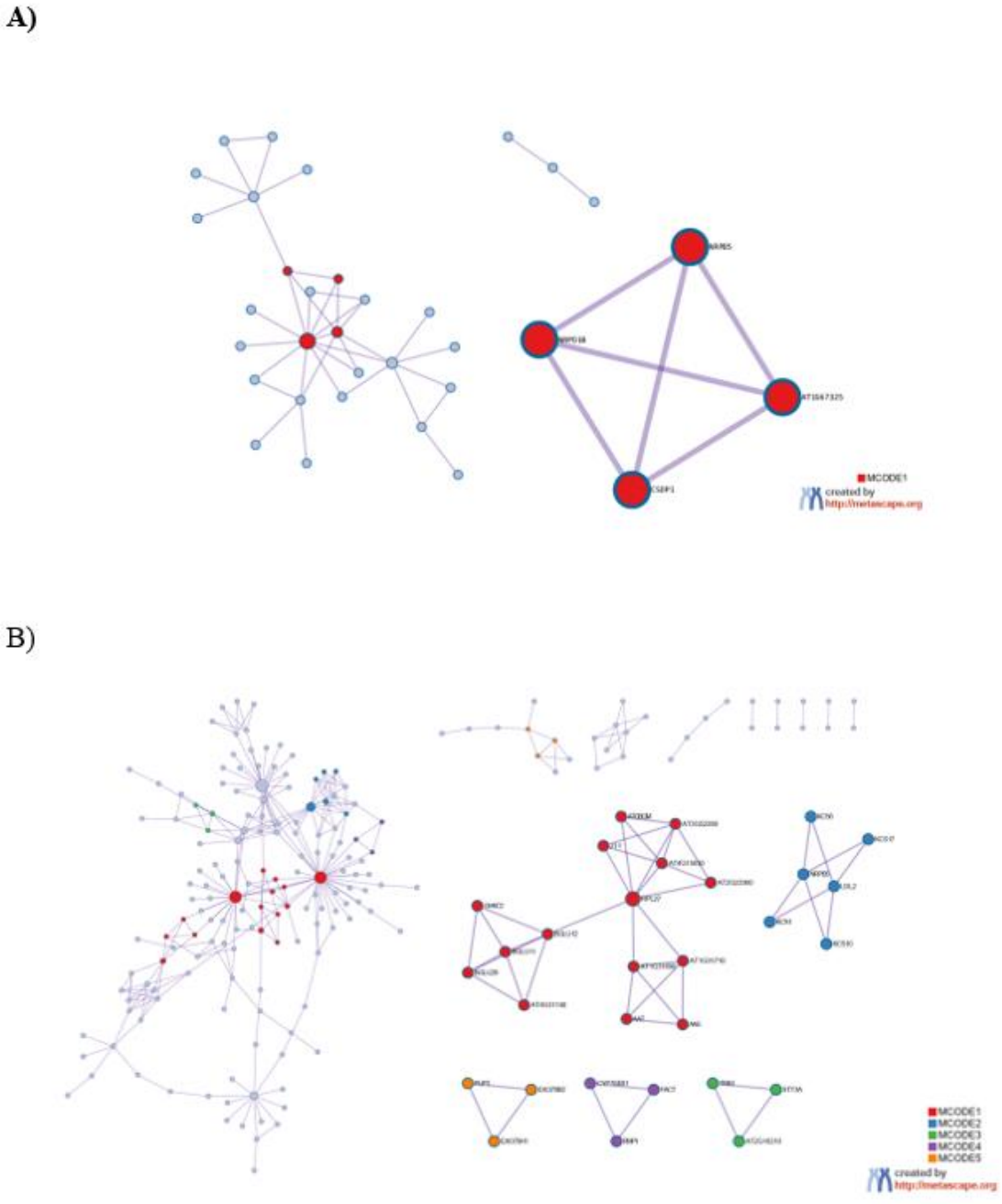

Figure 2.11: Interactome network and MCODE of A) 107 upregulated DEGs and B) 486 downregulated DEGs. Note that in the interactome network, the MCDOE complexes are coloured according to their identities

2.3.6 Transcription factors

A homology search of 595 shared DEGs with *Arabidopsis thaliana* genes identified 17 transcription factor families. Myeloblastosis (MYB), WRKY, DNA-binding One Zinc Finger (C2C2-Dof), and Cys2-His2 zinc-finger proteins (C2H2-ZF) transcription factor families were mostly expressed. Other expressed transcription factors were the MYB-related, bHLH, TCP, GRAS, LOB, bZIP, HB-HD-ZIP, NAC, HB-BELL, GARP-G2-like, and HSF. Interestingly, MYB, C2C2-Dof, and HSF transcription factors were found upregulated and downregulated in the expression.

2.3.7 Validation of DEGs

To validate the RNA-seq data, the expression profiles of selected DEGs (P32, P41, P51, and P58) were analysed using RT-qPCR. List of primers is tabulated in Table 2.9. The expression levels from each primer were normalised to a housekeeping gene Actin 2, and relative quantification was calculated using the $2^{-\Delta\Delta Ct}$ method. The RT-qPCR results generally corroborated with the RNA-seq expression patterns, with primers P32 and P41 corroborated with upregulated DEGs, while primers P51 and P58 corroborated with downregulated DEGs across Dalat, PPaloh and SgTalau populations. Minor qualitative differences observed between the two methods may be attributed to differences in sensitivity of machines used. Overall, the expression patterns confirmed by RT-qPCR support the transcriptomics findings and supports the reliability of the RNA-seq data. Figure 2.12 illustrates the expression fold changes between RNA-seq and RT-qPCR.

Figure 2.12: Validation of RNA-seq results by qPCR for four selected genes across Dalat, PPaloh, and SgTalau, showing A) $\log_2$ RT-qPCR ddct values and B) corresponding $\log_2$ RNA seq values with error bars indicating standard deviations

2.4 Discussion

2.4.1 Gene Ontology Terms of Upregulated DEGs

DAVID functional annotation revealed the top three molecular function GO terms of upregulated DEGs in trunking sago palm leaves were the 5S ribosomal RNA (rRNA) binding, binding to inositol hexaphosphate ($InsP_6$), and microRNA (miRNA) binding Meanwhile, the top three biological process GO terms were the RNA primers during DNA replication (GO: 0006269), the resolution of recombination intermediates (GO: 0071139) and polyphosphate biosynthesis process (GO: 0006799).

The 5S rRNA binding refers to the molecular function of binding to a 5S ribosomal RNA. Ribosomal 5S rRNA is an integral component of large ribosomal subunit essential for translating genetic information into proteins (Szymanski, 2002). In this work, Arabidospis Tóxicos en Levadura 5 (*ATL5*) was identified as the upregulated gene in this GO term. Belongs to the ATL family, a prominent Really Interesting New Gene (RING)-H2 finger protein which features a distinct RING zinc-finger domain (Han et al., 2022). There are several ATL members that have been reported to function in biotic and abiotic stress responses. For example, the AtATL2 is pathogen-induced and plays a role in salicylic acid- and jasmonic acid mediated defences, while the AtATL78 positively regulate drought stress response mediating abscisic acid (ABA)-dependent stomatal closure. However, most ATL family members have not been studied, and their functions remain unknown (He et al., 2023).

Previous work on *ATL5* was primarily reported in *Arabidopsis*. *AtATL5* was revealed to maintain *Arabidopsis* seed longevity by mediating degradation of Activator of Basal Transcription 1 (ABT1), minimising the negative effects caused by ABT1 (He et al., 2023). All ATLs share a common RING-H2 finger domain that facilitates the interaction of E3 ubiquitin ligases, which is responsible for degrading dysfunctional proteins in ubiquitin

proteasome system (UPS). This posttranslational protein modification process maintains protein balance and cellular homeostasis. The ubiquitination process is vastly studied where orchestration of ligases till E3 ligase recognise and ubiquitinate specific substrates to be processed by proteasomal degradation system. This protein degradation affects cellular activities including gene expression and signalling. Many studies have shown that RING-type E3 ligases are involved in regulating abiotic stress response such as drought and salt stress through ABA signalling. A work on a RING-type E3 ligase, salt-and drought-induced ring finger 1 (SDIR1) proved to be vital in abiotic stress and ABA signalling. SDIR1 functions as a positive regulator of ABA signalling binds to substrate of SDIR1-interacting protein 1 and modulates its turnover through the 26S proteasome system and promotes ABA-mediated responses via ABA-insensitive 3 (*ABI3*) and ABA-insensitive 5 (*ABI5*) transcription. Overexpressing SDIR1 in transgenic plants consistently mediates drought salt-stress response (Gao et al., 2011; Zhang et al., 2015). Additionally, another RING-type E3 ligase heat tolerance at seedling stage of *Oryza sativa* (*OsHTAS*) was shown to have positive effect on heat tolerance at early seedling stage by enhancing hydrogen peroxide induced stomatal closure. The increase in hydrogen peroxide in stomata aperture of rice leaves hence increased ABA biosynthesis (Liu et al., 2015; Sharma et al., 2016; Shu & Yang. 2017).

The upregulation of *ATL5* in trunking sago palms suggests a mechanism for maintaining protein turnover and cellular resilience under environmental stress. Although *ATL5* is not directly linked to trunk/stem development, its role in removal of misfolded or damaged proteins *via ATL5*-mediated degradation supports cellular homeostasis, conserves metabolic resources, and enables a dynamic remodelling of the proteome during plant growth and development. In parallel, ABA-mediated responses regulated by SDIR1 and *OsHTAS* enhance adaptive water conservation and oxidative stress tolerance, providing

protection and sustain the plant during water deficient stress. In contrast, reduced *ATL5* in non-trunking sago palms may suggests the palms are vulnerable to proteotoxic stress, limiting their ability to sustain trunk development and vertical growth.

The GO term of binding to inositol hexakisphosphate ($InsP_6$) also known as phytic acid is involved in cellular signalling such as RNA editing, DNA repair and protein-protein interactions. In this study, phosphate transporter (*PHO1*) was found upregulated in this GO term. Studies have found that the $InsP_6$ act as signalling molecules in various biological functions including phosphate homeostasis, immune responses, and hormone perception (Riemer et al., 2022). In leaves, $InsP_6$ was reported responsible to regulate stomata guard cells in response to ABA. For example, the application of ABA to *Solanum tuberosum* leaves significantly increase of $InsP_6$ levels in the plant's guard cells, which influenced the potassium currents ($I_{K,in}$), reducing K^+ ion flow into guard cells. This decreases guard cell turgor pressure subsequently close the plant stomata. This action is important to reduce water loss *via* transpiration and help plants to conserve water especially during drought stress (Lemtiri-Chlieh et al., 2000). *PHO1* functions to regulate Pi starvation responses. It translocate inorganic phosphate (Pi) from the root xylem to the shoot and is predominantly expressed in stomata guard cells (Xiao et al., 2022; Yang et al., 2024). Cryogenic electron microscopy (Cryo-EM) observed the binding of $InsP_6$ to the SPX domain of SPX-EXS family mediates dimerization and enhances AtPHO1:H1 activity acting like a 'channel-like' mechanism to transport Pi to enhance Pi homeostasis in *Arabidopsis* (Fang et al., 2025). Supporting evidence from rice revealed elevated *PHO1* in rice blade was shown to increase Pi acquisition to leaf and enhance photosynthesis rate, subsequently increase grain filling in rice (Ma et al., 2024). While *PHO1* is primarily known for phosphate transport, its SPX domain interaction with $InsP_6$ influence phosphate signalling pathways in ABA-mediated

stomatal closure. This is shown where experiment conducted on allelic mutants of *pho1.2* and *pho1.4* in *Arabidopsis* leaves found that the stomata apertures stay wide despite treatment with ABA despite sufficient Pi level (Zimmerli et al., 2012; Bechtaoui et al., 2021). The binding of $InsP_6$ to SPX domain of PHO1 play a role in Pi acquisition and stomatal regulation. The stomatal regulation helped in maintaining both photosynthesis and transpiration rate, crucial for plant adaptability toward environmental response (Land et al., 2021).

The upregulation of *PHO1* and its $InsP_6$-mediated regulation suggests a shift toward enhanced phosphate homeostasis and ABA–responsive stomatal control in trunking sago palms during drought stress. While $InsP_6$ promotes stomatal closure by reducing K^+ ion flow into guard cells, decreasing their turgor pressure, the *PHO1* facilitates the export of Pi from root cells into the xylem, ensuring Pi delivery to the leaves (Ma et al., 2024). Adequate Pi availability in leaves is crucial for adenosine triphosphate (ATP) synthesis *via* photophosphorylation, supports nicotinamide adenine dinucleotide phosphate (NADPH) production during light-dependent reactions, and activation of Rubisco as well as regeneration of ribulose-1,5-biphosphate (RuBP) in the Calvin cycle (Yan et al., 2022). These processes enhance carbon fixation efficiency, leading to higher net photosynthetic rates. Increased photosynthesis promotes carbohydrates accumulation, which can translocated to stem tissues to support starch deposition and structural development within the trunk. Thus, sufficient Pi availability not only sustains the biochemical machinery of photosynthesis but also provides the metabolic foundation for trunk development, linking molecular regulation in leaves to the emergence of the trunk formation (Suzuki et al., 2022). The coordinated roles of water conservation and nutrient transport in trunking sago palms suggest a physiological strategy that maintains photosynthetic capacity and cellular function

under environmental stress, contributing to growth, development, and structural resilience. Comparatively, non-trunking palms may lack efficient regulation of *PHO1* and $InsP_6$ pathways, resulting in reduced Pi transport and less effective stomatal control. This deficiency would compromise ATP and NADPH production, limit carbon fixation, and restrict carbohydrate allocation to stem tissues.

In the GO term associated with microRNA (miRNA) binding, Argonaute 10 (*AGO 10*) was significantly expressed in the GO term. The upregulation of *AGO10* gene in trunking sago palms suggests a multifaceted role in supporting the sago palm's growth and developmental stability. *AGO10* is involved in plant development, where it modulates the expression of certain transcription factors, preventing their excessive activity, which otherwise lead to growth defects. Functionally, *AGO10* sequesters microRNAs miR166/165 preventing repression of HD-ZIP III transcription factors activity. This regulation is critical for maintaining the integrity and activity of the SAM, essential for continuous stem elongation and initiation of vascular tissues essential for trunk formation (Zhu et al., 2011; Jiang et al., 2015; Ma et al., 2017). In contrast, the reduced expression of *AGO10* in non-trunking sago palms may suggest excessive transcription factor activity which could impair SAM function. Study in *Arabidopsis* observed loss of *AGO10* function led to abnormal SAM growth resulting in stunted growth due to mis regulation of HD-ZIP III transcription factors (Zhu et al., 2011). Beyond meristem maintenance, *AGO10* contributes to stress resilience by modulating transcription factor activity under adverse conditions. The transcription factor LBD12-1 is often upregulated during stress, leading to negative growth effects, including stunted growth, twisted leaves, abnormal anthers, and reduced SAM size. A study on *Oryza sativa* overexpressing LBD12-1 due to salt stress found that overexpression of AGO10 helped counteract these negative effects by maintaining proper SAM development (Ma et

al., 2017). Limiting the overexpression of factors such as LBD12-1 prevents maladaptive developmental shifts that could otherwise destabilise growth development. This buffering capacity highlights *AGO10* role as a fine-tuner of transcriptional networks, ensuring developmental plasticity without sacrificing structural stability.

Both miRNA and argonaute proteins (AGOs) are the central components in RNA interference. AGOs interact with miRNAs and guide miRNAs to specific target sites located in the 3' untranslated region (UTR) of target messenger RNA (mRNA) leading to translational repression and deadenylation-induced mRNA degradation (O'Brien et al., 2018). *AGO10* also plays a role in antiviral defence by participating in RNA silencing pathways that degrade viral RNAs and reduce biotic stress. This RNA silencing plays a crucial role in the defence mechanism against invading viruses in plants. Studies have shown that AGOs are key player in the plant's adaptive defence system against viral infections. Upon viral infections, plant induces sequence-specific RNA silencing, which triggered by self-folded viral genome, or double-stranded RNAs (dsRNAs) replication intermediates produced during replication. Plant dicer-like proteins (DCLs) break down the viral dsRNAs into small fragments, known as virus-derived small interfering RNAs (vsiRNAs). These vsiRNAs are recruited by AGOs forming RNA-induced silencing complexes (RISCs). The RISCs then identify and neutralise matching viral RNA by either cutting or blocking its translation, suppressing the virus from spreading. Each AGO protein family has its own virus-specific role in RNA virus defence. Studies reported that this argonaute protein (AGO10) help protect plants against *Bamboo mosaic* virus (BaMV) and *Turnip mosaic virus* (TuMV) infections in *Nicotioana benthamiana* and *Arabidopsis*, respectively (Garcia-Ruiz et al., 2015; Huang et al., 2019). Collectively, the upregulation of *AGO10* likely serves a molecular link between post-transcriptional regulation and the developmental processes

underpinning trunk formation in sago palms as well as serving as defence mechanism against viral infection.

The synthesis of RNA primers and the resolution of recombination intermediates are interconnected processes in DNA synthesis. These RNA primers provide the necessary 3'-hydroxyl termini for the elongation of the new DNA strand. This step is crucial as DNA polymerases cannot initiate synthesis *de novo*. The accurate and timely synthesis of RNA primers ensure proper initiation and progression of DNA replication (Zhang et al., 2024). Meanwhile, the resolution of recombination intermediates refers to the cleaving of intermediates such as Holliday junctions, formed during homologous recombination repair of double-strand breaks to repair DNA damage. Subsequent dissolution of intermediate is essential for correct chromosome separation and cell survival. In plants, BLM- TOP3α-RMI1 (BTR) complex dissolves Holliday junction (Hartung et al., 2008). The C-terminal domain of TOP3α contains zinc finger domains, which are crucial for its DNA binding and catalytic activities. This interaction is vital for resolution of these intermediates, ensuring accurate segregation of chromosomes and the repair of DNA double-strand breaks. This process ensures that genetic material is correctly exchanged and that two intact DNA molecules are produced (Dorn et al., 2018).

The gene enriched in the synthesis of RNA primers during DNA replication GO term was the RanBP2-type zinc finger protein (*Atg67325*). Although diversely distributed in plants, RanBP2-type zinc finger protein functions in plants remain largely unknown (Gao et al., 2022). Phylogenetic analysis of Arabidopsis proteins carrying RanBP2 zinc fingers revealed same grouping of the At1g67325 domain with known human Znf Ran binding domain-containing protein 2 (ZRANB2). The ZRANB2 is a splicing factor that involves in DNA damage response, ensuring correct splicing to maintain proper function of proteins

during replication stress (Tanaka et al., 2020). The RanBP2-Znf protein is prevalent in both organelle zinc finger 1 (OZ1) and organelle zinc finger 2 (OZ2). These domains specifically bind to single stranded RNA containing GGU motif (Loughlin et al., 2009). The high expression of RanBP2-type zinc finger proteins suggests an enhanced genome integrity and stress resilience in trunking sago palms. These proteins are known to participate in DNA replication fidelity, repair of strand breaks, and RNA editing, mitigating genotoxic stress and ensuring stable cellular function (Lu et al., 2022). Studies have shown that the RanBP2-Znf are crucial for RNA editing, specifically converting cytidine (C) to uridine (U) in chloroplasts to enable the plant to adapt to different conditions and maintain chloroplast function (Mohammed et al., 2022). In absence of such editing, misfolded or truncated proteins would compromise the assembly of photosynthetic complexes Photosystem I and II, ATP synthase, and electron transport chain components, all of which are necessary for photophosphorylation, leading to reduced efficiency and heightened susceptibility to photodamage. This process drives the production of adenosine triphosphate (ATP), and nicotamide adenine dinucleotide phosphate (NADPH) in the Calvin cycle (Caffarri et al., 2014; Sreeharsha & Mohan, 2024). This can be seen in the impaired RNA editing *Arabidopsis*, rice and *Zea mays* which exhibit severe chlorosis due to lack in chloroplast pigmentations (Wang et al., 2021; Gipson et al., 2022; Hua et al., 2024; Wang et al., 2025). Another study on *oz2* mutants found splicing defects of *nad* (NADH dehydrogenase) transcripts which resulted in reduced respiratory ability in *oz2* mutants' plants. The impairments of RanBP2-Znf domains in the OZs resulted in morphological alterations to the mutant plants including delayed plant development (Bentolila et al., 2021). Research has revealed *RanBP2-Znf* genes in tomato (*Solanum lycopersicum*) were induced after drought treatment, while the *RanBP2-Znf* genes in *Populus alba* were upregulated in the leaves of

salt-treated Populus seedlings (Gao et al., 2022; Bian et al., 2024). Such high expression of RanBP2-Znf activity during abiotic stresses postulated this protein protects against photoinhibition and oxidative stress, maintaining leaf vitality under fluctuating environmental conditions, resulting in sustainable photosynthetic output and carbohydrate accumulation. Such resilience is essential for trunk development, as assimilates from photosynthesis must be translocated to stem tissues for starch deposition and vascular reinforcement. By contrast, in non-trunking sago palms with reduced RanBP2-Znf expression likely to experience inefficient RNA editing, resulting in defective assembly of photosynthetic complexes, reduced ATP/NADPH production, and ultimately compromised carbon fixation.

The gene significantly upregulated in relation to the resolution of recombination intermediates is the Zinc transporter 4 (*Zip4*). Zip4 protein is actively required for normal progression of synapsis and 95% of crossovers during meiosis (Draeger et al., 2023). Study on *Tazip4-B2* mutant demonstrated reduced size in wheat pollen grain and reduced grain number (Alabdullah et al., 2021). Conversely, in this study, leaf tissue (somatic cells) was experimented. To date, no study has been reported on the ZIP4 protein involved in mitosis. However, studies have documented that ZIP4 is involved in Zn uptake and transport across the cell membrane. Zinc ions (Zn^{2+}) are crucial for Zn homeostasis in plants. Although there is no direct information on ZIP4 supplying Zn^{2+} ions to zinc finger, Zn^{2+} ions is crucial to maintain structural integrity of Zn finger proteins. The upregulation of *Zip4* in trunking sago palms may suggests the maintenance of C-terminal zinc domain of TOP3α, which plays a pivotal role in resolving DNA intermediate resolution, thus maintaining genome stability in photosynthetic organs (Han et al., 2020; Kiori et al., 2024). Displacement of zinc by metals such as cadmium or cobalt, disrupt zinc finger structure and interferes with cellular

processes, including genomic integrity (Hartwig, 2001). This is supported by a study in *Arabidopsis*, which showed that the deletion of the C-terminal zinc finger TOP3α impairs its activity, leading to dwarfism, fasciated organs, and increased cell death within the root meristem. The observation indicates the role of zinc and zinc finger of TOP3α in DNA repair by promoting dissolution of intermediates like Holliday junctions (Dorn et al., 2018). Similarly, TOP3α mutant in tomato lead to embryo lethality due to accumulation of unresolved aberrant replication intermediates (Whitbread et al., 2021). Additionally, there are numerous studies reporting detrimental effects in Zn-deficit plants including smaller leaf size, withered stems, and senescence within young leaves (Hamzah Saleem et al., 2022). Adequate zinc supply mediated by *Zip4* ensures proper folding and catalytic activity of Zn finger proteins, safeguarding chloroplast DNA under high UV-B stress (Chen et al., 2022). This protection is particularly important in photosynthetic organs where chloroplast DNA is highly vulnerable to oxidative stress and photodamage, thereby sustaining photosynthetic capacity in trunking sago palm leaves. This molecular resilience at leaf level supports leaf vitality and continuous assimilate production, which is essential for sustaining active shoot apical meristem (SAM) activity and vertical growth (Cao et al., 2025). Conversely in non-trunking sago palms, the plant is portrayed to suffers from impaired zinc transport, leading to destabilisation of zinc finger domains, resulting to inefficient DNA repair, and defective chloroplast transcript processing. Therefore, the elevated expression of *Zip4* in trunking sago palms highlights a multilayered resilience strategy that integrates stabilisation of genome integrity, protection of chloroplast functions, and sustained photosynthetic performance.

Similar to its role in the binding to $InsP_6$, the polyphosphate biosynthesis biological process GO term revealed phosphate transporter (*PHO1*) was significantly upregulated. Polyphosphate (polyP) biosynthesis involves in the synthesis of long chains of phosphate

molecules which closely linked to phosphate transport and availability. While PHO1 do not directly involve in polyP biosynthesis, the transport of Pi and adequate Pi availability is crucial in polyP synthesis. PolyP biosynthesis is driven by linking Pi into long-chain polyP molecules by polyphosphate kinases (PPKs). The polyP plays a crucial role against stress responses and act as storage form of phosphorus, providing energy source during limited Pi availability (Guan et al., 2023).

The Metascape analysis revealed vacuole organisation or vacuole biogenesis GO term was expressed in all trunking leaf samples. In this study, Sec1/munc18-like (SM) proteins superfamily (ATVPS33), autophagy-related protein (ATG11), and Lazarus1 homolog1 (LAZ1H1) were expressed suggesting an enhanced vacuolar biogenesis in trunking sago palm leaves. The SM protein, a Homotypic fusion and Vacuolar Protein Sorting (HOPS) complex, mediates vacuole fusion in plants by interacting with Soluble NSF Attachment Protein Receptor proteins (SNAREs) (Brillada et al., 2018). The ATG11 initiates autophagosome formation which fused with plant vacuole releasing its digestion content (Kang et al., 2018). The LAZ1H1, a novel tonoplast-localised proteins play a significant role in maintaining vacuole integrity and brassinosteroid signalling at the tonoplast (Martins et al., 2015). Studies have shown that vacuoles play a crucial role in against abiotic and biotic stress responses in plants by maintaining intracellular environment through detoxification, nutrient cycling, and hormonal signalling (Cui et al., 2020). This measure was reported to enhanced salt and drought stress in tobacco, *Arabidopsis*, and maize plants (Jiang et al., 2021). The upregulated genes involve in vacuole biogenesis suggests enhancing the ability of the plant to adapt to multitude stress and supporting the plant growth and development (Cui et al., 2020; Liu et al., 2022). Beyond providing structural shape to the cell, vacuoles are also critical for the storage of excess Pi. During periods of Pi

abundance, vacuoles sequester the excess, thereby controlling the cytosolic Pi levels, preventing cytotoxicity, and maintaining cellular homeostasis (Yang et al., 2017; Guo et al., 2025). This vacuolar buffering capacity is postulated to complements the upregulation of *PHO1*, that facilitates Pi transport across membranes. Together, the coordinated upregulation of *PHO1* and vacuole biogenesis genes suggests a dual strategy in trunking sago palms i.e. facilitating efficient Pi transport and enhanced vacuolar Pi storage capacity. This integrated phosphate management not only supports stress adaptability but also ensures a continuous supply of energy and carbohydrates to fuel cell division and expansion in internodes, sustaining persistent meristem activity, thereby contributing to trunking formation (Guan et al., 2023).

In summary, the upregulated genes in trunking sago palm leaves revealed a coordinated molecular strategy that sustains trunk formation under stress. *ATL5* support proteostasis through protein degradation, *PHO1* and $InsP_6$-mediated regulation enhance phosphate transport and photosynthesis, and vacuole biogenesis buffers excess Pi to maintain homeostasis. *AGO10* secures shoot apical meristem integrity and developmental stability, while RanBP2-type zinc finger proteins and *Zip4* reinforce genome stability through RNA editing. Together, these genes sustain photosynthetic efficiency, metabolic resource allocation, and shoot apical meristem integrity, enabling persistent stem elongation and expansion. Meanwhile in non-trunking sago palms, downregulation of the above genes making the sago palms vulnerable to proteotoxic stress, reduced energy production, defective DNA repair and chloroplast transcript processing, thereby leading to reduced photosynthesis rate.

2.4.2 Downregulated KEGG pathways involved in reduced lignin and flavonoids biosynthesis

Most of the KEGG pathways associated with the downregulated DEGs fall under the main metabolism category. The enriched KEGG pathways of downregulated DEGs from trunking sago palm leaves were the biosynthesis of secondary metabolites (ath01110), metabolic pathways (ath01100), phenylpropanoid biosynthesis (ath00940), and flavonoid biosynthesis (ath00941). These pathways are known to biosynthesise plant secondary metabolites such as terpenoids, phenolic compounds, alkaloids, and sulphur. These compounds contribute to organisms' homeostasis and are responsible for plant growth, development, adaptation and reproduction (Jan et al., 2021). Given the extensive pathway map for biosynthesis of secondary metabolites and metabolic pathways, only phenylpropanoid biosynthesis and flavonoids biosynthesis pathways were discussed.

The downregulation of phenylpropanoid biosynthesis pathways observed in this study is complementary to the previous study, where phenylpropanoid biosynthesis was reported significantly upregulated in the non-trunking sago palms (Yan, 2023, unpublished data). The phenylpropanoid metabolic pathway mainly involves the *PAL*, *C4H*, and *4CL* genes. *PAL*, gene located at the beginning of this pathway determines the metabolic flow of the entire pathway, while the *4CL* regulates the formation of coumaroyl-CoA, caffeoyl-CoA, and feruloyl-CoA, which determines the synthesis of lignin precursors (Rahim et al., 2023). According to the results, most DEGs transcribed in the phenylpropanoid biosynthesis pathway belong to peroxidases like peroxidase 3, 12, 37, 51, 52, and 72 and lignin biosynthesis enzymes such as caffeoyl-CoA-methyltransferase 1 (*CCoAOMT1*), flavone 3'-O-methyltransferase (*OMT1*), 4-coumarate—CoA ligase 2 (*4CL2*), 4-coumarate—CoA ligase 3 (*4CL3*), homogentisate solanesyltransferase (*HST*), and cinnamoyl-CoA reductase

1 (*CCR1*) were downregulated in trunking sago palm leaves. These genes catalyse reactions producing the monolignol precursors used in lignin biosynthesis. Despite previous research have reported dwarfism among lignin-deficient plants, downregulation of enzymes in lignin biosynthesis did not result dwarfism in the experimented plants. This observation aligns with the findings in mutant 4CL-cinnamoyl-CoA reductase (*4cl- ccr*) tobacco, where no visible morphological abnormalities were reported, and the plants maintained a normal phenotype (Chabannes et al., 2001; Xie et al., 2019). This suggests that the downregulation of enzymes related to lignin biosynthesis may be linked to the biosynthesis of other compounds/products. Research suggests that reduced lignification does not directly caused dwarfism in plants. Instead, the downregulation of certain enzymes in phenylpropanoid pathway caused hypo- and hyper-accumulation of intermediates such as cinnamate-derived compounds due to reduced C4H enzyme activity. The fluxes in this phenylpropanoid pathway affect auxin transport and signalling, leading to impaired auxin signalling causing dwarfism as observed in *ref3-2* mutants (Muro-Villanueva et al., 2019). Other studies have shown that decrease in lignin biosynthesis was due to increase in cellulose content whereby a 45% reduction in lignin was shown to increase cellulose and hemicellulose content by 17-57% (Hu et al., 1999; VanAcker et al., 2013; Shigeto et al., 2015). This shift in the lignin-to-carbohydrate ratio is associated with enhanced growth of all vegetative organs (Hu et al., 1999). The inhibition of lignin biosynthesis was found to increase cell expansion and carbohydrate accumulation in *Ipomoea batatas* (Liang et al., 2023). Moreover, the reduction of lignin content in leaves was reported beneficial against viral infection as shown in cotton leaves, which showed to have enhanced resistance to soil-borne fungus *Verticilium dahliae* (Xiao et al., 2021). Similarly, antimicrobial protection is better in reduced lignin leaves as this allows better

antimicrobial compound penetration leaving the plant resistant to bacterial infections (Saberi Riseh et al., 2024).

Enzymes such as flavonoid 3'-monooxygenase (*CYP75B1*), chalcone—flavone isomerase 1 (*CHI1*), *CCoAOMT1*, LRR receptor-like serine/threonine-protein kinase FLS2 (*FLS2*), *HST*, and chalcone synthase (*CHS*) were expressed in flavonoid biosynthesis. The deviation towards flavonoid biosynthesis instead of lignin biosynthesis is mediated by *CHS*, which catalyses the formation of naringenin chalcone. Naringenin chalcone isomerise to flavanone naringenin via CHI while enzyme CYP75B1 diversifies the types of flavonoids synthesised (Hassani et al., 2020). Downregulation of CHS resulted in reduced flavonoid biosynthesis and were observed to cause major changes in plants growth and development. For example, downregulation in apple leaf metabolism, resulted in significant alterations to apple plant structure including reduced leaf size and extreme shortened internodes (Dare et al., 2013). Conversely to apple plants, flax plants were not affected by *CHS* downregulation. Instead, flax stem was observed enlarged by two-fold accompanied with increased level of cellulose and hemicellulose (Zuk et al., 2016). Meanwhile, the silencing of *chs* in flax induces signal transduction cascade that leads to extensive modification in flax metabolism and caused flavone levels to peak during flower initiation stage (Zuk et al., 2019).

The downregulation of lignin biosynthesis enzymes in trunking sago palm leaves suggests enhanced cell wall plasticity and flexibility through the synthesis of cellulose and hemicellulose (Ain et al., 2022). The cellulose microfibrils providing structural reinforcement, while hemicelluloses contribute to cell wall loosening provide extensible walls that maintain tensile strength while maintain cell elasticity and vertical growth. The hemicellulose such as xyloglucan play a central role by cross-linking cellulose microfibrils, and its remodelling of tissue matrix by endotransglucosylase/hydrolase (XTHs) loosen the

matrix by enabling microfibrils to slide past one another under turgor pressure. (Bi et al., 2024). This dynamic process facilitates cell elongation and expansion, creating a structural environment that is capable to accommodate the continuous influx of photosynthates (Bi et al., 2024). Reduced lignification, combined with Pi transport and vacuolar buffering sustain assimilate production in leaves and cell expansion mediated by XTHs supports persistent meristem activity, internode elongation and ultimately trunk formation.

In parallel, the downregulation of flavonoid biosynthesis, suggest a reallocation of metabolic resources toward primary growth and carbohydrate accumulation (Li et al., 2021). This pathway competes with central carbon metabolism for key precursors such as phenylalanine, malonyl-CoA, and hexose phosphates, and its downregulation may redirect metabolic flux toward sucrose and structural carbohydrate synthesis (Li et al., 2021). Downregulation of the flavonoid biosynthesis genes, including CHS, CHI1, and CYP75B1, reduces the diversion of carbon skeletons and energy into secondary metabolite production, increasing the availability of UDP-sugars and nucleotide sugars like UDP-xylose for cell wall polysaccharide biosynthesis. This deviation of carbon flux promotes the accumulation of soluble sugars, starch, and structural carbohydrates, supporting energy storage and biomass buildup. Moreover, under nutrient deficiency environment such as nitrogen, the synthesis is nitrogen-rich compounds like proteins is restricted, further enhance the diversion of excess photosynthates into non-structural carbohydrates, which can be mobilised to support plant growth (Luo et al., 2022). This shift in carbon allocation contributes downregulation of flavonoid biosynthesis and favours carbohydrate accumulation. Study reported flavonoids particularly flavonols such as quercetin and kaempferol are known to inhibit auxin transport proteins namely the PIN-FORMED (PIN) proteins and ATP-binding cassette subfamily B (ABCB)/ P-glycoprotein (PGP) transporters (Teale et al., 2021). The

reduced level of flavonoids shown in trunking sago palm leaves suggests enhanced basipetal polar auxin transport from leaf tissue to trunk and root. This boost sink strength, facilitating carbohydrates unloading to sink organs, hence supporting cell expansion and increase biomass accumulation, potentially enhanced leaf and trunk development (Xiong & Jiao, 2019).

In summary, the downregulation of both lignin and flavonoid biosynthesis in trunking sago palms suggest a strategic conservation of metabolic energy, enhanced cell expansion *via* turgor-driven cell wall loosening, structural reinforcement through cellulose and hemicellulose deposition, and carbohydrate accumulation responsible for biomass buildup. Reduced flavonoid synthesis suggests increased carbohydrate biosynthesis and alleviates inhibition of auxin transport, strengthening sink capacity. The reprogramming by XTHs activity and microfibril slippage ensures cell wall remains flexible allowing cell enlargement while maintaining structural integrity. Together, the downregulation of lignin and flavonoid biosynthesis supports cell expansion, efficient assimilate translocation and biomass buildup, hence contributing to trunk formation in sago palms. Contrarily, the upregulation of lignin and flavonoid biosynthesis in non-trunking sago palms diverts metabolic energy toward secondary wall thickening, restricting cell wall flexibility, and impairs auxin transport. This metabolic constraint resulting to limited cell expansion and ultimately leading to dwarfism among non-trunking sago palms.

2.4.3 MCODE of PPI network

Proteins identified upregulated by MCODE were the RanBP2-type zinc finger protein (AT167325), cold shock domain protein 1 (CSDP1), and DNA-directed RNA polymerases II and IV subunit 5A (NRPB5). Meanwhile, the downregulated genes identified

by MCODEs 1 till 5 were involve in lignin biosynthesis. Thus, only upregulated genes determined by MCODE is discussed.

The upregulation of proteins in the PPI network highlights a coordinated enhancement in genome stability, transcript integrity, and stress resilience. The RNA editing in chloroplasts and mitochondria by RanBP2-Znf play a crucial role in ensuring RNA stability by correcting genomic mutations (Wang et al., 2025). Meanwhile the CSP1, belongs to the cold shock protein (CSP) family, facilitates stress-adaptive translations acting as mRNA chaperones, enabling efficient protein synthesis (Yang et al., 2024). Research have shown that overexpression of CSPs improved drought tolerance in wheat and *Arabidopsis thaliana* (Juntawong et al., 2013; Yu et al., 2017). Lastly, the NRPD1B, a key subunit of plant nuclear RNA polymerase IVb (Pol IVb) and Pol V is involved in the RNA-directed DNA methylation (RdDM) pathway. This RNA polymerase produced small interfering RNAs (siRNAs) that guide *de novo* DNA methylation at transposable elements (TEs) and repetitive sequences, thus lead to silencing of potentially disruptive genomic regions (Zhang et al., 2020). This epigenetic regulation is crucial for maintaining genome integrity especially during cell proliferation and organogenesis, preventing transcriptional noise and ensures proper gene expression, hence prevents abnormal plant growth (Kryovrysanaki et al., 2022).

The proteins within the PPI network in trunking sago palms highlights a coordinated enhancement of genome stability, transcript integrity, and stress resilience. RNA editing by RanBP2-Znf in chloroplasts and mitochondria ensures transcript fidelity by correcting genomic mutations, supporting photosynthesis rate and energy production. In parallel, the CSP1, which acts as an mRNA chaperone facilitate stress-adaptive translation to ensure continuous protein synthesis. This molecular mechanism is further reinforced by NRPD1B-meidated RNA-directed DNA methylation (RdDM), which silences transposable elements

and repetitive sequences, thereby preserving genomic integrity. Such epigenetic regulation prevents transcriptional noise and aberrant gene expression. The interrelation of these proteins reflects efficient developmental strategy of trunking sago palms.

2.4.4 Expression of transcription factors in sago palm leaves

Transcription factors is crucial in regulating plant growth, development and environmental adaptation of plants. They are essential for transcriptional control in cell, performing four key functions: DNA binding, transcription activation or repression, nuclear localisation, and oligomerisation. These factors drive changes in gene expression that are fundamental for cell fate transitions and environmental responses. In this study, several TFs were found significantly expressed, including MYB, WRKY, C2C2-Dof, C2C2-ZF, MYB-related, bZIP, NAC, and HSF.

The MYB TFs are among the largest families of TFs in plants, significantly influencing various aspects of plant growth and development, including synthesis of secondary metabolites, regulation of cell cycle, and responses to environmental stressors. Previous research shown that most MYB TFs are primarily involved in stress tolerance, particularly in response to drought and salinity stress via regulation of ABA pathway. For instance, in *Arabidopsis*, *AtMYB60* and *AtMYB96* have been shown to regulate stomatal movements and activate the transcription of epidermal wax biosynthesis under drought conditions (Li et al., 2019). Additionally, R2R3-MYB TFs such as *AtMYB44* and *AtMYB2* (*Arabidopsis*), *VhMYB2* (*Vitis vinifera*), and *BnMYB44* (*Brasicca napus*) are induced under salt-stress conditions (Shamloo-Dashtpagerdi et al., 2018; Wang et al., 2021; Ren et al., 2023). The MYB TFs are also reported to involve in DNA damage responses caused by UV radiation, reactive oxygen species (ROS), and genotoxic chemicals. Damage response activates the DNA damage response (DDR) pathways that inhibits the cyclin-dependent

kinase (CDK) activity, leading to cell cycle arrest for DNA repair (Gentric et al., 2021). The cell cycle inhibition results to the accumulation of repressor-type MYBs (Rep-MYBs) such as MYB3R3, MYB3R5, and R1R2R3 (Chen et al., 2017). Rep-MYBs form a complex with retinoblastoma-related protein and E2F TFs, known as the DREAM complex, which act as the master regulator of somatic DNA-repair. The Rep-MYBs repress G2/M-specific genes to prevent premature cell cycle progression ensuring cell do not enter mitosis with damaged DNA preventing genomic instability and mutations (Bujarrabal-Dueso et al., 2023). However, direct relation between MYB TFs and the dissolution of double Holliday junction or polyphosphate biosynthesis is not well documented.

The C2C2-Dof motif is a zinc finger structure found in the Dof domain of DNA-binding with one finger (Dof) proteins. It plays a role in environmental stress responses and regulates various plant biological processes including carbon and nitrogen assimilation. Studies have shown that C2C2-Dof TFs act as potential downstream regulators for two lateral organ boundaries (LOB) domain genes (*SILBD1* and *SILBD2*) influencing light response in tomatoes (Dong & Manghwar, 2023). Meanwhile, the C2C2-Dof TFs were reported to regulates photosynthetic carbon assimilation, malate transporter proteins, and metal ion transporter proteins in oat (*Avena sativa* L.) leaves. Their regulation in carbon dioxide conversion into organic compounds enhance photosynthesis efficiency of the plant (Siadjeu & Kadereit, 2024; Xu et al., 2024). Additionally, the C2C2-Dof, along with other TFs such as WRKY, MYB-related, HB-BELL, MYB, C3H, bZIP, DBB, and bHLH, were shown to involved in stomatal movement in soybean (*Glycine max*) during drought stress (Kasirajan et al., 2018). Similarly to MYB TFs, C2C2-Dof regulate flavonoid biosynthesis through binding to HCT genes to promote conversion of p-Coumaroyl-CoA to caffeoyl-

CoA, while the ERF and MYB further enhanced the expression of *CcoAOMT* genes, leading to the conversion of caffeoyl-CoA to feruloyl-CoA (Wang et al., 2022).

Cold shock proteins (CSPs) are a family of proteins that regulate gene transcription in response to cold temperature and act as RNA chaperones. The first functionally characterised plant cold shock domain (CSD) protein was identified in wheat (*Triticum aestivum*) cold shock domain protein1 (WCSP1). WCSP1 functions as RNA chaperone and cold acclimatisation in wheat (Karlson et al., 2002). Studies on transgenic wheat and rice expressing *Escherichia coli* CSPs (*Csp A* and *CspB*) were reported to improved drought and salt tolerance in wheat and rice by lowering the malondialdehyde (MDA) content, lower relative Na^+ content, and reduced the transpiration rates (Yu et al., 2017; Guddimalli et al., 2021) while CSP increased chlorophyll and proline content in rice blade leading to increased rice yield (Castiglioni et al., 2008). Furthermore, *Arabidopsis* cold shock domain protein 3 (AtCSP3) were found to be upregulated under salt and drought conditions. A study in *Arabidopsis* mutants *atcsp3-2* were found to have lower survival rates compared to wild type under drought and high salinity conditions (Kim et al., 2013).

Heat shock factors (HSFs) act as key regulators in heat stress response, crucial for plants to maintain protein homeostasis and manage protein misfolding, restoring cellular function and aiding recovery from stresses. High temperatures activate HSFs, which stimulate heat shock proteins (HSPs) that acts as molecular chaperones to prevent deleterious protein conformations and eliminate non-native aggregations (Vierling, 1991; Huang et al., 2023). Studies have shown that upregulation of several *HSPs* gene such as *TaHSP*, *CaHsp25.9*, *CaHSP18.1a*, *LsHSP20*, and *AeHSFA2b*, positively increased tolerance to heat, salt and drought in *Arabidopsis*, pepper, lettuce, and kiwifruit, respectively by enhancing sensitivity to ABA and increase superoxide dismutase activity of the plants (Wang et al.,

2020; Liu et al., 2021; Zhang et al., 2024). The importance of *HSPs* in salt and drought stress is evidenced by knockdown studies in rice, particularly targeting genes like the *OsHSFC1b*. Knockdown of *OsHSFC1b* demonstrated high sensitivity rice mutants to salt and observed reduced growth in rice mutants (Bakery et al., 2024).

MIKC-type MADS-box TFs belong to Type II MADS-box family, are essential for plant growth, reproductive development, and stress response. Phylogenetic analysis groups MIKC proteins from angiosperms into at least 14 distinct subclades, including AG/STK AGL11, AGL6, AGL12, AGL17. Extensive studies have shown that these TFs play broad regulatory roles in plants. Although closely related to flower development, they are expressed in various organs, such as roots, leaves, buds, embryos, and seeds, highlighting their diverse functions. For example, the SVP2 in kiwi (*Actinidia sp.*) participates in ABA-mediated dehydration pathways (Wu et al., 2018). Maize AGL2-like gene *ZMM7-Li* revealed to respond to various stresses like cold, high salinity, drought and exogenous ABA (Zhang et al., 2012). In rice, genes such as *OsMADS18* (SQUA), *OsMADS22* (STMADS11), *OsMADS26* (AGL12), and *OsMADS27* (AGL17) were upregulated in response to cold and drought conditions (Dai et al., 2023). In pepper (*Capsicum annuum L.*), an SEP/AGL2 subfamily MADS-box gene is induced by abiotic stresses and hormones, with transgenic *CaMAD*S-expressing plants have greater tolerance to low temperatures, high salinity and mannitol conditions compared to wild-type plants (Chen et al., 2019). Additional MIKC-type MADS-box genes associated with stress resistance have also been identified in wheat (*Triticum aestivum* L.), sheepgrass (*Leymus chinensis*), *Brassica napus*, and tomato (*Solanum lycopersicum*) (Zhao et al., 2021).

The Toesinte branched 1, cycloidea, PCF1 (TCP) TFs family is crucial for plant development from seed germination to flowering and fruit formation. The TCPs are

conserved across various plant species, including tomato, poplar, cotton, orchids, and *Arabidopsis*. Initially, TCPs were known for their role in cell cycle regulation, but later studies revealed broader role in in translating environmental and endogenous signals into growth responses. Sequence diversity of *Arabidopsis* amino acids residues within the TCP-domain, divides the domain into Class I and Class II subfamily. Class II subfamilies are known as CINCINNATA-like TCP (CIN-TCPs) (Rath et al., 2022). The Class I TCP TFs are involved in cell cycle regulation and cell proliferation. Studies on single and/or double mutants *Arabidopsis* of *AtTCP14* and *AtTCP15* show decreased expression of cell cycle (Zhang et al., 2018; Camoirano et al., 2020). Studies also showed Class I TCPs mediate the effects of gibberellins on growth. For instance, TCPs induce the synthesis of gibberellins and expression of *EXPANSIN* genes for growth regulation. Mutants in Class I TCP genes show defective growth responses to auxin (Ferrero et al., 2021). *TCP21* is particularly important during plant growth. Its low expression in rice makes rice to be susceptible to rice ragged stunt virus (RRSV), while overexpression lines of *TCP21* rice exhibited increased tiller bud length, biomass, and tiller number (Wang et al., 2021). Several studies also reported that Class I TCP is upregulated in plants under high salinity and drought conditions (Viola et al., 2023). For example, *PeTCP10* of moso bamboo (*Phyllostachys edulis*) alleviates salt and drought stress in transgenic *Arabidopsis* and rice (Liu et al., 2020).

The CIN-TCP proteins are crucial for cell elongation and leaf development, promoting the transition from cell division to differentiation. This timing of transition is vital for determining the final leaf shape, size, complexity, and flatness. Genetic and growth kinematic studies have shown that CIN-TCP proteins significantly affect cell growth. Study in snapdragon (*Antirrhinum majus*), loss of CIN function result in larger and crinkle leaves (Nath et al., 2003). In *Arabidopsis*, CIN-like TCPs have redundant and additive roles in leaf

morphogenesis. Single *tcp* mutant in *Arabidopsis* show no significant differences from wild type, but disruption in TCP4 and TCP10 resulted in larger, curled leaves (Challa et al., 2019). CIN-TCPs are necessary but not sufficient for cell growth. This is shown by the interaction between miR396-GRF and mi319-CIN-TCP modules, where GRFs promote cell proliferation and CIN-TCPs regulate transition to differentiation. Reduced CIN-TCP function delays the division-to-differentiation switch, causing more cells to remain in the division phase, whereas increased function accelerates division-to-differentiation (Challa et al., 2019). Moreover, CIN-TCPs are involved in thermomorphogenesis. High temperatures were found to induce TCP5-like CIN-TCPs expression in petioles rather than the leaf blade resulting in elongated petioles and reduced leaf blade areas, potentially alter growth pattern to reduce heat stress (Han et al., 2019). Mutants in tcp5, tcp13, and tcp17 were found to have shorter hypocotyls and petioles (Lan & Qin, 2020). Additionally, downregulation in CIN-TPCs results in light hypersensitivity in *Arabidopsis* (Tsai et al., 2014).

In this study, the MYB, WRKY, bHLH, GRAS, bZIP, HB-HD-ZIP, NAC, C2C2-Dof, HB-Bell, OFP, C2H2-ZFP, HSF, GARP-G2-like, and LOB TFs were found downregulated. These TFs play crucial roles in plant growth and development, environmental stress responses, and the initiation of signal transduction pathways. Research has demonstrated their potential in enhancing abiotic stress responses in transgenic plants (Erpen et al., 2018). Typically, these TFs are upregulated under stressful conditions such as drought, high salinity, and high temperatures. For example, *WRKY* genes promote stomatal closure, reduce transpiration rates, and decrease malondialdehyde (MDA) accumulation, thereby improving drought and salt tolerance in *Arabidopsis*, Siberian crab apple (*Malus baccata*), and groundnut (He et al., 2016; Gao et al., 2018; Han et al., 2018). The collaboration of bHLH with R2R3-MYB TFs subgroups through the MYB-basic-loop-helix-

WD40 repeat (MBW) complex confer tolerance to Jilin ginseng (*Panax ginseng* C. A. Mey) and foxtail millet (*Setaria italica* (L.) P. Beauv.) under high salinity and drought stress condition, respectively (Qian et al., 2021). Studies have also shown that bHLH TFs, in conjunction with R2R3-MYB TFs subgroups, regulate flavonoid biosynthesis in response to abiotic stress (Naik et al., 2022). C2H2-ZFPs often contain ethylene-responsive element binding factor-associated Amphiphilic Repression (EAR) motif domain, such as ZAT245, ZAT179, ZAT7, ZAT10, ZAT12 and AZF1/2/3. These zinc finger function as transcriptional repressor and play a critical role in abiotic stress tolerance (Xie et al., 2019). bHLH1 with EAR motif, induces iron deficiency-responsive genes in *Arabidopsis*, maize, and *Brassica rapa* (Chow et al., 2023). *GRAS* genes are known to stimulate stress-inducible promoters and confers cold, drought and salt tolerance in *Arabidopsis* (Fode et al., 2008; Yuan et al., 2016).

Although these TFs are often documented as being upregulated in response to abiotic stress, they can also positively impact stress responses even when downregulated. For example, studies in *Brachypodium distachyon* and soybean found that most of the *WRKY* genes were downregulated under salt stress. They suggest that *WRKY* genes are upregulated in root and are downregulated in aerial parts of the plants, reflecting functional divergence of the *WRKY* gene family (Wen et al., 2014; Yu et al., 2016). Specifically, *WRKY* genes such *AtWRKY70* and *AtWRKY54*, which belong to group III of WRKY TFs, responsible in osmotic stress tolerance in salt-treated *Populus* and tomato (Zhao et al., 2015; Abbasi et al., 2020). Additionally, suppression of GRAS (*SlGRAS6*) and downregulation of *SlGRAS10* in tomato enhanced disease resistance and increased abiotic stress tolerance by modulating the expression of stress-inducible genes involved in flavonoid biosynthesis, reactive oxygen species (ROS) scavenging system and chlorophyll biosynthesis pathways (Habib et al.,

2021). The downregulation of TFs reported in this study may be due to the studied organ, which is a leaf rather than a root.

The coordinated expression of transcription factors and stress-responsive proteins plays a pivotal role in regulating trunk formation in sago palms. In this study, an array of transcription factors including MYB, C2C2-Dof, MIKC-type MADS-box, TCP, CIN-TCP, CSPs, and HSFs responsible in orchestrating key molecular and physiological processes such as ABA signalling, DNA repair, cell cycle progression, photosynthetic carbon assimilation, and secondary metabolism. Notably, the MYB, C2C2-Dof, and HSFs transcription factors exhibited both upregulation and downregulation, suggesting a fine-tuned, tissue-specific regulatory dynamic. Their multifaceted roles including stress response regulations, meristem activity, vascular patterning highlight their roles in cell elongation and expansion, as well as reinforcement in plant cell structure (Wang et al., 2020; Zou & Sun, 2023; Imran et al., 2025). This interpretation is further supported by the observed downregulation of other stress-responsive TFs such as WRKY, GRAS, and bHLH in leaf tissues. Trunk formation in sago palm can be explained as a coordinated, hormone-driven reprogramming orchestrated by a network of transcription factors. Trunk formation in sago palm can be explained as a coordinated, hormone-driven reprogramming orchestrated by a network of transcription factors. Stress associated TFs such as HSF and WRKY during abiotic and biotic stress modulate ABA signalling to induce dormancy in plant including leaf abscission and senescence and bud dormancy to overcome environmental stresses. This modulation ultimately led to physiological changes that enhance plant survival against adverse environmental conditions (Mareri et al., 2022). The fine-tuning of MYB and C2C2-Dof gene expression contributes to the reprogramming processes whereby they act as negative regulators of ABA signalling and positive modulators of GA signalling. The

activation of GA signalling results in the DELLA protein degradation, a protein that repress growth programs, thereby enabling several growth TFs such as TCP, bHLH, and MADS-box factors to activate cell-cycle, stem elongation, and meristem activity (Shu et al., 2018, Xue et al., 2022). Concurrently, the reduced bHLH and MYB expression modulate auxin transporters and signalling component, creating auxin maxima, an auxin-rich zones that drive cell growth and vascular development, which is essential for cell expansion and trunk formation (Hussain et al., 2022). In contrast, the non-trunking sago palms altered gene expression favouring stress signalling shifting toward stress adaptation and away from active growth in non-trunking individuals, hence contributing to their failure to trunk formation.

2.5 Conclusion

Through the identification and functional characterisation of commonly expressed DEGs in leaf tissues of trunking sago palms, this study reveals a coordinated molecular framework that highlight persistent growth and trunk formation. The upregulation of *ATL5* supports protein balance and cellular homeostasis by removing misfolded or damaged proteins, while *PHO1* mediates phosphate homeostasis and ABA-responsive stomatal regulation, thereby ensuring continuous assimilate synthesis, providing energy and metabolic foundation for sustained meristem activity. Regulatory genes such as *AGO10* safeguard transcriptional balance by preventing excessive transcription factor activity and silencing viral RNAs, whereas RanBP2-type zinc finger proteins and *Zip4* maintain genome integrity and stress resilience, thereby supporting robust photosynthetic output and leaf vitality essential for assimilate production. Vacuolar sequestration of excess Pi complements this phosphate buffering maintaining osmotic balance and offering a readily mobilizable pool of assimilates transport to sink tissues.

At the structural level, the downregulation of lignin biosynthesis enhances cell wall plasticity and expansion through loosening, while maintaining reinforcement via cellulose and hemicellulose deposition. Simultaneously, flavonoid downregulation redirects carbon flux toward carbohydrate biosynthesis and alleviates inhibition of auxin transport, strengthening sink capacity and facilitating assimilate unloading to vegetative organs. The coordinated upregulation of RanBP2-Znf, CSP1, and NRPD1B further reinforces genome stability, transcript fidelity, and stress-adaptive protein synthesis, ensuring accurate chloroplast and mitochondrial function, efficient translation under stress, and epigenetic silencing of transposable elements to prevent transcriptional noise.

As a whole, these findings demonstrate that trunking sago palms integrate metabolic energy conservation, phosphate and carbohydrate homeostasis, cell wall remodelling, hormonal regulation, and genomic safeguards into a unified growth strategy. This molecular coordination sustains persistent meristem activity, internode elongation, and biomass accumulation, ultimately driving trunk formation and maintaining trunking stature.

CHAPTER 3

MICROBIAL AND PHYSICOCHEMICAL PROPERTIES IN SAGO PALMS GROWN IN PEAT SOILS

3.1 Introduction

Soil serves as an essential bedrock of terrestrial ecosystems. It plays a critical role in supporting plant life. The relationship between plants and soil is reciprocal, where plants not only affect soil properties but are also shaped by them. Soil physicochemical properties and soil microorganisms are the utmost influencing factors that support plant vegetation through the nutrients stored (Yang et al., 2021). Soil taxonomy categorises soil into various orders. Each soil order comprises different soil compositions, nutrient value, organic matter and soil microbial taxonomy (Islam et al., 2020).

3.1.1 Soil characteristics influences sago palm growth

An in-depth study on the relationship between peat soil characteristics and sago palm growth and development was conducted in Mukah and Dalat sago plantations. The report documented the mineral substation above mean sea level (MSL). Dalat sago palm plantation recorded MSL level of more than 7 m while the MSL at Mukah sago palm plantation is less than 2 m (Melling, 2000). The difference in the MSL at the peat soil influences the stratigraphy and rawness of peat soil due to water table fluctuations at the area. The growth and development of sago palm depend closely to the soil characteristics it is cultivated. The effects of the nature of soil types illustrated that the peat thickness can influence the growth rate of sago palm (Yamamoto et al., 2003). In deep peat soil, the sago palm growth rate is the slowest. Field observations at deep peat soil found the sago palms often maintain their non-trunking (stunted, trunkless) appearance despite being planted for more than 20 years

(Hussain et al., 2012). Studies reported constant waterlogging at deep peat soil plantation to be the main culprit to cause stunted growth in sago palms. Constant flooding cause low decomposition level of organic matter, which leads to the formation of springy root mats. Vacant space as tall as 0.5 m is often observed to form underneath the root mats. This structure limits water and nutrients access to sago palm roots especially during drier months. This condition is more pronounced at deep peat soil where non-trunking sago palms are observed along with dense forest floor vegetation of ferns and creepers reaching up to 2 m high (Melling, 2000).

3.1.2 Studies on peat soil microbial communities

A comprehensive environmental study focusing on soil properties and microbial communities is imperative. Microbes and plants coexist symbiotically *via* intricate interactions. Soil microorganisms, such as mycorrhizal fungi and rhizobia, play pivotal roles in plant growth and productivity in promoting the nutrient cycle (Enebe & Babalola, 2019; Vannier et al., 2019). Beneficial soil microbes such as the arbuscular mycorrhizal fungi (AMF) and the plant growth-promoting rhizobacteria (PGPR) aid in providing nutrients to plant roots (Sahib et al., 2020). Understanding the composition, diversity, function, and network structure of the rhizome microbiome in trunking and non-trunking sago palm soils in relation to soil physicochemical properties is important for plant health. Presently, the study on identifying soil microbiota present in sago palm soils is limited. It is hypothesised that different bacterial community structure and specific soil properties are associated with the phenotypic differences of the palms.

Initial studies about different genera of N-fixing bacteria have reported the presence of *K. pneumoniae*, *K. oxytoca*, *P. agglomerans*, *E. cloacae*, *Burkholderia* sp., *S. maltohilia*, and *B. megaterium* in sago palm roots *via* agar inoculation (Shrestha, 2006). Soils at the

rivers of Sg. Nunau, Sg Taap and Sg Petah intermediate, and Sg Ugui, at Dalat and Sago Research Plot, Kuching confirmed the presence of *L. sphaericus* and *B. thuringiensis* bacteria for N fixation using 16s rRNA sequencing (Lihan et al., 2021). A comparison study of nipa palm and sago palm roots sampled in Mukah revealed the *Burkholderia cepacia* complex (Bcc) of *B. vietnamiensis* was found in nipa palm roots while the non-Bcc *Burkholderia* species such as *B. unamae*, *B. phenazinium*, *B. mimosarum*, *B. nodosa*, *B. gladioli*, *B. tropica*, *B. phymatum*, *B. tropicalis*, and *B. fungorum* were identified in sago palm roots (Tang et al., 2010).

The comprehensive soil studies on tropical peat soils, especially those where sago palms are cultivated are still limited. While previous research has conducted physicochemical properties of peat soil supporting sago palms growth, none has been specifically compared the soils from trunking and non-trunking sago palm. Furthermore, the total boron content has not been reported in the studies of sago palm peat soils. Boron is essential micronutrient for cell wall formation and membrane integrity. Thus, understanding boron content in soil is important for optimising fertilisation practices to minimise nutrient waste and enhance crop productivity (Aytop et al., 2023). Although the study conducted by Lihan et al. (2021) provides beneficial attributes toward the growth of sago palm, the study did not investigate fungal taxonomy present in the soil. Additionally, the study by Asano et al. (2021) lacked biological replicates, leading to a less precise estimation of biological variation within the sample population (Badrick, 2021).

3.1.3 Research Objectives and Hypothesis

While previous studies have examined soil taxonomy and microbial diversity in peatlands, limited understanding on correlation between soil physicochemical properties and microbial community composition in influencing sago palm growth especially toward the trunking formation remains scarce. Research has focused on general soil-plant relationship or microbial diversity in agricultural system, but few have integrated these factors in the context of trunking versus non-trunking sago palms. This research gap limits our understanding behind the failure of trunk formation in sago palms despite being grown at similar location.

The aim of this study is to investigate the environmental factors associated with sago palm growth. It is hypothesised that the sago palms growth is supported by the peat soils with more favourable physicochemical properties such as higher pH value, better nutrient availability in the soil and enriched microbial communities that actively involved in organic carbon decomposition and nutrient cycling in the soils. Meanwhile the non-trunking sago palms growth are constrained by unfavourable environment such as waterlogging condition, nutrient leaching, and pollutant presence in the soil along with reduced microbial diversity and function. The objectives of the study were as follows:

i. To determine the physicochemical properties of peat soil collected from trunking and non-trunking sago palm plots.
ii. To identify the differences in microbial taxonomic communities between these plots.

3.2 Materials and Methods

This chapter describes the methodology employed to study peat soil physicochemical properties and discover bacterial communities present in sago palms' plantation soil. Amplicon sequencing was performed at Apical Scientific Sdn. Bhd. All soil physicochemical analyses except soil pH, electrical conductance (EC), and bulk density were conducted by Sarawak Plantation Sdn. Bhd. under standard operating procedures.

3.2.1 Soil collection

A total of 10 soil samples were collected at trunking sago palm, with peat thickness of less than 0.5 m (N 02°50'56.2" E 111°49' 41.5"), and non-trunking sago palm, with peat thickness more than 1.5 m (N 02°50'22.1'' E 111°50'02.2"), at the semi-wild Dalat Sago Palm Plantation, Mukah, Sarawak. Three replication plots (20 x 20 m) that were 100 m apart from each other were selected. Soil samples were collected at a distance of 1 m from plant base and at two depths of 0-15 cm and 15-20 cm using a half-cylindrical gouge auger (Eijelkamp; effective auger body 100 cm, ø 3 cm). Samples were composited by depth, placed in sterile labelled plastic bags and kept cold for transportation. The samples were stored at -20 °C until laboratory analyses were performed. Figure 3.1 shows the location of where soil samples were collected.

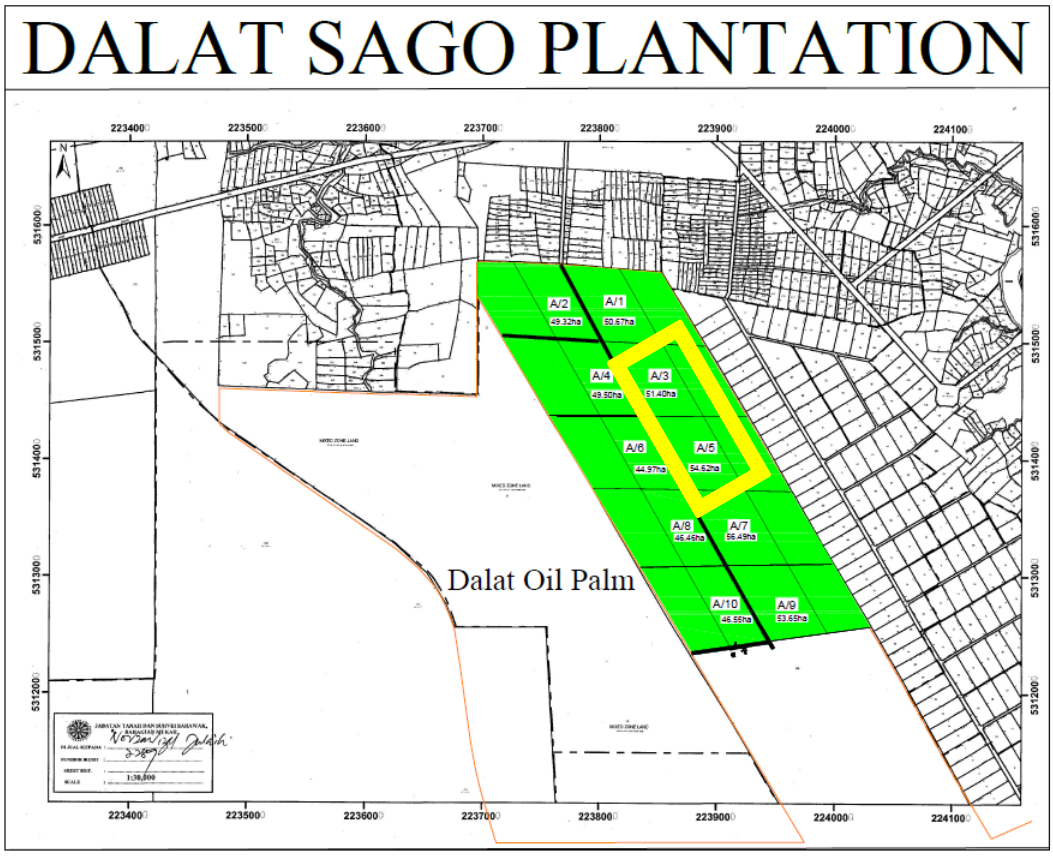

Figure 3.1: Soil collection were conducted at Block 3 and 5 indicated by yellow frame. Green field represents sago palm plantation. Source: Land Custody and Development Authority (LCDA)

3.2.2 Soil physicochemical analysis

All soil physicochemical analyses except soil pH, electrical conductance (EC), and bulk density were conducted by Sarawak Plantation Sdn. Bhd. under standard operating procedures.

3.2.2.1 Sample preparation

Soil samples for physicochemical analyses were air-dried on carboard and allowed for several days within a well-ventilated environment. The air-dried soil was sieved using a 2 mm mesh sieve to remove debris such as stones, sticks, and plant roots.

3.2.2.2 pH and electrical conductance (EC)

Soil pH and EC were determined using the potentiometric method (Xiong et al., 2021). A total of 10 g air-dried sieved soil was homogenised with 25 ml distilled water based on 1: 2.5 (w/v) soil-to-water ratio. The solution was uniformly mixed for 1 h using rotary mixer (Cole Palmer RotoFlex Sigma-Aldrich, USA) and left overnight to allow the suspension to settle down and form an aqueous layer. The pH and EC were recorded using pH meter (ST3100-B, OHAUS) and EC probe (EC150, EXTECH, USA).

3.2.2.3 Soil bulk density

The bulk density (BD) of the soil was determined using the dry bulk density method (Al-Shammary et al., 2018). A polypropylene tube (50 ml) was filled with fresh soil and dried in an oven at 105 °C for 24 h, and dried soil was weighed. The soil bulk density was calculated by using Equation 3.1. Where ρ_{bulk} is dry bulk density, m_{dry} is dry mass soil, and V represents soil volume.

$$\rho_{bulk} = \frac{m_{dry}}{V} \qquad \text{Equation 3.1}$$

3.2.2.4 Available phosphorus content

The available phosphorus (P) content in the soil was determined using the Bray I method (FAO, 2021). A total of 2 g of dried soil was weighed and mixed with an extracting solution of 0.03 M ammonium fluoride and 0.025 M hydrochloric acid. The solution was agitated for 5 min at 180 oscillations per minute and filtered through a Watman No. 42 filter paper. The filtrate was further treated with 2 ml boric acid and the homogenised solution left to stand for 1 h until the blue colour developed. The standard curve was plotted based on spectrometry readings set at 882 nm wavelength.

3.2.2.5 Total nitrogen content

The quantification of soil total nitrogen (N) was determined using Kjeldahl digestion and distillation method (Faithfull, 2002). A total of 5 g of air-dried soil was used in this experiment. The soil was first digested and subsequently distilled using a Markham semi-micro distiller. The total nitrogen content was determined by titrating the distillate with 0.01 M sulphuric acid until a colour change from green to purple was observed.

3.2.2.6 Total organic carbon content quantification

The total organic carbon content was determined using a Walkley-Black titration and colorimetric method (FAO, 2019). A total of 1 g of dried-sieved soil was used in this experiment. The soil was treated with potassium dichromate ($K_2Cr_2O_7$) solution and concentrated sulphuric acid (18.4 M) and filtered. Phosphoric acid and barium diphenylamine sulfonate indicator was added to the filtrate. The filtrate was then titrated with diphenylamine and ammonium ion sulphate until filtrate colour changed from deep violet-blue to brilliant green.

3.2.2.7 Cation Exchange Capacity (CEC) and exchangeable cations

The soil Cation Exchange Capacity (CEC) analysis was carried out using neutral ammonium acetate extraction in soil/solution ration of 1:5 (w/v) (Räty et al., 2021). The soil sample suspension was agitated for 1 h and left to stand overnight. The suspension was filtered, and the extraction method was repeated until reaching 100 ml. The filtrates were combined for exchangeable bases (K, Ca, Mg) analyses using inductively coupled plasma atomic emission spectroscopy (ICP-AES). The titratable acidity was determined using back-titration to pH 7.0. The CEC value was calculated as the sum of the extracted cations and titratable acid in meq%.

3.2.2.8 Total boron (TB)

The soil total boron (TB) was determined using hot water extraction-azomethine colorimetric method (FAO, 2024). Twenty-five grams of air-dried soil was dissolved in 50 ml distilled water. The slurry was heated in a water bath (80 °C) for 30 min and then filtered using Whatman No. 42 filter paper. The clear filtered was extracted with sodium EDTA solution and azomethine-H solution and diluted to 25 ml with distilled water. The solution was left to stand for an hour for colour development before absorbance reading using an UV-Vis spectrophotometer at an absorbance of 420 nm.

3.2.3 Soil amplicon study

Fresh soil samples were used for soil amplicon study. Following genomic DNA extraction from soil samples, amplicon sequencing was performed at Apical Scientific Sdn. Bhd.

3.2.3.1 Extraction of genomic DNA from soil samples

Soil gDNA was extracted from soil samples by using a NucleoSpin Soil (Macherey-Nagel, Germany) extraction kit following manufacturer protocol. The quality and quantity of the extracted gDNA were assessed with a Nanodrop instrument (DeNovix DS-11, USA) at A_{260}/A_{280} and A_{260}/A_{230} ratios and visualised on 1% (w/v) agarose gel before downstream applications. High-quality DNA sample sequencing was analysed *via* PCR amplification of universal primers 341F (5'- CCTACGGGNGGCWGCAG-3')/ 805R (5'- GACTACHVGGGTATCTAATCC-3') and ITSF1 (5'- GGAAGTAAAAGTCGTAACAAGG-3')/ ITSR1 (5'- GCTGCGTTCTTCATCGATGC-3') targeting V3 and V4 hypervariable region in the bacterial 16S rRNA gene and ITS1 gene region, respectively. Amplicon sequencing was performed on the Illumina MiSeq platform using PE strategy of 2 x 300 bp. All the sequence data generated were uploaded to NCBI under project ID PRJNA1067377.

3.2.3.2 Sequencing pre-processing and statistical analysis

Demultiplexed paired-end fastq files were processed into quality-filtered reads and merged using an error-corrected amplicon sequence variant (ASV) in DADA2 v1.18. The taxonomic assignment was annotated against SILVA non-redundant (nr) database v138.1 (updated on March 10, 2021). The ASV table with read counts affiliated with 'eukaryote', 'archeaea', 'chloroplast', and 'mitochondria' were removed before subsequent analyses. This filtration step is conducted to remove irrelevant sequences and ensure accurate representation of microbial community data as well as reducing dataset size for computational analysis efficiency (Xiong et al., 2021b). All statistical analyses were performed using R package v3.6.1. Alpha diversity was calculated using QIIME whilst alpha-diversity calculations, the ASV tables were normalised using function cumNorm from

R package metagenome Seq v1.12. The ordination analysis was carried out using Bray-Curtis dissimilarity matrix using Vegan package v2.3.2 implemented in the Phyloseq package v1.10 in R.

3.3 Results

3.3.1 Soil physicochemical properties

The physicochemical properties of peat soil are shown in Table 3.1. Nitrogen (N) content was observed (0.32-1.13%) in non-trunking soil sago palms plot at both soil levels. This total N value is lower than the reported optimum range (1.10-2.98%) (Othman et al., 2009; Reeza et al., 2014) which is attributed to most N present in organic form and nitrate leaching in the soil. The organic carbon content (16.5-39.57%) observed in the collected soils is considered high due to plant litter serving as the primary source material. The higher organic carbon content in the subsoil level supported significant organic matter accumulation at both sampling sites (Arabia et al., 2020). The C: N ratio shows no significant differences between sites or soil levels, with values ranging from 29.57 – 55.78 % (Melling et al., 2007).

Table 3.1: Peat physicochemical properties of collected soil samples from trunking and non-trunking sago palm plots

Soil properties (unit)	Topsoil (0-15 cm)			Subsoil (15-30cm)			Parameter ranges reported in other tropical peat soil studies	References
	Trunking	Non-trunking	*p*-value	Trunking	Non-trunking	*p*-value		
pH	4.54±0.12	4.13±0.35	0.053	4.28±0.15	3.61±0.12	0.000***	pH 3.33-3.40	Melling et al. (2008)
EC (dS cm^{-1})	58.30±39.12	52.70±10.31	0.771	20.5±56.8	277.5±215.5	0.110	0.48 – 0.92 dS cm^{-1}	Arabia et al. (2020)
N (%)	0.32±0.11	1.13±0.300	0.002***	0.40±0.25	0.97±0.20	0.000***	1.10 - 2.98%	Murtedza et al. (2002)
							1.21 - 2.98%	Othman et al. (2009)
AP (ppm)	26.80±29.28	30.80±16.58	0.820	9±2.86	24.25±8.06	0.000***	8-133 ppm	Fukasawa (2021)
							8 – 27 ppm	Akhmad Kadir et al. (2020)

Table 3.1 continued

Organic carbon (%)	16.38±10.84	33.21±9.23	0.030*	16.05±9.85	39.57±8.79	0.000***	15.27 - 17.54%	Akmad Kadir et al. (2020)
							48.34 - 54.92%	Arabia et al. (2020)
CEC (meq%)	36.95±14.68	58.93±4.91	0.026*	41.22±6.58	59.09±3.90	0.000***	34.36 -37.95%	Melling et al. (2008)
TB (mg/kg)	7.80±1.09	11.00±2.00	0.019*	7.40±2.07	9.60±1.14	0.080	None reported on tropical peatlands	
Exchangeable K (meq%)	0.11±0.03	0.22±0.04	0.001***	0.07±0.02	0.13±0.01	0.000***	1.07 -1.22%	Arabia et al. (2020)
Exchangeable Mg (meq%)	0.93±0.34	1.63±0.24	0.007***	0.85±0.34	1.95±0.41	0.000***	10.6 - 18.1%	Arabia et al. (2020)
							0.16 %	Devangsari et al. (2022)
Exchangeable Ca (meq%)	1.14±0.59	3.05±0.65	0.001***	0.78±0.52	2.64±0.87	0.000***	2.34 %	Devangsari et al. (2022)
Bulk density (g/cm^3)	0.42±0.27	0.26±0.13	0.266	0.31±0.09	0.16±0.04	0.020	0.12 - 0.16 g/cm^3	Melling et al. (2008)

Table 3.1 continued

C: N ratio	55.78±47.22	29.57±2.54	0.282	43.12±12.97	43.29±5.84	0.974	13.39-15.66	Akhmad Kadir et al. (2020)
							29.70-30.27	Melling et al. (2008)

Note: Peat soil physicochemical properties at top – and subsoil levels. Values mean ± standard deviation. Statistical significance was assessed by T-test and significant differences were accepted when *p*-value < 0.05 between the two groups. $p < 0.05$ (*), $p < 0.01$ (**), and $p < 0.001$ (***). Ec: Electrical conductance, AP: available phosphorus; CEC: cation exchange capacity; TB: total boron; K: potassium; Ca: calcium, Mg: magnesium, N; Nitrogen.

The soil pH is highly acidic, primarily influenced by naturally occurring acid sulphate in peat soil. The EC and CEC values range from 20 – 277 dS cm^{-1} and 36.95 – 59.09%, respectively. These values are higher than other tropical peatlands reported values (0.48 – 0.92 dS cm^{-1} and 35.36 – 37.95%) (Melling et al., 2008; Arabia et al., 2020) due to high organic content (Walter et al., 2013). The availability of ExC *i.e.*, Mg^{2+} (0.85 – 1.95%), Ca^{2+} (0.78 – 2.64%), and K^{+} (0.07 – 0.22%) are very low because it influenced by rainfall consistency (Arabia et al., 2020). The available P (9 – 30.80 ppm) is consistent with other peat soil studies (Akhmad Kadir et al., 2020), it can be decreased in peat soil due to P leaching and the formation of histosols (Oliveira et al., 2021; Kunarso et al., 2022). The TB content is higher in the topsoil of non-trunking soils. However, no comparative TB studies have been conducted on tropical peatlands. The bulk density of the peat soil 0.16 – 0.42 g/cm^3 is the resultant biological decomposition of sago plants (Könönen et al., 2015).

3.3.2 Amplicon dataset from trunking and non-trunking sago palm soils

Bacterial and fungal communities associated with the bulk soil samples of trunking and non-trunking sago palms characterised based on V3-V4 regions of the bacterial 16S rRNA and fungal ITS1 region generated a total of 1,907553 and 2,172982, ranging from 167,607 to 201,086 and 160,216 to 265,069 reads for each datasets following quality filtering with average length distribution of trimmed sequences of 300 bp and 280 bp, respectively. The rarefaction analysis of amplicon sequence variants (ASVs) at more than 50,000 reads reached a plateau for both 16s and ITS, representing sufficient sequencing depth to cover microbial diversity within individual samples (Li et al., 2022) (Appendix G).

3.3.3 Microbial composition in soil samples

Statistical analysis of sequence annotations revealed that the prokaryotes present at both collection sites were classified into 41 phyla, 110 classes, 231 orders, 31 families, 463 genera, and 475 species. Bacterial sequence assigned at the phylum level revealed that Acidobacteria (39±0.06%), Proteobacteria (26 ± 0.02%) and Actinobacteria (16 ± 0.06) were the top three dominant phyla found in all soil samples. Other dominant phyla ranging from 2-6% such as Desulfobacterota (2 ± 0.02%) and Nitrospirota (1 ± 0.01%) phyla were identified across all trunking soil samples except WPS-2 (2 ± 0.02%), which was detected only across non-trunking soil samples (Figure 3.2). The relative differential abundance revealed that Nitrospirota and Desulfobacterota phyla were found to be significantly higher across soil samples collected at trunking compared to non-trunking soil samples. Meanwhile Actinobacteriota and WPS-2 phyla were found to be significantly higher in soil samples collected from non-trunking soil samples (DESeq2 $p < 0.05$) (Figure 3.3).

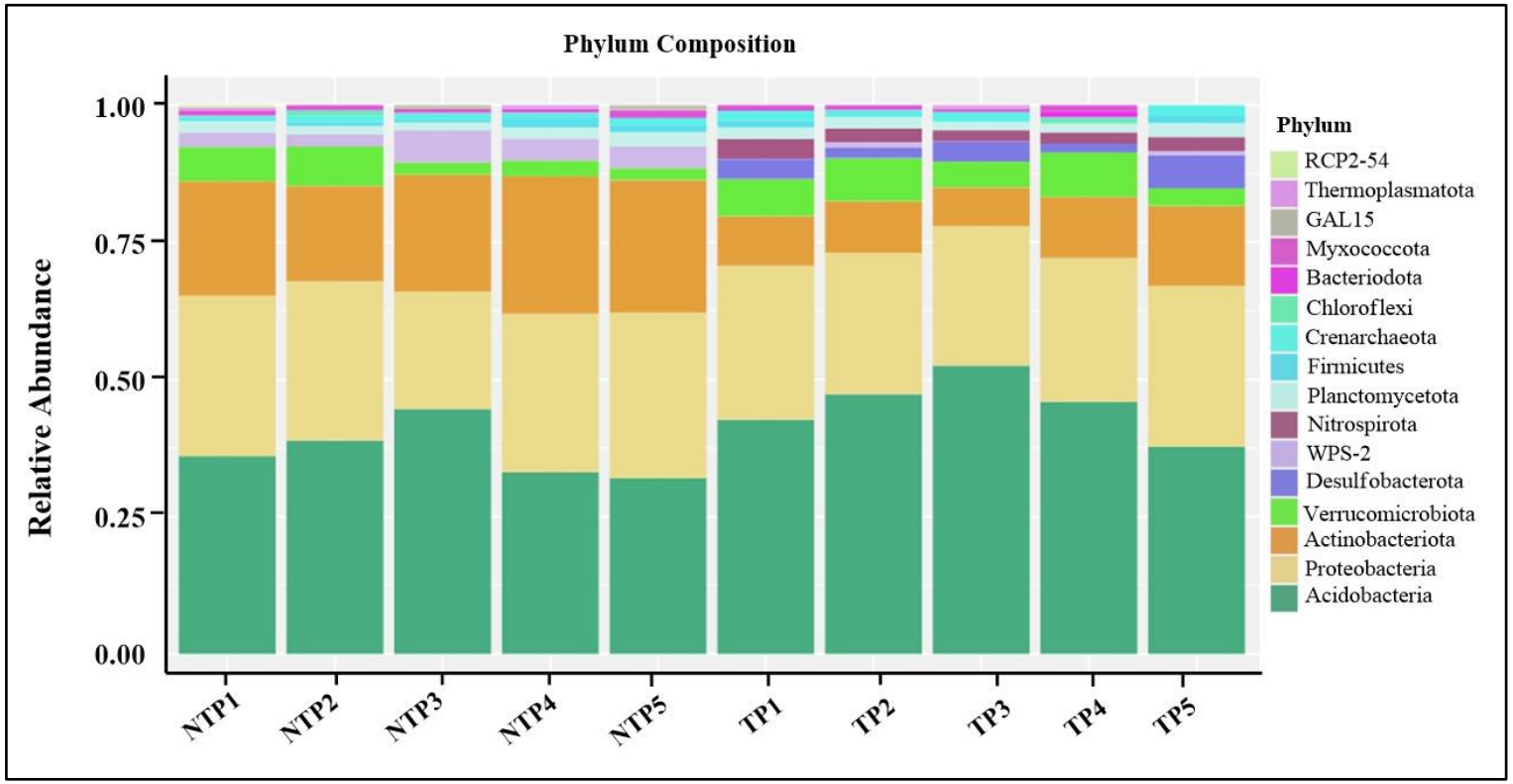

Figure 3.2: Relative abundance of bacterial phyla in trunking (TP1-TP5) and non-trunking (NTP1-NTP5) sago palm soils, showing Acidobacteria, Proteobacteria, Actinobacteria, and Verrucomicrobiota dominate across all samples, with minor contributions from multiple low-abundance phyla. Colour-coded bar plot shows the percentage of the major top 10 bacterial phyla. The y-axis represents the classification level of phyla, and the x-axis represents biological replicates

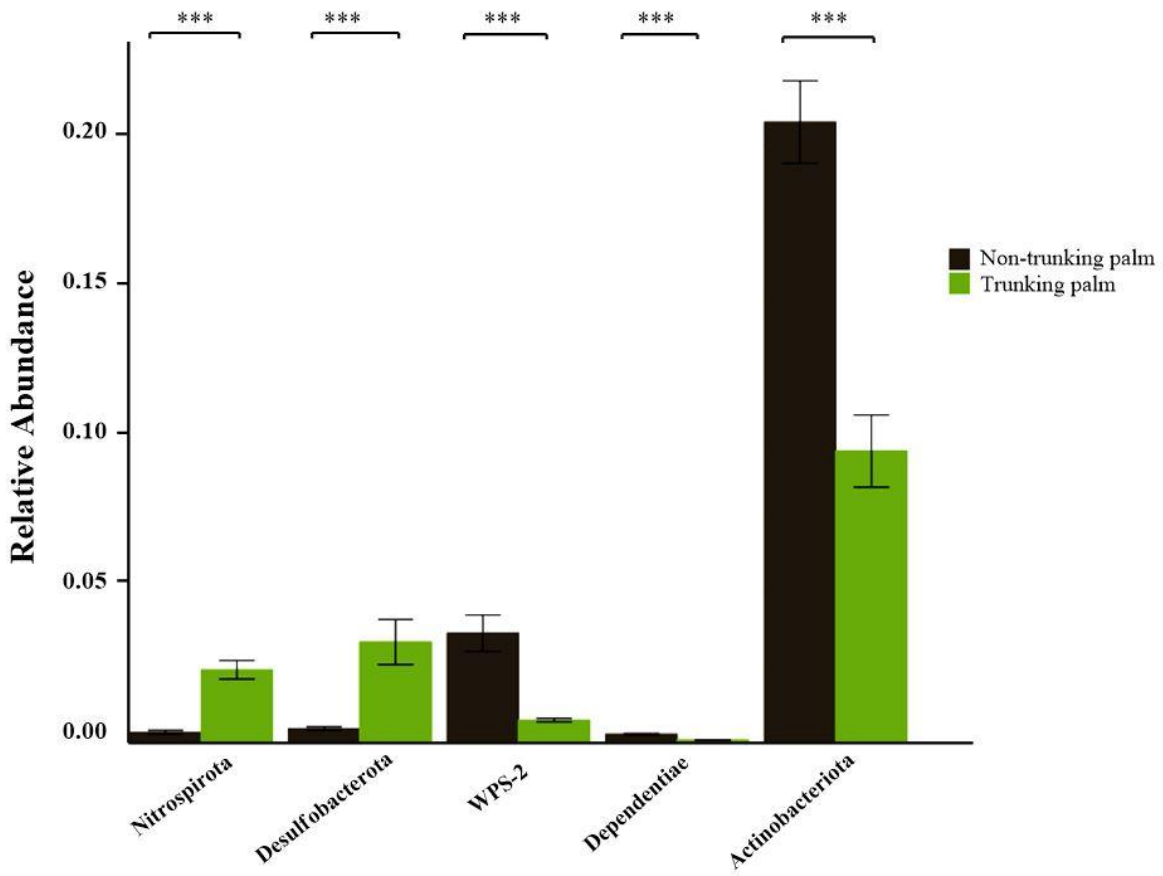

Figure 3.3: Differential relative abundance of key bacterial phyla (Nitrospirota, Desulfobacterota, WPS-2, Dependentiae, and Actinobacteria) in the soils of trunking and non-trunking sago palms with significance levels indicated as $p < 0.05$ (*), $p < 0.01$ (**), $p < 0.001$ (***)

The fungi ASVs were classified into 13 phyla, 44 classes, 116 orders, 222 families, 364 genera, and 507 species. Fungal sequence assigned at phyla level identified Ascomycota (73±0.10%), Basidiomycota (11±0.08%), Mucoromycota (11±0.09%), and Mortierellomycota (3±0.06%) emerged as the top dominant fungi phyla detected across all soil samples (Figure 3.4). Differential abundance analysis identified phylum Monoblepharomycota found slightly higher in their abundance in soil samples collected across trunking sago palms plot. In contrast, the relative abundance of phylum Calcarisporiellomycota is slightly higher in non-trunking soil samples (DESeq2, $p < 0.05$). However, phyla Mortierellomycota and Chytridiomycota were visualised higher in non-trunking and trunking soil samples, respectively (Figure 3.5).

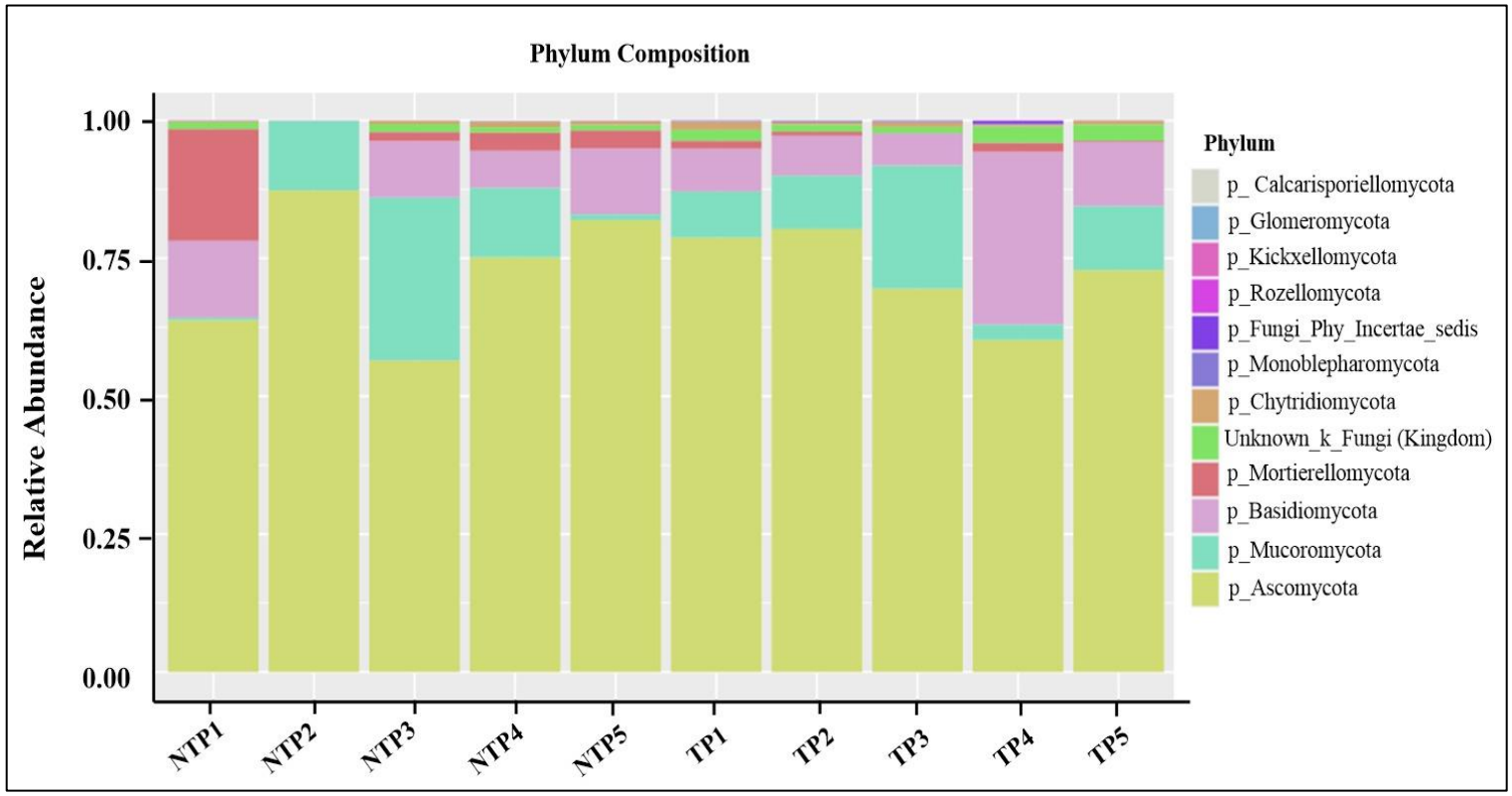

Figure 3.4: Relative abundance of fungal phyla in trunking (TP1-TP5) and non-trunking (NTP1-NTP5) sago palm soils, showing Ascomycota, Mucoromycota, Basidiomycota, and Mortierellomycota dominate across all samples, with minor contributions from multiple low-abundance phyla. Colour-coded bar plot shows the percentage of the major top 10 fungal phyla. The y-axis represents the classification level of phyla, and the x-axis represents biological replicates

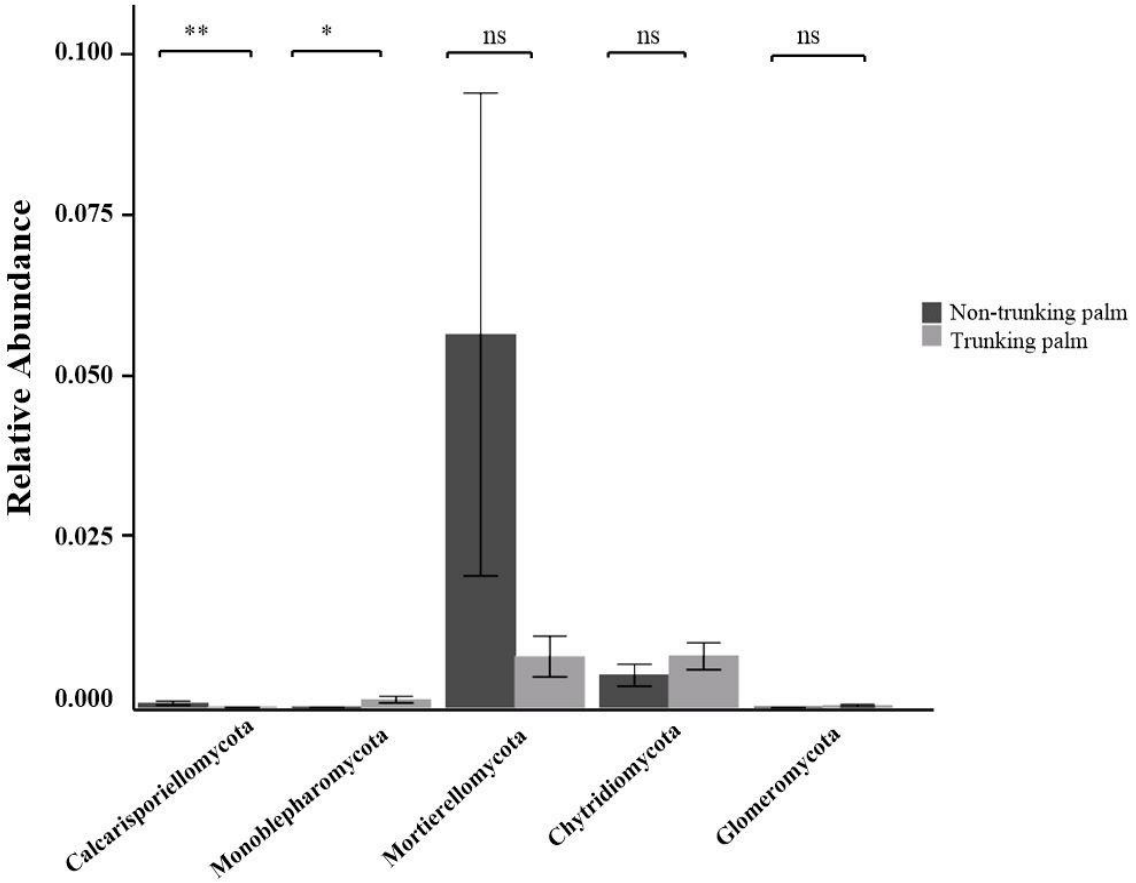

Figure 3.5: Differential relative abundance of key fungal phyla (Calcarisporiellomycota, Monoblepharomycota, Mortierellomycota, Chytridiomycota, and Glomeromycota) in the soils of trunking and non-trunking sago palms with significance levels indicated as $p < 0.05$ (*), $p < 0.01$ (**), $p < 0.001$ (***)

3.3.4 Microbial diversities in sago palm soils

The alpha diversity was evaluated for the richness and diversity of bacterial and fungal species Chao1 and Shannon diversity indices for two sampling plots (Table 3.2). The alpha diversity metrices do not show significant difference in bacterial taxa richness between soil samples collected from trunking and non-trunking sago palms soils (ANOVA, Chao1 = 0.87, Shannon = 0.65, $p > 0.05$). Similarly, there was no significant difference in fungal diversity richness observed between the two collection sites (ANOVA, Chao1 = 0.86; Shannon = 0.22, $p > 0.05$) (Figure 3.6).

Table 3.2: Alpha diversity matrices from trunking and non-trunking soil samples

Kingdoms	Indices	Trunking	Non-Trunking
Bacterial species	Chao1	652.074 ± 45	642.746 ± 31
	Shannon	5.822 ± 0.07	5.779 ± 0.05
Fungal species	Chao1	445.644 ± 68	467.883 ± 105
	Shannon	4.616 ± 0.09	3.917 ± 0.52

Note: Results are expressed as mean value ± standard error.

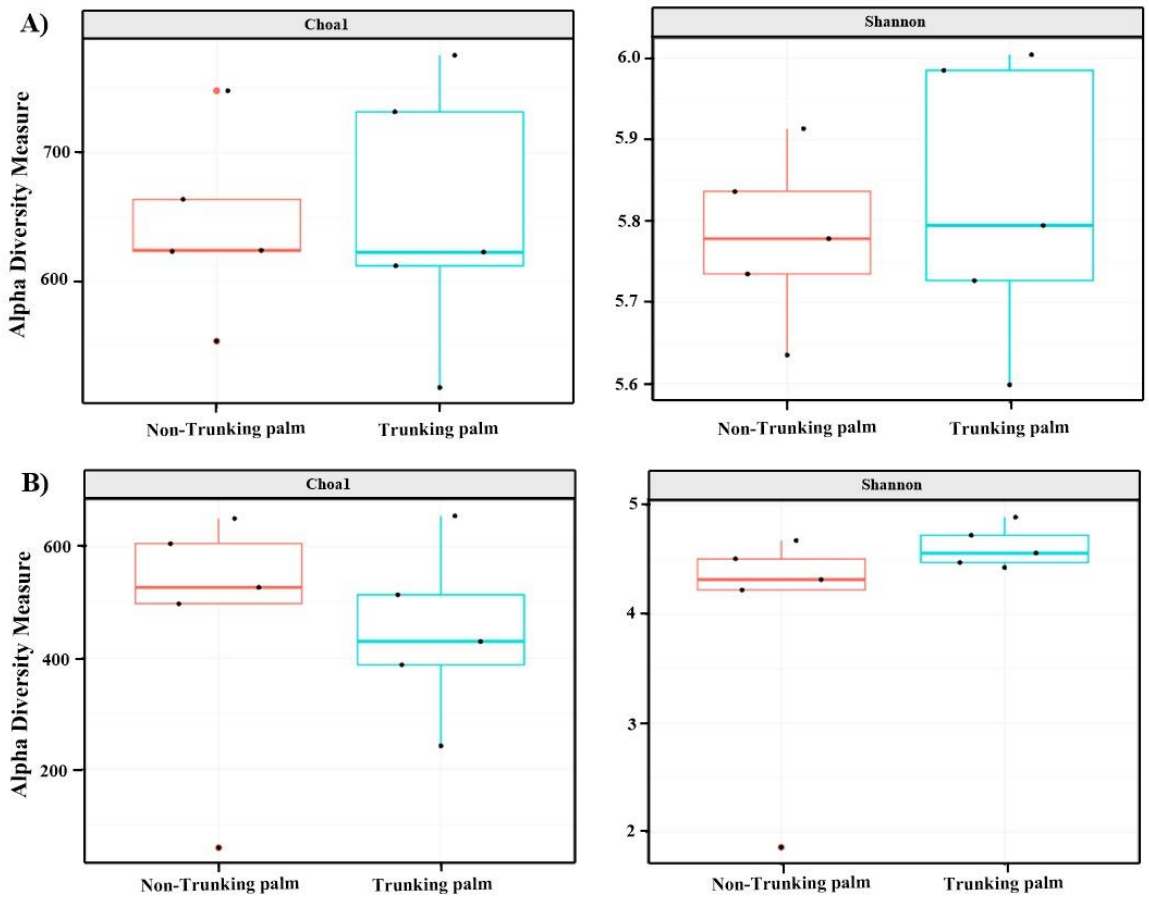

Figure 3.6: Alpha-diversity of the soil microbial community **A)** 16S and **B)** ITS of Chao1 and Shannon-relative abundance of microbial in trunking and non-trunking sago palm soils. No significant differences were detected, indicating that overall microbial richness and evenness are not the main drivers of trunking differences

Meanwhile, species diversity in all samples, as observed *via* Principal Coordinates Analysis (PCoA) based on Bray-Curtis distances revealed distinct clustering of microbial communities at different collection sites. The samples were separated at the biplot with Axis1 and Axis 2, denoting 59% and 37% variance for 16S and ITS at trunking and non-trunking soil samples, respectively. Analysis of similarity (ANOSIM) was conducted to assess the differences in microbial community composition based on the 16S rRNA gene and ITS sequence data. Significant separation was observed between samples (16S: R=0.772, $p < 0.05$; ITS: R=0.600, $p < 0.05$). These relatively high R-values suggest strong differentiation of microbial communities across plots, highlighting the impact of trunking status on microbial community composition (Figure 3.7).

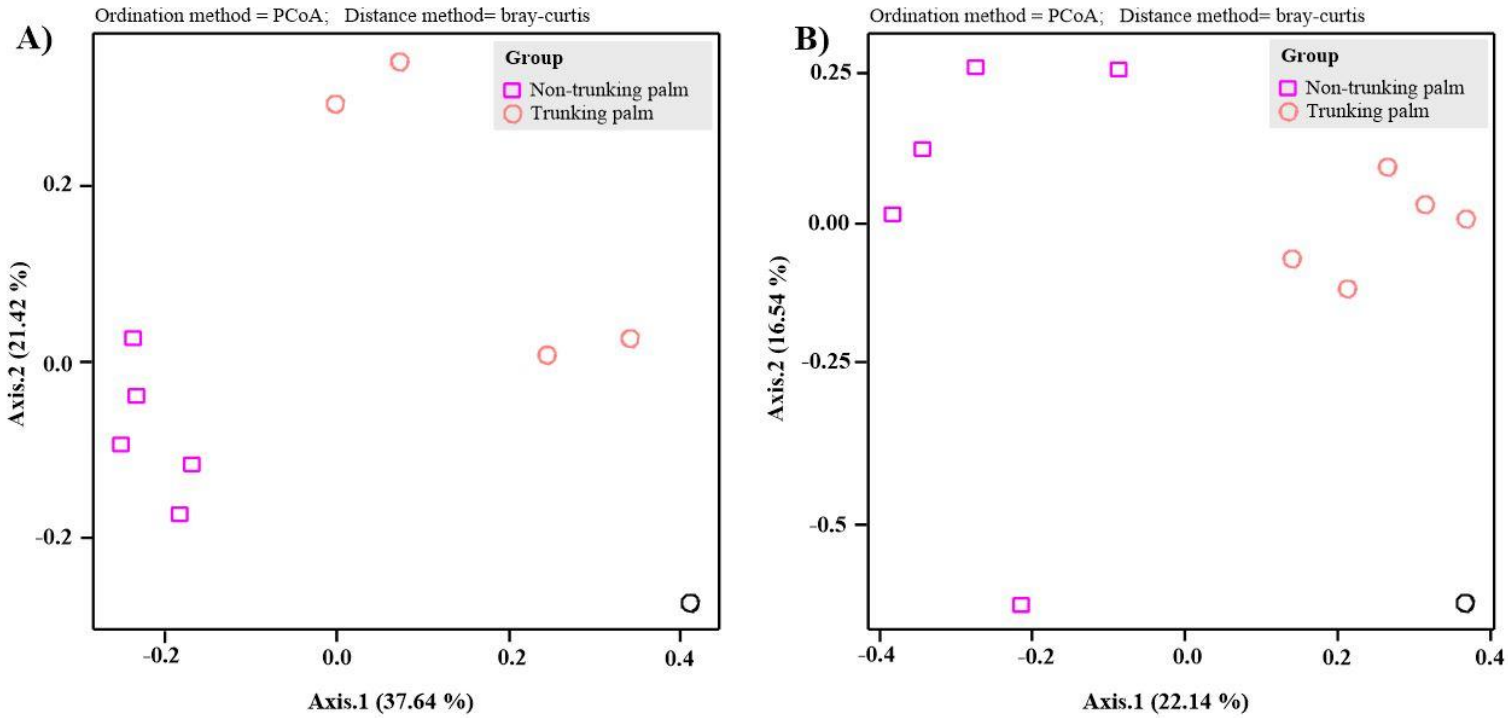

Figure 3.7: Principal coordinates analysis (PCoA) based on Bray-Curtis distance showing differences in soil microbial community structure between trunking and non-trunking sago palms for **A)** bacteria and **B)** archaea, with clear separation of samples along the first two axes

3.4 Discussion

Although Southeast Asia has the second-largest tropical peatlands, research on these wetlands is limited compared to those in the Northern Hemisphere. Often deemed unsuitable for agriculture, Malaysia's peatlands are utilised to grow various crops such as pineapples and oil palms. In Sarawak, sago palms are primarily cultivated in peat soils to boost local economic development. However, years (> 10 years) after cultivation, some sago palm plantations are experiencing dwarfism in their populations. While research has been conducted on these palms, there are fewer studies focused on the soil in which they are grown. Therefore, this study aims to address this gap by conducting physicochemical analysis of the peat soil and amplicon sequencing to investigate the microbial community composition at trunking and non-trunking plots at Dalat Sago Plantation, Mukah, Sarawak. It is important to note that the chosen sago palm plantation is semi-wild, which refers to the palms being cultivated with minimal maintenance and without proper treatments such as fertiliser applications, occasional weeding, and land clearing.

3.4.1 Peat physicochemical characteristics in studied soil samples

Soil is a dynamic entity where complex interactions occur between its biological, chemical, and physical components, determining its quality (Woldeyohannis et al., 2022). Soil pH describes the chemical environment of the soil, including cation exchange capacity (CEC) value and soil nutrient availability (Yin et al., 2021). Based on the physicochemical properties in Table 3.1, the analysis of variance for soil pH revealed that under both trunking and non-trunking sago plants, soil pH was acidic due to the naturally occurring acid sulphate in peat soil (Melling, 2016). The lower pH 3.61 – 4.13 at non-trunking compared to trunking (pH 4.28 – 4.54) is likely attributable to higher nitrogen accumulation in the soil, whereby the conversion of nitrogen to nitrate releases hydrogen ions (H^+) making the soil more acidic.

Moreover, nitrate commonly leach out of the soil along with other cations reducing the soil's ability to buffer acidity. This condition results in lower soil pH levels (Zhang et al., 2022).

Subtle differences in soil pH may suggest differences in nutrient dynamic at both trunking and non-trunking sago palm soils. The moderately higher soil pH at trunking sago palm soils suggest better nutrient retention and availability of essential base cations such as K^+, Mg^{2+}, Ca^{2+}, and Fe^{2+} in the soil (Solly et al., 2020). The non-trunking sago palms exhibited higher cation exchange capacity (CEC) due to elevated organic carbon, however, the effective availability of exchangeable cations (ExC) of base cations are reduced due to leaching and inherently low content of clay (< 6%) and mineral matters in peat (Narangerel et al., 2022). The excess organic carbon accumulation in the non-trunking sago palms soils, driven by low pH and poor microbial decomposition, further immobilised N and P in organic forms, further restricting nutrient turnover (Kadir et al., 2020; Breugem et al., 2024). Naturally, nutrients such as N and P are organically bound in soil, and microbial metabolic reactions convert these nutrients into usable forms for plants. In this study, N was found to be in a low concentration (0.32-1.13 %) compared to the reported value for both peat soil environments (1.10 – 2.98 %). The low N content is attributed to N often being in organic form (*i.e.,* lignoprotein) (Hoang et al., 2022). The anoxic environment and low pH of peat soil limit the decomposition and conversion of high organic matter to N by responsible microorganisms, as indicated by high C:N ratio values 29.57 – 55.78 (Breugem et al., 2024).

The higher levels of several nutrients such as N, organic carbon, CEC, and exchangeable bases (K^+, Mg^{2+}, Ca^{2+}) in both topsoil and subsoil of non-trunking soils do not confer growth advantages to non-trunking sago palms as depicted by the palms' poor growth performance. Instead, the nutrient abundances creates ionic disequilibrium with profound physiological consequences (Rietra et al., 2017). For example excessive K^+ uptake can

interfere with the Mg^{2+} uptake by saturating shared cationic transport pathways and channels in plant roots. Such antagonism extends to other micronutrients, including Zn^{2+}, and Mn^{2+} uptake leading to nutrient imbalances that affects photosynthetic efficiency and impair metabolic pathways that weakens the structural development, essential for sustaining trunk growth (Xie et al., 2021). By contrast, the lower nutrient concentrations in trunking sago palms soils suggested to have balance ionic composition in the soil, resulting in better nutrient absorption of the roots. As for AP, the result was consistent with the finding on peat swamp soil (Kadir et al., 2020). The finding showed there was a significant difference between the subsoils of trunking and non-trunking sago palms. This significant differences at the subsoils is likely due to leaching of the nutrient from the topsoil to the subsoil. This is supported by the lower BD value of peat soils at non-trunking soils which enhances porosity and solute movement. In addition, peat soil exhibit very high water-holding capacity (300-3000% of its dry weight) compared to mineral soil (20-35%), further promoting nutrient transport to the subsoil and depleting the nutrient pool (Dom et al., 2021). The high nutrient leaching in non-trunking soils imposes physiological stress toward the non-trunking palms. Hence, it is postulated that trunking sago palms soils has better drainage and reduced waterlogging conditions, which allows better microbial activity, nutrient cycling, and root respiration to enable proper growth condition to the palms (Kooch et al., 2025).

Boron (B) is an essential micronutrient for plant growth and development, and its deficiency can impair plant development and function (Brdar-Jokanović, 2020). Boron studies have reported a significant correlation between the amount of available B and plant growth and development, as long as it is within the non-toxic level (Vera-Maldonado et al., 2024). The optimum range of B in soil is between 0.5 – 2.0 mg kg^{-1} (de Mendonça et al., 2024). Based on the physicochemical properties in Table 3.1, both soils exhibited high B

concentrations exceeding the optimum agronomic range, whereby the B level in the trunking sago palm soil (7.40-7.40 mg kg^{-1}) was found to be lower than in non-trunking sago palm soil (9.60 – 11.00 mg kg^{-1}). Study found extreme B dose application to sago palms exhibited higher dry biomass in sago palm petiole and suckers, suggesting age- or stage-dependent to B tolerance (Kakuda et al., 2005). While clear B deficiency or toxicity symptoms remain undocumented in sago palms, combined deficiencies of K, Zn, and Cu are prevalent in wild sago palms (Kakuda et al., 2015). The enhanced vacuole biogenesis observed in the GO terms of trunking sago palms suggests an adaptive capacity of the palm to sequester excess B into vacuole. This compartmentalisation protects cytoplasmic metabolism from B toxicity, thereby sustaining enzymatic regulation, photosynthetic efficiency, and carbohydrate assimilation (Martínez-Cuenca et al., 2015; Luo et al., 2024). In contrast, non-trunking sago palms, which likely lacking vacuole compartment, the excessive B level in the soil directly induced toxicity in the plant. The resulting toxicity exhibited by interveinal chlorosis in leaves, reflecting impaired chlorophyll integrity and reduced efficiency of photosystem II and electron transport, which reduces photosynthetic capacity of the palm. Furthermore, B toxicity further disrupts carbohydrate metabolism by restricting phloem loading and assimilate translocation, thereby limiting the supply of energy and structural carbon to developing tissues. Overtime, the reduction in leaf biomass and its functional capacity resulted in impaired trunk development as what is observed in non-trunking sago palms (Riaz et al., 2021). Moreover, the high nutrient leaching in non-trunking soils may suggests enhanced B uptake into the palm as reported by a study in grapevines where cations deficiency especially Ca^{2+} shown to greatly increase B uptake into the vines leading to root deterioration and several structural impairment including short stature phenotype with small stem diameter (Duan et al., 2022).

The contrasting developmental outcomes between trunking and non-trunking sago palms can be explained by the combined effects ionic balance and B tolerance. In non-trunking palms, excess in exchangeable bases disrupts micronutrient uptake, impairing photosynthesis and metabolic pathways essential for sustaining meristematic activity. The elevated B levels in soil coupled with limited vacuolar compartmentalisation, further exacerbate the palm's stress. This dual constraint of ionic imbalance and boron toxicity impairs hormonal regulation, weakens structural reinforcement, and disrupts energy metabolism, ultimately restricting trunk formation.

3.4.2 Dominant microbial functions in sago palm plantation peat soils

Rarefaction analysis of ASVs at over 50,000 reads plateaued for both 16S and ITS, indicating sufficient sequencing depth to capture microbial diversity within samples. The major ASVs of 16S in the V3-V4 region identified in soil samples from both sites are linked to bacterial communities of Acidobacteria, Proteobacteria, and Actinobacteria. These are common dominant phyla in peatland ecosystems *i.e.,* Maludam National Park, Sarawak, Peninsular Malaysia, Indonesia, Brunei and Thailand (Tripathi et al., 2016; Too et al., 2018; Dom et al., 2021). Meanwhile, the major ASVs of ITS1 identified Ascomycota and Basidiomycota, as the dominant fungal phyla in the collected soils. This aligns with findings from peatlands and other terrestrial studies (Debeljak & Baltar, 2023). These hardy phyla are known to survive under stressful conditions including oligotrophic, low pH (acidic), high salinity, and heavy metal-polluted environment (Zhang et al., 2024). These phyla are important in the soil ecosystem, and each of them has its own functions.

Acidobacteria (32-51%), Proteobacteria (21-29%), and Actinobacteria (7-21%), Ascomycota (60-87%), and Basidiomycota (6-31%) exhibit similar functional abilities to decompose plant litter, with fungi recognised as the key decomposers thanks to the

specialised enzymes secreted by these microbes including carbohydrate-active enzymes (CAZymes) *i.e.,* glycosyl hydrolases, polysaccharide lyases, β-glucosidase, acetyl xylan esterase, cellobiohydrolase, arabinofuranosidase, ligninase and pectin lyase (Peltoniemi et al., 2012; Wang et al., 2020). Ascomycota and Basidiomycota are highly effective at degrading crop residues thanks to their complementary enzymes, which increase nutrient availability in the soil. Ascomycota is deemed more specialised in cellulose-hemicellulose degradation, whilst Basidiomycota is more specialised in lignin degradation (Fukasawa, 2021). Additionally, these fungi are categorised as arbuscular mycorrhizal and are known to facilitate the acquisition of low-mobility nutrients like phosphorus from the soil (Ezawa & Saito, 2018). The different lignocellulose-degrading enzymes produced by Ascomycota and Basidiomycota, suggest cellulose decomposition is more prevalent than lignin decomposition, reflecting the higher relative abundance of Ascomycota compared to Basidiomycota. A study showed that Ascomycota members dominated fungal communities during straw residue decomposition, highlighting their role as the primary decomposers of cellulose (Ma et al., 2013). The higher relative abundance of Ascomycota compared to Basidiomycota in the studied soils suggests leaf litter decomposition is more significant than woody litter decomposition (Leifheit et al., 2024). Additionally, the high lignin content in non-trunking sago palms as depicted by higher lignin deposition in their tissues may imply slower nutrient return in soils due to the lower presence of lignin decomposers. In peat soil environments, a high ground water-table results in continuous flooding is more common in deep peat areas. High moisture content in peat soils was found to reduce arbuscular mycorrhizal fungi (AMF) diversity and slower wood decomposition (Ma et al., 2013; Asano et al., 2021).

Apart from the active decomposers, the dominant bacterial taxa identified in this study are active plant growth-promoting rhizobacteria (PGPR). N fixation *nif genes* (i.e *nifA*, *nifB*, *nifD*, *nifH*, *nifJ*, *nifK*, *nifS*, and *nifW*) encoded in Acidobacteria and Proteobacteria, and dissimilatory sulphite metabolism including *dsrAB*, *dsrC*, *dsrD*, *dsrN*, *dsrT*, *dsrMKJOP* and *DsrL* in Acidobacteria indicate active N and S cycling participation of these taxa (Flieder et al., 2021; Rahimlou et al., 2021; Gonçalves et al., 2024). Acidobacteria and Actinobacteria synthesised exopolysaccharides (EPSs), siderophore, plant growth hormones and antibiotics which aid in soil aggregation and biofilm formation, enhancing nutrient uptake, soil stability, and root protection from pathogens (Boukhatem et al., 2022; Carezzano et al., 2023). Studies have shown soil water content, EC, TN and TP profoundly influence the composition and microbial communities in the soil (Boukhatem et al., 2022). Research conducted using chambers and wetlands demonstrated slower bacterial litter decomposition under oxygen-deprived conditions (Rejmánková & Houdková, 2006). Classified as k-strategist bacteria, Acidobacteria can tolerate harsh living conditions such as acidic soils, limited nutrient availability, and toxic compounds (Gonçalves et al., 2024). Decomposition by this bacterial taxon determined in this study is important in acidic oligotrophic wetlands. Studies have found that Acidobacteria help decompose organic matter and enrich soil in waterlogged areas where soybean and paddy are grown (Yu et al., 2022). In tobacco-rice cropping systems, these bacteria are associated with higher ammonium N levels, indicating their role in N cycling (Chen et al., 2021). Additionally, inoculating Acidobacteria into duckweeds environment supports the healthy growth of these aquatic plants, highlighting their importance in waterlogged and aquatic areas (Yoneda et al., 2021). Meanwhile Actinobacteria, which are abundant in nature, hold significant importance in agriculture due to their diverse metabolic properties. They can directly and indirectly ameliorate plant

growth hence, classifying them as potential PGPR (Yadav et al., 2018). Actinobacterial inoculations have contributed to protecting and improving plant growth under harsh conditions including acidic soil, drought and high salinity environments (Ebrahimi-Zarandi et al., 2023). This observation was supported by an Actinobacteria inoculation study in a coastal area, which reported increased mangrove dry biomass, demonstrating the bacteria's ability to thrive in high-saline environments and its positive association to mangrove growth (El-Tarabily et al., 2021). These qualities make Actinobacteria invaluable in agriculture to improve productivity and soil sustainability. The Proteobacteria include methanotrophs abundantly found in peatlands and other terrestrial soils. In this study, members of the classes Alphaproteobacteriota and Gammaproteobacteriota were identified as typical heterotrophic bacteria involved in nitric oxide dismutation, as evidenced by the presence of nitric oxide (*nod*) genes. The presence of these *nod* genes suggests that these bacterial classes function as oxygenic denitrifiers, converting nitric oxide (NO) into N_2 gas and oxygen, thereby enabling aerobic respiration in oxygen-deficit areas such as peatlands (Elbon et al., 2024). Additionally, Proteobacteria have been reported to involved in methane oxidation and heavy metal reduction (Mellado & Vera, 2021). Inoculation studies demonstrated that Proteobacteria can reduce heavy metal accumulation and enhance biomass and yield in crops such as maize and soybean (Bai et al., 2024).

3.4.3 Differences microbial relative abundance in soil samples

Principal Coordinates Analysis (PCoA) demonstrated distinct clustering between trunking and non-trunking sago palm soils (Figure 3.8). However, differential abundance analysis identified several phyla to be more abundant in a land plot. The different microbial communities between sampling sites may relate to the soil's anoxic conditions and heavy metal pollution (Yin et al., 2021). Different microbial phyla found in the soil samples were

the Desulfobacterota, Nitrospirota, and WPS-2. Nitrospirota and Desulfobacterota are important sulphate-reducing bacteria (SRB) that encode sulphur oxidation genes such as *sqr*, *sdo*, and *dsr* in their genome. These genes enable them to reduce sulphate to hydrogen sulphide and subsequently convert it back to sulphur or sulphate, contributing to the sulphur cycle in soil (Zhang et al., 2024). The significant relative abundance of Desulfobacterota (2-6%) and Nitrospirota (3%) in trunking soil samples suggests higher available sulphur for plant uptake and supports microbial nutrient cycling under anaerobic conditions (Rodriguez et al., 2025).

Nitrospirota is advantageous in nutrient-deficit environments like peatlands. Apart from sulphur reducing, Nitrospirota includes nitrate-oxidising bacteria. These chemoautotrophic bacteria play a significant role in N cycling. Several members of Nitrospirota includes *Nitrospira*, *Thermodesulfovibrio*, *Leptospirillum*, and 4-29-1 were identified in the soil samples of this study. The class *Thermodesulfovibriona* is equipped with genes that enable the reduction of nitrates and sulphates (Sakoula et al., 2021). *Nitrospira* and *Leptospirillum* are capable of nitrite oxidation and are involved in microaerobic-anaerobic iron oxidation (Mosley et al., 2024). Additionally, *Nitrospira* can perform complete nitrification processes, known as comammox, which involves a complete ammonia conversion into nitrite and then into nitrate by a single organism (Koch et al., 2019). Metagenome-Assembled Genomes (MAGs) revealed that *Nitrospira* contains genes involved in nitrite oxidation (*nxrA* and *nxrB*), the reduction of the tricarboxylic acid cycle for carbon dioxide fixation (rTCA), the pentose phosphate pathway, gluconeogenesis, and the oxidative Tricarboxylic Acid Cycle (TCA) cycle pathway (Palomo et al., 2022). These bacterial processes create a conducive environment for plant growth supplying nitrate and glucose in soil (Han et al., 2018). They also enrich soil carbon, improve soil fertility and

structure, and suppress pathogens in soil *via* rTCA and Pentose Phosphate Pathway (PPP) (Li et al., 2023). Inoculation and fertiliser application studies, led to better cycling of C, N, and P, and higher crop yields (Wu et al., 2022). This aligns with the application of biostimulator application like *Pseudomonas* sp. and *Azotobacter* sp., which also increase *Nitrospira* abundance. The increase in *Nitrospira* leads to higher nitrate levels and enhanced winter wheat yield (Dobrzyński et al., 2025). Studies on the effects of pH and inoculum with ammonia-oxidising bacteria (AOB) revealed that *Nitrospira* is the favoured nitrifiers in lower pH soils, supporting robust plant growth in aquaponics systems (Derikvand et al., 2024). Additionally, research on AMF inoculation in soybean soil showed positive impact on the S cycle and increased *Nitrospira* composition, resulting in improved sulphur absorption and growth in soybeans (Wu et al., 2022).

Desulfobacterota are strict anaerobes that thrive in oxygen-deficit environments. Desulfobacterota is involved in arsenic detoxification and mercury reduction in soil. In sulphur-rich media, Desulfobacterota and Nitrospirota work to convert dissolved arsenic (As) into immobile As-S minerals like orpiment (As_2S_3), realgar (AsS), and arsenopyrite (FeAsS) reducing toxicity in soil and prevent As uptake by plants (Tashan et al., 2021). A study on As-contaminated paddy soils found that the existence of the arsenic oxidation *arxA* and dissimilatory nitrite reductase *nrfA* genes in Desulfobacterota and Nitrospira, convert As to be less toxic and easier to remove from water (Zhao et al., 2024). Additionally, MAGs of Desulfobacterota revealed the presence of mercury reduction *merA* genes, indicating their potential mercury reducers in anoxic environments (Lu et al., 2016). Desulfobacterota is widely reported to facilitate the reduction of toxic ionic mercury (Hg^{2+}) to less toxic elemental mercury (Hg^{o}) (Rincón-Tomás et al., 2024). Bioremediation studies have shown that mercury detoxification by Desulfobacterota can significantly increase maize biomass by

30-50% in mercury-contaminated soils (Wu et al., 2024). Research on Desulfobacterota in fluctuating oxygen conditions found the bacteria drives sulphur cycling at oxic-anoxic interphases (Dyksma & Pester, 2024). Study on synergistic treatment of SRB and manganese fertiliser ($MnSO_4$) demonstrated enhanced cadmium (Cd) immobilisation by promoting the growth of Cd-tolerant bacteria like Desulfobacterota. This treatment increased sulphate reduction, elevated soil pH, and reduced the availability of Cd in paddy soils, leading to improved rice performance (Su et al., 2024). The experimental site in this study is located nearby a coal-fired power plant. This suggests potential mercury contamination in surrounding soils (Sia & Abdullah, 2015). The higher abundance of Desulfobacterota in trunking soils indicates a more favourable root environment in trunking sago palms compared to the non-trunking sago palms (Cabrol et al., 2023).

The Wittenberg-polluted soil (WPS-2), also known as *Candidatus eremiobacterota*, constitutes 2-6% of the soil samples collected in this study. This phylum is found abundant in polluted soils contaminated with polychlorinated biphenyls (PCBs) (Sazykina et al., 2022). Studies indicate a positive correlation between WPS-2 and pollutant content, especially polycyclic aromatic hydrocarbons (PAHs) (Sazykina et al., 2022). WPS-2 harbours genes encoding RuBisCO type 1E and high-affinity Group 1h (NiFe)-hydrogenase, which allows them to thrive in nutrient-poor soils by utilising hydrogen as an energy source (Sheremet et al., 2020). Interestingly, their genomes lack indications for autotrophy, phototrophy, or trace gas metabolism. Instead, they function as heterotrophic scavengers (Azizan et al., 2024). Accordingly, due to scarce information of WPS-2 functions in tropical peatlands, further study is required. There are no studies reported on the beneficial role of WPS-2 in relation to plant growth and health.

3.4.4 Microbial decomposition, nutrient cycling, and detoxification supporting trunk formation in sago palms

The dominance of Acidobacteria, Proteobacteria, Actinobacteria, Ascomycota, and Basidiomycota in the peat soils highlights the central role of microbial decomposition, nutrient cycling, and rhizosphere resilience in supporting sago palm trunk development. In fungal community, the higher percentage denoted by Ascomycota compared to Basidiomycota suggests higher turnover of nutrients happens in trunking sago palm soils as there is less lignified organic litter, as observed by lower lignin biosynthesis presented by the sago palm's leaf transcriptome analysis (Leifheit et al., 2024). These fungi also facilitate phosphorus acquisition, a macronutrient fundamental to plant metabolism. Phosphorus-deficient plants often showed stunted growth and poor root growth. Phosphorus sustains the meristematic activity through adenosine triphosphate (ATP) synthesis, which provides the energy required for cellular metabolism, thereby supporting rapid energy transfer for cell division and differentiation in the SAM (Xiao et al., 2024; Yang et al., 2024). Moreover, phosphorus is important in photosynthesis to ensure a continuous supply of sugars and energy to support meristematic cell division, while stabilising nucleic acids and phospholipids, which are essential for genome replication and membrane integrity (Khan et al., 2023).

The N and S cycling by the microbes further sustains meristem activity in the palm. N which provides the essential substrates for chlorophyll biosynthesis, directly enhance photosynthesis efficiency, assimilate production, and transport of assimilates to SAM, in order to cater rapid SAM activity and plant architecture (Camut et al., 2021; Liu et al., 2025). Meanwhile S cycling cater the meristem activity by synthesising cysteine and methionine. Cysteine ensures structural stability and redox protection of proteins, while methionine

ensures proper initiation of protein synthesis and epigenetic regulation (Wawrzyńska & Sirko, 2024). Together, they sustain meristem activity by enabling persistent internode elongation and biomass accumulation (Dimitriadi et al., 2025). Under impaired S cycling, less cysteine and methionine will be synthesized, contributing to weakens protein stability and enzyme regulation, thereby halting meristem activity in plants (Wawrzyńska & Sirko, 2024). The presence of Desulfobacterota and Nitrospirota at trunking sago palms soils suggest an advantage to trunking sago palms. Apart from supporting active nutrient cycling, these bacteria work synergistically to enhance heavy metal soil detoxification. Toxic heavy metals such as arsenic and mercury were immobilised by Desulfobacterota through the reduction process of sulphate to sulphide. In parallel, Nitrospirota recycle sulphur intermediates and contribute to nitrite oxidation, thereby maintaining redox balance and reinforcing N and S turnover (Rincón-Tomás et al., 2024). This synergistic action by these bacteria stabilises soil chemistry, which protects plant roots from arsenic and mercury toxicity, thus ensuring efficient nutrient uptake to sustain assimilate flow and enzyme stability in meristematic tissues (Sharma et al., 2025). Therefore, the presence of these rhizobacteria enables heavy metals detoxification in the soil, thereby suggesting better root environment to the trunking sago palm roots, thus enhancing the nutrient uptake by the roots.

3.5 Conclusion

This study investigated the environmental factors influencing sago palm growth by examining the physicochemical properties of peat soils and the microbial communities in the trunking and non-trunking sago palms soils. The contrasting developmental outcomes between trunking and non-trunking sago palms can be attributed to the interplay of ionic balance, B tolerance, pH level, and soil-microbial interactions. In non-trunking sago palms, excess exchangeable bases create ionic disequilibrium and toxicity thus impairs photosynthesis rate of the palm. Persistent waterlogging and high lignin content in organic matter in non-trunking sago palms soils affects microbial activity, resulting in limited nutrient turnover in the soils. On contrast, trunking sago palms suggested to benefit from the slightly lower nutrient concentrations in the soil which minimise ionic antagonism, alongside with enhanced vacuolar compartmentalisation that mitigates B toxicity. Moreover, Desulfobacterota and Nitrospirota contributed to enhanced N and S cycling while reducing heavy metal stress, reinforcing physiological resilience. Overall, the findings elucidate the synergistic interplay between soil physicochemical properties and microbial community as one of the critical determinant of sago palm growth and trunk development.

CHAPTER 4

GENERAL DISCUSSION AND CONCLUSION

4.1 Overview and Research Integration

This work presents the first comprehensive integration of leaf transcriptomics, soil physicochemical properties, and microbial community analyses to unravel the molecular and environmental factors associated with the trunk formation in *Metroxylon sagu* Rottb. While previous research largely focused on non-trunking sago palms with limited gene expression approaches, this study expands the scope to the productive trunking sago palms, bridging the critical knowledge gaps through transcriptomics, biochemical, and amplicon sequencing frameworks. The findings demonstrate that trunk formation in sago palm is not solely dictated by gene programming, but emerges from the coordinated interplay of plant molecular regulation, soil nutrient dynamics, and beneficial microbial associations.

It is hypothesised that trunking sago palms possess distinct molecular regulatory mechanisms that promote meristem activity, vascular bundle initiation and maturation, and carbon partitioning while being supported by slightly better soil properties and microbial communities. Functional enrichment highlighted upregulated pathways associated with stress response, genome stability, phosphate uptake and vacuole biogenesis, while downregulated pathways reflected reduced lignin and flavonoid biosynthesis. In parallel, soil analysis indicated acidic conditions of peat soils with high organic carbon content, yet different microbial community profiles identified in trunking and non-trunking sago palm soils, with higher relative abundance of Desulfobacterota and Nitrospirota in trunking sago palm soils, and WPS-2 was identified only in non-trunking sago palm soils.

This chapter synthesises the findings from Chapter 2 and 3, contextualising them within broader plant developmental biology, stress physiology, and soil-plant-microbe interactions. The discussion interprets how coordinated gene expression patterns, transcription factor dynamic, phosphate homeostasis, cell wall remodelling, and microbial-mediated nutrient cycling converge to enable sustained growth and trunk development in sago palms.

4.2 Molecular Mechanisms Driving Trunk Formation in Sago Palms

4.2.1 RNA editing, transcript integrity, and hormonal crosstalk for stress resilience in trunking sago palms

Coordination between cell signalling, hormone regulation, genetic mechanism, and epigenetic regulation is fundamental to plant development. In the present study, trunking sago palms exemplify a coordinated enhancement of genome stability, transcript integrity, and stress resilience. RNA editing mediated by RanBP2-type zinc finger proteins in chloroplasts and mitochondria ensures transcript fidelity by correcting genomic mutations, thereby sustaining photosynthetic efficiency and energy production. This mechanism is particularly critical in plants where cumulative mutations in organellar genomes could otherwise compromise metabolic performance. Concurrently, CSP1 functioning as an mRNA chaperone, facilitate stress-adaptive translation to maintain continuous protein synthesis under adverse conditions (Yang et al., 2024). Together, these processes mitigate genotoxic stress and prevent translational collapse, ensuring that meristematic activity is not compromised during environmental fluctuations.

This molecular framework is further reinforced by NRPD1B-mediated RNA-directed DNA methylation (RdDM). Together with AGO10, NRPD1B initiates the production of double-stranded RNA precursors for small interfering RNAs (siRNAs)

(Erdmann & Picard, 2020). These siRNAs are subsequently processed and loaded onto Argonaute proteins, which sequesters miR165/166 to prevent the degradation of HD-ZIP III transcription factors. HD-ZIP III proteins are required in establishing vascular tissue and organising auxin maxima for sustaining stem cell activity and trunk formation (Zhang & Zhang, 2012). Such epigenetic regulation reflects an efficient developmental strategy in trunking sago palms, where hormonal signalling, transcript fidelity, stress-adaptive translation, enabling trunk formation. The epigenetic regulation by NRPD1B prevents transcriptional noise and aberrant gene expression in trunking sago palm for resilience, long-term stability.

In parallel, the plant leaves, which are the primary organs are continuously exposed to environmental stresses such as prolonged exposure to extreme heat and ultraviolet (UV) radiation. This stress conditions elevates reactive oxygen species (ROS) levels in the plant leaf tissues. Excessive ROS production can stall replication forks, leading to DNA double-strand breaks (DSBs) that can threaten genome stability and cell survival. Efficient repair of DSBs is essential to maintain genomic integrity (Nisa et al., 2019). Stress-responsive proteins such as ATL5, RanBP2-Znf, CSP1, and Zip4 contribute to cellular homeostasis through diverse mechanisms. The elevated expression of RanBP2-type zinc finger proteins and CSP1 in trunking sago palms is suggested to play a pivotal role in mitigating genotoxic stress. RanBP2-Znf proteins contributes to RNA editing fidelity in chloroplasts and mitochondria, preserving transcript accuracy and supporting photosynthesis efficiency (Sreeharsha & Mohan, 2024), while CSP1 stabilises RNA to facilitate proper protein synthesis, preventing translational collapse. In parallel, the ATL5 facilitates the degradation of dysfunctional proteins (Wang et al., 2025). Collectively, these molecular responses

enhances cellular resilience and ensures the adaptation of the plant under stress does not compromise meristem function and reinforce genome integrity.

Beyond the molecular safeguards, the dynamic interplay between ABA-mediated stress responses and GA-driven growth is crucial for balancing survival and development in plants. The rapid activation of ABA signalling contributes to stress adaptation by inducing stomatal closure. This transient ABA response which facilitated by $InsP_6$-mediated reduction of potassium ion influx into guard cells, decreases turgor pressure. This suppresses photosynthetic activity, hence reflecting a trade-off between stress protection and growth (Li et al., 2017). Following stress alleviation, giberrellin (GA) signalling resumes plant growth by promoting DELLA protein ubiquitination, which activates multiple transcription factors to restore cell elongation and meristem activity (Panozzo et al., 2025).

The antagonistic yet complementary actions of ABA and GA, therefore establish a dynamic regulatory cycle that enables plants to maintain continuous meristematic activity and vascular initiation under fluctuating environmental conditions (Zhai et al., 2025). By coordinating hormonal signalling through RNA editing fidelity, stress-adaptive translation, and DNA repair, it can be postulated that trunking sago palms achieve a developmental strategy that balances environmental resilience with growth and development. This multilayered regulation underpins trunk formation, sustained growth and long-term resilience in challenging environments.

4.2.2 Metabolic reprogramming and auxin-mediated regulation for trunk formation

The downregulation of lignin and flavonoid biosynthesis is closely associated with increased SAM activity and enhanced auxin transport. The reduction in these enzymes suggested to enable vertical growth and trunk formation in sago palms. Flavonoids such as quercetin and kaempferol are well-established modulators of auxin transport, acting as

endogenous inhibitors of polar auxin flux. Reduced accumulation of these compounds alleviates the inhibitory constraint on auxin movement, therefore reinforcing basipetal auxin signalling from leaf tissues toward the stem apex (Xiong et al., 2019). The strengthened auxin gradient promotes progressive initiation and maturation of vascular bundle.

Brassinosteroids (BRs) act in close cooperation with auxin to promote trunk formation in monocots. The regulatory loop benefited from flavonoid downregulation and auxin reinforcement provides a developmental advantage to trunking sago palms. Enhanced auxin transport synergistically activates SAMs through ARF-mediated transcription regulation help to sustains the stem cell activity. This enable continuous organogenesis through continuous generation of undifferentiated daughter cells (Pernisová & Vernoux, 2021). During differentiation and expansion, auxin establishes localised maxima that result in direct meristematic activity, while BRs together with auxin participate in vascular bundle proliferation and xylem/phloem differentiation, thereby enhancing early procambial divisions (Furuya et al., 2024). This mechanism ensures functional connectivity between source organs and sink tissues, hence supporting the metabolic demands of trunk formation and expansion. In parallel, the cell wall reprogramming mediated by XTHs facilitates the microfibril slippage, which confers flexibility to the primary cell wall. This process allows cell enlargement while preserving structural integrity, hence accommodate the mechanical requirements of vertical growth while preserving tissue stability (Bi et al., 2024).

Moreover, the reduction in lignin biosynthesis further contributes to developmental plasticity. Reduced lignin deposition enhances cell wall extensibility, facilitating expansion of leaf laminae and therefore increase the photosynthesis surface area. This morphological adjustment increase light capture and carbon assimilation, leading to greater production of assimilates that can be translocated into sink organs (Liu et al., 2016). In summary, the

downregulation of lignin and flavonoid biosynthesis, coupled with enhanced auxin transport and cell wall reprogramming represents a coordinated developmental strategy in trunking sago palms highlighting the adaptive advantage of trunking sago palm in sustaining growth amid under environmental stress.

4.2.3 Vacuolar Pi mobilisation and cytokinin-ABA regulation supporting palm trunk formation

The dynamic interplay between hormonal signalling, nutrient homestasis, and stress adaptation is fundamental in sustaining trunk formation in sago palms. Vacuoles function as versatile reservoirs as they store Pi and sequester toxic ions, thereby stabilizing cytoplasmic homeostasis under adverse conditions. Mobilization of vacuolar Pi through transporters such as PHT5 elevates cytoplasmic Pi concentration, sustaining glycolysis and oxidative phosphorylation. This continuous ATP supply prevents energy depletion under stress, hence ensuring cell proliferation (Yang et al., 2017). This coupling mechanism in trunking sago palms preserves meristematic activity by sustaining cytoplasmic energy supply, preventing interruption of cell division and elongation.

Cytokinin signalling further reinforces this process by enhancing nutrient uptake and allocation. Through modulation of phosphate and nitrate transporter activity, cytokinin ensures that assimilates and micronutrients are directed toward SAM. The elevated cytokinin activity, along with sustained nutrient flow, supports progressive vascular bundle initiation and maturation, while simultaneously stimulating chloroplast biogenesis and photosynthetic capacity to strengthen source-sink relationships. Cytokinin also exerts direct control over plastid gene expression and ribosomal RNA maturation, thereby safeguarding transcript integrity within chloroplasts and ensures efficient translation of photosynthetic proteins (Pokimica et al., 2024). In parallel, ABA provides osmotic regulation, stabilizing osmotic

potential and protecting enzymatic activity despite ABA transiently suppresses growth. This protective mechanism preserves cellular integrity in expanding trunk tissues, ensuring that meristematic activity and vascular initiation are not compromised during stress (Du et al., 2025).

The crosstalk between cytokinin and ABA establishes a balance between growth and resilience, integrating nutrient homeostasis with osmotic regulation. Cytokinin promotes nutrient acquisition, meristem activity and guarding transcript integrity, while ABA enforces osmotic regulation and stress tolerance. Their integration with vacuolar function to sustain Pi storage and mobilization provides a buffering system that sustains ATP synthesis, cytoskeletal dynamics, and auxin-mediated vascular bundle initiation and maturation. In trunking sago palm, by coordinating nutrient homeostasis with osmotic regulation, cytokinin and ABA signalling provide trunking sago palms with as robust adaptive framework that ensures active SAM function, continuous incorporation of vascular bundles into expanding trunk, reinforcing continuous growth and trunk development, highlighting the adaptive advantage of trunking phenotypes.

4.3 Soil Nutrient and Microbial Contribution to Trunk Formation

4.3.1 Synergistic regulation of macronutrient N and P in regulating balanced growth and development

The synergistic mechanism of N and P is crucial in supplying nutrient to plant and maintain metabolic balance. N availability actively reprograms phosphate signalling ensuring phosphate starvation responses (PSR) are fully engaged when N supply is sufficient. This synergistic mechanism prevents disproportionate nutrient uptake and maintain balanced N:P ratios in plant tissue (Cui et al., 2019). P availability influence N acquisition through a feedback network of SPX-PHR sensing and Nitrate-inducible Garp-

type Transcriptional Repressor 1/ HRS1 homolog (NIGT1/HHO) transcriptional regulation. During sufficient Pi condition, SPX proteins bind to $InsP_6$ and interact with PHR transcription factors to suppress P starvation responses and limits the induction of NIGT1/HHO genes and allowing strong nitrate uptake and assimilation. Conversely, Pi deficiency alleviates the SPX-mediated inhibition, allowing PHR transcription factors to activates phosphate starvation genes, including the NIGT1/HHO genes. This expression represses nitrate uptake, thereby restricting nitrate influx during Pi deficiency. The PHR-NIGT1/HHO cascade also antagonizes NIN-like protein (NLP) - driven nitrate signalling outputs, hence declining the expression of nitrate assimilation and growth-related genes (Ueda et al., 2020). Through this mechanism, P availability exerts direct transcriptional control over N uptake, ensuring nitrate acquisition in dynamically scaled to Pi availability. The repression of nitrate uptake under Pi deficiency serves as protective strategy to prevent metabolic imbalance as nitrate assimilation requires adequate ATP, nucleotides, and phosphorylated intermediates. Excess nitrate influx during Pi deficiency results in energy depletion, accumulation of assimilated N and oxidative stress (Hu et al., 2025).

In this study, the contrasting morphologies of trunking and non-trunking individuals can be interpreted through the lens of N and P synergistic regulation. Although trunking sago palm soils exhibit lower N and P concentration, the positive morphology of trunking sago palms suggest nutrient efficiency rather than absolute abundance that underpinning the trunk development. Low nutrient pools in trunking sago palms soils may implies the activation of SPX-PHR-NIGHT1/HHO cascade, which restricts excessive nitrate influx under Pi deficient and aligns N assimilation with available phosphate-derived metabolites. This balanced regulation prevents metabolic stress and ensures that N:P uptake ratios remain favourable, hence channelling resources into structural growth and trunk formation. In contrast, the non-

trunking sago palm soils with higher N and P levels may bypass the regulatory safeguards, leading to disproportionate nutrient assimilation and less efficient allocation toward trunk development (Krouk & Kiba, 2020). Thus, this condition exemplifies a “low-input, high-efficiency” strategy, where synergistic N and P signalling optimises nutrient homeostasis and supports adaptive morphological outcomes (Ueda et al., 2020).

4.3.2 Plant-soil-microbe shaping hormone networks

The integration of soil chemistry with molecular regulation offers a mechanistic framework for understanding how edaphic factors translate into developmental outcomes in sago palms. Plants engage in dynamic crosstalk with various environmental signals, facilitating the integration of microbial communities which will influence the development of the plant (Trivedi et al., 2020). Plant roots secrete exudes, a complex mixture of sugars, amino acids, organic acids, and secondary metabolites that act as chemical cues that influence microbial composition, communities, and activities in the soil. In return, these microbes facilitate essential processes for plant growth such as organic matter decomposition, nitrogen fixation, and biosynthesis of phytohormones such as auxins, cytokinins, and strigolactones, as well as volatile organic compounds, siderophores, and enzymes.

During abiotic stresses such as high salinity or drought stress, plant roots exude 1-aminocyclopropane-1-carboxylic acid (ACC), the immediate precursor of ethylene. Elevated ACC pools drive ethylene biosynthesis which can inhibits root elongation and exacerbates stress symptoms by suppressing cell division and nutrient uptake (Gamalero et al., 2023). Beneficial rhizobacteria counteract this effect through the expression of ACC deaminase, a pyridoxal-5’-phosphate dependent enzyme that cleaves ACC into α-ketobutyrate and ammonia, lowering the substrate available for ethylene synthesis and reducing stress-

induced ethylene accumulation (Muhammad et al., 2024). In parallel, rhizobacteria synthesised indole-3-acetic acid (IAA), which enhances root proliferation, thereby enhancing nutrient uptake and adaptation to heavy metals by promoting phytoextraction of Pb, Zn, and cadmium (Cd) (Sytar et al., 2019; Shah et al., 2024). Complementing bacterial contributions, the interaction of arbuscular mycorrhizal (AM) fungi initiated by strigolactones, which is secreted by plant roots during nutrient deficiency stimulates fungal spore germination and hyphal branching. This root-fungal interaction enhances hydraulic conductivity during drought stress, facilitate N and P uptake in acidic or saline soils especially in low K availability soils and heavy metal detoxification (Gong et al., 2023). Moreover, AM fungi stimulate key antioxidant enzymes such as superoxide dismutase (SOD), peroxidases (POD), catalase (CAT), and ascorbate peroxidase (APX) which detoxify ROS by converting them into non-harmful molecules such as water and oxygen (Chandrasekaran et al., 2022). Together, these microbial associations support nutrient uptake and stress tolerance, thereby creating favourable conditions for trunk formation.

The persistent waterlogging and a shift toward anaerobic soil conditions in non-trunking sago palms result in reduced population of beneficial microbes, leading to impaired nutrient cycling. The limited Pi availability in soil, combined with impaired respiration under hypoxia, reduces ATP production and suppresses key growth regulators such as target of rapamycin (TOR) and cyclin-dependent kinases (CDKs). This condition activates sucrose non-fermenting 1-related protein kinase 1 (SnRK1) stress pathways, that halt the cell cycle (Margalha et al., 2019). Simultaneously, the shortages of sulphur-containing amino acids cysteine and methionine restrict protein synthesis, limit iron-sulphur (Fe-S) cluster assembly, forcing cells to divert resources toward redox defence and enhance antioxidant defence rather than protein synthesis. Depletion of S-adenosylmethionine (SAM) further

disrupts DNA and histone methylation as well as small-RNA regulation, resulting in reduced capacity for stem cell proliferation and tissue renewal (Azhar et al., 2022). The accumulation of toxic metals together with elevated ROS, worsen the cellular stress by inhibiting key enzymatic activity, damaging the mitochondria and disrupts the respiratory chain. These combined effects accelerate ATP depletion and destabilise protein function, thereby depleting cell energy (Mansoor et al., 2023). The chronic hypoxia and nutrient deficiencies induced by persistent waterlogging exacerbates these effects by turning on survival metabolism in the palms and further suppress protein translation and nutrient assimilation (Kęska et al., 2021). Ultimately, this cascade of low energy, limited amino acids, and methyl donors, metal toxicity, and hormonal imbalance may explains the collapse of SAM activity leading to failure in trunk formation in non-trunking sago palms.

The exclusive presence of WPS-2 in non-trunking soils suggest a microbial signature of environmental deterioration and stress. WPS-2 is typical to polluted, anaerobic and nutrient-impoverished soils. Its presence in the non-trunking soil suggest reduce in functional microbial diversity, coinciding with impaired nitrogen fixation, phosphate mobilisation imposed by persistent waterlogging condition at the plot. This condition may further suppress meristem activity and trunk development, hence positioning WPS-2 not only as a marker of poor soil quality but also as the contributor to the unfavourable conditions underlying the non-trunking phenotype.

4.4 Conclusion

This study highlights the integrated transcriptomic analysis of sago palm leaf tissues with peat soil characterization and microbial taxonomy profiling to address the knowledge gaps in *M. sagu* growth. Transcriptome study revealed that trunking sago palms exhibit enhanced molecular safeguards which includes RNA editing fidelity, stress-adaptive translation, and epigenetic regulation. The molecular regulations crucial to sustain meristematic activity and trunk formation despite facing abiotic stresses. Hormonal crosstalk particularly between cytokinin, brassinosteroids, and gibberellin reinforcing vascular initiation and vertical development in trunking sago palm.

Soil analyses demonstrated trunking sago palm soils associated with lower cations along with lower N, and P availability compared to non-trunking sago palm soils. This nutrient-efficient strategy enables metabolic balance and channels resources into trunk formation. In contrast to non-trunking sago palm, the persistent waterlogging results in impairs nutrient cycling in the soil. Microbial profiling further highlighted the role of beneficial taxa in nutrient mobilization, soil detoxification, and stress responses. In contrast, the non-trunking sago palm soils were characterised by microbial decline and the exclusive presence of WPS-2, a stress-associated bacterial group indicative of deteriorating soil quality.

4.5 Limitations and Future Recommendations

This study presents important insights into the molecular and microbial mechanisms associated with the trunking phenomenon in sago palm. However, it has several limitations that should be addressed in future research. On the transcriptomic side, leaf samples were collected from a limited number of sago palms within a single plantation, potentially limiting

the generalisability of the findings. Additionally, the study focused exclusively on a single developmental stage (*Pelawei manit*), without incorporating data from earlier or later stages, which restricts the understanding of gene expression dynamics across sago palm development. The absence of root transcriptome analysis further limits the scope of interpretation, as it overlooks key gene expression patterns that may be crucial in stress response, nutrient uptake, and plant-microbe interactions.

A key limitation of this study is that the soil samples were collected from a single site, Dalat Sago Palm Plantation in Mukah. Restricting the investigation to one plantation reduces ecological replication and limits the generalisability of the findings, as soil and microbial dynamics may vary across different peatland environments, management practices, and climatic conditions. This lack of replications constrains the robustness of the dataset and introduces the possibility of site-specific bias in data interpretation. Nevertheless, focusing on a single plantation also provides a controlled case study that reduces confounding variables and allows for a detailed examination of trunking versus non-trunking sago palm under consistent ecological and management conditions. As such, the Dalat plantation serves as a valuable baseline for understanding trunk formation in peat soils, and future studies incorporating multiple plantations and diverse peatland settings can build upon this foundation to strengthen the reliability and boarder applicability of the findings.

Building on the insights gained from the Dalat Sago Palm Plantation, future research should expand to include multiple plantations across different peatland regions to strengthen ecological replication and improve the generalizability of findings. Comparative studies across diverse soil types, hydrological conditions, and management practices would help disentangle site-specific effects from broader ecological drivers of trunk formation. Long-

term monitoring of soil nutrient dynamics, microbial community shifts, and phenotypic outcomes would provide valuable temporal resolution, revealing how seasonal changes and plantation management influence trunk development. Integrating transcriptomic data with soil and microbial analyses could further clarify the mechanistic pathways linking nutrient cycling, cambial activity, and trunk formation. Such multi-site, multi-layered approaches would not only validate the current findings but also establish a more comprehensive framework for improving sago palm cultivation and productivity in peatland ecosystems. Additionally, controlled growth conditions should be established, whereby the soil physiochemical are clearly defined to allow direct comparison. Such studies should be complemented with gnotobiotic or inoculation-based approaches to examine microbial potential in regulating host gene, especially the transcription of stress-related and nutrient responsive genes.

4.6 Recommendations to Sago Palms Plantation Management

The findings of this study underscore the need for an integrated management strategy to enhance *M. sagu* growth and development to cater sustainability of sago palm cultivation especially in peat soils. Previous exogenous N, P, K fertiliser application have consistently observed no positive developmental growth in sago palms grown on peat soils (Wang et al., 2020; Ming et al., 2018). This lack of efficacy is attributed to nutrient leaching which caused by waterlogging and the high adsorptions of cations due to low pH conditions typical of peat soils (Sasaki et al., 2025; Zainal et al., 2022). Consequently, the conventional fertilisation practices are insufficient to result in proper sago palm growth, hence necessitating approaches that integrate soil management, targeted nutrient delivery, biofertilizer application, and continuous monitoring.

Peat soils are common to waterlogging. Improved drainage systems are essential to mitigate waterlogging and restore aerobic condition, thereby enhancing microbial diversity and nutrient cycling (Espenberg et al., 2018). Soil treatment such as lime and biochar application can buffer peat soils acidity, enhance toxic metal adsorption, and improve nutrient retention. Furthermore, incorporating organic matter such as composted residues, enhances soil structure and supports beneficial microbial communities that facilitate nutrient mobilisation (Ahmed et al., 2023).

Phytohormones such as auxins, gibberellins, cytokinins, and ethylene are commonly applied in agriculture to induce fruiting and flowering in plants. Given the inefficiency of fertiliser application of peat soils, trunk injection to the stem of the plant has become the alternative method to deliver nutrients, hormones, pesticides, insecticides, and other plant growth promoting materials when foliar sprays or soil drenches fail to result in positive results (Archer et al., 2022). This method bypasses impaired root uptake and ensures targeted delivery to meristematic tissues. While phytohormones are widely used in agriculture to induce flowering and fruiting, their application to sago palms has thus far been limited to laboratory-based studies (Tajuddin et al., 2015). Field-based trials incorporating trunk injections of phytohormones including gibberellins and cytokinin may provide a promising solution to enhance vascular initiation and differentiation in both trunking and non-trunking sago palms.

The integration of biofertilizers enriched with NPK has demonstrated significant yield improvements in oil palm and rice cultivated on peat soils. Biofertiliser produced from rice straw and poultry manure (60:40) enriched with *Azospirillum* and phosphate solubilising bacteria increased rice grain yield by 252.63% compared to control, while oil palm fresh fruit brunches averaged 25.8 kg / bunch (Irawan et al., 2025; Marlina et al., 2025). It is

suggested to apply similar strategies for sago palm plantations to enhance nutrient efficiency, restore microbial diversity, thus support sago palm growth. Regular monitoring of soil nutrient profiles is essential to maintain balanced nutrient availability in the plantation especially in peat soils. Microbial community profiling should be employed to detect early shifts toward stress-associated taxa such as WPS-2. Growth performance indicator, including trunk initiation and leaf area index should be systematically tracked to evaluate plantation health.

In general, sago palm planters are advised to adopt a holistic management plan that integrates soil improvement, targeted nutrient and hormone delivery, biofertiliser application, and continuous monitoring. These measures directly address the contrasting conditions of trunking and non-trunking palms, ensuring sustainable growth, improved trunk information, and long-term productivity in peatland plantations.

REFERENCES

Abbasi, S., Sadeghi, A., & Safaie, N. (2020). Streptomyces alleviate drought stress in tomato plants and modulate the expression of transcription factors ERF1 and WRKY70 genes. *Scientia Horticulturae*, *265*, 109206. https://doi.org/10.1016/j.scienta.2020.109206

Abd-Aziz, S. (2002). Sago starch and its utilisation. *Journal of Bioscience and Bioenginnering*, *94*(6), 526–529.

Abrams, Z. B., Johnson, T. S., Huang, K., Payne, P. R. O., & Coombes, K. (2019). A protocol to evaluate RNA sequencing normalization methods. *BMC Bioinformatics*, *20*(S24), 679. https://doi.org/10.1186/s12859-019-3247-x

Adriaens, M., Jaillard, M., Waagmeester, A., Coort, S., Pico, A., & Evelo, C. (2008). The public road to high-quality curated biological pathways. *Drug Discovery Today*, *13*(19–20), 856–862. https://doi.org/10.1016/j.drudis.2008.06.013

Afiq, M., & Azura, A. R. (2013). Effect of sago starch loadings on soil decomposition of Natural Rubber Latex (NRL) composite film mechanical properties. *International Biodeterioration & Biodegradation*, *85*, 139–149.

Ahmed, T., Noman, M., Qi, Y., Shahid, M., Hussain, S., Masood, H. A., Xu, L., Ali, H. M., Negm, S., El-Kott, A. F., Yao, Y., Qi, X., & Li, B. (2023). Fertilization of microbial composts: a technology for improving stress resilience in plants. *Plants*, *12*(20), 3550. https://doi.org/10.3390/plants12203550

Ain, N., Haider, F. U., Fatima, M., Habiba, Zhou, Y., & Ming, R. (2022). Genetic determinants of biomass in C4 crops: molecular and agronomic approaches to increase biomass for biofuels. *Frontiers in Plant Science*, *13*. https://doi.org/10.3389/fpls.2022.839588

Akhmad Kadir, Rosye, H. R. T., Suharno, S., Basa, T. R., & Muhammad, A. R. (2020). Soil physicochemical and ethnobiological studies on the peat swamp forests of Southern Papua, Indonesia. *Biodiversitas Journal of Biological Diversity*, *21*(4). https://doi.org/10.13057/biodiv/d210454

Alabdullah, A. K., Moore, G., & Martín, A. C. (2021). A duplicated copy of the meiotic gene ZIP4 preserves up to 50% pollen viability and grain number in polyploid wheat. *Biology*, *10*(4), 290. https://doi.org/10.3390/biology10040290

Alberton, D., Valdameri, G., Moure, V. R., Monteiro, R. A., Pedrosa, F. de O., Müller-Santos, M., & de Souza, E. M. (2020). What did we learn from plant growth-promoting rhizobacteria (PGPR)-grass associations studies through proteomic and metabolomic approaches? *Frontiers in Sustainable Food Systems*, *4*. https://doi.org/10.3389/fsufs.2020.607343

Aleksander, S. A., Balhoff, J., Carbon, S., Cherry, J. M., Drabkin, H. J., Ebert, D., Feuermann, M., Gaudet, P., Harris, N. L., Hill, D. P., Lee, R., Mi, H., Moxon, S., Mungall, C. J., Muruganugan, A., Mushayahama, T., Sternberg, P. W., Thomas, P. D., Van Auken, K., … Westerfield, M. (2023). The gene ontology knowledgebase in 2023. *Genetics*, *224*(1). https://doi.org/10.1093/genetics/iyad031

Al-Shammary, A. A. G., Kouzani, A. Z., Kaynak, A., Khoo, S. Y., Norton, M., & Gates, W. (2018). Soil bulk density estimation methods: A review. *Pedosphere*, *28*(4), 581–596. https://doi.org/10.1016/S1002-0160(18)60034-7

Anders, S., Pyl, P. T., & Huber, W. (2015). HTSeq—A Python framework to work with high-throughput sequencing data. *Bioinformatics*, *31*(2), 166–169. https://doi.org/10.1093/bioinformatics/btu638

Applegate, G., Freeman, B., Tular, B., Sitadevi, L., & Jessup, T. C. (2022). Application of agroforestry business models to tropical peatland restoration. *Ambio*, *51*(4), 863–874. https://doi.org/10.1007/s13280-021-01595-x

Apryianto, A., Arsela, P., Felix, F., & Ajambang, W. (2024). Quality control on oil palm RNA samples for efficient genomic downstream applications. *Journal of Genomics*, *12*, 35–43. https://doi.org/10.7150/jgen.92209

Arabia, T., Basri, H., Manfarizah, Zainabun, & Mukhtaruddin. (2020). Physical and chemical characteristics in peat lands of Aceh Jaya District, Indonesia. *IOP Conference Series: Earth and Environmental Science*, *499*(1), 012004. https://doi.org/10.1088/1755-1315/499/1/012004

Archer, L., Crane, J. H., & Albrecht, U. (2022). Trunk injection as a tool to deliver plant protection materials—an overview of basic principles and practical considerations. *Horticulturae*, *8*(6), 552. https://doi.org/10.3390/horticulturae8060552

Asano, K., Kagong, W. V. A., Mohammad, S. M. Bin, Sakazaki, K., Talip, M. S. A., Sahmat, S. S., Chan, M. K. Y., Isoi, T., Kano-Nakata, M., & Ehara, H. (2021). Arbuscular mycorrhizal communities in the roots of sago palm in mineral and shallow peat soils. *Agriculture*, *11*(11), 1161. https://doi.org/10.3390/agriculture11111161

Aytop, H., Ateş, Ö., Dengiz, O., Yılmaz, C. H., & Demir, Ö. F. (2023). Environmental, ecological and health risks of boron in agricultural soils of Amik Plain under Mediterranean conditions. *Stochastic Environmental Research and Risk Assessment*, *37*(6), 2069–2081. https://doi.org/10.1007/s00477-023-02380-w

Azhar, A., Asano, K., Sugiura, D., Kano-Nakata, M., & Ehara, H. (2022). Waterlogged conditions influence the nitrogen, phosphorus, potassium, and sugar Distribution in sago palm (*Metroxylon sagu* Rottb.) at seedling stages. *Plants*, *11*(5), 710. https://doi.org/10.3390/plants11050710

Azhar, A., Makihara, D., Naito, H., & Ehara, H. (2020). Evaluating sago palm (*Metroxylon sagu* Rottb.) photosynthetic performance in waterlogged conditions: utilizing pulse-amplitude-modulated (PAM) fluorometry as a waterlogging stress indicator. *Journal of the Saudi Society of Agricultural Sciences*, *19*(1), 37–42. https://doi.org/10.1016/j.jssas.2018.05.004

Azizan, S. N. F., Murakami, S., McTaggart, I., Yusof, N., Sha'arani, S., Hara, H., & Noborio, K. (2024). Changes in specific microbial groups characterize the impact of land conversion to oil palm plantations on peat. *Frontiers in Forests and Global Change*, *7*. https://doi.org/10.3389/ffgc.2024.1305491

Badrick, T. (2021). Biological variation: understanding why it is so important? *Practical Laboratory Medicine*, *23*, e00199. https://doi.org/10.1016/j.plabm.2020.e00199

Bai, X., Bol, R., Chen, H., Cui, Q., Qiu, T., Zhao, S., & Fang, L. (2024). A meta-analysis on crop growth and heavy metals accumulation with PGPB inoculation in contaminated soils. *Journal of Hazardous Materials*, *471*, 134370. https://doi.org/10.1016/j.jhazmat.2024.134370

Bakery, A., Vraggalas, S., Shalha, B., Chauhan, H., Benhamed, M., & Fragkostefanakis, S. (2024). Heat stress transcription factors as the central molecular rheostat to optimize plant survival and recovery from heat stress. *New Phytologist*, *244*(1), 51–64. https://doi.org/10.1111/nph.20017

Barrau, J. (1959). The sago palm and other food plants of marsh dwellers in the South Pacific Islands. *Economic Botany*, *13*(1), 151–159.

Beccari, O. (1918). Asiatic palms - Lepidocaryeae. *Annals Royal Botanical Garden, Calcutta*, *12*, 156–195.

Bechtaoui, N., Rabiu, M. K., Raklami, A., Oufdou, K., Hafidi, M., & Jemo, M. (2021). Phosphate-dependent regulation of growth and stresses management in plants. *Frontiers in Plant Science*, *12*. https://doi.org/10.3389/fpls.2021.679916

Beg, M. D. H., Kormin, S., Bijarimi, M., & Zaman, H. U. (2016). Preparation and characterization of low-density polyethylene/thermoplastic starch composites. *Advances in Polymer Technology*, *35*(1). https://doi.org/10.1002/adv.21521

Bentolila, S., Gipson, A. B., Kehl, A. J., Hamm, L. N., Hayes, M. L., Mulligan, R. M., & Hanson, M. R. (2021). A RanBP2-type zinc finger protein functions in intron splicing in *Arabidopsis* mitochondria and is involved in the biogenesis of respiratory complex I. *Nucleic Acids Research*, *49*(6), 3490–3506. https://doi.org/10.1093/nar/gkab066

Bhat, J. A., Deshmukh, R., Zhao, T., Patil, G., Deokar, A., Shinde, S., & Chaudhary, J. (2020). Harnessing high-throughput phenotyping and genotyping for enhanced drought tolerance in crop plants. *Journal of Biotechnology*, *324*, 248–260. https://doi.org/10.1016/j.jbiotec.2020.11.010

Bi, H., Liu, Z., Liu, S., Qiao, W., Zhang, K., Zhao, M., & Wang, D. (2024). Genome-wide analysis of wheat xyloglucan endotransglucosylase/hydrolase (*XTH*) gene family revealed *TaXTH17* involved in abiotic stress responses. *BMC Plant Biology*, *24*(1), 640. https://doi.org/10.1186/s12870-024-05370-4

Bian, X.-Y., Xue, Y., Jiang, P.-F., Zeng, Q.-Y., & Liu, Y.-J. (2024). Genome-wide identification of key genes responding to salt stress in *Populus alba*. *Research square*, *1*, 1-34. https://doi.org/10.21203/rs.3.rs-4395721/v1

Bintoro, M. H., Iqbal Nurulhaq, M., Pratama, A. J., Ahmad, F., & Ayulia, L. (2018). Growing area of sago palm and its environment. In *Sago Palm Multiple Contributions to Food Security and Sustainable Livelihoods* (Ehara, H., Toyoda, T., & Johnson. D. V.), pp. 17–30. Springer Nature.

Bolger, A. M., Lohse, M., & Usadel, B. (2014). Trimmomatic: a flexible trimmer for Illumina sequence data. *Bioinformatics*, *30*(15), 2114–2120. https://doi.org/10.1093/bioinformatics/btu170

Boonsermsuk, S., Anai, T., Hasegawa, K., & Hisajima, S. (1997). Variation in random polymorphic DNA of sago palm (*Metroxylon* spp.) in Thailand. *Japanese Journal of Tropical Agriculture*, *41*(2), 89–92.

Boukhatem, Z. F., Merabet, C., & Tsaki, H. (2022). Plant growth promoting Actinobacteria, the most promising candidates as bioinoculants? *Frontiers in Agronomy*, *4*, 849911. https://doi.org/10.3389/fagro.2022.849911

Brdar-Jokanović, M. (2020). Boron toxicity and deficiency in agricultural plants. *International Journal of Molecular Sciences*, *21*(4), 1424. https://doi.org/10.3390/ijms21041424

Breugem, A., Kros, H., & de Vries, W. (2024). *Impacts of pH on mechanisms and rates of carbon and nitrogen mineralisation: a review*. Wageningen, Wageningen Environmental Research.

Brillada, C., Zheng, J., Krüger, F., Rovira-Diaz, E., Askani, J. C., Schumacher, K., & Rojas-Pierce, M. (2018). Phosphoinositides control the localization of HOPS subunit VPS41,

which together with VPS33 mediates vacuole fusion in plants. *Proceedings of the National Academy of Sciences*, *115*(35). https://doi.org/10.1073/pnas.1807763115

Bujang, K. (2018). Production, purification, and health benefits of sago sugar. In *Sago palm: multiple contributions to food security and sustainable livelihoods* (Ehara, H., Johnson, D. V., & Toyoda Y., 1st ed), pp. 229–308. Singapore: Springer Singapore.

Bujarrabal-Dueso, A., Sendtner, G., Meyer, D. H., Chatzinikolaou, G., Stratigi, K., Garinis, G. A., & Schumacher, B. (2023). The DREAM complex functions as conserved master regulator of somatic DNA-repair capacities. *Nature Structural & Molecular Biology*, *30*(4), 475–488. https://doi.org/10.1038/s41594-023-00942-8

Cabrol, L., Capo, E., van Vliet, D. M., von Meijenfeldt, F. A. B., Bertilsson, S., Villanueva, L., Sánchez-Andrea, I., Björn, E., G. Bravo, A., & Heimburger Boavida, L.-E. (2023). Redox gradient shapes the abundance and diversity of mercury-methylating microorganisms along the water column of the Black Sea. *MSystems*, 8e00537-23. https://doi.org/10.1128/msystems.00537-23

Caffarri, S., Tibiletti, T., Jennings, R., & Santabarbara, S. (2014). A comparison between plant photosystem i and photosystem ii architecture and functioning. *Current Protein & Peptide Science*, *15*(4), 296–331. https://doi.org/10.2174/1389203715666140327102218

Camoirano, A., Arce, A. L., Ariel, F. D., Alem, A. L., Gonzalez, D. H., & Viola, I. L. (2020). Class I TCP transcription factors regulate trichome branching and cuticle development in *Arabidopsis*. *Journal of Experimental Botany*, *71*(18), 5438–5453. https://doi.org/10.1093/jxb/eraa257

Cao, X., Li, Y., Zhang, Y., Zhong, Z., Bai, R., Yang, P., Pan, F., & Fu, X. (2025). Full-time sequence assessment of okra seedling vigor under salt stress based on leaf area and leaf

growth rate estimation using the YOLOv11-HSECal instance segmentation model. *Frontiers in Plant Science*, *16*. https://doi.org/10.3389/fpls.2025.1625154

Canzler, S., & Hackermüller, J. (2020). multiGSEA: a GSEA-based pathway enrichment analysis for multi-omics data. *BMC Bioinformatics*, *21*(1), 561. https://doi.org/10.1186/s12859-020-03910-x

Carezzano, M. E., Alvarez Strazzi, F. B., Pérez, V., Bogino, P., & Giordano, W. (2023). Exopolysaccharides synthesized by rhizospheric bacteria: a review focused on their roles in protecting plants against stress. *Applied Microbiology*, *3*(4), 1249–1261. https://doi.org/10.3390/applmicrobiol3040086

Castiglioni, P., Warner, D., Bensen, R. J., Anstrom, D. C., Harrison, J., Stoecker, M., Abad, M., Kumar, G., Salvador, S., D'Ordine, R., Navarro, S., Back, S., Fernandes, M., Targolli, J., Dasgupta, S., Bonin, C., Luethy, M. H., & Heard, J. E. (2008). Bacterial RNA chaperones confer abiotic stress tolerance in plants and improved grain yield in maize under water-limited conditions. *Plant Physiology*, *147*(2), 446–455. https://doi.org/10.1104/pp.108.118828

Chabannes, M., Barakate, A., Lapierre, C., Marita, J. M., Ralph, J., Pean, M., Danoun, S., Halpin, C., Grima-Pettenati, J., & Boudet, A. M. (2001). Strong decrease in lignin content without significant alteration of plant development is induced by simultaneous down-regulation of cinnamoyl CoA reductase (CCR) and cinnamyl alcohol dehydrogenase (CAD) in tobacco plants. *The Plant Journal*, *28*(3), 257–270. https://doi.org/10.1046/j.1365-313X.2001.01140.x

Challa, K. R., Rath, M., & Nath, U. (2019). The CIN-TCP transcription factors promote commitment to differentiation in *Arabidopsis* leaf pavement cells via both auxin-dependent

and independent pathways. *PLOS Genetics*, *15*(2), e1007988. https://doi.org/10.1371/journal.pgen.1007988

Chandrasekaran, M., & Paramasivan, M. (2022). Arbuscular mycorrhizal fungi and antioxidant enzymes in ameliorating drought stress: a meta-analysis. *Plant and Soil*, *480*(1–2), 295–303. https://doi.org/10.1007/s11104-022-05582-3

Chauhan, D. S., Quraishi, M. A., & Verma, C. (2022). Carbon nanodots: recent advances in synthesis and applications. *Carbon Letters*, *32*(7), 1603–1629. https://doi.org/10.1007/s42823-022-00359-1

Chen, P., Takatsuka, H., Takahashi, N., Kurata, R., Fukao, Y., Kobayashi, K., Ito, M., & Umeda, M. (2017). *Arabidopsis* R1R2R3-Myb proteins are essential for inhibiting cell division in response to DNA damage. *Nature Communications*, *8*(1), 635. https://doi.org/10.1038/s41467-017-00676-4

Chen, R., Ma, J., Luo, D., Hou, X., Ma, F., Zhang, Y., Meng, Y., Zhang, H., & Guo, W. (2019). CaMADS, a MADS-box transcription factor from pepper, plays an important role in the response to cold, salt, and osmotic stress. *Plant Science*, *280*, 164–174. https://doi.org/10.1016/j.plantsci.2018.11.020

Chen, S., Zhou, Y., Chen, Y., & Gu, J. (2018). fastp: an ultra-fast all-in-one FASTQ preprocessor. *Bioinformatics*, *34*(17), i884–i890. https://doi.org/10.1093/bioinformatics/bty560

Chen, T., Hu, R., Zheng, Z., Yang, J., Fan, H., Deng, X., Yao, W., Wang, Q., Peng, S., & Li, J. (2021). Soil bacterial community in the multiple cropping system increased grain yield within 40 cultivation years. *Frontiers in Plant Science*, *12*. https://doi.org/10.3389/fpls.2021.804527

Chen, T.-T., Liu, F.-F., Xiao, D.-W., Jiang, X.-Y., Li, P., Zhao, S.-M., Hou, B., & Li, Y. (2020). The *Arabidopsis* UDP-glycosyltransferase75B1, conjugates abscisic acid and affects plant response to abiotic stresses. *Plant Molecular Biology*, *102*(4–5), 389–401. https://doi.org/10.1007/s11103-019-00953-4

Chen, Z., Dong, Y., & Huang, X. (2022). Plant responses to UV-B radiation: signaling, acclimation and stress tolerance. *Stress Biology*, *2*(1), 51. https://doi.org/10.1007/s44154-022-00076-9

Chicco, D., & Agapito, G. (2022). Nine quick tips for pathway enrichment analysis. *PLOS Computational Biology*, *18*(8), e1010348. https://doi.org/10.1371/journal.pcbi.1010348

Chow, V., Kirzinger, M. W., & Kagale, S. (2023). Lend me your EARs: a systematic review of the broad functions of EAR motif-containing transcriptional repressors in plants. *Genes*, *14*(2), 270. https://doi.org/10.3390/genes14020270

Cole, L. E. S., Åkesson, C. M., Hapsari, K. A., Hawthorne, D., Roucoux, K. H., Girkin, N. T., Cooper, H. V., Ledger, M. J., O'Reilly, P., & Thornton, S. A. (2022). Tropical peatlands in the anthropocene: lessons from the past. *Anthropocene*, *37*, 100324. https://doi.org/10.1016/j.ancene.2022.100324

Cui, Y.-N., Li, X.-T., Yuan, J.-Z., Wang, F.-Z., Wang, S.-M., & Ma, Q. (2019). Nitrate transporter NPF7.3/NRT1.5 plays an essential role in regulating phosphate deficiency responses in Arabidopsis. *Biochemical and Biophysical Research Communications*, *508*(1), 314–319. https://doi.org/10.1016/j.bbrc.2018.11.118

Cui, Y., Zhao, Q., Hu, S., & Jiang, L. (2020). Vacuole biogenesis in plants: how many vacuoles, how many models? *Trends in Plant Science*, *25*(6), 538–548. https://doi.org/10.1016/j.tplants.2020.01.008

Dai, Y., Wang, Y., Zeng, L., Jia, R., He, L., Huang, X., Zhao, H., Liu, D., Zhao, H., Hu, S., Gao, L., Guo, A., Xia, W., & Ji, C. (2023). Genomic and transcriptomic insights into the evolution and divergence of MIKC-Type MADS-box genes in *Carica papaya*. *International Journal of Molecular Sciences*, *24*(18), 14039. https://doi.org/10.3390/ijms241814039

Dare, A. P., Tomes, S., Jones, M., McGhie, T. K., Stevenson, D. E., Johnson, R. A., Greenwood, D. R., & Hellens, R. P. (2013). Phenotypic changes associated with RNA interference silencing of chalcone synthase in apple (*Malus* × *domestica* **)**. *The Plant Journal*, *74*(3), 398–410. https://doi.org/10.1111/tpj.12140

Dimitriadi, D., Stylianidis, G. P., Tsirogiannis, I., Bouranis, L. D., Chorianopoulou, S. N., & Bouranis, D. L. (2025). Morphological Acclimation of Durum Wheat Spikes in Response to Foliar Micronutrient Applications. *Plants*, *14*(19), 3079. https://doi.org/10.3390/plants14193079

de Mendonça, G. W., Aguilar, J. V., de Marcos Lapaz, A., da Silva de Paiva, W., Ferreira, T. C., Souza, L. A., Justino, G. C., & de Camargos, L. S. (2024). How does boron modify the growth of *Crotalaria juncea*? A legume with phytostabilizing potential. *International Journal of Environmental Studies*, *81*(4), 1918–1932. https://doi.org/10.1080/00207233.2023.2207895

Debeljak, P., & Baltar, F. (2023). Fungal diversity and community composition across ecosystems. *Journal of Fungi*, *9*(5), 510. https://doi.org/10.3390/jof9050510

Deng, W.-J., Li, Q.-Q., Shuai, H.-N., Wu, R.-X., Niu, S.-F., Wang, Q.-H., & Miao, B.-B. (2024). Whole-genome sequencing analyses reveal the evolution mechanisms of typical biological features of *Decapterus maruadsi*. *Animals*, *14*(8), 1202. https://doi.org/10.3390/ani14081202

Derbyshire, M. C., Batley, J., & Edwards, D. (2022). Use of multiple omics techniques to accelerate the breeding of abiotic stress tolerant crops. *Current Plant Biology*, *32*, 100262. https://doi.org/10.1016/j.cpb.2022.100262

Derikvand, P., Sauter, B., Keddie, A., & Stein, L. Y. (2024). Inoculum and pH effects on ammonium removal and microbial community dynamics in aquaponics systems. *IScience*, *27*(3), 109073. https://doi.org/10.1016/j.isci.2024.109073

Devangsari, I. M., Nurudin, M., Sartohadi, J., & Karmila, Y. A. (2022). Characteristics of peat functional group in Padang Island, Indonesia. *IOP Conference Series: Earth and Environmental Science*, *1005*(1), 012022. https://doi.org/10.1088/1755-1315/1005/1/012022

Dobin, A., Davis, C. A., Schlesinger, F., Drenkow, J., Zaleski, C., Jha, S., Batut, P., Chaisson, M., & Gingeras, T. R. (2013). STAR: ultrafast universal RNA-seq aligner. *Bioinformatics*, *29*(1), 15–21. https://doi.org/10.1093/bioinformatics/bts635

Dobrzyński, J., Kulkova, I., Jakubowska, Z., & Wróbel, B. (2025). Non-native PGPB consortium consisting of *Pseudomonas* sp. G31 and *Azotobacter* sp. PBC2 promoted winter wheat growth and slightly altered the native bacterial community. *Scientific Reports*, *15*(1), 3248. https://doi.org/10.1038/s41598-025-86820-3

Dom, S. P., Ikenaga, M., Lau, S. Y. L., Radu, S., Midot, F., Yap, M. L., Chin, M. Y., Lo, M. L., Jee, M. S., Maie, N., & Melling, L. (2021). Linking prokaryotic community composition to

carbon biogeochemical cycling across a tropical peat dome in Sarawak, Malaysia. *Scientific Reports*, *11*(1). https://doi.org/10.1038/s41598-021-81865-6

Dong, L., & Manghwar, H. (2023). Genome-wide expression analysis of *LBD* genes in tomato (*Solanum lycopersicum* L.) under different light conditions. *Plant Signaling & Behavior*, *18*(1). https://doi.org/10.1080/15592324.2023.2290414

Dorn, A., Röhrig, S., Papp, K., Schröpfer, S., Hartung, F., Knoll, A., & Puchta, H. (2018). The topoisomerase 3α zinc-finger domain T1 of *Arabidopsis thaliana* is required for targeting the enzyme activity to Holliday junction-like DNA repair intermediates. *PLOS Genetics*, *14*(9), e1007674. https://doi.org/10.1371/journal.pgen.1007674

Draeger, T. N., Rey, M.-D., Hayta, S., Smedley, M., Alabdullah, A. K., Moore, G., & Martín, A. C. (2023). ZIP4 is required for normal progression of synapsis and for over 95% of crossovers in wheat meiosis. *Frontiers in Plant Science*, *14*, 118998. https://doi.org/10.3389/fpls.2023.1189998

Du, B., Franzisky, B. L., Muhammad, W., Alfarraj, S., Geilfus, C., & Rennenberg, H. (2025). How to cope with stress in the desert—the date palm approach. *Plant, Cell & Environment*, *48*(1), 768–780. https://doi.org/10.1111/pce.15188

Duan, S., Zhang, C., Song, S., Ma, C., Zhang, C., Xu, W., Bondada, B., Wang, L., & Wang, S. (2022). Understanding calcium functionality by examining growth characteristics and structural aspects in calcium-deficient grapevine. *Scientific Reports*, *12*(1), 3233. https://doi.org/10.1038/s41598-022-06867-4

Dyksma, S., & Pester, M. (2024). Growth of sulfate-reducing Desulfobacterota and Bacillota at periodic oxygen stress of 50% air-O2 saturation. *Microbiome*, *12*(1), 191. https://doi.org/10.1186/s40168-024-01909-7

Ebrahimi-Zarandi, M., Etesami, H., & Glick, B. R. (2023). Fostering plant resilience to drought with Actinobacteria: unveiling perennial allies in drought stress tolerance. *Plant Stress*, *10*, 100242. https://doi.org/10.1016/j.stress.2023.100242

Ehara, H. (2009). Potency of sago palm as carbohydrate resource for strengthening food security program. *Indonesian Journal of Agronomy*, *37*(3), 209–219.

Ehara, H., Kakuda, K., Miyazaki, A., Naito, H., Nakamura, S., Nitta, Y., Okazaki, M., Sasaki, Y., Toyota, K., Watanabe, A., Watanabe, M., Yamamoto, Y., Goto, Y., & Kimura, S. D. (2021). Sago palm in peatland. In *Tropical peatland eco-management* (Osaki, M., Tsuji, N., Foead, N., & Rieley, J. pp. 477–508. Singapore: Springer Singapore.

Ehara, H., Naito, H., Tarimo, A. J., Bintoro, M. H., & Takamura, T. Y. (2006). Introduction of sago palm seeds and seedlings into Tanzania. *Sago Palm*, *14*(2), 65–71.

Ehara, H., Toyoda, Y., & Johnson, D. V. (2018). Sago palm: Multiple contributions to food security and sustainable livelihoods. In *Sago Palm: Multiple Contributions to Food Security and Sustainable Livelihoods* (Ehara, H., Toyoda, Y., & Johnson, D. V.) pp 31-42. Singapore: Springer Singapore.

Ellen, R. (2006). Local knowledge and management of sago palm (*Metroxylon sagu* Rottboel) diversity in South Central Seram, Maluku, Eastern Indonesia. *Journal of Ethnobiology*, *26*(2), 258–298.

El-Tarabily, K. A., Sham, A., Elbadawi, A. A., Hassan, A. H., Alhosani, B. K. K., El-Esawi, M. A., AlKhajeh, A. S., & AbuQamar, S. F. (2021). A consortium of rhizosphere-competent

actinobacteria exhibiting multiple plant growth-promoting traits improves the growth of *Avicennia marina* in the United Arab Emirates. *Frontiers in Marine Science*, *8*. https://doi.org/10.3389/fmars.2021.715123

Enebe, M. C., & Babalola, O. O. (2019). The impact of microbes in the orchestration of plants' resistance to biotic stress: a disease management approach. *Applied Microbiology and Biotechnology*, *103*(1), 9–25. https://doi.org/10.1007/s00253-018-9433-3

Erdmann, R. M., & Picard, C. L. (2020). RNA-directed DNA Methylation. *PLOS Genetics*, *16*(10), e1009034. https://doi.org/10.1371/journal.pgen.1009034

Erpen, L., Devi, H. S., Grosser, J. W., & Dutt, M. (2018). Potential use of the DREB/ERF, MYB, NAC and WRKY transcription factors to improve abiotic and biotic stress in transgenic plants. *Plant Cell, Tissue and Organ Culture (PCTOC)*, *132*(1), 1–25. https://doi.org/10.1007/s11240-017-1320-6

Ezawa, T., & Saito, K. (2018). How do arbuscular mycorrhizal fungi handle phosphate? New insight into fine-tuning of phosphate metabolism. *New Phytologist*, *220*(4), 1116–1121. https://doi.org/10.1111/nph.15187

Faithfull, N. T. (2002). *Methods in Agricultural Chemical Analysis* (1st ed., Vol. 1). CABI Publishing.

Fang, S., Yang, Y., Zhang, X., Yang, Z., Zhang, M., Zhao, Y., Zhang, C., Yu, F., Wang, Y.-F., & Zhang, P. (2025). Structural mechanism underlying PHO1;H1-mediated phosphate transport in *Arabidopsis*. *Nature Plants*, *11*(2), 309–320. https://doi.org/10.1038/s41477-024-01895-6

Food and Agriculture Organization. (2024). *Standard operating procedure for boron determination in soil: Hot water extraction*. Rome: FAO. https://doi.org/10.4060/cd0604en

Food and Agriculture Organization. (2021) *Standard operating procedure for soil available phosphorus Bray I and Bray II method*. Rome: FAO.

Food and Agriculture Organization. (2019) *Standard operating procedure for soil organic carbon Walkley-Black method Titration and colorimetric method*. Rome: FAO.

Ferrero, L. V., Gastaldi, V., Ariel, F. D., Viola, I. L., & Gonzalez, D. H. (2021). Class I TCP proteins TCP14 and TCP15 are required for elongation and gene expression responses to auxin. *Plant Molecular Biology*, *105*(1–2), 147–159. https://doi.org/10.1007/s11103-020-01075-y

Flach, M. (1997). *Sago palm: Metroxylon sagu Rottb.: Promoting the conservation and use of underutilized and neglected crops*, 1st ed., Rome International Plant Genetic Resources Institute.

Flach, M., & Schuiling, D. L. (1988). Revival of an ancient starch crop: a review of the agronomy of the sago palm. *Agroforestry Systems*, *7*(3), 259–281. https://doi.org/10.1007/BF00046972

Flieder, M., Buongiorno, J., Herbold, C. W., Hausmann, B., Rattei, T., Lloyd, K. G., Loy, A., & Wasmund, K. (2021). Novel taxa of Acidobacteriota implicated in seafloor sulfur cycling. *The ISME Journal*, *15*(11), 3159–3180. https://doi.org/10.1038/s41396-021-00992-0

Fode, B., Siemsen, T., Thurow, C., Weigel, R., & Gatz, C. (2008). The *Arabidopsis* GRAS protein SCL14 interacts with class II TGA transcription factors and is essential for the activation of stress-inducible promoters. *The Plant Cell*, *20*(11), 3122–3135. https://doi.org/10.1105/tpc.108.058974

Fukasawa, Y. (2021). Ecological impacts of fungal wood decay types: a review of current knowledge and future research directions. *Ecological Research*, *36*(6), 910–931. https://doi.org/10.1111/1440-1703.12260

Furuya, T., Ohashi-Ito, K., & Kondo, Y. (2024). Multiple Roles of Brassinosteroid Signaling in Vascular Development. *Plant And Cell Physiology*, *65*(10), 1601–1607. https://doi.org/10.1093/pcp/pcae037

Gaafar, A.-R. Z., Al-Qurainy, F., Alshameri, A., Khan, S., Nadeem, M., Tarroum, M., Alansi, S., Shaikhaldein, H. O., Salih, A. M., & Arrak Alenezi, N. (2021). High RNA quality extracted from the tolerant crop *Cyamopsis tetragonoloba* (L.) despite possession of low RNA integrity number. *Biotechnology & Biotechnological Equipment*, *35*(1), 608–618. https://doi.org/10.1080/13102818.2021.1910567

Gamalero, E., Lingua, G., & Glick, B. R. (2023). Ethylene, ACC, and the Plant Growth-Promoting Enzyme ACC Deaminase. *Biology*, *12*(8), 1043. https://doi.org/10.3390/biology12081043

Gao, H., Wang, Y., Xu, P., & Zhang, Z. (2018). Overexpression of a WRKY transcription factor TaWRKY2 enhances drought stress tolerance in transgenic wheat. *Frontiers in Plant Science*, *9*. https://doi.org/10.3389/fpls.2018.00997

Gao, T., Wu, Y., Zhang, Y., Liu, L., Ning, Y., Wang, D., Tong, H., Chen, S., Chu, C., & Xie, Q. (2011). *OsSDIR1* overexpression greatly improves drought tolerance in transgenic rice. *Plant Molecular Biology*, *76*(1–2), 145–156. https://doi.org/10.1007/s11103-011-9775-z

Gao, Y., Li, N., Ruan, J., Li, Y., Liao, X., & Yang, C. (2022). Genome-wide identification, cloning and expression profile of RanBP2-type zinc finger protein genes in tomato. *Horticulturae*, *8*(11), 985. https://doi.org/10.3390/horticulturae8110985

Garcia-Ruiz, H., Carbonell, A., Hoyer, J. S., Fahlgren, N., Gilbert, K. B., Takeda, A., Giampetruzzi, A., Garcia Ruiz, M. T., McGinn, M. G., Lowery, N., Martinez Baladejo, M. T., & Carrington, J. C. (2015). Roles and programming of *Arabidopsis* ARGONAUTE

proteins during turnip mosaic virus infection. *PLOS Pathogens*, *11*(3), e1004755. https://doi.org/10.1371/journal.ppat.1004755

Gentric, N., Genschik, P., & Noir, S. (2021). Connections between the cell cycle and the DNA damage response in plants. *International Journal of Molecular Sciences*, *22*(17), 9558. https://doi.org/10.3390/ijms22179558

Gipson, A. B., Hanson, M. R., & Bentolila, S. (2022). The RanBP2 zinc finger domains of chloroplast RNA editing factor OZ1 are required for protein–protein interactions and conversion of C to U. *The Plant Journal*, *109*(1), 215–226. https://doi.org/10.1111/tpj.15569

Gonçalves, O. S., Fernandes, A. S., Tupy, S. M., Ferreira, T. G., Almeida, L. N., Creevey, C. J., & Santana, M. F. (2024). Insights into plant interactions and the biogeochemical role of the globally widespread Acidobacteriota phylum. *Soil Biology and Biochemistry*, *192*, 109369. https://doi.org/10.1016/j.soilbio.2024.109369

Gong, M., Bai, N., Wang, P., Su, J., Chang, Q., & Zhang, Q. (2023). Co-inoculation with arbuscular mycorrhizal fungi and dark septate endophytes under drought stress: synergistic or competitive effects on maize growth, photosynthesis, root hydraulic properties and aquaporins? *Plants*, *12*(14), 2596. https://doi.org/10.3390/plants12142596

Guan, Z., Chen, J., Liu, R., Chen, Y., Xing, Q., Du, Z., Cheng, M., Hu, J., Zhang, W., Mei, W., Wan, B., Wang, Q., Zhang, J., Cheng, P., Cai, H., Cao, J., Zhang, D., Yan, J., Yin, P., … Liu, Z. (2023). The cytoplasmic synthesis and coupled membrane translocation of eukaryotic polyphosphate by signal-activated VTC complex. *Nature Communications*, *14*(1), 718. https://doi.org/10.1038/s41467-023-36466-4

Guddimalli, R., Somanaboina, A. K., Palle, S. R., Edupuganti, S., Kummari, D., Palakolanu, S. R., Naravula, J., Gandra, J., Qureshi, I. A., Marka, N., Polavarapu, R., & Kavi Kishor, P. B.

(2021). Overexpression of RNA -binding bacterial chaperones in rice leads to stay-green phenotype, improved yield and tolerance to salt and drought stresses. *Physiologia Plantarum*, *173*(4), 1351–1368. https://doi.org/10.1111/ppl.13369

Guo, J., Huang, Z., Sun, J., Cui, X., & Liu, Y. (2021). Research progress and future development trends in medicinal plant transcriptomics. *Frontiers in Plant Science*, *12*. https://doi.org/10.3389/fpls.2021.691838

Guo, Z., Zhang, C., Zhao, H., Liu, Y., Chen, X., Zhao, H., Chen, L., Ruan, W., Chen, Y., Yuan, L., Yi, K., Xu, L., & Zhang, J. (2025). Vacuolar phosphate efflux transporter ZmVPEs mediate phosphate homeostasis and remobilization in maize leaves. *Journal of Integrative Plant Biology*, *67*(2), 311–326. https://doi.org/10.1111/jipb.13811

Habib, S., Lwin, Y. Y., & Li, N. (2021). Down-regulation of *SlGRAS10* in tomato confers abiotic stress tolerance. *Genes*, *12*(5), 623. https://doi.org/10.3390/genes12050623

Hamzah S., M., Usman, K., Rizwan, M., Al Jabri, H., & Alsafran, M. (2022). Functions and strategies for enhancing zinc availability in plants for sustainable agriculture. *Frontiers in Plant Science*, *13*. https://doi.org/10.3389/fpls.2022.1033092

Han, G., Lu, C., Guo, J., Qiao, Z., Sui, N., Qiu, N., & Wang, B. (2020). C2H2 zinc finger proteins: master regulators of abiotic stress responses in plants. *Frontiers in Plant Science*, *11*. https://doi.org/10.3389/fpls.2020.00115

Han, G., Qiao, Z., Li, Y., Yang, Z., Wang, C., Zhang, Y., Liu, L., & Wang, B. (2022). RING zinc finger proteins in plant abiotic stress tolerance. *Frontiers in Plant Science*, *13*. https://doi.org/10.3389/fpls.2022.877011

Han, S., Li, X., Luo, X., Wen, S., Chen, W., & Huang, Q. (2018). Nitrite-oxidizing bacteria community composition and diversity are influenced by fertilizer regimes, but are

independent of the soil aggregate in acidic subtropical red soil. *Frontiers in Microbiology*, *9*. https://doi.org/10.3389/fmicb.2018.00885

Han, X., Yu, H., Yuan, R., Yang, Y., An, F., & Qin, G. (2019). *Arabidopsis* transcription factor TCP5 controls plant thermomorphogenesis by positively regulating PIF4 activity. *IScience*, *15*, 611–622. https://doi.org/10.1016/j.isci.2019.04.005

Hardcastle, T. J., & Kelly, K. A. (2010). baySeq: empirical bayesian methods for identifying differential expression in sequence count data. *BMC Bioinformatics*, *11*(1), 422. https://doi.org/10.1186/1471-2105-11-422

Hartung, F., Suer, S., Knoll, A., Wurz-Wildersinn, R., & Puchta, H. (2008). Topoisomerase 3α and RMI1 suppress somatic crossovers and are essential for resolution of meiotic recombination intermediates in *Arabidopsis thaliana*. *PLoS Genetics*, *4*(12), e1000285. https://doi.org/10.1371/journal.pgen.1000285

Hartwig, A. (2001). Zinc finger proteins as potential targets for toxic metal ions: differential effects on structure and function. *Antioxidants & Redox Signaling*, *3*(4), 625–634. https://doi.org/10.1089/15230860152542970

Hassani, D., Fu, X., Shen, Q., Khalid, M., Rose, J. K. C., & Tang, K. (2020). Parallel transcriptional regulation of artemisinin and flavonoid biosynthesis. *Trends in Plant Science*, *25*(5), 466–476. https://doi.org/10.1016/j.tplants.2020.01.001

He, G.-H., Xu, J.-Y., Wang, Y.-X., Liu, J.-M., Li, P.-S., Chen, M., Ma, Y.-Z., & Xu, Z.-S. (2016). Drought-responsive WRKY transcription factor genes TaWRKY1 and TaWRKY33 from wheat confer drought and/or heat resistance in *Arabidopsis*. *BMC Plant Biology*, *16*(1), 116. https://doi.org/10.1186/s12870-016-0806-4

He, W., Wang, R., Zhang, Q., Fan, M., Lyu, Y., Chen, S., Chen, D., & Chen, X. (2023). E3 ligase ATL5 positively regulates seed longevity by mediating the degradation of ABT1 in *Arabidopsis*. *New Phytologist*, *239*(5), 1754–1770. https://doi.org/10.1111/nph.19080

Hirao, K., Kondo, T., Kainuma, K., & Takahashi, S. (2018). Starch properties and uses as food for human health and welfare. In *Sago palm: multiple contributions to food security and sustainable livelihoods* (Ehara, H., Johnson, D. V., & Toyoda, Y. 1st ed.), pp. 285–288. Singapore: Springer Singapore.

Hoang, H. G., Thuy, B. T. P., Lin, C., Vo, D.-V. N., Tran, H. T., Bahari, M. B., Le, V. G., & Vu, C. T. (2022). The nitrogen cycle and mitigation strategies for nitrogen loss during organic waste composting: A review. *Chemosphere*, *300*, 134514. https://doi.org/10.1016/j.chemosphere.2022.134514

Hu, D., Zhang, J., Yang, Y., Yu, D., Zhang, H., & Zhang, D. (2025). Molecular mechanisms underlying plant responses to low phosphate stress and potential applications in crop improvement. *New Crops*, *2*, 100064. https://doi.org/10.1016/j.ncrops.2024.100064

Hu, T., Chitnis, N., Monos, D., & Dinh, A. (2021). Next-generation sequencing technologies: an overview. *Human Immunology*, *82*(11), 801–811. https://doi.org/10.1016/j.humimm.2021.02.012

Hu, W.-J., Harding, S. A., Lung, J., Popko, J. L., Ralph, J., Stokke, D. D., Tsai, C.-J., & Chiang, V. L. (1999). Repression of lignin biosynthesis promotes cellulose accumulation and growth in transgenic trees. In *Nature Biotechnology*, *17*, 808-812.

Hua, H. Y., Santibanez, P. I., Ngo, V. T., & Hayes, M. L. (2024). RIP-Seq analysis of non-PPR chloroplast editing factors reveals broad RNA interactions and enrichment of less efficiently

translated RNAs by OZ1 and ORRM1 complexes. *The Plant Journal*, *117*(5), 1528–1542. https://doi.org/10.1111/tpj.16581

Huang, Y., An, J., Sircar, S., Bergis, C., Lopes, C. D., He, X., Da Costa, B., Tan, F.-Q., Bazin, J., Antunez-Sanchez, J., Mammarella, M. F., Devani, R., Brik-Chaouche, R., Bendahmane, A., Frugier, F., Xia, C., Rothan, C., Probst, A. V., Mohamed, Z., … Benhamed, M. (2023). HSFA1a modulates plant heat stress responses and alters the 3D chromatin organization of enhancer-promoter interactions. *Nature Communications*, *14*(1), 469. https://doi.org/10.1038/s41467-023-36227-3

Huang, Y. W., Hu, C. C., Tsai, C. H., Lin, N. S., & Hsu, Y. H. (2019). *Nicotiana benthamiana* Argonaute10 plays a pro-viral role in *Bamboo mosaic virus* infection. *New Phytologist*, *224*(2), 804–817. https://doi.org/10.1111/nph.16048

Hussain, H., Edward-Atit, A. S., Julaihi, N., Tommy, R., Nisar, M., Hamdan, N., & Ehara, H. (2022). Identification of differentially expressed transcripts for trunk formation in sago palm using annealing control primer GeneFishing technique. *Journal of Applied Biology and Biotechnology*, *10*(2), 2–4.

Hussain, H., Kamal, M., Atit, A., Kamarol, S. I., Yan, W. J., Ngaini, Z., Al-Obaidi, J., & Mohd-Yusuf, Y. (2012). Proteomics of trunking and non-trunking sago palm (*Metroxylon sagu* Rottb.). *2nd ASEAN Sago Symposium* .

Hussain, H., Mustafa Kamal, M., Al-Obaidi, J. R., Hamdin, N. E., Ngaini, Z., & Mohd-Yusuf, Y. (2020). Proteomics of sago palm towards identifying contributory proteins in stress-tolerant cultivar. *Protein Journal*, *39*(1), 62–72. https://doi.org/10.1007/s10930-019-09878-9

Hussain, H., Yan, W.-J., Ngaini, Z., Julaihi, N., Tommy, R., & Bhawani, S. A. (2021). Differential metabolites markers from trunking and stressed non-trunking sago palm (*Metroxylon sagu*

Rottb.). *Current Chemical Biology*, *14*(4), 262–278. https://doi.org/10.2174/2212796814999200930120925

Imran, M., Wu, Q., Guanming, C., & Zhou, L. (2025). Multifaceted roles and regulatory mechanisms of MYB transcription factors in plant development, secondary metabolism, and stress adaptation: current insights and future prospects. *GM Crops & Food*, *16*(1), 626–655. https://doi.org/10.1080/21645698.2025.2559489

Irawan, R., Sudrajat, S., & Supijatno, S. (2025). Increasing palm oil productivity with a combination of inorganic fertilizers and biofertilizers. *Journal of Ecological Engineering*.

Ishizaki, A. (1997). Concluding remarks for the 6th international sago symposium. *6th International Sago Symposium*, 22–24.

Islam, W., Noman, A., Naveed, H., Huang, Z., & Chen, H. Y. H. (2020). Role of environmental factors in shaping the soil microbiome. *Environmental Science and Pollution Research*, *27*(33), 41225–41247. https://doi.org/10.1007/s11356-020-10471-2

Jan, R., Asaf, S., Numan, M., Lubna, & Kim, K.-M. (2021). Plant secondary metabolite biosynthesis and transcriptional regulation in response to biotic and abiotic stress conditions. *Agronomy*, *11*(5), 968. https://doi.org/10.3390/agronomy11050968

Jayarathne, T., Stockwell, C. E., Gilbert, A. A., Daugherty, K., Cochrane, M. A., Ryan, K. C., Putra, E. I., Saharjo, B. H., Nurhayati, A. D., Albar, I., Yokelson, R. J., & Stone, E. A. (2018). Chemical characterization of fine particulate matter emitted by peat fires in Central Kalimantan, Indonesia, during the 2015 El Niño. *Atmospheric Chemistry and Physics*, *18*(4), 2585–2600. https://doi.org/10.5194/acp-18-2585-2018

Jia, A., Xu, L., & Wang, Y. (2021). Venn diagrams in bioinformatics. *Briefings in Bioinformatics*, *22*(5). https://doi.org/10.1093/bib/bbab108

Jiang, C.-K., Ma, J.-Q., Apostolides, Z., & Chen, L. (2019). Metabolomics for a millenniums-old crop: tea plant (*Camellia sinensis*). *Journal of Agricultural and Food Chemistry*, *67*(23), 6445–6457. https://doi.org/10.1021/acs.jafc.9b01356

Jiang, H., Sheong, F. K., Zhu, L., Gao, X., Bernauer, J., & Huang, X. (2015). Markov state models reveal a two-step mechanism of mirna loading into the human argonaute protein: selective binding followed by structural re-arrangement. *PLOS Computational Biology*, *11*(7), e1004404. https://doi.org/10.1371/journal.pcbi.1004404

Jiang, Y.-T., Yang, L.-H., Ferjani, A., & Lin, W.-H. (2021). Multiple functions of the vacuole in plant growth and fruit quality. *Molecular Horticulture*, *1*(1), 4. https://doi.org/10.1186/s43897-021-00008-7

Jong, F. S. (1995). *Research for the development of sago palm (Metroxylon sagu Rottb.) cultivation in Sarawak, Malaysia* [Ph. D. thesis]. Agriculture.

Jong, F. S., & Flach, M. (1995). The sustainability of sago palm (*Metroxylon sagu*) cultivation on deep peat in Sarawak. *SAGO PALM* , *3*, 13–20.

Juntawong, P., Sorenson, R., & Bailey-Serres, J. (2013). Cold shock protein 1 chaperones mRNAs during translation in *Arabidopsis thaliana*. *The Plant Journal*, *74*(6), 1016–1028. https://doi.org/10.1111/tpj.12187

Kanehisa, M., Furumichi, M., Sato, Y., Ishiguro-Watanabe, M., & Tanabe, M. (2021). KEGG: integrating viruses and cellular organisms. *Nucleic Acids Research*, *49*(D1), D545–D551. https://doi.org/10.1093/nar/gkaa970

Kaneko, T., Okazaki, M., Kasuya, N., Yamaguchi, T., & Hassan, A. H. (1996). Growth and biomass of sago palm (*Metroxylon sagu*) on deep and shallow peat soils of Dalat District, Sarawak. *SAGO PALM*, *4*, 21–24.

Kang, S., Shin, K. D., Kim, J. H., & Chung, T. (2018). Autophagy-related (ATG) 11, ATG9 and the phosphatidylinositol 3-kinase control ATG2-mediated formation of autophagosomes in *Arabidopsis*. *Plant Cell Reports*, *37*(4), 653–664. https://doi.org/10.1007/s00299-018-2258-9

Kanokratana, P., Uengwetwanit, T., Rattanachomsri, U., Bunterngsook, B., Nimchua, T., Tangphatsornruang, S., Plengvidhya, V., Champreda, V., & Eurwilaichitr, L. (2011). Insights into the phylogeny and metabolic potential of a primary tropical peat swamp forest microbial community by metagenomic analysis. *Microbial Ecology*, *61*(3), 518–528. https://doi.org/10.1007/s00248-010-9766-7

Karim, A. A., Tie, A. P. L., Manan, D. M. A., & Zaidul, I. S. M. (2008). Starch from the sago (*Metroxylon sagu*) palm tree - properties, prospects, and challenges as a new industrial source for food and other uses. *Comprehensive Reviews in Food Science and Food Safety*, *7*(3), 215–228. https://doi.org/10.1111/j.1541-4337.2008.00042.x

Kaur, M., Manchanda, P., Kalia, A., Ahmed, F. K., Nepovimova, E., Kuca, K., & Abd-Elsalam, K. A. (2021). Agroinfiltration mediated scalable transient gene expression in genome edited crop plants. *International Journal of Molecular Sciences*, *22*(19), 10882. https://doi.org/10.3390/ijms221910882

Karlson, D., Nakaminami, K., Toyomasu, T., & Imai, R. (2002). A cold-regulated nucleic acid-binding protein of winter wheat shares a domain with bacterial cold shock proteins. *Journal of Biological Chemistry*, *277*(38), 35248–35256. https://doi.org/10.1074/jbc.M205774200

Kasirajan, L., Hoang, N. V., Furtado, A., Botha, F. C., & Henry, R. J. (2018). Transcriptome analysis highlights key differentially expressed genes involved in cellulose and lignin

biosynthesis of sugarcane genotypes varying in fiber content. *Scientific Reports*, *8*(1), 11612. https://doi.org/10.1038/s41598-018-30033-4

Kęska, K., Szcześniak, M. W., Makałowska, I., & Czernicka, M. (2021). Long-term waterlogging as factor contributing to hypoxia stress tolerance enhancement in cucumber: comparative transcriptome analysis of waterlogging sensitive and tolerant accessions. *Genes*, *12*(2), 189. https://doi.org/10.3390/genes12020189

Khan, F., Siddique, A. B., Shabala, S., Zhou, M., & Zhao, C. (2023). Phosphorus plays key roles in regulating plants' physiological responses to abiotic stresses. *Plants*, *12*(15), 2861. https://doi.org/10.3390/plants12152861

Kim, D., Pertea, G., Trapnell, C., Pimentel, H., Kelley, R., & Salzberg, S. L. (2013). TopHat2: accurate alignment of transcriptomes in the presence of insertions, deletions and gene fusions. *Genome Biology*, *14*(4), R36. https://doi.org/10.1186/gb-2013-14-4-r36

Kim, M.-H., Sato, S., Sasaki, K., Saburi, W., Matsui, H., & Imai, R. (2013). Cold shock domain protein 3 is involved in salt and drought stress tolerance in *Arabidopsis*. *FEBS Open Bio*, *3*(1), 438–442. https://doi.org/10.1016/j.fob.2013.10.003

Kim, W. S., & Haj-Ahmad, Y. (2016). *Evaluation of plant RNA Integrity Number (RIN) generated using an Agilent BioAnalyzer 2100*. Ontario: Norgen Biotek Corporation.

Kimura, S. D., Matsumura, S., Lina, S. B., Igura, M., Okazaki, M., Quevedo, M. A., & Loreto, A. B. (2008). Influence of slow-release fertilizers on sago palm growth in the early growth stage in a sago-taro intercropping field. *Sago Palm*, *16*(1), 1–9.

Koch, H., van Kessel, M. A. H. J., & Lücker, S. (2019). Complete nitrification: insights into the ecophysiology of comammox *Nitrospira*. *Applied Microbiology and Biotechnology*, *103*(1), 177–189. https://doi.org/10.1007/s00253-018-9486-3

Könönen, M., Jauhiainen, J., Laiho, R., Kusin, K., & Vasander, H. (2015). Physical and chemical properties of tropical peat under stabilised land uses. *Mires and peat* (*16*), 1-13.

Konuma, H. (2018). Status and outlook of global food security and the role of underutilized food resources: sago palm. In *Sago palm: multiple contributions to food security and sustainable livelihoods* (Ehara, H., Toyoda, T., & Johnson. D. V.), pp. 3–16). Singapore: Springer Singapore.

Kooch, Y., Heidari, F., Frouz, J., Haghverdi, K., & Francaviglia, R. (2025). Soil drainage reduces the negative impact of excessive soil moisture contents by improving the N dynamics in coastal forests. *Science of The Total Environment*, *1000*, 180471. https://doi.org/10.1016/j.scitotenv.2025.180471

Krouk, G., & Kiba, T. (2020). Nitrogen and phosphorus interactions in plants: from agronomic to physiological and molecular insights. *Current Opinion in Plant Biology*, *57*, 104–109. https://doi.org/10.1016/j.pbi.2020.07.002

Kryovrysanaki, N., James, A., Tselika, M., Bardani, E., & Kalantidis, K. (2022). RNA silencing pathways in plant development and defense. *The International Journal of Developmental Biology*, *66*(1-2–3), 163–175. https://doi.org/10.1387/ijdb.210189kk

Kuleshov, M. V., Jones, M. R., Rouillard, A. D., Fernandez, N. F., Duan, Q., Wang, Z., Koplev, S., Jenkins, S. L., Jagodnik, K. M., Lachmann, A., McDermott, M. G., Monteiro, C. D., Gundersen, G. W., & Ma'ayan, A. (2016). Enrichr: a comprehensive gene set enrichment analysis web server 2016 update. *Nucleic Acids Research*, *44*(W1), W90–W97. https://doi.org/10.1093/nar/gkw377

Kunarso, A., Bonner, M. T. L., Blanch, E. W., & Grover, S. (2022). Differences in tropical peat soil physical and chemical properties under different land uses: a systematic review and

meta-analysis. *Journal of Soil Science and Plant Nutrition*, *22*(4), 4063–4083. https://doi.org/10.1007/s42729-022-01008-2

Kwon, M. J., Haraguchi, A., & Kang, H. (2013). Long-term water regime differentiates changes in decomposition and microbial properties in tropical peat soils exposed to the short-term drought. *Soil Biology and Biochemistry*, *60*, 33–44. https://doi.org/10.1016/j.soilbio.2013.01.023

Lan, J., & Qin, G. (2020). The regulation of CIN-like TCP transcription factors. *International Journal of Molecular Sciences*, *21*(12), 4498. https://doi.org/10.3390/ijms21124498

Land, E. S., Cridland, C. A., Craige, B., Dye, A., Hildreth, S. B., Helm, R. F., Gillaspy, G. E., & Perera, I. Y. (2021). A role for inositol pyrophosphates in the metabolic adaptations to low phosphate in *Arabidopsis*. *Metabolites*, *11*(9), 601. https://doi.org/10.3390/metabo11090601

Langmead, B., & Salzberg, S. L. (2012). Fast gapped-read alignment with Bowtie 2. *Nature Methods*, *9*(4), 357–359. https://doi.org/10.1038/nmeth.1923

Leifheit, E. F., Camenzind, T., Lehmann, A., Andrade-Linares, D. R., Fussan, M., Westhusen, S., Wineberger, T. M., & Rillig, M. C. (2024). Fungal traits help to understand the decomposition of simple and complex plant litter. *FEMS Microbiology Ecology*, *100*(5). https://doi.org/10.1093/femsec/fiae033

Lemtiri-Chlieh, F., MacRobbie, E. A. C., & Brearley, C. A. (2000). Inositol hexakisphosphate is a physiological signal regulating the K^+-inward rectifying conductance in guard cells. *Proceedings of the National Academy of Sciences*, *97*(15), 8687–8692. https://doi.org/10.1073/pnas.140217497

Leng, N., Dawson, J. A., Thomson, J. A., Ruotti, V., Rissman, A. I., Smits, B. M. G., Haag, J. D., Gould, M. N., Stewart, R. M., & Kendziorski, C. (2013). EBSeq: an empirical Bayes

hierarchical model for inference in RNA-seq experiments. *Bioinformatics*, *29*(8), 1035–1043. https://doi.org/10.1093/bioinformatics/btt087

Li, H., & Durbin, R. (2010). Fast and accurate long-read alignment with Burrows–Wheeler transform. *Bioinformatics*, *26*(5), 589–595. https://doi.org/10.1093/bioinformatics/btp698

Li, H., Handsaker, B., Wysoker, A., Fennell, T., Ruan, J., Homer, N., Marth, G., Abecasis, G., & Durbin, R. (2009). The sequence alignment/map format and SAMtools. *Bioinformatics*, *25*(16), 2078–2079. https://doi.org/10.1093/bioinformatics/btp352

Li, J., Han, G., Sun, C., & Sui, N. (2019). Research advances of MYB transcription factors in plant stress resistance and breeding. *Plant Signaling & Behavior*, *14*(8), 1613131. https://doi.org/10.1080/15592324.2019.1613131

Li, J., & Tibshirani, R. (2013). Finding consistent patterns: a nonparametric approach for identifying differential expression in RNA-Seq data. *Statistical Methods in Medical Research*, *22*(5), 519–536. https://doi.org/10.1177/0962280211428386

Li, J., Wang, Y., & Suh, J. H. (2022). Multi-omics approach in tea polyphenol research regarding tea plant growth, development and tea processing: current technologies and perspectives. *Food Science and Human Wellness*, *11*(3), 524–536. https://doi.org/10.1016/j.fshw.2021.12.010

Li, J., Witten, D. M., Johnstone, I. M., & Tibshirani, R. (2012). Normalization, testing, and false discovery rate estimation for RNA-sequencing data. *Biostatistics*, *13*(3), 523–538. https://doi.org/10.1093/biostatistics/kxr031

Li, J., Zhai, Y., Ge, G., Xu, Y., Wang, C., Hu, A., Han, Y., Shan, N., Liu, B., Chen, J., & Wang, W. (2022). Bacterial community composition and function of tropical river ecosystem along

the Nandu River on Hainan Island, China. *International Journal of Environmental Research and Public Health*, *20*(1), 382. https://doi.org/10.3390/ijerph20010382

Li, P., Li, Y., Wang, B., Yu, H., Li, Q., & Hou, B. (2017). The *Arabidopsis* UGT87A2, a stress-inducible family 1 glycosyltransferase, is involved in the plant adaptation to abiotic stresses. *Physiologia Plantarum*, *159*(4), 416–432. https://doi.org/10.1111/ppl.12520

Li, S., Liu, J., Zhao, M., Su, Y., Cong, B., & Wang, Z. (2024). RNA quality score evaluation: a preliminary study of RNA integrity number (RIN) and RNA integrity and quality number (RNA IQ). *Forensic Science International*, *357*, 111976. https://doi.org/10.1016/j.forsciint.2024.111976

Li, Y., Wang, C., Chang, H., Zhang, Y., Liu, S., & He, W. (2023). Metagenomics reveals the effect of long-term fertilization on carbon cycle in the maize rhizosphere. *Frontiers in Microbiology*, *14*. https://doi.org/10.3389/fmicb.2023.1170214

Li, Y., Yang, X., Liu, H., Wang, W., Wang, C., Ding, G., Xu, F., Wang, S., Cai, H., Hammond, J. P., White, P. J., Shabala, S., Yu, M., & Shi, L. (2022). Local and systemic responses conferring acclimation of *Brassica napus* roots to low phosphorus conditions. *Journal of Experimental Botany*, *73*(14), 4753–4777. https://doi.org/10.1093/jxb/erac177

Li, Z., Jiang, H., Yan, H., Jiang, X., Ma, Y., & Qin, Y. (2021). Carbon and nitrogen metabolism under nitrogen variation affects flavonoid accumulation in the leaves of *Coreopsis tinctoria*. *PeerJ*, *9*, e12152. https://doi.org/10.7717/peerj.12152

Liang, Q., Chen, H., Chang, H., Liu, Y., Wang, Q., Wu, J., Liu, Y., Kumar, S., Chen, Y., Chen, Y., & Zhu, G. (2023). Influence of planting density on sweet potato storage root formation by regulating carbohydrate and lignin metabolism. *Plants*, *12*(10), 2039. https://doi.org/10.3390/plants12102039

Lihan, S., Benet, F., Husaini, A. A. S. A., Apun, K., Roslan, H. A., & Hassan, H. (2021). Isolation and identification of plant growth promoting rhizobacteria from sago palm (*Metroxylon sagu* Rottb.). *Tropical Life Sciences Research*, *32*(3), 39–51. https://doi.org/10.21315/tlsr2021.32.3.3

Liu, H., Gao, X., Fan, W., & Fu, X. (2025). Optimizing carbon and nitrogen metabolism in plants: from fundamental principles to practical applications. *Journal of Integrative Plant Biology*, *67*(6), 1447–1466. https://doi.org/10.1111/jipb.13919

Liu, H., Gao, Y., Wu, M., Shi, Y., Wang, H., Wu, L., & Xiang, Y. (2020). TCP10, a TCP transcription factor in moso bamboo (*Phyllostachys edulis*), confers drought tolerance to transgenic plants. *Environmental and Experimental Botany*, *172*, 104002. https://doi.org/10.1016/j.envexpbot.2020.104002

Liu, H., Shen, C., Hassani, D., Fang, W., Wang, Z., Lu, Y., Zhu, R., & Zhao, Q. (2022). Vacuoles in bryophytes: properties, biogenesis, and evolution. *Frontiers in Plant Science*, *13*. https://doi.org/10.3389/fpls.2022.863389

Liu, J., Kim, J. I., Cusumano, J. C., Chapple, C., Venugopalan, N., Fischetti, R. F., & Makowski, L. (2016). The impact of alterations in lignin deposition on cellulose organization of the plant cell wall. *Biotechnology for Biofuels*, *9*(1), 126. https://doi.org/10.1186/s13068-016-0540-z

Liu, J., Zhang, C., Wei, C., Liu, X., Wang, M., Yu, F., Xie, Q., & Tu, J. (2015). The RING finger ubiquitin E3 ligase OsHTAS enhances heat tolerance by promoting H_2O_2-induced stomatal closure in rice. *Plant Physiology*, *170*(1), 429–443. https://doi.org/10.1104/pp.15.00879

Liu, S., Abdellaoui, A., Verweij, K. J. H., & van Wingen, G. A. (2023). Gene expression has distinct associations with brain structure and function in major depressive disorder. *Advanced Science*, *10*(7). https://doi.org/10.1002/advs.202205486

Liu, Y., Xiao, L., Chi, J., Li, R., Han, Y., Cui, F., Peng, Z., Wan, S., & Li, G. (2022). Genome-wide identification and expression of SAUR gene family in peanut (*Arachis hypogaea L.*) and functional identification of *AhSAUR3* in drought tolerance. *BMC Plant Biology*, *22*(1), 178. https://doi.org/10.1186/s12870-022-03564-2

Liu, Y.-L., Liu, S., Xiao, J.-J., Cheng, G.-X., ul, H. S., & Gong, Z.-H. (2021). CaHSP18.1a, a small heat shock protein from pepper (*Capsicum annuum L.*), positively responds to heat, drought, and salt tolerance. *Horticulturae*, *7*(5), 117. https://doi.org/10.3390/horticulturae7050117

Livak, K. J., & Schmittgen, T. D. (2001). Analysis of relative gene expression data using real-time quantitative PCR and the 2−ΔΔCT Method. *Methods*, *25*(4), 402–408. https://doi.org/10.1006/meth.2001.1262

Loughlin, F. E., Mansfield, R. E., Vaz, P. M., McGrath, A. P., Setiyaputra, S., Gamsjaeger, R., Chen, E. S., Morris, B. J., Guss, J. M., & Mackay, J. P. (2009). The zinc fingers of the SR-like protein ZRANB2 are single-stranded RNA-binding domains that recognize 5′ splice site-like sequences. *Proceedings of the National Academy of Sciences*, *106*(14), 5581–5586. https://doi.org/10.1073/pnas.0802466106

Lourenco, M., Fitchett, J. M., & Woodborne, S. (2023). Peat definitions: a critical review. *Progress in Physical Geography: Earth and Environment*, *47*(4), 506–520. https://doi.org/10.1177/03091333221118353

Love, M. I., Huber, W., & Anders, S. (2014). Moderated estimation of fold change and dispersion for RNA-seq data with DESeq2. *Genome Biology*, *15*(12), 550. https://doi.org/10.1186/s13059-014-0550-8

Lu, D., Zhang, Y., Zhang, A., & Lu, C. (2022). Non-photochemical quenching: from light perception to photoprotective gene expression. *International Journal of Molecular Sciences*, *23*(2), 687. https://doi.org/10.3390/ijms23020687

Lu, X., Liu, Y., Johs, A., Zhao, L., Wang, T., Yang, Z., Lin, H., Elias, D. A., Pierce, E. M., Liang, L., Barkay, T., & Gu, B. (2016). Anaerobic mercury methylation and demethylation by *Geobacter bemidjiensis* Bem. *Environmental Science & Technology*, *50*(8), 4366–4373. https://doi.org/10.1021/acs.est.6b00401

Luo, C., Yan, J., He, C., Liu, W., Xie, D., & Jiang, B. (2022). Genome-wide identification of the *SAUR* gene family in wax gourd (*Benincasa hispida*) and functional characterization of *BhSAUR60* during fruit development. *International Journal of Molecular Sciences*, *23*(22), 14021. https://doi.org/10.3390/ijms232214021

Luo, G., Li, J., Guo, S., Li, Y., & Jin, Z. (2022). Photosynthesis, nitrogen allocation, non-structural carbohydrate allocation, and C:N:P stoichiometry of *Ulmus elongata* seedlings exposed to different light intensities. *Life*, *12*(9), 1310. https://doi.org/10.3390/life12091310

Luo, Z., Zhang, L., Hu, W., Wang, Y., Tao, J., Jia, Y., Miao, R., Chen, L.-S., & Guo, J. (2024). Excessive boron fertilization-induced toxicity is related to boron transport in field-grown pomelo trees. *Frontiers in Plant Science*, *15*. https://doi.org/10.3389/fpls.2024.1438664

Lv, W., He, X., Guo, H., Lan, H., Jiao, Y., Li, L., Lian, Y., Wang, Z., Xin, Z., Ren, Y., & Lin, T. (2022). Genome-wide identification of *TaSAUR* gene family members in hexaploid wheat and functional characterization of *TaSAUR66-5B* in improving nitrogen use efficiency.

International Journal of Molecular Sciences, *23*(14), 7574. https://doi.org/10.3390/ijms23147574

Lyu, Y., He, W., Zhou, X., Gao, X., Fan, M., Chen, D., & Chen, X. (2025). Clathrin light chain 2 is a substrate of ubiquitin ligase ATL5 and negatively regulates seed longevity in Arabidopsis. *Journal of Experimental Botany*, *76*(16), 4684–4695. https://doi.org/10.1093/jxb/eraf231

Ma, A., Zhuang, X., Wu, J., Cui, M., Lv, D., Liu, C., & Zhuang, G. (2013). Ascomycota members dominate fungal communities during straw residue decomposition in arable soil. *PLoS ONE*, *8*(6), e66146. https://doi.org/10.1371/journal.pone.0066146

Ma, B., Zhang, Y., Fan, Y., Zhang, L., Li, X., Zhang, Q.-Q., Shu, Q., Huang, J., Chen, G., Li, Q., Gao, Q., Zhu, X.-G., He, Z., & Wang, P. (2024). Genetic improvement of phosphate-limited photosynthesis for high yield in rice. *Proceedings of the National Academy of Sciences*, *121*(34). https://doi.org/10.1073/pnas.2404199121

Ma, W., Wu, F., Sheng, P., Wang, X., Zhang, Z., Zhou, K., Zhang, H., Hu, J., Lin, Q., Cheng, Z., Wang, J., Zhu, S., Zhang, X., Guo, X., Wang, H., Wu, C., Zhai, H., & Wan, J. (2017). The LBD12-1 transcription factor suppresses apical meristem size by repressing argonaute 10 expression. *Plant Physiology*, *173*(1), 801–811. https://doi.org/10.1104/pp.16.01699

Marçais, G., Delcher, A. L., Phillippy, A. M., Coston, R., Salzberg, S. L., & Zimin, A. (2018). MUMmer4: a fast and versatile genome alignment system. *PLOS Computational Biology*, *14*(1), e1005944. https://doi.org/10.1371/journal.pcbi.1005944

Mansoor, S., Ali, A., Kour, N., Bornhorst, J., AlHarbi, K., Rinklebe, J., Abd El Moneim, D., Ahmad, P., & Chung, Y. S. (2023). Heavy metal induced oxidative stress mitigation and ROS scavenging in plants. *Plants*, *12*(16), 3003. https://doi.org/10.3390/plants12163003

Mareri, L., Parrotta, L., & Cai, G. (2022). Environmental stress and plants. *International Journal of Molecular Sciences*, *23*(10), 5416. https://doi.org/10.3390/ijms23105416

Margalha, L., Confraria, A., & Baena-González, E. (2019). SnRK1 and TOR: modulating growth–defense trade-offs in plant stress responses. *Journal of Experimental Botany*, *70*(8), 2261–2274. https://doi.org/10.1093/jxb/erz066

Marlina, N., Haitami, A., Gusmiatun, G., Meidelima, D., Aluyah, C., Gribaldi, G., & Asmawati, A. (2025). Optimization of rice production in tidal swamps by combining bio-organic fertilizers and cropping systems. *Journal of Ecological Engineering*, *26*(9).

Martens, M., Ammar, A., Riutta, A., Waagmeester, A., Slenter, D. N., Hanspers, K., A. Miller, R., Digles, D., Lopes, E. N., Ehrhart, F., Dupuis, L. J., Winckers, L. A., Coort, S. L., Willighagen, E. L., Evelo, C. T., Pico, A. R., & Kutmon, M. (2021). WikiPathways: connecting communities. *Nucleic Acids Research*, *49*(D1), D613–D621. https://doi.org/10.1093/nar/gkaa1024

Martin, M. (2011). Cutadapt removes adapter sequences from high-throughput sequencing reads. *EMBnet.Journal*, *17*(1), 10. https://doi.org/10.14806/ej.17.1.200

Martins, S., Dohmann, E. M. N., Cayrel, A., Johnson, A., Fischer, W., Pojer, F., Satiat-Jeunemaître, B., Jaillais, Y., Chory, J., Geldner, N., & Vert, G. (2015). Internalization and vacuolar targeting of the brassinosteroid hormone receptor BRI1 are regulated by ubiquitination. *Nature Communications*, *6*(1), 6151. https://doi.org/10.1038/ncomms7151

Martínez-Cuenca, M.-R., Martínez-Alcántara, B., Quiñones, A., Ruiz, M., Iglesias, D. J., Primo-Millo, E., & Forner-Giner, M. Á. (2015). Physiological and molecular responses to excess boron in *Citrus macrophylla* W. *PLOS ONE*, *10*(7), e0134372. https://doi.org/10.1371/journal.pone.0134372

McDermaid, A., Monier, B., Zhao, J., Liu, B., & Ma, Q. (2019a). Interpretation of differential gene expression results of RNA-seq data: review and integration. *Briefings in Bioinformatics*, *20*(6), 2044–2054. https://doi.org/10.1093/bib/bby067

McDermaid, A., Monier, B., Zhao, J., Liu, B., & Ma, Q. (2019b). Interpretation of differential gene expression results of RNA-seq data: review and integration. *Briefings in Bioinformatics*, *20*(6), 2044–2054. https://doi.org/10.1093/bib/bby067

Mellado, M., & Vera, J. (2021). Microorganisms that participate in biochemical cycles in wetlands. *Canadian Journal of Microbiology*, *67*(11), 771–788. https://doi.org/10.1139/cjm-2020-0336

Melling, L. (2000). *Dalat & Mukah sago plantation peat soil study. Final Report Lulie Melling Soils Branch Department of Agriculture Sarawak*.

Melling, L. (2016). Peatland in Malaysia. In *Tropical Peatland Ecosystems* (Osaki, M. & Tsuji N.), pp. 59–73. Tokyo: Springer Japan. https://doi.org/10.1007/978-4-431-55681-7_4

Melling, L., Goh, K. J., Hatano, R., Uyo, L. J., Sayok, A., & Nik, A. R. (2008). Characteristics of natural tropical peatland and their influence on C flux in Loagan Bunut National Park, Sarawak, Malaysia. *After Wise Use-The Future of Peatlands. Proceedings 13th International Peat Congress Tullamore, Ireland*, 8–12.

Melling, L., Goh, K. J., Uyo, L. J., Sayok, A., & Hatano, R. (2007). Biophysical characteristics of tropical peatland. *Proceedings of the Soil Science Conference of Malaysia*, 1–11.

Mi, H., Ebert, D., Muruganujan, A., Mills, C., Albou, L.-P., Mushayamaha, T., & Thomas, P. D. (2021). PANTHER version 16: a revised family classification, tree-based classification tool, enhancer regions and extensive API. *Nucleic Acids Research*, *49*(D1), D394–D403. https://doi.org/10.1093/nar/gkaa1106

Ming, R. Y. C., Sobeng, Y., Zaini, F., & Busri, N. (2018). Suitability of peat swamp areas for commercial production of sago palms: The Sarawak Experience. In *Sago Palm Multiple Contributions to Food Security and Sustainable Livelihoods* (Ehara, H., Toyoda, T., & Johnson. D. V.), pp. 91–108. Singapore: Springer Singapore.

Mohamad Naim, H., Yaakub, A. N., & Awang Hamdan, D. A. (2016). Commercialization of sago through estate plantation scheme in Sarawak: The Way Forward. *International Journal of Agronomy*, *2016*, 1–6. https://doi.org/10.1155/2016/8319542

Mohamed, R., Mutalib, N. W. A., Norizan, M. N., Hirzin, R. S. N., & Isa, S. A. M. 2018. Effect of different plasticizers on tensile properties of PVA/sago starch system before and after weathering exposure. *AIP Conference Proceedings*, Shah Alam, Malaysia, 21-22 October 2017. AIP Publishing. https://doi.org/10.1063/1.5047163

Mohammed, T., Firoz, A., & Ramadan, A. M. (2022). RNA editing in chloroplast: advancements and opportunities. *Current Issues in Molecular Biology*, *44*(11), 5593–5604. https://doi.org/10.3390/cimb44110379

Mora-Poblete, F., Heidari, P., & Fuentes, S. (2023). Editorial: integrating advanced high-throughput technologies to improve plant resilience to environmental challenges. *Frontiers in Plant Science*, *14*. https://doi.org/10.3389/fpls.2023.1218691

Mosley, O. E., Gios, E., & Handley, K. M. (2024). Implications for nitrogen and sulphur cycles: phylogeny and niche-range of *Nitrospirota* in terrestrial aquifers. *ISME Communications*, *4*(1). https://doi.org/10.1093/ismeco/ycae047

Muhammad, A., Kong, X., Zheng, S., Bai, N., Li, L., Khan, M. H. U., Fiaz, S., & Zhang, Z. (2024). Exploring plant-microbe interactions in adapting to abiotic stress under climate change: a review. *Frontiers in Plant Science*, *15*. https://doi.org/10.3389/fpls.2024.1482739

Murdiyarso, D., Lilleskov, E., & Kolka, R. (2019). Tropical peatlands under siege: the need for evidence-based policies and strategies. *Mitigation and Adaptation Strategies for Global Change*, *24*(4), 493–505. https://doi.org/10.1007/s11027-019-9844-1

Muro-Villanueva, F., Mao, X., & Chapple, C. (2019). Linking phenylpropanoid metabolism, lignin deposition, and plant growth inhibition. *Current Opinion in Biotechnology*, *56*, 202–208. https://doi.org/10.1016/j.copbio.2018.12.008

Murtedza, M., Padmanabhan, E., Mei, B. L. H., & Siong, W. B. (2002). *The Peat Soils of Sarawak, STRAPEAT Status Report*. *UNIMAS: Sarawak, Malaysia,* 1-16.

Musich, R., Cadle-Davidson, L., & Osier, M. V. (2021). Comparison of short-read sequence aligners indicates strengths and weaknesses for biologists to consider. *Frontiers in Plant Science*, *12*. https://doi.org/10.3389/fpls.2021.657240

Naik, J., Misra, P., Trivedi, P. K., & Pandey, A. (2022). Molecular components associated with the regulation of flavonoid biosynthesis. *Plant Science*, *317*, 111196. https://doi.org/10.1016/j.plantsci.2022.111196

Nakamura, S. (2018). Morphogenesis of sago palm. In *Sago Palm Multiple Contributions to Food Security and Sustainable Livelihoods* (Ehara, H., Toyoda, T., & Johnson. D. V.), pp. 169–180. Singapore: Springer Singapore.

Narangerel, S., Jamsran, U., Asano, M., & Tamura, K. (2022). Morphological feature and physicochemical characteristics of soils under *Festuca* spp. dominant steppe at high mountain and mountain of Khuvsgul, Mongolia. *Open Journal of Soil Science*, *12*(09), 446–474. https://doi.org/10.4236/ojss.2022.129018

Nath, U., Crawford, B. C. W., Carpenter, R., & Coen, E. (2003). Genetic control of surface curvature. *Science*, *299*(5611), 1404–1407. https://doi.org/10.1126/science.1079354

Nisa, M.-U., Huang, Y., Benhamed, M., & Raynaud, C. (2019). The plant DNA damage response: signaling pathways leading to growth inhibition and putative role in response to stress conditions. *Frontiers in Plant Science*, *10*. https://doi.org/10.3389/fpls.2019.00653

Nishimura, Y. (2018). Sago starch: transformation of extraction and consumption processes in traditional Indonesian societies. In *Sago Palm Multiple Contributions to Food Security and Sustainable Livelihoods* (Ehara, H., Toyoda, T., & Johnson. D. V.), pp. 221–230. Singapore: Springer Singapore.

O'Brien, J., Hayder, H., Zayed, Y., & Peng, C. (2018). Overview of microRNA biogenesis, mechanisms of actions, and circulation. *Frontiers in Endocrinology*, *9*. https://doi.org/10.3389/fendo.2018.00402

Okamura, S., Mumtahina, N., Shimono, H., & Matsunami, M. (2021). Root sampling and RNA extraction methods for field-based gene expression analysis of soybeans. *Plant Production Science*, *24*(3), 339–345. https://doi.org/10.1080/1343943X.2020.1834867

Okazaki, M., & Sasaki, Y. (2018). Soil environment in sago palm forest. In *Sago Palm Multiple Contributions to Food Security and Sustainable Livelihoods* (Ehara, H., Toyoda, T., & Johnson. D. V.), pp. 193–206. Singapore: Springer Singapore.

Oliveira Filho, J. de S., Santos, O. A. Q. dos, Tavares, O. C. H., Fagundes, H. de S., Diniz, Y. V. de F. G., Pinto, L. A. da S. R., Silva Neto, E. C. da, & Pereira, M. G. (2021). Changes in soil phosphorus pools induced by drainage in tropical peatlands: evidence in monoculture and intercropping long-term systems. *Soil and Tillage Research*, *211*, 105056. https://doi.org/10.1016/j.still.2021.105056

Otasek, D., Morris, J. H., Bouças, J., Pico, A. R., & Demchak, B. (2019). Cytoscape automation: empowering workflow-based network analysis. *Genome Biology*, *20*(1), 185. https://doi.org/10.1186/s13059-019-1758-4

Othman, H., Darus, F. M., & Mohammed, A. T. (2009). Experiences in peat development for oil palm planting in the MPOB Research Station at Sessang, Sarawak. *Oil Palm Bulletin*, *58*, 1–13.

Palomo, A., Dechesne, A., Pedersen, A. G., & Smets, B. F. (2022). Genomic profiling of *Nitrospira* species reveals ecological success of comammox *Nitrospira*. *Microbiome*, *10*(1), 204. https://doi.org/10.1186/s40168-022-01411-y

Panozzo, A., Bolla, P. K., Barion, G., Botton, A., & Vamerali, T. (2025). Phytohormonal regulation of abiotic stress tolerance, leaf senescence and yield response in field crops: a comprehensive review. *BioTech*, *14*(1), 14. https://doi.org/10.3390/biotech14010014

Peltoniemi, K., Straková, P., Fritze, H., Iráizoz, P. A., Pennanen, T., & Laiho, R. (2012). How water-level drawdown modifies litter-decomposing fungal and actinobacterial communities in boreal peatlands. *Soil Biology and Biochemistry*, *51*, 20–34. https://doi.org/10.1016/j.soilbio.2012.04.013

Pendi, F. H., Hussain, H. (2024). Transcriptome dataset of *Metroxylon sagu* palms from multiple sago plantations in Sarawak. *BMC Research Note*.

Pernisová, M., & Vernoux, T. (2021). Auxin does the SAMba: auxin signaling in the shoot apical meristem. *Cold Spring Harbor Perspectives in Biology*, *13*(12), a039925. https://doi.org/10.1101/cshperspect.a039925

Pertea, M., Pertea, G. M., Antonescu, C. M., Chang, T.-C., Mendell, J. T., & Salzberg, S. L. (2015). StringTie enables improved reconstruction of a transcriptome from RNA-seq reads. *Nature Biotechnology*, *33*(3), 290–295. https://doi.org/10.1038/nbt.3122

Pimentel, H., Bray, N. L., Puente, S., Melsted, P., & Pachter, L. (2017). Differential analysis of RNA-seq incorporating quantification uncertainty. *Nature Methods*, *14*(7), 687–690. https://doi.org/10.1038/nmeth.4324

Pokimica, N., Ćosić, T., Uzelac, B., Ninković, S., & Raspor, M. (2024). Dissecting the roles of the cytokinin signaling network: the case of *de novo* shoot apical meristem formation. *Biomolecules*, *14*(3), 381. https://doi.org/10.3390/biom14030381

Qi, F., Wang, F., Xiaoyang, C., Wang, Z., Lin, Y., Peng, Z., Zhang, J., Wang, N., & Zhang, J. (2023). Gene expression analysis of different organs and identification of AP2 transcription factors in flax (*Linum usitatissimum* L.). *Plants*, *12*(18), 3260. https://doi.org/10.3390/plants12183260

Qi, S., Wang, J., Wan, L., Dai, Z., da Silva Matos, D. M., Du, D., Egan, S., Bonser, S. P., Thomas, T., & Moles, A. T. (2022). Arbuscular mycorrhizal fungi contribute to phosphorous uptake and allocation strategies of *Solidago canadensis* in a phosphorous-deficient environment. *Frontiers in Plant Science*, *13*. https://doi.org/10.3389/fpls.2022.831654

Qian, Y., Zhang, T., Yu, Y., Gou, L., Yang, J., Xu, J., & Pi, E. (2021). Regulatory mechanisms of bHLH transcription factors in plant adaptive responses to various abiotic stresses. *Frontiers in Plant Science*, *12*. https://doi.org/10.3389/fpls.2021.677611

Rahim, M. A., Zhang, X., & Busatto, N. (2023). Editorial: phenylpropanoid biosynthesis in plants. *Frontiers in Plant Science*, *14*. https://doi.org/10.3389/fpls.2023.1230664

Rahimlou, S., Bahram, M., & Tedersoo, L. (2021). Phylogenomics reveals the evolution of root nodulating alpha- and beta-Proteobacteria (rhizobia). *Microbiological Research*, *250*, 126788. https://doi.org/10.1016/j.micres.2021.126788

Ramnath, V., Sekar, S., Sankar, S., Sankaranarayanan, C., & Sastry, T. P. (2012). Preparation and evaluation of biocomposites as wound dressing material. *Journal of Materials Science: Materials in Medicine*, *23*(12), 3083–3095. https://doi.org/10.1007/s10856-012-4765-5

Rath, M., Challa, K. R., Sarvepalli, K., & Nath, U. (2022). Cincinnata-like TCP transcription factors in cell growth – an expanding portfolio. *Frontiers in Plant Science*, *13*. https://doi.org/10.3389/fpls.2022.825341

Räty, M., Keskinen, R., Yli-Halla, M., Hyvönen, J., & Soinne, H. (2021). Estimating cation exchange capacity and clay content from agricultural soil testing data. *Agricultural and Food Science*, *30*(4). https://doi.org/10.23986/afsci.111107

Rauwerdink, J. (1984). On the taxonomy of *Metroxylon*: the status of the sago palm in Papua New Guinea. *Department of Plant Taxonomy, Agricultural University, Wageningen, the Netherlands*, 42.

Reeza, A. A., Hussin, A., Hanif, A. H. M., & Sukari, M. A. M. (2014). Effect of liming and fertilizer application in hemic and sapric of tropical peat: phosphorus mineralisation, infra-red spectroscopy and microscopy. *American Journal of Agricultural and Biological Sciences*, *9*(3), 321–333. https://doi.org/10.3844/ajabssp.2014.321.333

Rejmánková, E., & Houdková, K. (2006). Wetland plant decomposition under different nutrient conditions: what is more important, litter quality or site quality? *Biogeochemistry*, *80*(3), 245–262. https://doi.org/10.1007/s10533-006-9021-y

Ren, C., Li, Z., Song, P., Wang, Y., Liu, W., Zhang, L., Li, X., Li, W., & Han, D. (2023). Overexpression of a grape MYB transcription factor gene VhMYB2 increases salinity and drought tolerance in *Arabidopsis thaliana*. *International Journal of Molecular Sciences*, *24*(13), 10743. https://doi.org/10.3390/ijms241310743

Riaz, M., Kamran, M., El-Esawi, M. A., Hussain, S., & Wang, X. (2021). Boron-toxicity induced changes in cell wall components, boron forms, and antioxidant defense system in rice seedlings. *Ecotoxicology and Environmental Safety*, *216*, 112192. https://doi.org/10.1016/j.ecoenv.2021.112192

Riemer, E., Pullagurla, N. J., Yadav, R., Rana, P., Jessen, H. J., Kamleitner, M., Schaaf, G., & Laha, D. (2022). Regulation of plant biotic interactions and abiotic stress responses by inositol polyphosphates. *Frontiers in Plant Science*, *13*. https://doi.org/10.3389/fpls.2022.944515

Rietra, R. P. J. J., Heinen, M., Dimkpa, C. O., & Bindraban, P. S. (2017). Effects of nutrient antagonism and synergism on yield and fertilizer use efficiency. *Communications in Soil Science and Plant Analysis*, *48*(16), 1895–1920. https://doi.org/10.1080/00103624.2017.1407429

Rincón-Tomás, B., Lanzén, A., Sánchez, P., Estupiñán, M., Sanz-Sáez, I., Bilbao, M. E., Rojo, D., Mendibil, I., Pérez-Cruz, C., Ferri, M., Capo, E., Abad-Recio, I. L., Amouroux, D., Bertilsson, S., Sánchez, O., Acinas, S. G., & Alonso-Sáez, L. (2024). Revisiting the mercury cycle in marine sediments: a potential multifaceted role for Desulfobacterota. *Journal of Hazardous Materials*, *465*, 133120. https://doi.org/10.1016/j.jhazmat.2023.133120

Ritchie, M. E., Phipson, B., Wu, D., Hu, Y., Law, C. W., Shi, W., & Smyth, G. K. (2015). limma powers differential expression analyses for RNA-sequencing and microarray studies. *Nucleic Acids Research*, *43*(7), e47–e47. https://doi.org/10.1093/nar/gkv007

Robinson, M. D., McCarthy, D. J., & Smyth, G. K. (2010). edgeR: a Bioconductor package for differential expression analysis of digital gene expression data. *Bioinformatics*, *26*(1), 139–140. https://doi.org/10.1093/bioinformatics/btp616

Rodriguez, K., Ricci, F., Ni, G., Iram, N., Palfreyman, R., Gonzalez-Garcia, R. A., Heffernan, J., Greening, C., Adame, M. F., & Marcellin, E. (2025). Abundant and active acetogens enhance the carbon dioxide sink of Blue Carbon ecosystems. *bioRxiv*, 2025-01. https://doi.org/10.1101/2025.01.07.631696

Rong, M., Xing, X., & Zhang, R. (2024). Muscle transcriptome analysis of mink at different growth stages using RNA-Seq. *Biology*, *13*(5), 283. https://doi.org/10.3390/biology13050283

Rosati, D., Palmieri, M., Brunelli, G., Morrione, A., Iannelli, F., Frullanti, E., & Giordano, A. (2024). Differential gene expression analysis pipelines and bioinformatic tools for the identification of specific biomarkers: a review. *Computational and Structural Biotechnology Journal*, *23*, 1154–1168. https://doi.org/10.1016/j.csbj.2024.02.018

Rothfels, K., Milacic, M., Matthews, L., Haw, R., Sevilla, C., Gillespie, M., Stephan, R., Gong, C., Ragueneau, E., May, B., Shamovsky, V., Wright, A., Weiser, J., Beavers, D., Conley, P., Tiwari, K., Jassal, B., Griss, J., Senff-Ribeiro, A., … Stein, L. (2023). Using the reactome database. *Current Protocols*, *3*(4). https://doi.org/10.1002/cpz1.722

Ruddle, K. (2010). The geographical distribution of sago-producing palms. *National Museum of Ethnology*, *3*(3), 572–594.

Saberi Riseh, R., Fathi, F., Lagzian, A., Vatankhah, M., & Kennedy, J. F. (2024). Modifying lignin: a promising strategy for plant disease control. *International Journal of Biological Macromolecules*, *271*, 132696. https://doi.org/10.1016/j.ijbiomac.2024.132696

Sahib, M. R., Pervaiz, Z. H., Williams, M. A., Saleem, M., & DeBolt, S. (2020). Rhizobacterial species richness improves sorghum growth and soil nutrient synergism in a nutrient-poor greenhouse soil. *Scientific Reports*, *10*(1). https://doi.org/10.1038/s41598-020-72516-3

Sakoula, D., Koch, H., Frank, J., Jetten, M. S. M., van Kessel, M. A. H. J., & Lücker, S. (2021). Enrichment and physiological characterization of a novel comammox *Nitrospira* indicates ammonium inhibition of complete nitrification. *The ISME Journal*, *15*(4), 1010–1024. https://doi.org/10.1038/s41396-020-00827-4

Sano, N., & Marion-Poll, A. (2021). ABA metabolism and homeostasis in seed dormancy and germination. *International Journal of Molecular Sciences*, *22*(10), 5069. https://doi.org/10.3390/ijms22105069

Sasaki, Y., Ando, H., Kakuda, K.-I., Melling, L., & Watanabe, A. (2025). Efficient nitrogen fertilization for sustainable sago palm (*Metroxylon sagu* Rottb.) cultivation in tropical peatland. *Plant Production Science*, *28*(1), 23–33. https://doi.org/10.1080/1343943X.2024.2423977

Sasi, S., Krishnan, S., Kodackattumannil, P., Shamisi, A. AL, Aldarmaki, M., Lekshmi, G., Kottackal, M., & Amiri, K. M. A. (2023). DNA-free high-quality RNA extraction from 39 difficult-to-extract plant species (representing seasonal tissues and tissue types) of 32 families, and its validation for downstream molecular applications. *Plant Methods*, *19*(1), 84. https://doi.org/10.1186/s13007-023-01063-5

Sato, T., Yamaguchi, T., & Takamura, T. (1979). Cultivation, harvesting and processing of sago palm. *Japanese Journal of Tropical Agriculture*, *23*(1), 130–136.

Sazykina, M. A., Minkina, T. M., Konstantinova, E. Yu., Khmelevtsova, L. E., Azhogina, T. N., Antonenko, E. M., Karchava, Sh. K., Klimova, M. V., Sushkova, S. N., Polienko, E. A., Birukova, O. A., Mandzhieva, S. S., Kudeevskaya, E. M., Khammami, M. I., Rakin, A. V., & Sazykin, I. S. (2022). Pollution impact on microbial communities composition in natural and anthropogenically modified soils of Southern Russia. *Microbiological Research*, *254*, 126913. https://doi.org/10.1016/j.micres.2021.126913

Schroeder, A., Mueller, O., Stocker, S., Salowsky, R., Leiber, M., Gassmann, M., Lightfoot, S., Menzel, W., Granzow, M., & Ragg, T. (2006). The RIN: an RNA integrity number for assigning integrity values to RNA measurements. *BMC Molecular Biology*, *7*(1), 3. https://doi.org/10.1186/1471-2199-7-3

Shamloo-Dashtpagerdi, R., Razi, H., Ebrahimie, E., & Niazi, A. (2018). Molecular characterization of *Brassica napus* stress related transcription factors, BnMYB44 and BnVIP1, selected based on comparative analysis of *Arabidopsis thaliana* and *Eutrema salsugineum* transcriptomes. *Molecular Biology Reports*, *45*(5), 1111–1124. https://doi.org/10.1007/s11033-018-4262-0

Sharma, B., Joshi, D., Yadav, P. K., Gupta, A. K., & Bhatt, T. K. (2016). Role of ubiquitin-mediated degradation system in plant biology. *Frontiers in Plant Science*, *7*. https://doi.org/10.3389/fpls.2016.00806

Sharma, N., Negi, N., Kaur, H., Sharma, V., Kumari, V., & Thakur, N. (2025). Metabolic adaptations in plants: navigating heavy metal stress for sustainable plant growth. *Discover Applied Sciences*, *7*(10), 1041. https://doi.org/10.1007/s42452-025-06715-w

Sheng, C., Song, S., Zhou, W., Dossou, S. S. K., Zhou, R., Zhang, Y., Li, D., You, J., & Wang, L. (2023). Integrating transcriptome and phytohormones analysis provided insights into plant height development in sesame. *Plant Physiology and Biochemistry*, *198*, 107695. https://doi.org/10.1016/j.plaphy.2023.107695

Sheremet, A., Jones, G. M., Jarett, J., Bowers, R. M., Bedard, I., Culham, C., Eloe-Fadrosh, E. A., Ivanova, N., Malmstrom, R. R., Grasby, S. E., Woyke, T., & Dunfield, P. F. (2020). Ecological and genomic analyses of candidate phylum WPS-2 bacteria in an unvegetated soil. *Environmental Microbiology*, *22*(8), 3143–3157. https://doi.org/10.1111/1462-2920.15054

Sherman, B. T., Hao, M., Qiu, J., Jiao, X., Baseler, M. W., Lane, H. C., Imamichi, T., & Chang, W. (2022). DAVID: a web server for functional enrichment analysis and functional annotation of gene lists (2021 update). *Nucleic Acids Research*, *50*(W1), W216–W221. https://doi.org/10.1093/nar/gkac194

Shrestha, A. (2006). Nitrogen fixing activity in different parts of sago palm (*Metroxylon sagu*) and characterization of aerobic nitrogen fixing bacteria colonizing sago palm. *Sago Palm*, 20–32.

Shu, K., & Yang, W. (2017). E3 ubiquitin ligases: ubiquitous actors in plant development and abiotic stress responses. *Plant and Cell Physiology*, *58*(9), 1461–1476. https://doi.org/10.1093/pcp/pcx071

Shu, K., Zhou, W., & Yang, W. (2018). APETALA 2-domain-containing transcription factors: focusing on abscisic acid and gibberellins antagonism. *New Phytologist*, *217*(3), 977–983. https://doi.org/10.1111/nph.14880

Sia, S.-G., & Abdullah, W. H. (2015). Mercury and chlorine in the Balingian coal from Sarawak, Malaysia. *Natural Resources Research*, *24*(2), 197–207. https://doi.org/10.1007/s11053-014-9249-5

Siadjeu, C., & Kadereit, G. (2024). C4-like *Sesuvium sesuvioides* (Aizoaceae) exhibits CAM in cotyledons and putative C4-like + CAM metabolism in adult leaves as revealed by transcriptome analysis. *BMC Genomics*, *25*(1), 688. https://doi.org/10.1186/s12864-024-10553-2

Sim, E. S., & Ahmed, M. I. (1978). Variation of flour yield in the sago palm. *Malaysian Journal of Sustainable Agriculture*, *51*, 351–358.

Singh, P., Meshram, A., Singh, R. K., ur Rahman, L., & Morya, V. K. (2024). Synergistic enhancement of cauliflower yield: harnessing phosphate-solubilizing bacteria and nitrogen-fixing microbes for sustainable agriculture. *Journal of Pure and Applied Microbiology*, *18*(4), 2582–2591. https://doi.org/10.22207/JPAM.18.4.31

Singh, V. V., Naseer, A., Sellamuthu, G., & Jakuš, R. (2024). An optimized and cost-effective RNA extraction method for secondary metabolite-enriched tissues of Norway spruce (*Picea abies*). *Plants*, *13*(3), 389. https://doi.org/10.3390/plants13030389

Singhal, R. S., Kennedy, J. F., Gopalakrishnan, S. M., Kaczmarek, A., Knill, C. J., & Akmar, P. F. (2008). Industrial production, processing, and utilization of sago palm-derived products. *Carbohydrate Polymers*, *72*(1), 1–20.

Smolikova, G., Gorbach, D., Lukasheva, E., Mavropolo-Stolyarenko, G., Bilova, T., Soboleva, A., Tsarev, A., Romanovskaya, E., Podolskaya, E., Zhukov, V., Tikhonovich, I., Medvedev, S., Hoehenwarter, W., & Frolov, A. (2020). Bringing new methods to the seed proteomics

platform: challenges and perspectives. *International Journal of Molecular Sciences*, *21*(23), 9162. https://doi.org/10.3390/ijms21239162

Solly, E. F., Weber, V., Zimmermann, S., Walthert, L., Hagedorn, F., & Schmidt, M. W. I. (2020). A critical evaluation of the relationship between the effective cation exchange capacity and soil organic carbon content in Swiss forest soils. *Frontiers in Forests and Global Change*, *3*. https://doi.org/10.3389/ffgc.2020.00098

Song, B., Ning, W., Wei, D., Jiang, M., Zhu, K., Wang, X., Edwards, D., Odeny, D. A., & Cheng, S. (2023). Plant genome resequencing and population genomics: current status and future prospects. *Molecular Plant*, *16*(8), 1252–1268. https://doi.org/10.1016/j.molp.2023.07.009

Sreeharsha, R. V., & Venkata Mohan, S. (2024). Structural and functional dynamics of microbial photosystem complexes. In *Microbial Photosynthesis* (pp. 23–41). Springer Nature Singapore. https://doi.org/10.1007/978-981-97-1253-3_2

Steinacher, C., Rieder, D., Turner, J. E., Solanky, N., Nishio, S., Usami, S., Hausott, B., Schrott-Fischer, A., & Dudas, J. (2024). Validation of RNA extraction methods and suitable reference genes for gene expression studies in developing fetal human inner ear tissue. *International Journal of Molecular Sciences*, *25*(5), 2907. https://doi.org/10.3390/ijms25052907

Su, Y., Shi, Q., Li, Z., Deng, H., Zhou, Q., Li, L., Zhao, L., Yuan, S., Liu, Q., & Chen, Y. (2024). *Rhodopseudomonas palustris* shapes bacterial community, reduces Cd bioavailability in Cd contaminated flooding paddy soil, and improves rice performance. *Science of The Total Environment*, *926*, 171824. https://doi.org/10.1016/j.scitotenv.2024.171824

Suzuki, Y., Ishiyama, K., Yoon, D.-K., Takegahara-Tamakawa, Y., Kondo, E., Suganami, M., Wada, S., Miyake, C., & Makino, A. (2022). Suppression of chloroplast triose phosphate

isomerase evokes inorganic phosphate-limited photosynthesis in rice. *Plant Physiology*, *188*(3), 1550–1562. https://doi.org/10.1093/plphys/kiab576

Syahariza, Z. A., & Yong, H. Y. (2017). Evaluation of rheological and textural properties of texture-modified rice porridge using tapioca and sago starch as thickener. *Journal of Food Measurement and Characterization*, *11*(4), 1586–1591. https://doi.org/10.1007/s11694-017-9538-x

Szklarczyk, D., Gable, A. L., Nastou, K. C., Lyon, D., Kirsch, R., Pyysalo, S., Doncheva, N. T., Legeay, M., Fang, T., Bork, P., Jensen, L. J., & von Mering, C. (2021). The STRING database in 2021: customizable protein–protein networks, and functional characterization of user-uploaded gene/measurement sets. *Nucleic Acids Research*, *49*(D1), D605–D612. https://doi.org/10.1093/nar/gkaa1074

Szymanski, M. (2002). 5S ribosomal RNA database. *Nucleic Acids Research*, *30*(1), 176–178. https://doi.org/10.1093/nar/30.1.176

Tajuddin, T., Sukarnih, T., & Haska, N. (2015). The combination of growth hormones increased the *in vitro* shoots multiplication on sago palm (*Metroxylon sagu* Rottb.). *Journal Bioteknologi dan Biosains Indonesia*, *2* (1), 27-33.

Tan, H. L., Wong, Y. Y., Muniyandy, S., Hashim, K., & Pushpamalar, J. (2016). Carboxymethyl sago pulp/carboxymethyl sago starch hydrogel: effect of polymer mixing ratio and study of controlled drug release. *Journal of Applied Polymer Science*, *133*(28). https://doi.org/10.1002/app.43652

Tanaka, I., Chakraborty, A., Saulnier, O., Benoit-Pilven, C., Vacher, S., Labiod, D., Lam, E. W. F., Bièche, I., Delattre, O., Pouzoulet, F., Auboeuf, D., Vagner, S., & Dutertre, M. (2020). ZRANB2 and SYF2-mediated splicing programs converging on ECT2 are involved in breast

cancer cell resistance to doxorubicin. *Nucleic Acids Research*, *48*(5), 2676–2693. https://doi.org/10.1093/nar/gkz1213

Tang, S.-Y., Hara, S., Melling, L., Goh, K.-J., & Hashikodo, Y. (2010). *Burkholderia vietnamiensis* isolated from root tissues of nipa palm (*Nypa fruticans*) in Sarawak, Malaysia, proved to be its major endophytic nitrogen-fixing bacterium. *Bioscience, Biotechnology, and Biochemistry*, *74*(9), 1972–1975. https://doi.org/10.1271/bbb.100397

Tarazona, S., García, F., Ferrer, A., Dopazo, J., & Conesa, A. (2012). NOIseq: a RNA-seq differential expression method robust for sequencing depth biases. *EMBnet.Journal*, *17*(B), 18. https://doi.org/10.14806/ej.17.B.265

Tashan, H., Harighi, B., Rostamzadeh, J., & Azizi, A. (2021). Characterization of arsenic-resistant endophytic bacteria from alfalfa and chickpea plants. *Frontiers in Plant Science*, *12*. https://doi.org/10.3389/fpls.2021.696750

Teale, W. D., Pasternak, T., Dal Bosco, C., Dovzhenko, A., Kratzat, K., Bildl, W., Schwörer, M., Falk, T., Ruperti, B., V Schaefer, J., Shahriari, M., Pilgermayer, L., Li, X., Lübben, F., Plückthun, A., Schulte, U., & Palme, K. (2021). Flavonol-mediated stabilization of PIN efflux complexes regulates polar auxin transport. *The EMBO Journal*, *40*(1). https://doi.org/10.15252/embj.2020104416

Thompson, M. S., Yan, T. H., Mikal, K. M., Shamsudin, S. M., Rasheed, A., & Sarbini, S. R. (2023). An in vivo study: prebiotic evaluation of the resistant starch from *Metroxylon sagu* on obesity using fat-induced rats. *Bioactive Carbohydrates and Dietary Fibre*, *30*, 100365.

Thudi, M., Palakurthi, R., Schnable, J. C., Chitikineni, A., Dreisigacker, S., Mace, E., Srivastava, R. K., Satyavathi, C. T., Odeny, D., Tiwari, V. K., Lam, H.-M., Hong, Y. Bin, Singh, V. K., Li, G., Xu, Y., Chen, X., Kaila, S., Nguyen, H., Sivasankar, S., … Varshney, R. K. (2021).

Genomic resources in plant breeding for sustainable agriculture. *Journal of Plant Physiology*, *257*, 153351. https://doi.org/10.1016/j.jplph.2020.153351

Too, C. C., Keller, A., Sickel, W., Lee, S. M., & Yule, C. M. (2018). Microbial community structure in a Malaysian tropical peat swamp forest: the influence of tree species and depth. *Frontiers in Microbiology*, *9*. https://doi.org/10.3389/fmicb.2018.02859

Toyoda, Y. (2018). Life and livelihood in sago-growing areas. In *Sago Palm Multiple Contributions to Food Security and Sustainable Livelihoods* (Ehara, H., Toyoda, T., & Johnson. D. V.), pp. 31–44. Singapore: Springer Singapore.

Tripathi, B. M., Song, W., Slik, J. W. F., Sukri, R. S., Jaafar, S., Dong, K., & Adams, J. M. (2016). Distinctive tropical forest variants have unique soil microbial communities, but not always low microbial diversity. *Frontiers in Microbiology*, *7*. https://doi.org/10.3389/fmicb.2016.00376

Trisia, M. A., Takeshita, H., Kikuta, M., & Ehara, H. (2020). Factors determining sago starch import demand: empirical evidence from Japan. *Journal of International Logistics and Trade*, *18*(4), 159–167. https://doi.org/10.24006/jilt.2020.18.4.159

Trivedi, P., Leach, J. E., Tringe, S. G., Sa, T., & Singh, B. K. (2020). Plant–microbiome interactions: from community assembly to plant health. *Nature Reviews Microbiology*, *18*(11), 607–621. https://doi.org/10.1038/s41579-020-0412-1

Tsai, H.-L., Li, Y.-H., Hsieh, W.-P., Lin, M.-C., Ahn, J. H., & Wu, S.-H. (2014). HUA enhancer 1 is involved in posttranscriptional regulation of positive and negative regulators in *Arabidopsis* Photomorphogenesis. *The Plant Cell*, *26*(7), 2858–2872. https://doi.org/10.1105/tpc.114.126722

Tyagi, P., Singh, D., Mathur, S., Singh, A., & Ranjan, R. (2022). Upcoming progress of transcriptomics studies on plants: an overview. *Frontiers in Plant Science*, *13*. https://doi.org/10.3389/fpls.2022.1030890

Ueda, Y., Kiba, T., & Yanagisawa, S. (2020). Nitrate-inducible NIGT1 proteins modulate phosphate uptake and starvation signalling via transcriptional regulation of *SPX* genes. *The Plant Journal*, *102*(3), 448–466. https://doi.org/10.1111/tpj.14637

Untergasser, A., Cutcutache, I., Koressaar, T., Ye, J., Faircloth, B. C., Remm, M., & Rozen, S. G. (2012). Primer3—new capabilities and interfaces. *Nucleic Acids Research*, *40*(15), e115–e115. https://doi.org/10.1093/nar/gks596

Vamadevan, V., Bertoft, E., & Seetharaman, K. (2018). Impact of different structural types of amylopectin on retrogradation. *Food Hyrocolloids*, *80*(1), 88–96.

Van Acker, R., Vanholme, R., Storme, V., Mortimer, J. C., Dupree, P., & Boerjan, W. (2013). Lignin biosynthesis perturbations affect secondary cell wall composition and saccharification yield in *Arabidopsis thaliana*. *Biotechnology for Biofuels*, *6*(1). https://doi.org/10.1186/1754-6834-6-46

Vannier, N., Agler, M., & Hacquard, S. (2019). Microbiota-mediated disease resistance in plants. *PLOS Pathogens*, *15*(6), e1007740. https://doi.org/10.1371/journal.ppat.1007740

Vera-Maldonado, P., Aquea, F., Reyes-Díaz, M., Cárcamo-Fincheira, P., Soto-Cerda, B., Nunes-Nesi, A., & Inostroza-Blancheteau, C. (2024). Role of boron and its interaction with other elements in plants. *Frontiers in Plant Science*, *15*. https://doi.org/10.3389/fpls.2024.1332459

Verhaar, H. M., 1976. Chromosome pattern of the sago palm (*M. sagu* Rottb.). In K. Tan (Ed.), *Proceedings of the. 1st International Sago Symposium*, Kuching, Malaysia 5-7 July 1976.

Viola, I. L., Alem, A. L., Jure, R. M., & Gonzalez, D. H. (2023). Physiological roles and mechanisms of action of class I TCP transcription factors. *International Journal of Molecular Sciences*, *24*(6), 5437. https://doi.org/10.3390/ijms24065437

Walter, J., Lück, E. & Zeitz, J. (2013). Characterization of peat-electrical properties by means of geophysical measurements. In *EGU General Assembly Conference Abstracts*, Vienna, Austria 7-12 April 2013.

Wang, J., Gao, X., Dong, J., Tian, X., Wang, J., Palta, J. A., Xu, S., Fang, Y., & Wang, Z. (2020). Over-expression of the heat-responsive wheat gene *TaHSP23.9* in transgenic *Arabidopsis* conferred tolerance to heat and salt stress. *Frontiers in Plant Science*, *11*. https://doi.org/10.3389/fpls.2020.00243

Wang, J., Zhang, L., Qi, L., & Zhang, S. (2022). Integrated transcriptomic and metabolic analyses provide insights into the maintenance of embryogenic potential and the biosynthesis of phenolic acids and flavonoids involving transcription factors in *Larix kaempferi* (Lamb.) Carr. *Frontiers in Plant Science*, *13*. https://doi.org/10.3389/fpls.2022.1056930

Wang, M., Li, R., & Zhao, Q. (2023). Multi-omics techniques in genetic studies and breeding of forest plants. *Forests*, *14*(6), 1196. https://doi.org/10.3390/f14061196

Wang, R., Yang, X., Guo, S., Wang, Z., Zhang, Z., & Fang, Z. (2021). MiR319-targeted *OsTCP21* and *OsGAmyb* regulate tillering and grain yield in rice. *Journal of Integrative Plant Biology*, *63*(7), 1260–1272. https://doi.org/10.1111/jipb.13097

Wang, S., Meade, A., Lam, H.-M., & Luo, H. (2020). Evolutionary timeline and genomic plasticity underlying the lifestyle diversity in *Rhizobiales*. *MSystems*, *5*(4). https://doi.org/10.1128/mSystems.00438-20

Wang, X., An, Y., Xu, P., & Xiao, J. (2021). Functioning of PPR proteins in organelle RNA metabolism and chloroplast biogenesis. *Frontiers in Plant Science*, *12*. https://doi.org/10.3389/fpls.2021.627501

Wang, X., Niu, Y., & Zheng, Y. (2021). Multiple functions of MYB transcription factors in abiotic stress responses. *International Journal of Molecular Sciences*, *22*(11), 6125. https://doi.org/10.3390/ijms22116125

Wang, Z., Mao, Y., Guo, Y., Gao, J., Liu, X., Li, S., Lin, Y.-C. J., Chen, H., Wang, J. P., Chiang, V. L., & Li, W. (2020). MYB transcription factor161 mediates feedback regulation of secondary wall-associated *NAC-Domain1* family genes for wood formation. *Plant Physiology*, *184*(3), 1389–1406. https://doi.org/10.1104/pp.20.01033

Wang, Z., Zhu, Z., Li, M., Xie, X., Hao, P., Tan, J., Chen, Y., Bai, W., Guo, L., & Hu, M. (2025). OsOZ1, a zinc finger motif-containing protein, is essential for chloroplast development through RNA editing and intron splicing in rice. *Plant Growth Regulation*. https://doi.org/10.1007/s10725-025-01283-w

Watanabe, S. (2005). Research on sago palm plantation sustainability in Tebing Tinggi, Indonesia. *Sago Palm*, *13*, 12–15.

Wawrzyńska, A., & Sirko, A. (2024). Sulfate availability and hormonal signaling in the coordination of plant growth and development. *International Journal of Molecular Sciences*, *25*(7), 3978. https://doi.org/10.3390/ijms25073978

Whitbread, A. L., Dorn, A., Röhrig, S., & Puchta, H. (2021). Different functional roles of RTR complex factors in DNA repair and meiosis in *Arabidopsis* and tomato. *The Plant Journal*, *106*(4), 965–977. https://doi.org/10.1111/tpj.15211

Widodo, R. T., & Hassan, A. (2015). Compression and mechanical properties of directly compressible pregelatinized sago starches. *Powder Technology*, *269*, 15–21. https://doi.org/10.1016/j.powtec.2014.08.039

Wodrich, M. D., Sawatlon, B., Busch, M., & Corminboeuf, C. (2021). The genesis of molecular volcano plots. *Accounts of Chemical Research*, *54*(5), 1107–1117. https://doi.org/10.1021/acs.accounts.0c00857

Woldeyohannis, Y. S., Hiremath, S. S., Tola, S., & Wako, A. (2022). Investigation of soil physiochemical properties effects on soil compaction for a long year tilled farmland. *Applied and Environmental Soil Science*, *2022*, 1–9. https://doi.org/10.1155/2022/8626200

Wu, C., Tang, D., Dai, J., Tang, X., Bao, Y., Ning, J., Zhen, Q., Song, H., St. Leger, R. J., & Fang, W. (2022). Bioremediation of mercury-polluted soil and water by the plant symbiotic fungus *Metarhizium robertsii*. *Proceedings of the National Academy of Sciences*, *119*(47). https://doi.org/10.1073/pnas.2214513119

Wu, R., Wang, T., Warren, B. A. W., Thomson, S. J., Allan, A. C., Macknight, R. C., & Varkonyi-Gasic, E. (2018). Kiwifruit SVP2 controls developmental and drought-stress pathways. *Plant Molecular Biology*, *96*(3), 233–244. https://doi.org/10.1007/s11103-017-0688-3

Wu, Y., Sun, Z., Liu, R., Wang, L., & Cai, B. (2024). Enhancing sulfur absorption in soybean rhizosphere through arbuscular mycorrhizal fungi inoculation: Implications for soil health and crop growth. *Journal of Cleaner Production*, *463*, 142759. https://doi.org/10.1016/j.jclepro.2024.142759

Xiao, S., Hu, Q., Shen, J., Liu, S., Yang, Z., Chen, K., Klosterman, S. J., Javornik, B., Zhang, X., & Zhu, L. (2021). GhMYB4 downregulates lignin biosynthesis and enhances cotton

resistance to *Verticillium dahliae*. *Plant Cell Reports*, *40*(4), 735–751. https://doi.org/10.1007/s00299-021-02672-x

Xie, H., Engle, N. L., Venketachalam, S., Yoo, C. G., Barros, J., Lecoultre, M., Howard, N., Li, G., Sun, L., Srivastava, A. C., Pattathil, S., Pu, Y., Hahn, M. G., Ragauskas, A. J., Nelson, R. S., Dixon, R. A., Tschaplinski, T. J., Blancaflor, E. B., & Tang, Y. (2019). Combining loss of function of *folylpolyglutamate synthetase1* and *caffeoyl-coa 3-o-methyltransferase1* for lignin reduction and improved saccharification efficiency in *Arabidopsis thaliana*. *Biotechnology for Biofuels*, *12*(1), 108. https://doi.org/10.1186/s13068-019-1446-3

Xie, K., Cakmak, I., Wang, S., Zhang, F., & Guo, S. (2021). Synergistic and antagonistic interactions between potassium and magnesium in higher plants. *The Crop Journal*, *9*(2), 249–256. https://doi.org/10.1016/j.cj.2020.10.005

Xie, M., Sun, J., Gong, D., & Kong, Y. (2019). The roles of *Arabidopsis* c1-2i subclass of C_2H_2-type zinc-finger transcription factors. *Genes*, *10*(9), 653. https://doi.org/10.3390/genes10090653

Xiong, W., Jousset, A., Li, R., Delgado-Baquerizo, M., Bahram, M., Logares, R., Wilden, B., de Groot, G. A., Amacker, N., Kowalchuk, G. A., Shen, Q., & Geisen, S. (2021). A global overview of the trophic structure within microbiomes across ecosystems. *Environment International*, *151*, 106438. https://doi.org/10.1016/j.envint.2021.106438

Xiong, Y., & Jiao, Y. (2019). The diverse roles of auxin in regulating leaf development. *Plants*, *8*(7), 243. https://doi.org/10.3390/plants8070243

Xu, J., Morris, P. J., Liu, J., & Holden, J. (2018). PEATMAP: refining estimates of global peatland distribution based on a meta-analysis. *Catena*, *160*, 134–140. https://doi.org/10.1016/j.catena.2017.09.010

Xu, Y., Jiang, L., Gao, J., Zhang, W., Zhang, M., Liu, C., & Jia, J. (2024). Molecular regulation of photosynthetic carbon assimilation in oat leaves under drought stress. *Plants*, *13*(23), 3317. https://doi.org/10.3390/plants13233317

Xue, H., Gao, X., He, P., & Xiao, G. (2022). Origin, evolution, and molecular function of DELLA proteins in plants. *The Crop Journal*, *10*(2), 287–299. https://doi.org/10.1016/j.cj.2021.06.005

Yadav, A. N., Verma, P., Kumar, S., Kumar, V., Kumar, M., Kumari Sugitha, T. C., Singh, B. P., Saxena, A. K., & Dhaliwal, H. S. (2018). Actinobacteria from rhizosphere. In *New and Future Developments in Microbial Biotechnology and Bioengineering* (pp. 13–41). Elsevier. https://doi.org/10.1016/B978-0-444-63994-3.00002-3

Yamamoto, Y., Yoshida, T., Goto, Y., Nitta, Y., Kakuda, K., Jong, F., Hillary, L., & Hassan, A. (2003). Differences in growth and starch yield of sago palms (*Metroxylon sagu* Rottb.) among soil types in Sarawak, Malaysia. *Japanese Journal of Tropical Agriculture*, *47*(4), 250–259. https://doi.org/10.11248/jsta1957.47.250

Yan, S., Bhawal, R., Yin, Z., Thannhauser, T. W., & Zhang, S. (2022). Recent advances in proteomics and metabolomics in plants. *Molecular Horticulture*, *2*(1), 17. https://doi.org/10.1186/s43897-022-00038-9

Yan, W. J., Pendi, F. H., & Hussain, H. (2022). Improved CTAB method for RNA extraction of thick waxy leaf tissues from sago palm (*Metroxylon sagu* Rottb.). *Chemical and Biological Technologies in Agriculture*, *9*(1). https://doi.org/10.1186/s40538-022-00329-9

Yan, J., Ye, X., Song, Y., Ren, T., Wang, C., Li, X., Cong, R., Lu, Z., & Lu, J. (2023). Sufficient potassium improves inorganic phosphate-limited photosynthesis in *Brassica napus* by

enhancing metabolic phosphorus fractions and rubisco activity. *The Plant Journal*, *113*(2), 416–429. https://doi.org/10.1111/tpj.16057

Yang, M., Zhou, D., Hang, H., Chen, S., Liu, H., Su, J., Lv, H., Jia, H., & Zhao, G. (2024). Effects of balancing exchangeable cations Ca, Mg, and K on the growth of tomato seedlings (solanum lycopersicum L.) based on increased soil cation exchange capacity. *Agronomy*, *14*(3), 629. https://doi.org/10.3390/agronomy14030629

Yang, S.-Y., Huang, T.-K., Kuo, H.-F., & Chiou, T.-J. (2017). Role of vacuoles in phosphorus storage and remobilization. *Journal of Experimental Botany*, 3045–3055. https://doi.org/10.1093/jxb/erw481

Yang, S.-Y., Lin, W.-Y., Hsiao, Y.-M., & Chiou, T.-J. (2024). Milestones in understanding transport, sensing, and signaling of the plant nutrient phosphorus. *The Plant Cell*, *36*(5), 1504–1523. https://doi.org/10.1093/plcell/koad326

Yang, X., Long, Y., Sarkar, B., Li, Y., Lü, G., Ali, A., Yang, J., & Cao, Y. E. (2021). Influence of soil microorganisms and physicochemical properties on plant diversity in an arid desert of Western China. *Journal of Forestry Research*, *32*(6), 2645–2659. https://doi.org/10.1007/s11676-021-01292-1

Yang, Y., Zhou, T., Xu, J., Wang, Y., Pu, Y., Qu, Y., & Sun, G. (2024). Genome-wide identification and expression analysis unveil the involvement of the cold shock protein (*CSP*) gene family in cotton hypothermia stress. *Plants*, *13*(5), 643. https://doi.org/10.3390/plants13050643

Yatsugi, T. (1986). Problems of sago starch manufacturing. *Proceeding of the Third Sago Symposium "The Equatorial Swamp as a Natural Resource,"* Tokyo, Japan, 20-23 May 1985. Sago Palm Research Fund.

Yin, X., Zhao, L., Fang, Q., & Ding, G. (2021). Differences in soil physicochemical properties in different-aged *Pinus massoniana* plantations in Southwest China. *Forests*, *12*(8), 987. https://doi.org/10.3390/f12080987

Yoneda, Y., Yamamoto, K., Makino, A., Tanaka, Y., Meng, X.-Y., Hashimoto, J., Shin-ya, K., Satoh, N., Fujie, M., Toyama, T., Mori, K., Ike, M., Morikawa, M., Kamagata, Y., & Tamaki, H. (2021). Novel plant-associated Acidobacteria promotes growth of common floating aquatic plants, duckweeds. *Microorganisms*, *9*(6), 1133. https://doi.org/10.3390/microorganisms9061133

Yu, T., Cheng, L., Liu, Q., Wang, S., Zhou, Y., Zhong, H., Tang, M., Nian, H., & Lian, T. (2022). Effects of waterlogging on soybean rhizosphere bacterial community using V4, LoopSeq, and PacBio 16S rRNA sequence. *Microbiology Spectrum*, *10*(1). https://doi.org/10.1128/spectrum.02011-21

Yu, T.-F., Xu, Z.-S., Guo, J.-K., Wang, Y.-X., Abernathy, B., Fu, J.-D., Chen, X., Zhou, Y.-B., Chen, M., Ye, X.-G., & Ma, Y.-Z. (2017). Improved drought tolerance in wheat plants overexpressing a synthetic bacterial cold shock protein gene *SeCspA*. *Scientific Reports*, *7*(1), 44050. https://doi.org/10.1038/srep44050

Yu, Y., Wang, N., Hu, R., & Xiang, F. (2016). Genome-wide identification of soybean WRKY transcription factors in response to salt stress. *SpringerPlus*, *5*(1). https://doi.org/10.1186/s40064-016-2647-x

Yuan, Y., Fang, L., Karungo, S. K., Zhang, L., Gao, Y., Li, S., & Xin, H. (2016). Overexpression of VaPAT1, a GRAS transcription factor from *Vitis amurensis*, confers abiotic stress tolerance in *Arabidopsis*. *Plant Cell Reports*, *35*(3), 655–666. https://doi.org/10.1007/s00299-015-1910-x

Zhai, J., Teng, Z., Zheng, C., Lv, J., Song, T., Zhang, J., & Ye, N. (2025). Abscisic acid mediates the trade-off between growth and abiotic stress defense. *Crop and Environment*. https://doi.org/10.1016/j.crope.2025.09.004

Zainal, Z., Ismail, M., Zulkifli, R., & Omar, R. (2022). Growth performance of young sago palm (*Metroxylon sago* Rottb.) in peat fertilised using compound fertilisers. *International Journal of Agriculture, Forestry and Plantation*, *12*(2), 1-9.

Zhang, D., Liu, F., Al, M. A., Yang, Y., Yu, H., Li, M., Wu, K., Niu, M., Wang, C., He, Z., & Yan, Q. (2024). Nitrogen and sulfur cycling and their coupling mechanisms in eutrophic lake sediment microbiomes. *Science of The Total Environment*, *928*, 172518. https://doi.org/10.1016/j.scitotenv.2024.172518

Zhang, G., Liu, X., Quan, Z., Cheng, S., Xu, X., Pan, S., Xie, M., Zeng, P., Yue, Z., Wang, W., Tao, Y., Bian, C., Han, C., Xia, Q., Peng, X., Cao, R., Yang, X., Zhan, D., Hu, J., … Wang, J. (2012). Genome sequence of foxtail millet (*Setaria italica*) provides insights into grass evolution and biofuel potential. *Nature Biotechnology*, *30*(6), 549–554. https://doi.org/10.1038/nbt.2195

Zhang, H., Cui, F., Wu, Y., Lou, L., Liu, L., Tian, M., Ning, Y., Shu, K., Tang, S., & Xie, Q. (2015). The RING finger ubiquitin E3 ligase SDIR1 Targets sdir1-interacting protein1 for degradation to modulate the salt stress response and ABA signaling in *Arabidopsis*. *The Plant Cell*, *27*(1), 214–227. https://doi.org/10.1105/tpc.114.134163

Zhang, N., Wang, Z., Bao, Z., Yang, L., Wu, D., Shu, X., & Hua, J. (2018). MOS1 functions closely with TCP transcription factors to modulate immunity and cell cycle in *Arabidopsis*. *The Plant Journal*, *93*(1), 66–78. https://doi.org/10.1111/tpj.13757

Zhang, Q., Dai, B., Fan, M., Yang, L., Li, C., Hou, G., Wang, X., Gao, H., & Li, J. (2024). Genome-wide profile analysis of the Hsp20 family in lettuce and identification of its response to drought stress. *Frontiers in Plant Science*, *15*. https://doi.org/10.3389/fpls.2024.1426719

Zhang, S., Wu, X.-Q., Xie, H.-T., Zhao, S.-S., & Wu, J.-G. (2020). Multifaceted roles of RNA polymerase IV in plant growth and development. *Journal of Experimental Botany*, *71*(19), 5725–5732. https://doi.org/10.1093/jxb/eraa346

Zhang, S., Zhang, L., Tai, Y., Wang, X., Ho, C.-T., & Wan, X. (2018). Gene discovery of characteristic metabolic pathways in the tea plant (*Camellia sinensis*) using 'omics'-based network approaches: a future perspective. *Frontiers in Plant Science*, *9*. https://doi.org/10.3389/fpls.2018.00480

Zhang, W., Yang, Z., Wang, W., & Sun, Q. (2024). Primase promotes the competition between transcription and replication on the same template strand resulting in DNA damage. *Nature Communications*, *15*(1), 73. https://doi.org/10.1038/s41467-023-44443-0

Zhang, Y., Park, C., Bennett, C., Thornton, M., & Kim, D. (2021). Rapid and accurate alignment of nucleotide conversion sequencing reads with HISAT-3N. *Genome Research*, *31*(7), 1290–1295. https://doi.org/10.1101/gr.275193.120

Zhang, Y., Ye, C., Su, Y., Peng, W., Lu, R., Liu, Y., Huang, H., He, X., Yang, M., & Zhu, S. (2022). Soil acidification caused by excessive application of nitrogen fertilizer aggravates soil-borne diseases: evidence from literature review and field trials. *Agriculture, Ecosystems & Environment*, *340*, 108176. https://doi.org/10.1016/j.agee.2022.108176

Zhang, Z., & Zhang, X. (2012). Argonautes compete for miR165/166 to regulate shoot apical meristem development. *Current Opinion in Plant Biology*, *15*(6), 652–658. https://doi.org/10.1016/j.pbi.2012.05.007

Zhao, S., Ye, Z., & Stanton, R. (2020). Misuse of RPKM or TPM normalization when comparing across samples and sequencing protocols. *RNA*, *26*(8), 903–909. https://doi.org/10.1261/rna.074922.120

Zhao, W., Zhang, L.-L., Xu, Z.-S., Fu, L., Pang, H.-X., Ma, Y.-Z., & Min, D.-H. (2021). Genome-wide analysis of MADS-Box genes in foxtail millet (*Setaria italica L.*) and functional assessment of the role of *SiMADS51* in the drought stress response. *Frontiers in Plant Science*, *12*. https://doi.org/10.3389/fpls.2021.659474

Zhao, X.-D., Gao, Z.-Y., Peng, J., Konstantinidis, K. T., & Zhang, S.-Y. (2024). Various microbial taxa couple arsenic transformation to nitrogen and carbon cycling in paddy soils. *Microbiome*, *12*(1), 238. https://doi.org/10.1186/s40168-024-01952-4

Zhao, Y., Li, M.-C., Konaté, M. M., Chen, L., Das, B., Karlovich, C., Williams, P. M., Evrard, Y. A., Doroshow, J. H., & McShane, L. M. (2021). TPM, FPKM, or normalized counts? A comparative study of quantification measures for the analysis of RNA-seq data from the NCI patient-derived models repository. *Journal of Translational Medicine*, *19*(1), 269. https://doi.org/10.1186/s12967-021-02936-w

Zheng, Y., Jiao, C., Sun, H., Rosli, H. G., Pombo, M. A., Zhang, P., Banf, M., Dai, X., Martin, G. B., Giovannoni, J. J., Zhao, P. X., Rhee, S. Y., & Fei, Z. (2016). iTAK: a program for genome-wide prediction and classification of plant transcription factors, transcriptional regulators, and protein kinases. *Molecular Plant*, *9*(12), 1667–1670. https://doi.org/10.1016/j.molp.2016.09.014

Zhou, Y., Li, A., Du, T., Qin, Z., Zhang, L., Wang, Q., Li, Z., & Hou, F. (2024). A small auxin-Up RNA gene, *IbSAUR36*, regulates adventitious root development in transgenic sweet potato. *Genes*, *15*(6), 760. https://doi.org/10.3390/genes15060760

Zhou, Y., Zhou, B., Pache, L., Chang, M., Khodabakhshi, A. H., Tanaseichuk, O., Benner, C., & Chanda, S. K. (2019). Metascape provides a biologist-oriented resource for the analysis of systems-level datasets. *Nature Communications*, *10*(1), 1523. https://doi.org/10.1038/s41467-019-09234-6

Zhu, F. (2019). Recent advances in modifications and applications of sago starch. *Food Hydrocolloids*, *96*(1), 412-423. https://doi.org/10.1016/j.foodhyd.2019.05.035

Zhu, H., Hu, F., Wang, R., Zhou, X., Sze, S.-H., Liou, L. W., Barefoot, A., Dickman, M., & Zhang, X. (2011). *Arabidopsis* argonaute10 specifically sequesters miR166/165 to regulate shoot apical meristem development. *Cell*, *145*(2), 242–256. https://doi.org/10.1016/j.cell.2011.03.024

Zhu, Q., Zheng, H., Hu, X., Liu, Y., Zheng, X., Li, L., & Tang, M. (2024). Genome-wide analysis of the SAUR gene family and its expression profiles in response to salt stress in *Santalum album*. *Plants*, *13*(10), 1286. https://doi.org/10.3390/plants13101286

Zimmerli, C., Ribot, C., Vavasseur, A., Bauer, H., Hedrich, R., & Poirier, Y. (2012). *PHO1* expression in guard cells mediates the stomatal response to abscisic acid in *Arabidopsis*. *The Plant Journal*, *72*(2), 199–211. https://doi.org/10.1111/j.1365-313X.2012.05058.x

Zou, X., Liu, Q., Guan, Q., Zhao, M., Zhu, X., Pan, Y., Liu, L., & Gao, Z. (2024). Muscle fiber characteristics and transcriptome analysis in slow- and fast-growing *Megalobrama amblycephala*. *Genes*, *15*(2), 179. https://doi.org/10.3390/genes15020179

Zou, X., & Sun, H. (2023). DOF transcription factors: Specific regulators of plant biological processes. *Frontiers in Plant Science*, *14*. https://doi.org/10.3389/fpls.2023.1044918

Zuk, M., Działo, M., Richter, D., Dymińska, L., Matuła, J., Kotecki, A., Hanuza, J., & Szopa, J. (2016). Chalcone synthase (*CHS*) gene suppression in flax leads to changes in wall synthesis and sensing genes, cell wall chemistry and stem morphology parameters. *Frontiers in Plant Science*, *7*. https://doi.org/10.3389/fpls.2016.00894

Zuk, M., Szperlik, J., Hnitecka, A., & Szopa, J. (2019). Temporal biosynthesis of flavone constituents in flax growth stages. *Plant Physiology and Biochemistry*, *142*, 234–245. https://doi.org/10.1016/j.plaphy.2019.07.009

APPENDICES

Appendix A: Top 25 upregulated and downregulated DEGs from Dalat dataset.

DALAT				
UPREGULATED DEGS				
Gene_id	**Accession**	**Description**	**Log_2 Fold Change**	**padj**
g15325	Q9T080	UDP-Glycosyltransferase superfamily protein (AT4G27560)	3.01	7.1E-55
g15906	O22456	K-box region and MADS-box transcription factor family protein (SEP3)	5.18	4.2E-51
g1336	Q9SGU2	SAUR-like auxin-responsive protein family (AT1G56150)	4.38	4.9E-43
g33621	Q94KJ7	Sec1/munc18-like (SM) proteins superfamily (ATVPS33)	4.21	5.5E-38
g18622	Q9FNN6	Duplicated homeodomain-like superfamily protein (AT5G08520)	2.91	4.3E-25
g16136	Q9LT79	plant U-box 25 (PUB25)	3.78	4.2E-24
g35382	Q6NQJ7	FAR1-related sequence 4 (FRS4)	3.45	2.1E-22
g18499	Q39183	D6 protein kinase like 2 (D6PKL2)	4.70	1.3E-21
g21592	Q94CA0	organic solute transporter ostalpha protein (DUF300) (AT1G77220)	3.18	6.2E-21
g13341	Q9C5J8	outer envelope protein of 80 kDa (OEP80)	7.12	1.2E-20
g26409	Q9FXB6	GDSL-like Lipase/Acylhydrolase superfamily protein (AT1G56670)	3.75	1.3E-19
g35081	Q8S403	EXS (ERD1/XPR1/SYG1) family protein (PHO1;H1)	5.02	3.6E-19
g21013	Q9FIX8	Pre-mRNA cleavage complex II (AT5G43620)	3.71	1.2E-17
g13545	#N/A	#N/A	3.18	2.0E-17

Appendix A continued

g17401	Q8GXT3	basic helix-loop-helix (bHLH) DNA-binding superfamily protein (AT3G20640)	2.77	1.7E-16
g14375	O64587	Glycolipid transfer protein (GLTP) family protein (ACD11)	3.57	1.8E-16
g727	F4HT49	proteasome subunit PAB1 (PAB1)	2.89	5.4E-16
g29242	Q9LQL2	nitrate transporter 1.5 (NRT1.5)	2.81	5.2E-15
g25148	Q9SVV6	Ca2+ activated outward rectifying K+ channel 6 (KCO6)	2.25	6.2E-15
g20867	Q9LX82	myb domain protein 48 (MYB48)	3.27	8.5E-15
g19289	#N/A	#N/A	2.07	2.0E-14
g29994	Q9M069	O-Glycosyl hydrolases family 17 protein (AT4G34480)	4.36	3.0E-13
g16126	O65639	cold shock domain protein 1 (CSDP1)	3.18	5.2E-13
g21043	Q9M331	Major facilitator superfamily protein (AT3G53960)	3.04	3.0E-12
g27246	Q9C6B8	peptidylprolyl cis/trans isomerase, NIMA-interacting 1 (PIN1AT)	2.90	3.1E-12
DOWNREGULATED DEGS				
Gene_id	**Accession**	**Description**	**Log_2 Fold Change**	**padj**
g15621	P93751	zinc finger protein 8 (ZFP8)	-4.25119	5.95E-49
g2745	P0C897	Tetratricopeptide repeat (TPR)-like superfamily protein (AT3G02650)	-5.66881	9.18E-45
g9533	Q9M354	ARF-GAP domain 6 (AGD6)	-6.40015	2.54E-42
g9257	P37702	thioglucoside glucohydrolase 1 (TGG1)	-6.17847	5.81E-40
g5109	Q9M1X2	Chalcone-flavanone isomerase family protein (FAP1)	-3.55615	6.87E-36

Appendix A continued

g33537	Q9XF91	Chlorophyll A-B binding family protein (NPQ4)	-5.9415	6.07E-35
g27635	Q8GYW8	HXXXD-type acyl-transferase family protein (AT2G25150)	-5.19652	7.28E-34
g10864	Q8RX77	nitrate transporter 1.7 (NRT1.7)	-4.68417	1.37E-32
g15924	Q9C7F7	glycosylphosphatidylinositol-anchored lipid protein transfer 1 (LTPG1)	-3.18979	1.48E-31
g18425	O65390	aspartic proteinase A1 (APA1)	-2.14062	5.33E-29
g12364	O64759	cationic amino acid transporter 5 (CAT5)	-4.22824	4.56E-28
g4495	Q8LPK2	P-glycoprotein 2 (ABCB2)	-3.32871	8.31E-28
g20448	Q08298	BURP domain-containing protein (RD22)	-2.91413	1.89E-24
g3302	O65677	3-ketoacyl-CoA synthase 17 (KCS17)	-5.92907	2.23E-24
g2381	Q9ZWA9	RmlC-like cupins superfamily protein (AT1G03890)	-6.04323	1.70E-23
g17622	Q9SSM3	Mannose-binding lectin superfamily protein (AT1G73040)	-5.77004	7.30E-23
g31697	Q94K41	NAD(P)-binding Rossmann-fold superfamily protein (SDR5)	-4.6126	1.17E-22
g13208	P56786	Ycf2 (ycf2)	-6.75099	2.47E-22
g35239	Q41951	delta tonoplast integral protein (DELTA-TIP)	-5.60462	1.35E-20
g23392	Q9SK82	UDP-Glycosyltransferase superfamily protein (UGT85A1)	-5.57719	5.62E-20
g24519	Q39224	senescence-related gene 1 (SRG1)	-3.37125	6.81E-20
g5373	P38605	cycloartenol synthase 1 (CAS1)	-2.61187	1.40E-19
g33350	Q9STL2	cytochrome P450, family 71, subfamily A, polypeptide 21 (CYP71A21)	-4.67329	2.27E-18

Appendix A continued

g7699	Q9C8K0	disease resistance protein (CC-NBS-LRR class) family protein (AT1G51480)	-6.65971	2.52E-18
g17266	O64989	Cytochrome P450 superfamily protein (DWF4)	-4.59791	5.38E-18

Appendix B: Top 25 upregulated and downregulated DEGs from Paya Paloh dataset

Paya Paloh				
UPREGULATED DEGS				
Gene_id	**Accession**	**Description**	**Log_2 Fold Change**	**padj**
g33621	Q94KJ7	Sec1/munc18-like (SM) proteins superfamily (ATVPS33)	3.74	7.0E-29
g20867	Q9LX82	myb domain protein 48 (MYB48)	4.48	1.8E-26
g1336	Q9SGU2	SAUR-like auxin-responsive protein family (AT1G56150)	4.02	1.2E-25
g13341	Q9C5J8	outer envelope protein of 80 kDa (OEP80)	6.56	5.1E-24
g15906	O22456	K-box region and MADS-box transcription factor family protein (SEP3)	4.76	1.8E-21
g21592	Q94CA0	organic solute transporter ostalpha protein (DUF300) (AT1G77220)	3.28	1.8E-21
g18622	Q9FNN6	Duplicated homeodomain-like superfamily protein (AT5G08520)	3.69	1.1E-20
g13545	#N/A	#N/A	3.79	1.1E-18
g15325	Q9T080	UDP-Glycosyltransferase superfamily protein (AT4G27560)	2.41	5.1E-17
g35081	Q8S403	EXS (ERD1/XPR1/SYG1) family protein (PHO1;H1)	4.96	7.1E-16
g13486	Q9MAM4	IQ-domain 18 (IQD18)	3.75	4.1E-14
g26496	Q96533	GroES-like zinc-binding dehydrogenase family protein (HOT5)	3.57	4.4E-14
g26497	Q9LQQ0	Disease resistance-responsive (dirigent-like protein) family protein (AT1G07730)	4.46	8.9E-13
g21013	Q9FIX8	Pre-mRNA cleavage complex II (AT5G43620)	3.69	4.8E-12
g27246	Q9C6B8	peptidylprolyl cis/trans isomerase, NIMA-interacting 1 (PIN1AT)	3.15	8.1E-12

Appendix B continued

g1462	#N/A	#N/A	2.47	1.1E-11
g33956	O80982	heat shock transcription factor A2 (HSFA2)	6.02	1.6E-11
g13961	Q9XGW1	Stabilizer of iron transporter SufD / Polynucleotidyl transferase (AGO10)	3.48	4.2E-11
g25148	Q9SVV6	Ca2+ activated outward rectifying K+ channel 6 (KCO6)	2.13	4.3E-11
g706	Q9ZUC1	Oxidoreductase, zinc-binding dehydrogenase family protein (AOR)	3.25	4.4E-11
g19289	#N/A	#N/A	2.27	7.1E-11
g18499	Q39183	D6 protein kinase like 2 (D6PKL2)	4.11	6.8E-10
g19123	O22785	MOS4-associated complex 3B (MAC3B)	2.76	9.5E-10
g31900	Q9LSE7	Auxin-responsive family protein (AT3G25290)	2.89	1.8E-09
g29242	Q9LQL2	nitrate transporter 1.5 (NRT1.5)	2.92	5.4E-09
DOWNREGULATED DEGS				
Gene_id	**Accession**	**Description**	**Log_2 Fold Change**	**padj**
g9533	Q9M354	ARF-GAP domain 6 (AGD6)	-6.03345	1.83E-47
g31726	Q9LV10	Major facilitator superfamily protein (GTR2)	-3.02946	5.93E-35
g2745	P0C897	Tetratricopeptide repeat (TPR)-like superfamily protein (AT3G02650)	-3.60918	1.31E-30
g12364	O64759	cationic amino acid transporter 5 (CAT5)	-2.4966	5.60E-28
g20093	Q9LF88	late embryogenesis abundant protein, putative / LEA protein (AT3G53040)	-4.16724	4.86E-27

Appendix B continued

g759	Q9FZ90	Integrase-type DNA-binding superfamily protein (AT1G28160)	-4.6008	3.58E-23
g7423	Q9FJ45	GDSL-like Lipase/Acylhydrolase superfamily protein (AT5G45910)	-4.62889	1.38E-22
g9257	P37702	thioglucoside glucohydrolase 1 (TGG1)	-4.99464	2.52E-20
g24519	Q39224	senescence-related gene 1 (SRG1)	-3.15161	1.12E-19
g13208	P56786	Ycf2 (ycf2)	-4.45427	1.29E-19
g4495	Q8LPK2	P-glycoprotein 2 (ABCB2)	-2.84795	7.90E-19
g18425	O65390	aspartic proteinase A1 (APA1)	-2.1133	8.38E-19
g33350	Q9STL2	cytochrome P450, family 71, subfamily A, polypeptide 21 (CYP71A21)	-4.49202	2.80E-18
g25302	Q94A73	Phototropic-responsive NPH3 family protein (AT5G66560)	-3.68171	6.78E-18
g33537	Q9XF91	Chlorophyll A-B binding family protein (NPQ4)	-6.61218	9.24E-18
g16222	Q9FGC7	zeaxanthin epoxidase (ZEP) (ABA1) (ABA1)	-6.35678	2.46E-17
g7995	O65649	filament-like protein (DUF869) (AT4G36120)	-6.37921	4.62E-16
g30633	O82081	uclacyanin 1 (UCC1)	-5.068	9.25E-16
g10245	Q9XI31	Lactoylglutathione lyase / glyoxalase I family protein (GLYI4)	-3.70259	9.35E-16
g31634	Q9C7T7	Leucine-rich receptor-like protein kinase family protein (AT1G72180)	-3.60432	9.72E-16
g23050	Q94AK6	senescence associated gene 20 (SAG20)	-4.66867	1.39E-15
g10783	P52577	NmrA-like negative transcriptional regulator family protein (AT1G75280)	-6.52765	3.21E-15
g19434	Q9C7U7	myb domain protein 20 (MYB20)	-5.45953	5.93E-15

Appendix B continued

g35197	F4IV45	SNF2 domain-containing protein / helicase domain-containing protein (ASG3)	-4.25795	1.05E-14
g22285	O81765	Leucine-rich repeat (LRR) family protein (AT4G33970)	-5.74188	1.09E-14

Appendix C: Top 25 upregulated and downregulated DEGs from Paya Paloh dataset

Sungai Talau				
UPREGULATED DEGS				
Gene_id	**Accession**	**Description**	**Log_2 Fold Change**	**padj**
g15906	O22456	K-box region and MADS-box transcription factor family protein (SEP3)	5.04	1.59E-43
g18622	Q9FNN6	Duplicated homeodomain-like superfamily protein (AT5G08520)	3.57	3.47E-41
g1336	Q9SGU2	SAUR-like auxin-responsive protein family (AT1G56150)	3.57	5.09E-26
g3724	Q38806	HSP20-like chaperones superfamily protein (ATHSP22.0)	8.06	5.78E-20
g25148	Q9SVV6	Ca2+ activated outward rectifying K+ channel 6 (KCO6)	2.25	2.08E-19
g26496	Q96533	GroES-like zinc-binding dehydrogenase family protein (HOT5)	4.06	4.61E-18
g13545	#N/A	#N/A	3.43	0.37529
g13341	Q9C5J8	outer envelope protein of 80 kDa (OEP80)	6.13	5.47E-17
g35081	Q8S403	EXS (ERD1/XPR1/SYG1) family protein (PHO1;H1)	4.58	9.09E-17
g26497	Q9LQQ0	Disease resistance-responsive (dirigent-like protein) family protein (AT1G07730)	5.37	4.21E-15
g13486	Q9MAM4	IQ-domain 18 (IQD18)	3.58	1.13E-14
g19123	O22785	MOS4-associated complex 3B (MAC3B)	2.83	1.8E-14
g33621	Q94KJ7	Sec1/munc18-like (SM) proteins superfamily (ATVPS33)	2.68	1.36E-13

Appendix C continued

g26409	Q9FXB6	GDSL-like Lipase/Acylhydrolase superfamily protein (AT1G56670)	3.10	2.25E-13
g19289	#N/A	#N/A	2.10	0.261209
g26498	Q8GUH2	Erythronate-4-phosphate dehydrogenase family protein (AT1G01500)	5.18	2.72E-12
g29351	Q9SSC1	uncharacterized protein (AT1G80180)	3.11	5.36E-12
g35382	Q6NQJ7	FAR1-related sequence 4 (FRS4)	2.21	2.9E-10
g22547	Q7XZF5	ARM repeat superfamily protein (RST1)	9.05	1.44E-09
g15325	Q9T080	UDP-Glycosyltransferase superfamily protein (AT4G27560)	2.24	1.45E-09
g25813	P26569	winged-helix DNA-binding transcription factor family protein (AT2G30620)	8.56	1.46E-09
g27246	Q9C6B8	peptidylprolyl cis/trans isomerase, NIMA-interacting 1 (PIN1AT)	2.73	2.6E-09
g20680	Q9ZPH9	S-adenosyl-L-methionine-dependent methyltransferases superfamily protein (AT4G00750)	2.31	3.33E-09
g1710	A1A6M1	plastid transcriptionally active 5 (PTAC5)	2.14	3.68E-09
g27597	Q8GS71	P-loop containing nucleoside triphosphate hydrolases superfamily protein (FRA1)	2.88	4.06E-09

Appendix C continued

DOWNREGULATED DEGS				
Gene_id	**Accession**	**Description**	**Log_2 Fold Change**	**padj**
g9533	Q9M354	ARF-GAP domain 6 (AGD6)	-6.92828	2.73E-57
g2745	P0C897	Tetratricopeptide repeat (TPR)-like superfamily protein (AT3G02650)	-4.38384	4.26E-41
g9257	P37702	thioglucoside glucohydrolase 1 (TGG1)	-5.67903	1.25E-37
g15621	P93751	zinc finger protein 8 (ZFP8)	-3.51111	6.39E-37
g33537	Q9XF91	Chlorophyll A-B binding family protein (NPQ4)	-6.60018	1.57E-35
g33017	Q9LE63	myb domain protein 106 (MYB106)	-3.90943	1.72E-29
g5109	Q9M1X2	Chalcone-flavanone isomerase family protein (FAP1)	-2.46511	1.93E-27
g31726	Q9LV10	Major facilitator superfamily protein (GTR2)	-3.56927	3.68E-25
g759	Q9FZ90	Integrase-type DNA-binding superfamily protein (AT1G28160)	-4.22997	2.30E-20
g18766	O80992	PYR1-like 2 (PYL2)	-4.7425	4.00E-20
g16222	Q9FGC7	zeaxanthin epoxidase (ZEP) (ABA1) (ABA1)	-5.62817	2.04E-18
g18425	O65390	aspartic proteinase A1 (APA1)	-2.04029	7.33E-18
g17624	Q9SSM3	Mannose-binding lectin superfamily protein (AT1G73040)	-5.41714	8.81E-18
g30333	Q9MA90	peroxisomal adenine nucleotide carrier 1 (PNC1)	-3.53818	1.79E-17
g13208	P56786	Ycf2 (ycf2)	-5.66553	3.67E-17
g25204	P0C945	Zinc finger C-x8-C-x5-C-x3-H type family protein (AT1G21580)	-5.03759	5.79E-17

Appendix C continued

g10783	P52577	NmrA-like negative transcriptional regulator family protein (AT1G75280)	-4.33555	8.28E-16
g2835	Q9FHB6	MATE efflux family protein (AT5G52450)	-2.53288	8.64E-16
g10864	Q8RX77	nitrate transporter 1.7 (NRT1.7)	-3.66578	9.75E-16
g33350	Q9STL2	cytochrome P450, family 71, subfamily A, polypeptide 21 (CYP71A21)	-4.74578	2.74E-15
g27635	Q8GYW8	HXXXD-type acyl-transferase family protein (AT2G25150)	-3.8394	2.74E-15
g25302	Q94A73	Phototropic-responsive NPH3 family protein (AT5G66560)	-3.24565	1.04E-14
g17622	Q9SSM3	Mannose-binding lectin superfamily protein (AT1G73040)	-5.92026	1.13E-14
g20093	Q9LF88	late embryogenesis abundant protein, putative / LEA protein (AT3G53040)	-4.11998	1.80E-14
g30633	O82081	uclacyanin 1 (UCC1)	-5.09166	4.31E-14

Appendix D: Upregulated DEGs Gene Ontology (GO) enrichment analysis

Category	Gene Ontology Term	Enrichment	Pop Hits	Benjamini
Biological process	GO:0006269~DNA replication, synthesis of RNA primer	188.63	2/17920	7.95E-01
Biological process	GO:0006799~polyphosphate biosynthetic process	188.63	2/17920	7.95E-01
Biological process	GO:0071139~resolution of recombination intermediates	188.63	2/17920	7.95E-01
Biological process	GO:0009909~regulation of flower development	8.03	94/17920	7.95E-01
Biological process	GO:0090173~regulation of synaptonemal complex assembly	125.75	3/17920	7.95E-01
Biological process	GO:0051726~regulation of cell cycle	13.47	42/17920	8.66E-01
Biological process	GO:0010338~leaf formation	75.45	5/17920	9.03E-01
Biological process	GO:0000712~resolution of meiotic recombination intermediates	53.89	7/17920	9.03E-01
Biological process	GO:0007143~female meiotic division	47.16	8/17920	9.03E-01
Biological process	GO:0030643~cellular phosphate ion homeostasis	41.92	9/17920	9.03E-01
Biological process	GO:0010358~leaf shaping	41.92	9/17920	9.03E-01
Biological process	GO:0048826~cotyledon morphogenesis	41.92	9/17920	9.03E-01
Biological process	GO:0065003~macromolecular complex assembly	41.92	9/17920	9.03E-01
Biological process	GO:0003333~amino acid transmembrane transport	37.73	10/17920	9.07E-01
Biological process	GO:0009640~photomorphogenesis	7.97	71/17920	9.07E-01
Biological process	GO:0006417~regulation of translation	7.26	78/17920	9.33E-01
Biological process	GO:0048316~seed development	7.26	78/17920	9.33E-01

Appendix D continued

Biological process	GO:0032880~regulation of protein localization	29.02	13/17920	9.33E-01
Biological process	GO:0071577~zinc II ion transmembrane transport	25.15	15 / 17920	9.77E-01
Biological process	GO:0035194~posttranscriptional gene silencing by RNA	23.58	16 / 17920	9.77E-01
Biological process	GO:0007140~male meiosis	23.58	16 / 17920	9.77E-01
Biological process	GO:0006270~DNA replication initiation	22.19	17 / 17920	9.83E-01
Biological process	GO:0009408~response to heat	3.75	201 / 17920	9.83E-01
Cellular component	GO:0005886~plasma membrane	1.99	3209 / 25765	6.74E-02
Cellular component	GO:0005737~cytoplasm	1.66	4434 / 25765	1.83E-01
Cellular component	GO:0005658~alpha DNA polymerase: primase complex	245.38	2 / 25765	2.20E-01
Cellular component	GO:0005783~endoplasmic reticulum	2.63	932 / 25765	2.54E-01
Cellular component	GO:0005730~nucleolus	3.44	500 / 25765	2.54E-01
Cellular component	GO:0005773~vacuole	3.81	386 / 25765	2.54E-01
Cellular component	GO:0009925~basal plasma membrane	81.79	6 / 25765	2.54E-01
Cellular component	GO:0005802~trans-Golgi network	4.41	278 / 25765	2.54E-01
Cellular component	GO:0045177~apical part of cell	70.11	7 / 25765	2.54E-01
Cellular component	GO:0009506~plasmodesma	2.26	979 / 25765	3.66E-01
Cellular component	GO:0022626~cytosolic ribosome	4.57	215 / 25765	4.22E-01
Cellular component	GO:0019773~proteasome core complex, alpha-subunit complex	24.54	20 / 25765	5.27E-01

Appendix D continued

Cellular component	GO:0009705~plant-type vacuole membrane	6.19	119 / 25765	5.27E-01
Molecular functions	GO:0005515~protein binding	1.43	4515 / 18777	1
Molecular functions	GO:0008097~5S rRNA binding	80.76	5 / 18777	1
Molecular functions	GO:0000822~inositol hexakisphosphate binding	50.48	8 / 18777	1
Molecular functions	GO:0035198~miRNA binding	33.65	12 / 18777	1
Molecular functions	GO:0010329~auxin efflux transmembrane transporter activity	31.06	13 / 18777	1
Molecular functions	GO:0000175~3'-5'-exoribonuclease activity	25.24	16 / 18777	1
Molecular functions	GO:0015114~phosphate ion transmembrane transporter activity	22.43	18 / 18777	1
Molecular functions	GO:0005385~zinc ion transmembrane transporter activity	20.19	20 / 18777	1

Appendix E: Downregulated DEGs Gene Ontology (GO) enrichment analysis

Category	Gene Ontology Term	Enrichment	Pop Hits	Benjamini
Biological process	GO:0006979~response to oxidative stress	3.41	299 / 17920	2.30E-03
Biological process	GO:0009809~lignin biosynthetic process	8.41	52 / 17920	2.86E-03
Biological process	GO:0071555~cell wall organization	3.21	303 / 17920	3.33E-03
Biological process	GO:0009611~response to wounding	3.31	235 / 17920	1.57E-02
Biological process	GO:0009813~flavonoid biosynthetic process	10.79	27 / 17920	2.02E-02
Biological process	GO:0009737~response to abscisic acid	2.44	458 / 17920	2.02E-02
Biological process	GO:0009741~response to brassinosteroid	7.08	48 / 17920	3.47E-02
Biological process	GO:0009620~response to fungus	4.30	113 / 17920	3.84E-02
Biological process	GO:0042744~hydrogen peroxide catabolic process	4.70	93 / 17920	4.14E-02
Biological process	GO:0009826~unidimensional cell growth	3.71	131 / 17920	8.81E-02
Biological process	GO:0002237~response to molecule of bacterial origin	6.78	43 / 17920	9.34E-02
Biological process	GO:0009407~toxin catabolic process	6.33	46 / 17920	9.94E-02
Biological process	GO:0009753~response to jasmonic acid	3.22	166 / 17920	9.94E-02
Biological process	GO:0009416~response to light stimulus	3.04	192 / 17920	9.94E-02
Biological process	GO:0016132~brassinosteroid biosynthetic process	12.14	16 / 17920	1.50E-01
Biological process	GO:0009409~response to cold	2.20	376 / 17920	1.77E-01
Biological process	GO:0000038~very long-chain fatty acid metabolic process	10.79	18 / 17920	1.87E-01

Appendix E continued

Biological process	GO:0010431~seed maturation	6.74	36 / 17920	1.94E-01
Biological process	GO:0009963~positive regulation of flavonoid biosynthetic process	20.81	7 / 17920	2.36E-01
Biological process	GO:0042761~very long-chain fatty acid biosynthetic process	9.25	21 / 17920	2.36E-01
Biological process	GO:0009651~response to salt stress	2.07	399 / 17920	2.36E-01
Biological process	GO:0006611~protein export from nucleus	18.21	8 / 17920	2.81E-01
Biological process	GO:0090333~regulation of stomatal closure	5.52	44 / 17920	3.07E-01
Biological process	GO:0009414~response to water deprivation	2.03	382 / 17920	3.07E-01
Biological process	GO:0006777~Mo-molybdopterin cofactor biosynthetic process	16.19	9 / 17920	3.14E-01
Biological process	GO:0071215~cellular response to abscisic acid stimulus	5.28	46 / 17920	3.18E-01
Biological process	GO:0080027~response to herbivore	7.47	26 / 17920	3.20E-01
Biological process	GO:0010224~response to UV-B	4.10	71 / 17920	3.20E-01
Biological process	GO:0008610~lipid biosynthetic process	7.19	27 / 17920	3.40E-01
Biological process	GO:0010555~response to mannitol	6.94	28 / 17920	3.45E-01
Biological process	GO:0055085~transmembrane transport	2.06	330 / 17920	3.45E-01
Biological process	GO:0010236~plastoquinone biosynthetic process	13.24	11 / 17920	3.53E-01
Biological process	GO:0010025~wax biosynthetic process	6.70	29 / 17920	3.54E-01
Biological process	GO:0009058~biosynthetic process	3.55	82 / 17920	4.36E-01

Appendix E continued

Biological process	GO:0045892~negative regulation of transcription, DNA-templated	2.48	176 / 17920	4.62E-01
Biological process	GO:0009411~response to UV	5.71	34 / 17920	4.95E-01
Biological process	GO:0042183~formate catabolic process	48.56	2 / 17920	5.52E-01
Biological process	GO:0051574~positive regulation of histone H3-K9 methylation	48.56	2 / 17920	5.52E-01
Biological process	GO:0006898~receptor-mediated endocytosis	48.56	2 / 17920	5.52E-01
Biological process	GO:0033310~chlorophyll a catabolic process	48.56	2 / 17920	5.52E-01
Biological process	GO:0051555~flavonol biosynthetic process	9.71	15 / 17920	5.52E-01
Biological process	GO:0006865~amino acid transport	3.68	66 / 17920	6.19E-01
Biological process	GO:0006997~nucleus organization	8.09	18 / 17920	6.56E-01
Biological process	GO:0048544~recognition of pollen	4.74	41 / 17920	6.56E-01
Biological process	GO:0030244~cellulose biosynthetic process	4.63	42 / 17920	6.78E-01
Biological process	GO:0010223~secondary shoot formation	7.67	19 / 17920	6.89E-01
Biological process	GO:0042631~cellular response to water deprivation	4.52	43 / 17920	6.89E-01
Biological process	GO:0071266~'de novo' L-methionine biosynthetic process	32.38	3 / 17920	7.02E-01
Biological process	GO:0046244~salicylic acid catabolic process	24.28	4 / 17920	8.12E-01
Biological process	GO:1904585~response to putrescine	24.28	4 / 17920	8.12E-01
Biological process	GO:0015812~gamma-aminobutyric acid transport	24.28	4 / 17920	8.12E-01

Appendix E continued

Biological process	GO:0043447~alkane biosynthetic process	24.28	4 / 17920	8.12E-01
Biological process	GO:0030187~melatonin biosynthetic process	24.28	4 / 17920	8.12E-01
Biological process	GO:1902074~response to salt	4.05	48 / 17920	8.12E-01
Biological process	GO:0006952~defense response	1.49	651 / 17920	8.12E-01
Biological process	GO:0010038~response to metal ion	5.83	25 / 17920	9.26E-01
Biological process	GO:0060149~negative regulation of posttranscriptional gene silencing	19.43	5 / 17920	9.51E-01
Biological process	GO:0002239~response to oomycetes	5.60	26 / 17920	9.51E-01
Cellular component	GO:0016020~membrane	1.57	5721 / 25765	3.45E-07
Cellular component	GO:0005773~vacuole	3.23	386 / 25765	8.54E-04
Cellular component	GO:0005886~plasma membrane	1.57	3209 / 25765	1.13E-03
Cellular component	GO:0005829~cytosol	1.66	2450 / 25765	1.54E-03
Cellular component	GO:0000326~protein storage vacuole	17.33	18 / 25765	3.30E-03
Cellular component	GO:0005777~peroxisome	2.93	362 / 25765	4.46E-03
Cellular component	GO:0000325~plant-type vacuole	2.17	749 / 25765	6.81E-03
Cellular component	GO:0005783~endoplasmic reticulum	2.01	932 / 25765	6.81E-03
Cellular component	GO:0048046~apoplast	2.33	536 / 25765	1.27E-02
Cellular component	GO:0009505~plant-type cell wall	2.32	510 / 25765	1.56E-02
Cellular component	GO:0005576~extracellular region	1.40	3287 / 25765	1.91E-02

Appendix E continued

Cellular component	GO:0009536~plastid	1.82	1031 / 25765	1.91E-02
Cellular component	GO:0099503~secretory vesicle	3.47	180 / 25765	1.91E-02
Cellular component	GO:0005794~Golgi apparatus	1.81	1036 / 25765	1.91E-02
Cellular component	GO:0009941~chloroplast envelope	2.01	589 / 25765	4.69E-02
Cellular component	GO:0009506~plasmodesma	1.72	979 / 25765	5.23E-02
Cellular component	GO:0009705~plant-type vacuole membrane	3.67	119 / 25765	7.25E-02
Cellular component	GO:0031969~chloroplast membrane	3.06	163 / 25765	8.69E-02
Cellular component	GO:0005737~cytoplasm	1.25	4434 / 25765	8.69E-02
Cellular component	GO:0098552~side of membrane	2.75	159 / 25765	2.15E-01
Cellular component	GO:0045335~phagocytic vesicle	41.59	3 / 25765	2.25E-01
Cellular component	GO:0031966~mitochondrial membrane	3.35	93 / 25765	2.71E-01
Cellular component	GO:0009507~chloroplast	1.17	5071 / 25765	2.71E-01
Cellular component	GO:0005797~Golgi medial cisterna	4.30	58 / 25765	2.74E-01
Cellular component	GO:0005789~endoplasmic reticulum membrane	1.67	523 / 25765	3.12E-01
Cellular component	GO:0005635~nuclear envelope	3.06	102 / 25765	3.12E-01
Cellular component	GO:0042807~central vacuole	20.79	6 / 25765	3.41E-01
Molecular function	GO:0005506~iron ion binding	3.10	351 /18777	2.29E-03
Molecular function	GO:0020037~heme binding	2.88	394 /18777	2.29E-03

Appendix E continued

Molecular function	GO:0016491~oxidoreductase activity	2.70	420 /18777	4.12E-03
Molecular function	GO:0004497~monooxygenase activity	3.02	266 /18777	1.73E-02
Molecular function	GO:0080030~methyl indole-3-acetate esterase activity	23.65	8 /18777	3.75E-02
Molecular function	GO:0016705~oxidoreductase activity, acting on paired donors, with incorporation or reduction of molecular oxygen	2.80	270 /18777	3.93E-02
Molecular function	GO:0008194~UDP-glycosyltransferase activity	3.97	119 /18777	3.93E-02
Molecular function	GO:0010355~homogentisate farnesyltransferase activity	47.30	3 /18777	3.93E-02
Molecular function	GO:0047172~shikimate O-hydroxycinnamoyltransferase activity	47.30	3 /18777	3.93E-02
Molecular function	GO:0010357~homogentisate solanesyltransferase activity	47.30	3 /18777	3.93E-02
Molecular function	GO:0010356~homogentisate geranylgeranyltransferase activity	47.30	3 /18777	3.93E-02
Molecular function	GO:0032440~2-alkenal reductase [NAD(P)] activity	47.30	3 /18777	3.93E-02
Molecular function	GO:0047205~quinate O-hydroxycinnamoyltransferase activity	47.30	3 /18777	3.93E-02
Molecular function	GO:0015267~channel activity	6.76	42 /18777	5.06E-02
Molecular function	GO:0009922~fatty acid elongase activity	8.76	27 /18777	6.04E-02
Molecular function	GO:0004675~transmembrane receptor protein serine/threonine kinase activity	12.61	15 /18777	8.53E-02
Molecular function	GO:0015189~L-lysine transmembrane transporter activity	23.65	6 /18777	1.36E-01
Molecular function	GO:0080032~methyl jasmonate esterase activity	23.65	6 /18777	1.36E-01

Appendix E continued

Molecular function	GO:0005313~L-glutamate transmembrane transporter activity	20.27	7 /18777	1.69E-01
Molecular function	GO:0004659~prenyltransferase activity	20.27	7 /18777	1.69E-01
Molecular function	GO:0051723~protein methylesterase activity	9.01	21 /18777	1.73E-01
Molecular function	GO:0004364~glutathione transferase activity	4.58	62 /18777	1.74E-01
Molecular function	GO:0030151~molybdenum ion binding	17.74	8 /18777	1.93E-01
Molecular function	GO:0003700~transcription factor activity, sequence-specific DNA binding	1.41	1641 /18777	2.09E-01
Molecular function	GO:0022857~transmembrane transporter activity	2.27	250 /18777	2.67E-01
Molecular function	GO:0005049~nuclear export signal receptor activity	14.19	10 /18777	2.67E-01
Molecular function	GO:0035251~UDP-glucosyltransferase activity	7.01	27 /18777	2.70E-01
Molecular function	GO:0045735~nutrient reservoir activity	6.76	28 /18777	2.87E-01
Molecular function	GO:0008422~beta-glucosidase activity	4.55	52 /18777	3.20E-01
Molecular function	GO:0008131~primary amine oxidase activity	10.14	14 /18777	4.27E-01
Molecular function	GO:0015250~water channel activity	5.26	36 /18777	4.27E-01
Molecular function	GO:0016788~hydrolase activity, acting on ester bonds	2.78	119 /18777	4.27E-01
Molecular function	GO:1990465~aldehyde oxygenase (deformylating) activity	47.30	2 /18777	4.27E-01
Molecular function	GO:0061599~molybdopterin molybdotransferase activity	47.30	2 /18777	4.27E-01
Molecular function	GO:0008863~formate dehydrogenase (NAD+) activity	47.30	2 /18777	4.27E-01

Appendix E continued

Molecular function	GO:0009924~octadecanal decarbonylase activity	47.30	2 /18777	4.27E-01
Molecular function	GO:0061598~molybdopterin adenylyltransferase activity	47.30	2 /18777	4.27E-01
Molecular function	GO:0017096~acetylserotonin O-methyltransferase activity	47.30	2 /18777	4.27E-01
Molecular function	GO:0000976~transcription regulatory region sequence-specific DNA binding	1.53	710 /18777	4.65E-01
Molecular function	GO:0030246~carbohydrate binding	2.01	259 /18777	4.65E-01
Molecular function	GO:0042937~tripeptide transporter activity	8.35	17 /18777	4.65E-01
Molecular function	GO:0030170~pyridoxal phosphate binding	2.99	95 /18777	4.69E-01
Molecular function	GO:0071916~dipeptide transmembrane transporter activity	7.47	19 /18777	5.42E-01
Molecular function	GO:0047215~indole-3-acetate beta-glucosyltransferase activity	31.53	3 /18777	5.48E-01
Molecular function	GO:0102483~scopolin beta-glucosidase activity	4.20	45 /18777	5.68E-01
Molecular function	GO:0046872~metal ion binding	1.21	2467 /18777	5.68E-01
Molecular function	GO:0071949~FAD binding	3.07	77 /18777	5.68E-01
Molecular function	GO:0010297~heteropolysaccharide binding	23.65	4 /18777	5.68E-01
Molecular function	GO:0008705~methionine synthase activity	23.65	4 /18777	5.68E-01
Molecular function	GO:0015180~L-alanine transmembrane transporter activity	23.65	4 /18777	5.68E-01
Molecular function	GO:0052595~aliphatic-amine oxidase activity	23.65	4 /18777	5.68E-01
Molecular function	GO:0010308~acireductone dioxygenase (Ni2+-requiring) activity	23.65	4 /18777	5.68E-01

Appendix E continued

Molecular function	GO:0003871~5-methyltetrahydropteroyltriglutamate-homocysteine S-methyltransferase activity	23.65	4 / 18777	5.68E-01
Molecular function	GO:0008940~nitrate reductase activity	23.65	4 /18777	5.68E-01
Molecular function	GO:0015185~gamma-aminobutyric acid transmembrane transporter activity	23.65	4 /18777	5.68E-01
Molecular function	GO:0010309~acireductone dioxygenase [iron(II)-requiring] activity	23.65	4 /18777	5.68E-01

Appendix F: KEGG Pathway Functional Enrichment of downregulated DEGs

Term	Pathway	Count	p-value
ath01110	Biosynthesis of secondary metabolites	62	6.18E-12
ath01100	Metabolic pathways	84	9.32E-10
ath00940	Phenylpropanoid biosynthesis	13	1.35E-05
ath00941	Flavonoid biosynthesis	6	1.46E-04
ath00380	Tryptophan metabolism	8	3.60E-04
ath00073	Cutin, suberine and wax biosynthesis	5	0.0073
ath00130	Ubiquinone and other terpenoid-quinone biosynthesis	5	0.008803
ath00350	Tyrosine metabolism	5	0.010494
ath00950	Isoquinoline alkaloid biosynthesis	4	0.010562
ath00480	Glutathione metabolism	7	0.020344
ath00360	Phenylalanine metabolism	4	0.031655
ath00062	Fatty acid elongation	4	0.039591
ath00960	Tropane, piperidine and pyridine alkaloid biosynthesis	4	0.039591
ath00410	beta-Alanine metabolism	4	0.076251
ath00904	Diterpenoid biosynthesis	3	0.096934

Appendix G

A) 16S amplicon statistics

Sample	Raw reads	Trimmed reads	Filtered	Denoised F	Denoised R	Merged	Nonchimeric	Read length (bp)
NTP1	198291	197931	8703	78417	79115	51711	72622	300
NTP2	190169	189892	83718	74580	76079	50672	69329	300
NTP3	205219	204877	90600	81775	83009	54926	76415	300
NTP4	185481	185190	80371	69831	73215	47198	64789	300
NTP5	201419	201086	89118	80373	82074	54942	75932	300
TP1	190077	189705	82155	68598	72544	41922	65784	300
TP2	195250	194869	86833	77613	78573	50197	73838	300
TP3	167893	167607	75183	67007	67556	42985	61565	300
TP4	190944	190584	84671	74946	77327	50322	70674	300
TP5	186108	185812	81820	72491	75160	49684	70300	300
Total	1910851	1907553						

B) ITS1 amplicon statistics

Sample	Raw reads	Trimmed reads	Filtered	Denoised F	Denoised R	Merged	Nonchimeric	Read length (bp)
NTP1	190205	189849	44649	42445	39382	36036	41328	276
NTP2	215033	214599	92940	90319	88014	85899	85012	283
NTP3	202110	201727	58610	56088	54166	51304	55077	276
NTP4	209081	208662	71377	69275	66687	62975	68699	280
NTP5	254438	253949	79056	76071	72343	69249	75096	280
TP1	238318	237886	50369	46891	44854	41937	46570	269
TP2	265588	265069	81637	76068	73177	65104	75727	282
TP3	220240	219858	18498	16461	14964	12433	16432	243
TP4	221569	221167	63034	60530	56264	49665	60497	278
TP5	160468	160216	33303	29611	27714	24552	29569	276
Total	2177050	2172982						

C) 16S rarefraction curve

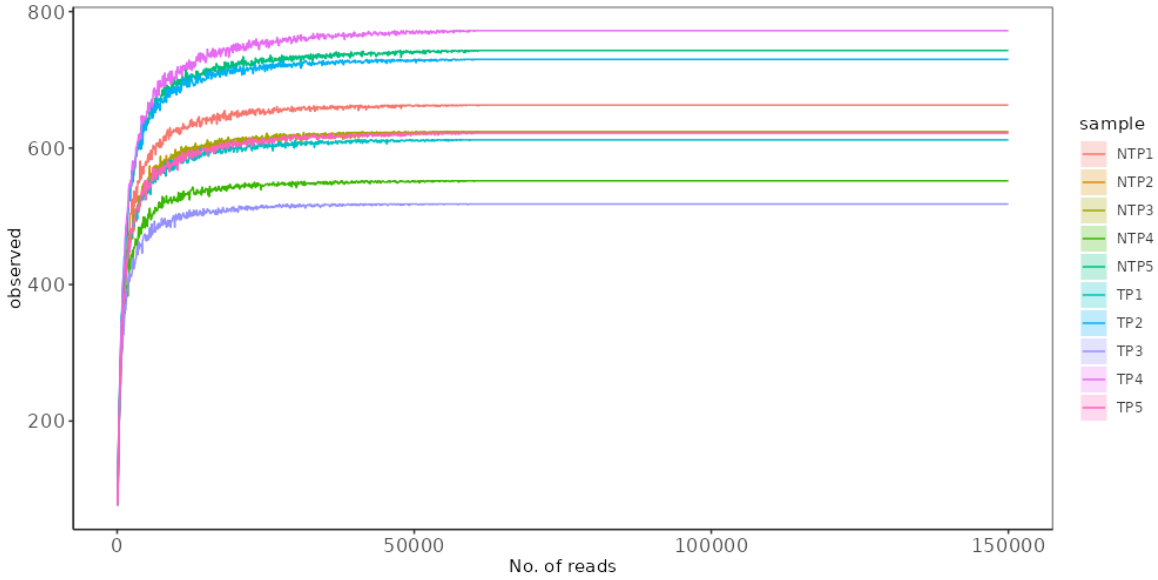

D) ITS1 rarefraction curve

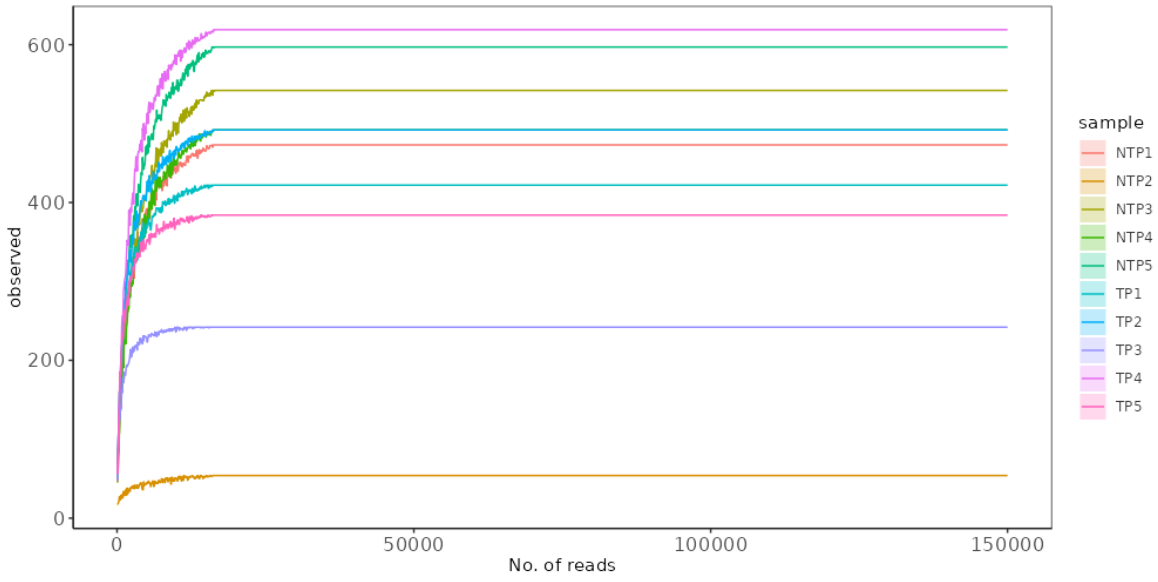

Appendix H

A) Actin 2

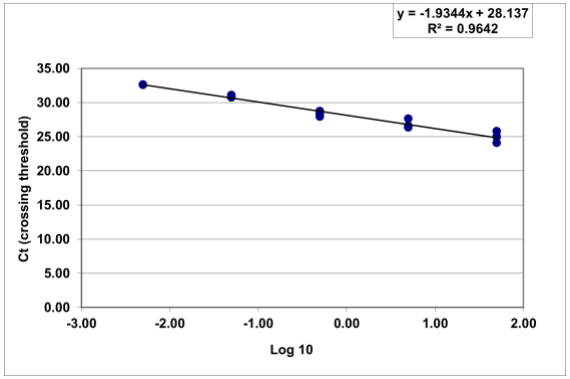

B) Primer 32

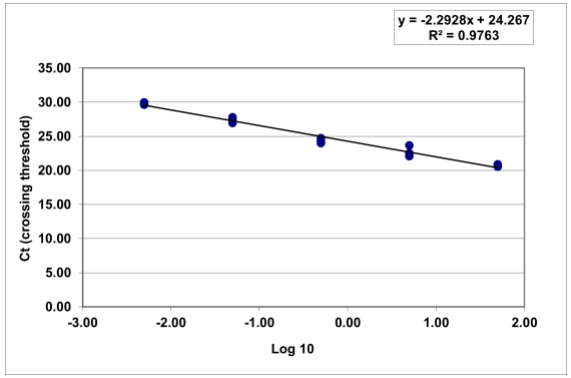

C) Primer 41

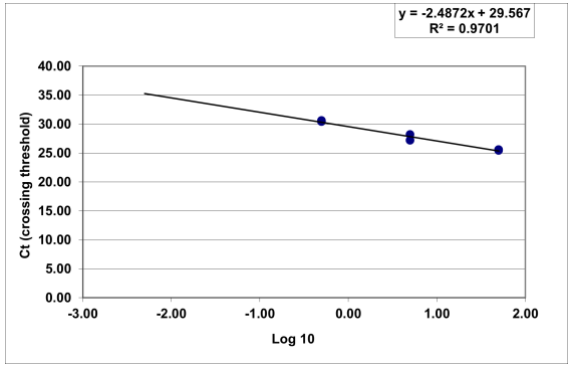

D) Primer 51

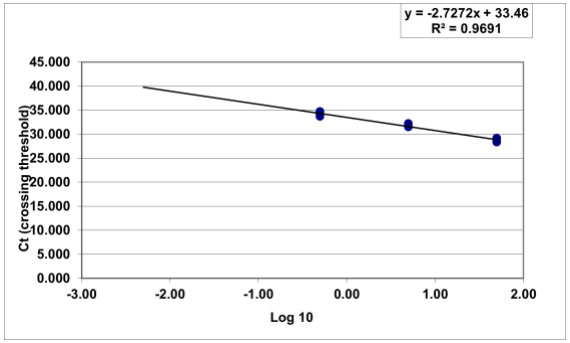

E) Primer 58

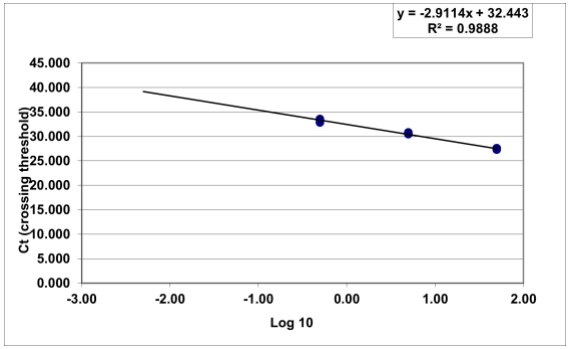

Appendix I

Gene Ontology (GO) enrichment analysis of 595 DEGs

Gene Ontology Upregulated Genes								
Term	**Description**	***P-value***	**Genes**	**List Total**	**Pop Hits**	**Pop Total**	**Fold Enrichment**	**Benjamini**
Biological process	GO:0006269~DNA replication, synthesis of RNA primer	1.05E-02	Q8GZ43	95	2	17920	188.6316	7.95E-01
Biological process	GO:0071139~resolution of recombination intermediates	1.05E-02	O04089	95	2	17920	188.6316	7.95E-01
Biological process	GO:0006799~polyphosphate biosynthetic process	1.05E-02	Q8S403	95	2	17920	188.6316	7.95E-01
Biological process	GO:0090173~regulation of synaptonemal complex assembly	1.57E-02	O04089	95	3	17920	125.7544	7.95E-01

Appendix I continued

Biological process	GO:0009909~regulation of flower development	1.33E-02	Q9SX27, F4K5X6, Q9C6B8	95	94	17920	8.026876	7.95E-01
Biological process	GO:0051726~regulation of cell cycle	2.05E-02	Q9C6B8, Q9FKB5	95	42	17920	13.47368	8.66E-01
Biological process	GO:0010338~leaf formation	2.60E-02	Q9C6B8	95	5	17920	75.45263	9.03E-01
Biological process	GO:0000712~resolution of meiotic recombination intermediates	3.62E-02	O04089	95	7	17920	53.89474	9.03E-01
Biological process	GO:0007143~female meiotic division	4.12E-02	O04089	95	8	17920	47.15789	9.03E-01
Biological process	GO:0048826~cotyledon morphogenesis	4.62E-02	Q9C6B8	95	9	17920	41.91813	9.03E-01
Biological process	GO:0030643~cellular phosphate ion homeostasis	4.62E-02	Q8S403	95	9	17920	41.91813	9.03E-01

Appendix I continued

Biological process	GO:0065003~macromolecular complex assembly	4.62E-02	Q9LZJ6	95	9	17920	41.91813	9.03E-01
Biological process	GO:0010358~leaf shaping	4.62E-02	Q9C6B8	95	9	17920	41.91813	9.03E-01
Biological process	GO:0003333~amino acid transmembrane transport	5.12E-02	Q38967, O81845	95	10	17920	37.72632	9.07E-01
Biological process	GO:0009640~photomorphogenesis	5.36E-02	Q8GXJ1, Q9C6B8	95	71	17920	7.970348	9.07E-01
Biological process	GO:0032880~regulation of protein localization	6.61E-02	Q9C6B8	95	13	17920	29.02024	9.33E-01
Biological process	GO:0048316~seed development	6.32E-02	Q96533, Q500U8, Q7XZF5	95	78	17920	7.255061	9.33E-01
Biological process	GO:0006417~regulation of translation	6.32E-02	Q9XGW1, F4HT49	95	78	17920	7.255061	9.33E-01

Appendix I continued

Biological process	GO:0071577~zinc II ion transmembrane transport	7.59E-02	O04089	95	15	17920	25.15088	9.77E-01
Biological process	GO:0007140~male meiosis	8.07E-02	O04089	95	16	17920	23.57895	9.77E-01
Biological process	GO:0035194~posttranscriptional gene silencing by RNA	8.07E-02	Q8W566, Q5D869	95	16	17920	23.57895	9.77E-01
Biological process	GO:0006270~DNA replication initiation	8.56E-02	Q8GZ43	95	17	17920	22.19195	9.83E-01
Biological process	GO:0009408~response to heat	8.90E-02	Q8GXJ1, A1A6M1, O80982, Q38806	95	201	17920	3.753862	9.83E-01

Appendix I continued

Cellular component	GO:0005886~plasma membrane	8.21E-04	Q8L7S6, Q9LW07, Q38967, Q9LFB9, Q6AWW5, Q9C6B8, Q9LQL2, Q9FLV9, O81905, Q6NQG7, Q9ZUK3, O65639, B8XCH5, Q39183, Q9SSC1, O04089, Q94F08, Q8VY13, Q9LFS4, Q9MAM4, Q9LSE7, Q8S403, Q7XZF5	105	3209	25765	1.988129	0.067361

Appendix I continued

Cellular component	GO:0005737~cytoplasm	0.004469	Q9LE20, Q9LFB9, F4HT49, Q96533, Q9M331, A3KPE8, Q9SGU2, Q9MAM4, P49637, Q7XZF5, O22820, Q8GS71, Q9M0C5, O64587, Q9FLQ7, Q6AWW5, Q9C6B8, O64647, O65639, Q8GXJ1, Q0WPX7, Q8W566, Q39183, Q9XGW1, O80982, Q9LFS4, Q9LZJ6	105	4434	25765	1.660223	0.183214

Appendix I continued

Cellular component	GO:0005658~alpha DNA polymerase:primase complex	0.008057	Q8GZ43	105	2	25765	245.381	0.22022
Cellular component	GO:0005783~endoplasmic reticulum	0.013152	Q9SIE7, O22785, Q9FNA9, Q6AWW5, Q38806, Q9C6B8, Q500U8, Q8L762, Q9M643	105	932	25765	2.632843	0.254371
Cellular component	GO:0005730~nucleolus	0.015947	Q8GXJ1, Q39183, Q5D869, P26569, Q8RX78, Q9LZJ6, Q8LE43	105	500	25765	3.435333	0.254371
Cellular component	GO:0005773~vacuole	0.020249	Q9SIE7, O22213, Q94KJ7, Q9SVV6, Q9LZJ6, O81905	105	386	25765	3.814212	0.254371

Appendix I continued

Cellular component	GO:0009925~basal plasma membrane	0.023978	Q9C6B8	105	6	25765	81.79365	0.254371
Cellular component	GO:0005802~trans-Golgi network	0.026342	Q9LE20, Q9ZPH9, Q8S403, Q9CA75	105	278	25765	4.413326	0.254371
Cellular component	GO:0045177~apical part of cell	0.027919	Q9C6B8	105	7	25765	70.10884	0.254371
Cellular component	GO:0009506~plasmodesma	0.044604	B8XCH5, Q8GZ43, Q9SUG7, Q9C6B8, O81845, O81905, Q9LSE7, P49637	105	979	25765	2.2558	0.365752
Cellular component	GO:0022626~cytosolic ribosome	0.056553	Q9LZJ6, F4HT49, P49637	105	215	25765	4.565227	0.421574
Cellular component	GO:0019773~proteasome core complex, alpha-subunit complex	0.077735	F4HT49	105	20	25765	24.5381	0.527497

Appendix I continued

Cellular component	GO:0009705~plant-type vacuole membrane	0.083628	Q94CA0, Q94KJ7, Q9SVV6	105	119	25765	6.186074	0.527497
Molecular function	GO:0005515~protein binding	0.023074	O22456, Q9FNN6, Q9FLV9, Q9LT79, Q9LRR4, B8XCH5, A1A6M1, A3KPE8, Q9FIX8, Q8RX78, Q7XZF5, Q8GS71, F4K5X6, O64587, Q9C6B8, O64647, Q8GXJ1, Q9SX27, Q39183, O04089, Q9XGW1, O80982, Q5D869, Q9SUG7, Q8GXT3, Q8GUP1, Q9LFS4, Q9FKB5, Q9LZJ6, Q500U8, Q9CA75	93	4515	18777	1.430986	1
Molecular function	GO:0008097~5S rRNA binding	0.024262	Q9LZJ6	93	5	18777	80.76129	1
Molecular function	GO:0000822~inositol hexakisphosphate binding	0.038538	Q8S403	93	8	18777	50.47581	1

Molecular function	GO:0035198~miRNA binding	0.057253	Q9XGW1, A3KPE8	93	12	18777	33.65054	1
Molecular function	GO:0010329~auxin efflux transmembrane transporter activity	0.061875	Q9C6B8	93	13	18777	31.06203	1
Molecular function	GO:0000175~3'-5'-exoribonuclease activity	0.075607	Q8W566, A3KPE8	93	16	18777	25.2379	1
Molecular function	GO:0015114~phosphate ion transmembrane transporter activity	0.084651	Q8S403	93	18	18777	22.43369	1
Molecular function	GO:0005385~zinc ion transmembrane transporter activity	0.093608	O04089	93	20	18777	20.19032	1

Gene Ontology Downregulated Genes								
Term	Description	P-value	Genes	List Total	Pop Hits	Pop Total	Fold Enrichment	Benjamini
Biological process	GO:0006979~response to oxidative stress	4.03E-06	Q8LPL3, Q9SZE7, O23044, Q9FLC0, Q9M815, Q42578, P13114, Q8S8K8, O04922, P52577, Q96520, P25819, Q9XI31, Q9LDN9, Q39172, Q39173, Q9FJZ9, Q8VZ59, Q41906	369	299	17920	3.410827	0.002297
Biological process	GO:0009809~lignin biosynthetic process	1.00E-05	O49499, Q9FLC0, Q9FJZ9, Q1ACB3, Q9S9N9, Q9FK25	369	52	17920	8.405253	0.002856
Biological process	GO:0071555~cell wall organization	1.75E-05	Q0WVN5, O48766, Q6R0C4, Q9SS43, Q9FT97, Q42059, O22977, Q8VZK9, Q9FFQ7, O81765, Q6DBP4, O22807, Q1ACB3, Q9FMY1, Q9LIS1, Q8RX83, Q940Q8	369	303	17920	3.205524	0.003327
Biological process	GO:0009611~response to wounding	1.10E-04	Q8RY79, P19172, Q9SAH7, Q9FNL7, P13114, F4IAX0,	369	235	17920	3.306464	0.015744

			Q9S725, F4IAX1, A4FVP2, P15456, Q570B4, Q9XI31, Q9LDR8, Q8RY23, Q93YV0, Q9SD05					
Biological process	GO:0009813~flavonoid biosynthetic process	1.98E-04	Q9FLV0, Q9SD85, P41088, Q9FL28, P13114	369	27	17920	10.79193	0.020194
Biological process	GO:0009737~response to abscisic acid	2.13E-04	Q9LRJ9, Q9SJ56, Q9FLD5, Q6R0C4, Q9LD83, Q9FNL7, P37702, F4IAX0, F4IAX1, P15456, Q5EAF2, Q08298, P46604, Q9LLR7, Q9LKR6, B9DHT4, Q9LDR8, Q9ZU50, Q8GXW1, Q9FGY3	369	458	17920	2.438788	0.020194
Biological process	GO:0009741~response to brassinosteroid	4.27E-04	Q9FN92, Q9ZU50, Q9XF92, O64989, Q3E936	369	48	17920	7.082204	0.034739
Biological process	GO:0009620~response to fungus	5.38E-04	Q9LUZ6, Q9SXB6, Q9FLV0, Q94AK6, Q06588, Q8VY27, Q9LMJ4, Q9SD05, Q9S725, Q6NLC8	369	113	17920	4.297671	0.038356
Biological process	GO:0042744~hydrogen peroxide catabolic process	6.54E-04	P25819, Q96520, Q9SZE7, Q9LDN9, O23044, Q9FLC0, Q9FJZ9, Q42578	369	93	17920	4.699712	0.041418
Biological process	GO:0009826~unidimensional cell growth	1.55E-03	Q9XF43, O22874, Q9FN92, Q9SHY6, F4K128, O48818, Q39111, Q9LF24, O64989	369	131	17920	3.707152	0.088115
Biological process	GO:0002237~response to molecule of bacterial origin	1.80E-03	Q9SAH7, Q8VY27, Q8VZG8, Q9LJ86, Q9LMJ4, F4JY11	369	43	17920	6.776328	0.093383
Biological process	GO:0009407~toxin catabolic process	2.44E-03	Q9FUS8, Q9ZW24, Q9CA57, Q9ZVQ3, Q9SLM6, Q9LZI9	369	46	17920	6.334394	0.099375
Biological process	GO:0009753~response to jasmonic acid	2.31E-03	Q9XI31, Q9FNL7, Q8RY23, F4IAX0, P13114, Q93YV0, Q9SD05, F4IAX1, O64989, A4FVP2, Q5EAF2	369	166	17920	3.218076	0.099375

Biological process	GO:0009416~response to light stimulus	2.12E-03	P25819, Q9XF43, Q570B4, Q9LD83, Q940V4, Q8GT75, Q9MAM3, Q9FJ07	369	192	17920	3.03523	0.099375
Biological process	GO:0016132~brassinosteroid biosynthetic process	3.94E-03	Q940V4, Q9ZU50, O64989	369	16	17920	12.14092	0.149839
Biological process	GO:0009409~response to cold	4.97E-03	Q9C5X8, Q9FLD5, P19172, O23044, P15456, P25819, Q9XF43, Q570B4, Q9XI31, Q9S9N9, Q9MAM3, Q41906, Q9LTC4	369	376	17920	2.195699	0.176977
Biological process	GO:0000038~very long-chain fatty acid metabolic process	5.57E-03	Q9XF43, Q570B4, O65677, Q9MAM3	369	18	17920	10.79193	0.186888
Biological process	GO:0010431~seed maturation	6.14E-03	Q9FLD5, Q9ZWA9, P15456	369	36	17920	6.744956	0.194301
Biological process	GO:0009963~positive regulation of flavonoid biosynthetic process	8.25E-03	Q1ACB3	369	7	17920	20.81301	0.235636
Biological process	GO:0042761~very long-chain fatty acid biosynthetic process	8.68E-03	Q9SCU7, Q9FMY1, Q9LIS1, Q9MAM3	369	21	17920	9.250226	0.235636
Biological process	GO:0009651~response to salt stress	8.57E-03	Q9FUS8, Q9FFA5, Q9C5X8, Q9FLD5, Q8LPL3, P19172, F4IAX0, Q5EAF2, Q08298, Q93ZH9, Q9C7A2, F4I9E1, B9DHT4, Q8GXW1, Q93ZY3, Q9LTC4	369	399	17920	2.069129	0.235636
Biological process	GO:0006611~protein export from nucleus	1.09E-02	Q1ACB3	369	8	17920	18.21138	0.281123
Biological process	GO:0090333~regulation of stomatal closure	1.24E-02	Q9LD83, Q8GZ99, Q9T003, Q9LMJ4, Q9FK25	369	44	17920	5.518601	0.306549
Biological process	GO:0009414~response to water deprivation	1.29E-02	Q9FGC7, F4HVY0, Q9FLD5, Q6R0C4, P33154, F4IAX0, Q9LMJ4, Q8S8K8, F4IAX1, P46604, Q9LLR7, Q8GUQ8, Q9XI31, Q41906, Q9LTC4	369	382	17920	2.034081	0.306549

Biological process	GO:0006777~Mo-molybdopterin cofactor biosynthetic process	1.38E-02	P29402, Q9C5X8	369	9	17920	16.1879	0.313783
Biological process	GO:0071215~cellular response to abscisic acid stimulus	1.45E-02	Q39086, B9DGI8, P15456, Q9SYK9	369	46	17920	5.278661	0.317643
Biological process	GO:0080027~response to herbivore	1.57E-02	P43082, Q8VZG8, Q93YV0, A4FVP2	369	26	17920	7.471336	0.320392
Biological process	GO:0010224~response to UV-B	1.53E-02	Q9SZP1, Q9XI31, P41088, P13114, Q5XF20, Q9FJ07	369	71	17920	4.103973	0.320392
Biological process	GO:0008610~lipid biosynthetic process	1.74E-02	F4HVY0, Q570B4, Q9AST3, Q8H1Z0	369	27	17920	7.19462	0.340086
Biological process	GO:0010555~response to mannitol	1.92E-02	Q9FFA5, Q9C7T7, Q9T003, Q9FK25	369	28	17920	6.937669	0.344735
Biological process	GO:0055085~transmembrane transport	1.94E-02	Q8LPK2, Q9FKF2, Q9FNL7, Q41951, O64515, O64759, Q9LV10, P25819, Q9C6D3, Q8W036, Q9M174, Q9ZU50, Q8GT75, P26587	369	330	17920	2.060278	0.344735
Biological process	GO:0010236~plastoquinone biosynthetic process	2.05E-02	Q1ACB3	369	11	17920	13.24464	0.353476
Biological process	GO:0010025~wax biosynthetic process	2.11E-02	Q9XF43, F4HVY0, Q8H1Z0, Q9MAM3	369	29	17920	6.698439	0.354485
Biological process	GO:0009058~biosynthetic process	2.68E-02	Q9S7E9, Q9M2Y8, Q9LQ10, Q9SIE1, P13114, Q9SD05	369	82	17920	3.55344	0.436419
Biological process	GO:0045892~negative regulation of transcription, DNA-templated	2.92E-02	F4HY56, Q9SZP1, Q9C9G7, Q9C7U7, Q96320, Q9SAH7, Q9FMC8, Q9C519, Q9FKL2	369	176	17920	2.48337	0.462367
Biological process	GO:0009411~response to UV	3.21E-02	Q9SD85, P41088, Q9S725, Q9S777	369	34	17920	5.713375	0.495047
Biological process	GO:0042183~formate catabolic process	4.07E-02	Q570B4	369	2	17920	48.56369	0.55169
Biological process	GO:0051574~positive regulation of histone H3-K9 methylation	4.07E-02	O50008	369	2	17920	48.56369	0.55169
Biological process	GO:0006898~receptor-mediated endocytosis	4.07E-02	Q9FL28	369	2	17920	48.56369	0.55169

Biological process	GO:0033310~chlorophyll a catabolic process	4.07E-02	O23512, Q9SRQ1	369	2	17920	48.56369	0.55169
Biological process	GO:0051555~flavonol biosynthetic process	3.70E-02	Q9FL28, Q9FK25, Q9FJ07	369	15	17920	9.712737	0.55169
Biological process	GO:0006865~amino acid transport	4.67E-02	P25819, Q9ZU50, O64759	369	66	17920	3.679067	0.618647
Biological process	GO:0006997~nucleus organization	5.18E-02	Q9SGD1	369	18	17920	8.093948	0.656401
Biological process	GO:0048544~recognition of pollen	5.16E-02	Q9LZR8, O81832, Q39086, O81905	369	41	17920	4.737921	0.656401
Biological process	GO:0030244~cellulose biosynthetic process	5.48E-02	Q0WVN5, Q9FG35, Q8RX83, Q8VZK9	369	42	17920	4.625113	0.67843
Biological process	GO:0010223~secondary shoot formation	5.72E-02	Q9SQR3, Q8VY26, O04017	369	19	17920	7.66795	0.688688
Biological process	GO:0042631~cellular response to water deprivation	5.80E-02	Q3E9F7, P19172, P15456, Q9SYK9	369	43	17920	4.517552	0.688688
Biological process	GO:0071266~'de novo' L-methionine biosynthetic process	6.04E-02	O50008	369	3	17920	32.37579	0.702077
Biological process	GO:0046244~salicylic acid catabolic process	7.97E-02	Q9ZSA7, Q9FLV0	369	4	17920	24.28184	0.811508
Biological process	GO:1904585~response to putrescine	7.97E-02	F4IAX0, F4IAX1	369	4	17920	24.28184	0.811508
Biological process	GO:0015812~gamma-aminobutyric acid transport	7.97E-02	Q9ZU50	369	4	17920	24.28184	0.811508
Biological process	GO:0043447~alkane biosynthetic process	7.97E-02	F4HVY0, Q8H1Z0	369	4	17920	24.28184	0.811508
Biological process	GO:0030187~melatonin biosynthetic process	7.97E-02	Q9T003, Q9FK25	369	4	17920	24.28184	0.811508
Biological process	GO:1902074~response to salt	7.55E-02	Q9XI31, Q6R0C4, Q8S8K8, Q9FGY3	369	48	17920	4.046974	0.811508
Biological process	GO:0006952~defense response	7.97E-02	Q3ED38, Q9SXB6, Q8LPL3, Q06588, P33154, Q9M2P8, Q9SS01, Q9LMJ4, Q9LUZ6, Q9XI31, Q9M2T2, Q9M088,	369	651	17920	1.491972	0.811508

			Q8VY27, Q9LDR8, Q9C8K0, Q9LMU2, Q9LXG8, O49353, Q8GXW1, Q41906					
Biological process	GO:0010038~response to metal ion	9.26E-02	P29402, Q8VZ59	369	25	17920	5.827642	0.926045
Biological process	GO:0060149~negative regulation of posttranscriptional gene silencing	9.86E-02	P0C945, Q9ZVT7	369	5	17920	19.42547	0.951493
Biological process	GO:0002239~response to oomycetes	9.90E-02	Q9FLV0, Q9SRH6, Q9SLM6	369	26	17920	5.603502	0.951493
	Term	PValue	Genes	List Total	Pop Hits	Pop Total	Fold Enrichment	Benjamini
Cellular componen t	GO:0016020~membrane	3.45E-09	Q9FHB6, Q9LD83, Q84W04, Q9XF91, Q5M721, Q9XF92, Q9STL1, Q9STL2, Q94C59, Q9LUZ6, Q9LQ10, Q9M331, F4HWL3, Q9M174, Q9C7A2, Q8W036, Q6NQ66, Q9LSE7, Q8LPK2, B9DFI7, Q9SRQ1, Q9C788, Q8H1Z0, Q8L7R8, Q9SZY3, F4K6R7, F4JY11, Q8LG88, Q9SD53, Q6DBP4, F4I9E1, Q8RX83, Q9FNL8, Q0WVN5, Q93Z38, O22874, F4HVY0, Q9LZR8, Q9LPF6, Q9FKF2, Q38956, Q9FNL7, Q9SGD1, O64515, Q9LV10, O64759, F4HXL0, Q9LXV0, O81000, Q9SYP3, P0C897, Q940V4, Q9LIP4, Q8RX77, Q9C5S9, Q9MAM3, Q93Z27, O65790, P29402, Q8GYA4, Q9AST3, P56786, Q9SS43, O65677, Q8VZG8, Q41951, O64989, Q9XF43, Q9C6D3,	413	5721	25765	1.570257	3.45E-07

			Q9C7F7, Q39086, Q9SIZ4, Q9LJ86, Q9FMY1, Q8GT75, Q9LJY5, Q9FZ95, Q9M815, Q9SU13, Q9FN92, Q9FG35, Q9SHY6, Q9ZU50, Q9SD05, Q9FGC7, Q9C6S7, O48818, Q9SZU1, A4FVP2, Q9S777, Q9LTS3, P25819, Q9SZ46, Q9M363, Q9M088, Q93ZH9, Q8GZ99, O22807, Q8VY27, Q93ZY3, P26587, Q9FZP1, Q94A34, Q9FLD5, Q9C7T7, O22397, Q9LT15, Q42578, Q9LIL4, Q9LXA5, Q1ACB3, Q8RUN2, Q9LUC5, Q9FME8, Q9SXB6, Q9SU40, Q9LYS9, Q9FL28, Q9LSW9, Q8VZK9, Q940Y9, Q570B4, O81832, Q9STK8, Q9SUE0, Q9SZG0, Q9S9N9, O82081, Q058N4, Q2HIV9					
Cellular component	GO:0005773~vacuole	1.71E-05	P29402, Q9SZE7, P43082, Q38956, O23044, Q9FLC0, P38605, Q42578, Q8S8K8, O81905, Q9LTS3, Q96520, Q8LG88, Q9LDN9, Q9M088, Q9FJZ9, O65390, Q9SD05, Q9SJZ7	413	386	25765	3.232383	8.54E-04
Cellular component	GO:0005886~plasma membrane	3.39E-05	Q9LD83, Q9SLL2, Q9M6N7, O49499, Q9M815, Q8RWD5, Q9LMJ4, O22977, O81905, Q9SU13, Q94C59, Q5EAF2, Q8GUQ8, Q9XI31, Q9FN92, Q9C7A2, F4HWL3, Q8L9B5,	413	3209	25765	1.574691	0.001129

			Q9SRH6, O50008, Q9LSE7, P47998, Q944C1, Q9M7K4, Q8H1Z0, F4K6R7, P25819, Q9ZUF4, Q9M088, Q9SD53, Q8GZ99, Q9ASQ7, Q8W108, Q9ZT81, Q0WVN5, Q94A34, Q6NQE2, Q9C7T7, O22397, Q38956, Q9LT15, O64515, O04922, O64759, B3H5Q1, O23207, Q9LV10, P52577, O80992, Q39173, Q9LXA5, Q9ZPR1, Q8RX77, Q9C5S9, Q3E936, Q9SXB6, Q9SU40, Q9FL28, O22707, Q9ZVJ5, Q8VZG8, Q41951, Q8S8E3, Q9C7F7, Q39086, Q9SUE0, B9DHT4, Q9SIZ4, Q9LJ86, Q8L8Z1, O82081, F4IC29, Q8GT75					
Cellular componen t	GO:0005829~cytosol	6.14E-05	O49499, Q06588, F4JLM5, O64733, Q9LMJ4, Q9SU13, Q9LX30, Q94C59, Q01525, Q9SRH6, Q9M1X2, P48528, O50008, P47998, Q9FUS8, Q944C1, Q8LPK2, Q9SRQ1, Q9SLM6, Q9SZY3, Q9FK25, A4FVP2, P15456, P25819, Q9SZ46, Q7Y175, P41088, Q8VY27, Q9LF24, Q8W108, Q9LRJ9, Q9ZW24, Q6NQE2, Q9ZVQ3, O82616, Q9LRR9, O04922, P52577, Q8LJW1, Q9M354, Q39172, Q8GY23, Q9LZI9, Q1ACB3, Q8RUN2,	413	2450	25765	1.655112	0.001535

			Q9C5S9, Q9LK73, Q9LUC5, Q3E936, Q9S7E9, Q8GYA4, Q9SU40, Q9T003, Q570B4, Q9CA57, Q9ZUH5, Q9LJ86, Q9LF88					
Cellular component	GO:0000326~protein storage vacuole	1.65E-04	Q9ZWA9, Q41951, P26587, P15456	413	18	25765	17.32916	0.003301
Cellular component	GO:0005777~peroxisome	2.67E-04	Q9S7E9, Q9FFE6, P37702, Q9LRR9, Q9SS01, Q9MA90, F4IAX0, F4IAX1, O04922, P15456, P25819, Q570B4, O50008, P47998	413	362	25765	2.929682	0.004457
Cellular component	GO:0000325~plant-type vacuole	4.80E-04	P29402, Q9LRJ9, Q9FHB6, Q9SU40, Q8VZJ2, Q38956, P37702, P38605, Q41951, P15456, Q9SU13, P25819, Q96520, Q01525, Q9LIL4, Q9LDN9, Q8GZ99, Q9SRH6, O65390, O50008, P47998, Q0WPR4	413	749	25765	2.165567	0.006814
Cellular component	GO:0005783~endoplasmic reticulum	5.45E-04	Q9FLD5, O23044, Q9LUZ6, Q9LIL4, Q940V4, Q9ZU50, Q9SD05, Q9MAM3, O65790, P29402, Q9AST3, O65677, Q9SZU1, P54968, P13114, O64989, Q9LTS3, Q8VZK9, Q9XF43, Q570B4, P41088, Q9C7F7, Q9LMU2, Q9FMY1, Q8RX83, Q93ZY3	413	932	25765	2.0081	0.006814
Cellular component	GO:0048046~apoplast	1.14E-03	Q9SR40, Q9FIC6, Q9SU40, Q9FLI4, Q9FLC0, Q9FT97, P37702, P33154, Q9LRR9, Q9FID0, P15456, Q8LG89,	413	536	25765	2.327798	0.012651

			Q9LLR7, Q9LMU2, Q8RY23, Q9SI72, O50008, P47998, Q84WE4					
Cellular component	GO:0009505~plant-type cell wall	1.56E-03	P29402, Q9LRJ9, Q9M8K5, Q9FZ35, Q9SU40, Q8VZJ2, Q9FLC0, Q9FT97, O48818, P33154, Q41951, Q9SZY3, Q96520, Q9LLR7, Q9C7F7, Q9FJZ9, Q9LMU2, Q8RY23	413	510	25765	2.324147	0.015563
Cellular component	GO:0005576~extracellular region	2.19E-03	O48766, P43082, Q8LPL3, Q941F1, P19172, Q8VZJ2, Q06588, P33154, Q9FID0, O22977, Q9SU13, Q9SD85, Q9FN92, F4HWL3, Q9FJZ9, Q9ZWA9, Q9SHY6, O65390, Q6NMK1, Q41906, Q6NQ66, Q9SR40, Q9FIC6, Q9FLI4, F4JJH4, P37702, O48818, Q9ZSB0, Q9SZY3, P15456, Q9LTS3, Q96520, Q9FH03, Q9FJ45, Q9FXD8, Q8LG89, Q9M363, Q9SA75, Q6DBP4, Q9LMU2, O49353, Q0WPR4, Q93Z38, Q9FZP1, O22874, Q9LRJ9, Q9FZ35, Q9LZR8, Q9SZE7, O23044, Q42059, Q42578, B3H5Q1, F4HXL0, Q9LLR7, Q9CA68, Q944R1, Q9LDN9, O81765, Q9LXA5, O80470, Q9SXB6, Q94A68, Q9SU40, Q9FIA1, Q9FLC0, F4IAX1, Q08298, O81832, Q9C7F7, Q39086, Q9LJ86, Q8GT75	413	3287	25765	1.404469	0.019145

Cellular component	GO:0009536~plastid	2.49E-03	Q9FNB0, Q9FHB6, Q9FLD5, Q8LPL3, Q9FLN4, Q9XF91, Q39172, Q39173, Q9M1X2, Q1ACB3, Q9FJA6, Q3E936, Q9FFA5, Q9FGC7, P56786, Q9FIA1, P37702, Q9FK25, Q940Y9, Q9FYB5, Q570B4, Q9FFQ7, Q8GZ99, Q93ZY3, Q058N4	413	1031	25765	1.815276	0.019145
Cellular component	GO:0099503~secretory vesicle	2.54E-03	Q9LRJ9, Q8LG89, P43082, Q8VZJ2, Q9C7F7, Q9FT97, P37702, Q9LMU2, P33154, O65390	413	180	25765	3.465833	0.019145
Cellular component	GO:0005794~Golgi apparatus	2.68E-03	Q9LZR8, Q9ZVY5, Q42578, Q8VZJ7, Q01525, Q9M354, Q9LIL4, F4HWL3, Q39173, Q9FG35, Q6NMK1, Q9SXB6, Q9AST3, Q9C6S7, B9DFI7, Q9SS43, Q9FLC0, Q41951, P15456, F4JY11, Q08298, Q8VZK9, Q9LR44, Q9FH03, Q9STK8, Q9C7F7, O22807, Q8RX83, Q940Q8	413	1036	25765	1.806515	0.019145
Cellular component	GO:0009941~chloroplast envelope	7.04E-03	Q9FGC7, Q9FLD5, P56786, Q94A68, Q9FLN4, O22707, Q41951, Q8S8K8, P15456, Q940Y9, Q9SUE0, Q9M1X2, Q1ACB3, Q058N4, Q9SJZ7	413	589	25765	2.012419	0.046941
Cellular component	GO:0009506~plasmodesma	8.36E-03	P29402, Q9SXB6, Q6NQE2, Q9SU40, Q9M6N7, O48818, Q8VZG8, Q9LRR9, Q41951, Q9FK25, O81905, P15456, Q9LV10, Q96520, Q9M088, Q9FN92, Q8GY23, Q9SA75,	413	979	25765	1.720526	0.05227

			Q9SRH6, Q8L8Z1, O65390, Q9FJA6, O50008, Q9LSE7					
Cellular component	GO:0009705~plant-type vacuole membrane	1.23E-02	P25819, P41088, Q41951, P13114, O64515, P26587	413	119	25765	3.669705	0.072537
Cellular component	GO:0031969~chloroplast membrane	1.62E-02	F4HXL0, Q9FLD5, Q1ACB3, Q8S8K8, Q058N4	413	163	25765	3.06184	0.086911
Cellular component	GO:0005737~cytoplasm	1.65E-02	Q6NMC6, Q8RY79, Q9M6N7, Q9SQR3, Q9SJL2, Q0WL81, Q06588, F4JLM5, O64733, Q9LMJ4, O22977, Q9LX30, Q94C59, Q5EAF2, Q01525, Q9XI31, Q9M331, Q9FLV0, Q9LKR6, Q9C7A2, Q8W036, Q8VZ59, Q9SND9, Q9ZU50, Q39111, Q9FNA2, O50008, Q9FUS8, Q9ZVT7, Q9SLM6, Q94K41, P13114, Q9C585, Q9FK25, Q94CD1, Q9C9D0, Q9FFQ7, Q9M2Y8, Q84TF0, Q39224, Q8W108, P26587, Q9SJZ7, Q9C5X8, Q9ZW24, Q9SJ56, Q6NQE2, Q9ZVQ3, Q9T030, Q84MC1, O81769, Q9LRR9, Q9FJT8, O04922, O23207, P52577, O80992, Q9LIL4, Q39172, Q39173, Q8RV79, Q9LZI9, Q1ACB3, Q93YV0, Q9MAM3, Q3E9F7, O23512, P29402, Q9S7E9, Q9M8K5, Q9T003, Q9FZ21, O65677, Q9FL28, O22707, Q9ZVJ5,	413	4434	25765	1.252202	0.086911

			Q9LRQ8, Q9LSS8, Q8S8E3, Q9XF43, Q570B4, Q9CA57, Q84Y18, Q9ZUH5, B9DHT4, Q9S9N9					
Cellular component	GO:0098552~side of membrane	4.30E-02	Q9M088, Q9SU40, Q9C7F7, O82081, Q9LJ86, F4K6R7, Q9SU13	413	159	25765	2.746509	0.215114
Cellular component	GO:0045335~phagocytic vesicle	4.72E-02	Q8VY27, Q9LMJ4	413	3	25765	41.58999	0.224814
Cellular component	GO:0031966~mitochondrial membrane	6.22E-02	O81000, Q9FLD5, Q9ZU50	413	93	25765	3.354032	0.271441
Cellular component	GO:0009507~chloroplast	6.24E-02	Q38854, Q9FNB0, Q9FZ95, Q941F1, Q84W04, Q0WL81, Q9FLN4, Q8RWD5, Q9XF91, Q5M721, O81905, Q9ZSA7, Q8W036, Q9M1X2, Q9SD05, O50008, Q9LSE7, P47998, Q84WE4, Q9FFA5, Q9FUS8, Q9FGC7, Q8LPK2, Q9C6S7, Q9C626, Q9FFE6, Q9SRQ1, Q9FV02, Q9SIK1, Q9SLM6, P37702, O64843, A4FVP2, Q9S777, P15456, F4JY11, Q9FYB5, Q9SZ46, P41088, Q9SD53, Q9SIC9, Q8VY26, Q9ASQ7, Q8RY23, Q93ZY3, Q9SJZ7, Q9SYK9, Q94A34, Q9LPF6, Q9FLD5, Q9ZVY5, Q94A73, O82616, Q9LRR9, Q9MA90, F4HXL0, Q9LXV0, Q9LIP4, Q8RX77, Q8RV79, Q1ACB3,	413	5071	25765	1.168719	0.271441

			Q8RUN2, P0C7P8, Q9C5S9, Q93YV0, Q9LUC5, O80470, P29402, Q9FLC2, Q9S7E9, P56786, Q9SXB6, Q94A68, Q9FIA1, Q9FZ21, Q9SIE1, Q9SS01, P54968, F4IAX0, Q9ZVN2, Q9C7J9, Q940Y9, Q9LR44, Q570B4, Q39086, Q9SUE0, Q8GXT2, Q9SIZ4, Q8S528, Q9FMY1, Q9LJY5, Q058N4					
Cellular component	GO:0005797~Golgi medial cisterna	6.58E-02	B9DFI7, Q9C6S7, Q8VZJ7, Q940Q8	413	58	25765	4.302413	0.274033
Cellular component	GO:0005789~endoplasmic reticulum membrane	7.87E-02	P29402, Q9XF43, F4HVY0, Q570B4, Q9AST3, Q9SD85, Q9SRQ1, Q8H1Z0, Q9FMY1, Q9MAM3, Q93ZY3, Q8VZJ7	413	523	25765	1.669961	0.312295
Cellular component	GO:0005635~nuclear envelope	8.12E-02	Q1ACB3, Q9SGD1, F4ID16	413	102	25765	3.058088	0.312295
Cellular component	GO:0042807~central vacuole	9.22E-02	Q41951, P26587	413	6	25765	20.795	0.341474
	Term	PValue	Genes	List Total	Pop Hits	Pop Total	Fold Enrichment	Benjamini
Molecular function	GO:0005506~iron ion binding	5.98E-06	O65790, F4HVY0, Q9AST3, Q9SRQ1, Q9C788, Q9SZU1, Q8H1Z0, Q9STL1, O64989, Q9STL2, Q8VZJ7, Q9SZ46, Q8GUQ8, Q9SD85, Q9STK8, Q9LIP4, Q940V4, Q9FMY1,	397	351	18777	3.099249	0.002287

			Q8W108, Q9LUC5, Q9LJY5, Q9SJZ7					
Molecular function	GO:0020037~heme binding	1.18E-05	O65790, Q9SZE7, Q9SRQ1, O23044, Q9FLC0, Q9C788, Q9SZU1, Q42578, Q9STL1, O64989, Q9STL2, Q96520, P25819, Q9SZ46, Q9LDN9, Q9SD85, Q9STK8, Q9LIP4, Q940V4, Q9FJZ9, Q9FMY1, Q9LUC5, Q9LJY5	397	394	18777	2.881049	0.002287
Molecular function	GO:0016491~oxidoreductase activity	3.18E-05	Q9FLC2, F4HVY0, Q9AST3, Q9T030, Q94A68, Q9SU40, Q9FZ21, Q9FL28, Q94K41, Q06588, O22707, Q8H1Z0, Q9LRR9, Q9LID0, P52577, Q9ZSA7, Q8GUQ8, Q9FLV0, Q84TF0, Q8S528, Q39111, Q39224, Q9FNA2	397	420	18777	2.702699	0.004117
Molecular function	GO:0004497~monooxygenase activity	1.78E-04	O65790, Q9FLC2, Q9SRQ1, Q9C788, Q9SZU1, Q9STL1, O64989, Q9STL2, Q9SZ46, Q9SD85, Q9STK8, Q9LIP4, Q940V4, Q8VZ59, Q9FMY1, Q9LUC5, Q9LJY5	397	266	18777	3.022755	0.017325
Molecular function	GO:0080030~methyl indole-3-acetate esterase activity	4.82E-04	O23512, Q8S8S9, Q9SG92, O23171	397	8	18777	23.64861	0.037485
Molecular function	GO:0016705~oxidoreductase activity, acting on paired donors, with incorporation or reduction of molecular oxygen	6.48E-04	O65790, Q9SRQ1, Q9C788, Q9SZU1, Q9STL1, O64989, Q9STL2, Q8VZJ7, Q9SZ46, Q9SD85, Q9STK8, Q9LIP4, Q940V4, Q9FMY1, Q9LUC5, Q9LJY5	397	270	18777	2.802799	0.039271
Molecular function	GO:0008194~UDP-glycosyltransferase activity	9.47E-04	Q9SJL0, Q9LXV0, Q9LR44, Q9ZVY5, Q9SK82, Q9M051,	397	119	18777	3.974557	0.039271

			O64733, Q9LK73, Q5XF20, Q9SYK9					
Molecular function	GO:0010355~homogentisate farnesyltransferase activity	1.31E-03	Q1ACB3	397	3	18777	47.29723	0.039271
Molecular function	GO:0047172~shikimate O-hydroxycinnamoyltransferase activity	1.31E-03	Q1ACB3	397	3	18777	47.29723	0.039271
Molecular function	GO:0010357~homogentisate solanesyltransferase activity	1.31E-03	Q1ACB3	397	3	18777	47.29723	0.039271
Molecular function	GO:0010356~homogentisate geranylgeranyltransferase activity	1.31E-03	Q1ACB3	397	3	18777	47.29723	0.039271
Molecular function	GO:0032440~2-alkenal reductase [NAD(P)] activity	1.31E-03	Q39172, Q39173	397	3	18777	47.29723	0.039271
Molecular function	GO:0047205~quinate O-hydroxycinnamoyltransferase activity	1.31E-03	Q1ACB3	397	3	18777	47.29723	0.039271
Molecular function	GO:0015267~channel activity	1.82E-03	Q8W036, Q41951, Q8GT75, P26587	397	42	18777	6.756747	0.050611
Molecular function	GO:0009922~fatty acid elongase activity	2.33E-03	Q9XF43, Q570B4, O65677, Q9MAM3	397	27	18777	8.758746	0.060389
Molecular function	GO:0004675~transmembrane receptor protein serine/threonine kinase activity	3.51E-03	Q8GZ99, Q9FL28, O81905	397	15	18777	12.61259	0.085275
Molecular function	GO:0015189~L-lysine transmembrane transporter activity	6.29E-03	Q9ZU50, O64759	397	6	18777	23.64861	0.135963
Molecular function	GO:0080032~methyl jasmonate esterase activity	6.29E-03	O23512, Q8S8S9, O23171	397	6	18777	23.64861	0.135963
Molecular function	GO:0005313~L-glutamate transmembrane transporter activity	8.69E-03	Q9ZU50, O64759	397	7	18777	20.27024	0.168933
Molecular function	GO:0004659~prenyltransferase activity	8.69E-03	Q1ACB3	397	7	18777	20.27024	0.168933
Molecular function	GO:0051723~protein methylesterase activity	9.34E-03	O23512, Q8S8S9, Q9SG92, O23171	397	21	18777	9.008996	0.172966

Molecular function	GO:0004364~glutathione transferase activity	9.84E-03	Q9FUS8, Q9ZW24, Q9CA57, Q9ZVQ3, Q9SLM6, Q9LZI9	397	62	18777	4.577151	0.174051
Molecular function	GO:0030151~molybdenum ion binding	1.14E-02	P29402, Q9C5X8	397	8	18777	17.73646	0.193148
Molecular function	GO:0003700~transcription factor activity, sequence-specific DNA binding	1.29E-02	Q9LE63, Q9SJ56, Q8LDF9, Q8VWJ2, Q9FHH8, Q9SAH7, Q9M9P4, Q9FLJ2, Q9SGD1, Q9FZ90, Q9FKL2, Q9FYA2, P46604, F4HY56, Q9SZP1, Q9CA46, Q9C9G7, P93751, Q9SCU7, Q9LDR8, Q9LXG8, P46665, P0C7P8, Q0WT24, Q8GXW1, O50008, Q9LTC4, Q84TE6, Q6R0C4, Q9C7U7, Q8VWK4, O04017, B9DGI8, Q9FKG1, Q700D9, Q42485, Q9FJ07, Q9FN69, Q9M2Y9, Q96320, Q9C519, Q8VZQ2, Q9C9H1, Q9SVC5, Q9FGY3, Q2HIV9	397	1641	18777	1.412288	0.208742
Molecular function	GO:0022857~transmembrane transporter activity	1.75E-02	P25819, Q9FKF2, Q9M174, Q9FNL7, Q8RX77, Q9ZU50, O64515, O64759, Q9C5Y4, Q9LV10	397	250	18777	2.270267	0.267056
Molecular function	GO:0005049~nuclear export signal receptor activity	1.78E-02	Q1ACB3	397	10	18777	14.18917	0.267056
Molecular function	GO:0035251~UDP-glucosyltransferase activity	1.87E-02	Q9LR44, Q9ZVY5, Q5XF20, Q9SYK9	397	27	18777	7.006997	0.269624
Molecular function	GO:0045735~nutrient reservoir activity	2.06E-02	Q9ZWA9, P15456, Q08298	397	28	18777	6.756747	0.28674
Molecular function	GO:0008422~beta-glucosidase activity	2.38E-02	Q9FH03, P19172, P37702, Q8GXT2, B3H5Q1	397	52	18777	4.547811	0.319595

Molecular function	GO:0008131~primary amine oxidase activity	3.42E-02	F4IAX0, F4IAX1, Q9LTS3	397	14	18777	10.13512	0.427241
Molecular function	GO:0015250~water channel activity	3.98E-02	Q8W036, Q41951, Q8GT75, P26587	397	36	18777	5.255248	0.427241
Molecular function	GO:0016788~hydrolase activity, acting on ester bonds	4.04E-02	O23512, Q9FJ45, Q9CA68, Q8S8S9, Q9SG92, O23171, O80470	397	119	18777	2.78219	0.427241
Molecular function	GO:1990465~aldehyde oxygenase (deformylating) activity	4.17E-02	F4HVY0, Q8H1Z0	397	2	18777	47.29723	0.427241
Molecular function	GO:0061599~molybdopterin molybdotransferase activity	4.17E-02	P29402	397	2	18777	47.29723	0.427241
Molecular function	GO:0008863~formate dehydrogenase (NAD+) activity	4.17E-02	Q570B4	397	2	18777	47.29723	0.427241
Molecular function	GO:0009924~octadecanal decarbonylase activity	4.17E-02	F4HVY0, Q8H1Z0	397	2	18777	47.29723	0.427241
Molecular function	GO:0061598~molybdopterin adenylyltransferase activity	4.17E-02	P29402	397	2	18777	47.29723	0.427241
Molecular function	GO:0017096~acetylserotonin O-methyltransferase activity	4.17E-02	Q9T003, Q9FK25	397	2	18777	47.29723	0.427241
Molecular function	GO:0000976~transcription regulatory region sequence-specific DNA binding	4.72E-02	Q6R0C4, Q9C7U7, Q9FHH8, Q8VWK4, Q9SAH7, O04017, Q9FKG1, Q700D9, Q9FZ90, Q9FKL2, Q9FYA2, P46604, Q01525, Q9SZP1, P93751, Q9SCU7, Q9C519, Q8VZQ2, P46665, Q9C9H1, Q9FGY3, F4HZD1	397	710	18777	1.532164	0.464646
Molecular function	GO:0030246~carbohydrate binding	4.87E-02	Q9C7J9, P29402, O81832, Q9LKR6, Q9FV02, Q39086, Q9LXA5, Q42059, Q9SSM3, O81905	397	259	18777	2.008763	0.464646
Molecular function	GO:0042937~tripeptide transporter activity	4.90E-02	Q9FNL8, Q9M331, Q9FNL7	397	17	18777	8.34657	0.464646

Molecular function	GO:0030170~pyridoxal phosphate binding	5.06E-02	Q9C5X8, Q9S7E9, Q9M2Y8, Q9LQ10, Q8RY79, Q9SIE1	397	95	18777	2.987193	0.46857
Molecular function	GO:0071916~dipeptide transmembrane transporter activity	5.99E-02	Q9FNL8, Q9M331, Q9FNL7	397	19	18777	7.467984	0.541995
Molecular function	GO:0047215~indole-3-acetate beta-glucosyltransferase activity	6.19E-02	Q9LR44, Q9ZVY5	397	3	18777	31.53149	0.547669
Molecular function	GO:0102483~scopolin beta-glucosidase activity	6.90E-02	Q9FH03, P37702, Q8GXT2, B3H5Q1	397	45	18777	4.204198	0.567756
Molecular function	GO:0046872~metal ion binding	7.73E-02	Q38854, O49499, Q9SJL2, Q0WL81, Q06588, Q9ZSA7, Q9FLV0, Q9FJZ9, Q39111, P48528, O50008, Q9LSE7, P37702, P25819, Q96520, Q9FXD8, Q8LG89, Q941Q3, Q9M363, Q93ZH9, Q8VY26, Q39224, Q9C9H1, Q93ZY3, Q9SJZ7, Q9SZE7, O23044, Q9SGD1, Q42578, Q9M354, Q944R1, Q9M2T2, Q9LDN9, P93751, Q8GWS3, Q9C5S9, Q0WT24, F4HZD1, P29402, Q9M8K5, Q9LYS9, Q9FZ21, Q9FLC0, Q9FL28, Q9ZVJ5, P54968, Q9LSW9, Q42485, P0C945, Q9SZG0, O82081, Q8GT75, F4IC29, Q9SSE9, Q9SVC5	397	2467	18777	1.207834	0.567756
Molecular function	GO:0071949~FAD binding	7.97E-02	Q9FLC2, Q9FGC7, Q8GUQ8, Q6NQ66, Q9LTS3	397	77	18777	3.071249	0.567756
Molecular function	GO:0010297~heteropolysaccharide binding	8.17E-02	Q8W108, P15456	397	4	18777	23.64861	0.567756
Molecular function	GO:0008705~methionine synthase activity	8.17E-02	O50008	397	4	18777	23.64861	0.567756

Molecular function	GO:0015180~L-alanine transmembrane transporter activity	8.17E-02	Q9ZU50	397	4	18777	23.64861	0.567756
Molecular function	GO:0052595~aliphatic-amine oxidase activity	8.17E-02	F4IAX0, F4IAX1	397	4	18777	23.64861	0.567756
Molecular function	GO:0010308~acireductone dioxygenase (Ni2+-requiring) activity	8.17E-02	Q8W108	397	4	18777	23.64861	0.567756
Molecular function	GO:0003871~5-methyltetrahydropteroyltriglutamate -homocysteine S-methyltransferase activity	8.17E-02	O50008	397	4	18777	23.64861	0.567756
Molecular function	GO:0008940~nitrate reductase activity	8.17E-02	P29402	397	4	18777	23.64861	0.567756
Molecular function	GO:0015185~gamma-aminobutyric acid transmembrane transporter activity	8.17E-02	Q9ZU50	397	4	18777	23.64861	0.567756
Molecular function	GO:0010309~acireductone dioxygenase [iron(II)-requiring] activity	8.17E-02	Q8W108	397	4	18777	23.64861	0.567756